UNIVERSIDADE
BEIRA INTERIOR

Water-Emulsified Diesel Fuel in a CI Engine Tested for Aeronautical Applications

Pedro Manuel Pimenta da Silva Oliveira

Tese para obtenção do Grau de Doutor em
Engenharia Aeronáutica
(3º ciclo de estudos)

Orientador: Prof. Doutor Francisco Miguel Ribeiro Proença Brójo
Co-orientador: Prof. Doutor Rogério Pedro Fernandes Serôdio

Covilhã, junho de 2025

Composição do Júri

Presidente

Doutor Mário Marques Freire

Professor catedrático da Universidade da Beira Interior

Vogais

Doutor Afzal Suleman

Professor catedrático do Instituto Superior Técnico da Universidade de Lisboa (Arguente)

Doutora Marya Reyes Garcia Contreras

Professora associada da Escuela de Ingeniería Industrial y Aeroespacial da Universidad de Castilla-La Mancha UCLM (Arguente)

Doutor Miguel Ângelo Rodrigues Silvestre

Professor auxiliar da Faculdade de Engenharia da Universidade da Beira Interior (Arguente)

Doutor Jorge Manuel Pereira Gregório

Professor adjunto do Instituto Politécnico da Guarda

Doutor Francisco Carrusca Pimenta Brito

Professor auxiliar da Escola de Engenharia da Universidade do Minho

Orientador

Doutor Francisco Miguel Proença Brójo

Professor auxiliar da Faculdade de Engenharia da Universidade da Beira Interior

Provas públicas realizadas a 18 de junho de 2025

Declaração de Integridade

Eu, Pedro Manuel Pimenta da Silva Oliveira, que abaixo assino, estudante com o número de inscrição D2858 do curso de 3º ciclo Engenharia Aeronáutica da Faculdade de Engenharia, declaro ter desenvolvido o presente trabalho e elaborado o presente texto em total consonância com o **Código de Integridades da Universidade da Beira Interior**.

Mais concretamente afirmo não ter incorrido em qualquer das variedades de Fraude Académica, e que aqui declaro conhecer, que em particular atendi à exigida referenciação de frases, extratos, imagens e outras formas de trabalho intelectual, e assumindo assim na íntegra as responsabilidades da autoria.

Universidade da Beira Interior, Covilhã, 26 de junho de 2025

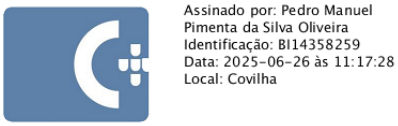

Dedication

To my family and everyone who supported me.

"We crave for new sensations but soon become indifferent to them. The wonders of yesterday are today common occurrences."

Nikola Tesla

"To myself I am only a child playing on the beach, while vast oceans of truth lie undiscovered before me."

Isaac Newton

Acknowledgements

First and foremost, I would like to thank my supervisor Prof. Doutor Francisco Brójo for his support, guidance, and availability throughout the entire journey of this research. Their expertise, constructive feedback, and encouragement were instrumental in shaping the direction of this work. Also, I want to thank my co-supervisor Prof. Doutor Rogério Serôdio for all the discussions, help, and availability whenever requested, especially in the analysis portion of this project. A sincere thanks to Eng. João Serôdio for all the help, knowledge, suggestions, motivation, and countless hours of troubleshooting to develop the best possible work and reach the most precise conclusions.

A special thanks to all the people who have worked alongside me in the lab, especially Eng. João Antunes for all the help provided during the experimental section of this work, which was fundamental for the success of this thesis.

I would like to thank C-MAST, University of Castilla La-Mancha, Department of Fuels and Engines, and Chemical Department of UBI for the space, equipment, and materials provided during the development of this work. I would also like to thank Santander Totta-UBI through Faculty of Engineering individual PhD Grant 2020, FCT through individual PhD Grant 2021.07535.BD, and C-MAST through projects UIDB/00151/2020 (https://doi.org/10.54499/UIDB/00151/2020) and UIDP/00151/2020 (https://doi.org/10.54499/UIDP/00151/2020) for funding this investigation.

I must express my very profound gratitude to my parents and grandparents, for the love they raised me with and all the honest values they taught me, inspiring me to stay motivated and reach all my goals without ever giving up. Finally, thanks to all my friends and especially my girlfriend for the continuous support and encouragement throughout these years. Your love has been the fuel that propelled me through this thesis.

C-MAST | Center for Mechanical and Aerospace Science and Technologies

Resumo

Emulsões de água em diesel como combustível alternativo estão a surgir como uma opção viável para fazer frente ao consumo global de combustíveis fósseis e às restrições de emissões sem a necessidade de modificações no motor. Numa emulsão, dois líquidos imiscíveis são misturados com a ajuda de surfatantes, onde gotas de um líquido estão dispersas numa fase contínua.

Esta tese pretende comparar diesel emulsificado com água com diesel europeu comercialmente disponível (EN590) relativamente ao desempenho do motor e emissões. Os testes foram conduzidos num motor a diesel monocilíndrico de injeção direta (Hatz 1B40) através de um dinamómetro de correntes de Foucault, um analisador de gases de escape e um opacímetro. Com o objetivo de testar o motor e os combustíveis alternativos para condições de operação encontradas frequentemente em veículos aéreos equipados com motores diesel (princípios de operação semelhantes), os testes foram executados para condições de ralenti (simulando o movimento de táxi de uma aeronave), 100% de carga do motor (simulando as manobras de descolagem e de subida), 50% de carga do motor (representando as fases de descida, aproximação e aterragem) e 75% de carga do motor (representado a componente de cruzeiro do perfil de voo de uma aeronave) a diferentes rotações do motor.

Misturas de combustível diesel EN590, água deionizada e surfatantes foram produzidas em laboratório através de homogeneização mecânica para obter as concentrações ideais dos diferentes reagentes a serem replicadas mais tarde a uma escala maior e usando um método de mistura de baixa energia. As emulsões foram desenvolvidas para estarem otimizadas à temperatura de operação do motor e aquecidas acima da temperatura de operação do gasóleo de forma a alcançar viscosidades semelhantes durante os procedimentos de teste.

Os resultados sugerem que adicionar água como uma fase dispersa no combustível permite obter uma eficiência térmica superior e menores emissões de óxidos de azoto e fumo em algumas condições comparado com o diesel tradicional. Por outro lado, emissões de hidrocarbonetos, monóxido de carbono e dióxido de carbono aumentaram, possivelmente devido a diferenças no atraso de injeção entre os combustíveis.

Ao priorizar o desempenho em detrimento da estabilidade através da adoção de uma formulação de emulsão hidrofílica, alinhada com a dificuldade de otimização adicional

em motores a gasolina na aviação geral e a ampla disponibilidade de combustível diesel, pode-se concluir que emulsões de água em diesel podem ser uma alternativa viável para alcançar o objetivo de melhorar taxas de consumo de combustível em algumas condições, reduzir emissões de óxido de azoto, fumo e diminuir custos, quando otimizadas para condições de operação específicas de veículos aéreos movidos a diesel.

Palavras-chave

Poluição, combustíveis fósseis, motores de combustão interna, motor diesel, combustíveis emulsificados, emulsão de água em diesel, combustíveis aeronáuticos, desempenho, emissões

Resumo Alargado

Emulsões de água em diesel como combustível alternativo estão a surgir como uma opção viável para fazer frente ao consumo global de combustíveis fósseis e às restrições de emissões sem a necessidade de modificações no motor. Numa emulsão, dois líquidos imiscíveis são misturados através de vários processos químicos e mecânicos com a ajuda de surfatantes, onde gotas de um líquido estão dispersas numa fase contínua. Emulsões de água em diesel pertencem à categoria de emulsões de água em óleo, onde o diesel corresponde à fase contínua e a água corresponde à fase dispersa.

Esta tese pretende comparar diesel emulsificado com água com diesel europeu comercialmente disponível (EN590) relativamente ao desempenho do motor e emissões. No que diz respeito ao desempenho, os parâmetros analisados foram a velocidade, o binário, a potência, o consumo específico, o rendimento e a temperatura do motor. Em termos de emissões, os gases de escape analisados foram o monóxido de carbono, dióxido de carbono, hidrocarbonetos, óxido nítrico, oxigénio e fumo. Os testes foram conduzidos num motor diesel monocilíndrico de injeção direta, naturalmente aspirado e arrefecido a ar (Hatz 1B40) através de um dinamómetro de correntes de Foucault, um analisador de gases de escape e um opacímetro. Com o objetivo de testar o motor e os combustíveis alternativos para condições de operação encontradas frequentemente em veículos aéreos equipados com motores a diesel (princípios de operação semelhantes), os testes foram executados para condições de ralenti (simulando o movimento de táxi de uma aeronave), 100% de carga do motor (simulando as manobras de descolagem e de subida), 50% de carga do motor (representando as fases de descida, aproximação e aterragem) e 75% de carga do motor (representado a componente de cruzeiro do perfil de voo de uma aeronave) a diferentes rotações do motor. A variação da carga no motor foi conseguida através da variação da corrente nas bobines que viriam a alterar a intensidade das correntes induzidas no disco rotativo do dinamómetro. Para cada carga do motor, os testes foram conduzidos a quatro velocidades diferentes (1500, 2000, 2500 e 3000 rotações por minuto).

Misturas de combustível diesel EN590, água deionizada e surfatantes foram produzidas em laboratório através de homogeneização mecânica para obter as concentrações ideais dos diferentes reagentes a serem replicadas mais tarde a uma escala maior e utilizando um misturador acoplado a um berbequim como um método de mistura de baixa energia. As emulsões foram desenvolvidas para estarem otimizadas à temperatura de operação

do motor e aquecidas acima da temperatura de operação do diesel de forma a alcançar viscosidades semelhantes durante os procedimentos de teste. Duas emulsões diferentes foram produzidas. A primeira com 8% de água, 89% de diesel e 3% de mistura de surfatantes e a segunda com 16% de água, 78% de diesel e 6% de mistura de surfatantes, em massa. Parâmetros como a massa volúmica e a viscosidade a diferentes temperaturas foram medidos para os três combustíveis através de um hidrómetro e de um viscosímetro, respetivamente. O poder calorífico dos diferentes combustíveis foi também medido a partir de um calorímetro de bomba.

Os resultados obtidos foram posteriormente analisados e tratatos recorrendo à linguagem de programação R de forma a proporcionar um elevado rigor estatístico aos dados em estudo. Estes resultados sugerem que adicionar água como uma fase dispersa no combustível permite obter uma eficiência térmica superior e menores emissões de óxidos de azoto e fumo em algumas condições comparado com o diesel tradicional. Por outro lado, emissões de hidrocarbonetos, monóxido de carbono e dióxido de carbono aumentaram, possivelmente devido a diferenças no atraso de injeção entre os combustíveis.

Ao priorizar o desempenho em detrimento da estabilidade através da adoção de uma formulação de emulsão hidrofílica, em contraste com o recomendado para emulsões de água em óleo, alinhada com a dificuldade de otimização adicional em motores a gasolina na aviação geral, o elevado preço da gasolina para aviação e a ampla disponibilidade de combustível diesel, pode-se concluir que emulsões de água em diesel podem ser uma alternativa viável para alcançar o objetivo de melhorar o consumo específico, reduzir emissões e diminuir custos, quando otimizadas para condições de operação específicas de veículos aéreos movidos a diesel. Contudo, e de forma a que a utilização de emulsões de água em diesel na aviação geral possa ser considerada, é fundamental otimizar os seus parâmetros e assegurar a estabilidade da mistura em diferentes condições de pressão e temperatura caraterísticas da maior dinâmica e variabilidade ambiental às quais os veículos aéreos estão sujeitos. Estes problemas poderiam ser resolvidos através de um sistema de produção de emulsões a bordo.

Abstract

Water-in-diesel emulsions as an alternative fuel are emerging as a viable option to fight global fossil fuel consumption and emissions restrictions without the need for engine modifications. In an emulsion, two immiscible liquids are mixed with the help of surfactants, where droplets of one liquid are dispersed in a continuous flow.

This thesis aims to compare water-emulsified diesel fuel with European commercially available diesel (EN590) when it comes to engine performance and emissions. The tests were performed in a single-cylinder, direct injection diesel engine (Hatz 1B40) using an eddy current dynamometer, an exhaust gas analyser, and an opacimeter. With the objective of testing the engine and the alternative fuels for operating conditions often found in aerial vehicles equipped with diesel engines (same operating principles), the tests were performed for idle settings (simulating the taxiing movement of an aircraft), 100% engine load (simulating the take-off and climbing manoeuvres), 50% engine load (representing the descent, approach, and landing phases), and 75% engine load (representing the cruise component of an aircraft's flight profile) at different engine speeds.

Mixtures of EN590 diesel fuel, deionised water, and surfactants were performed in laboratory by mechanical homogenization to obtain the ideal concentrations of the different reagents to be later replicated on a bigger scale using a low-energy mixing method. The emulsions were developed to be optimised at the engine's operating temperature and heated above the diesel fuel operating temperature to reach similar viscosities during the test procedures.

The results suggest that adding water as a dispersed phase in the fuel allows to obtain overall better thermal efficiency and lower emissions of nitrogen oxides and smoke in some conditions when compared to traditional diesel. On the other hand, carbon monoxide, hydrocarbons, and carbon dioxide emissions have increased, possibly due to differences in the injection delay between the fuels.

By focusing on performance over stability through the adoption of a hydrophilic emulsion formulation in line with the difficulty of further optimisation in general aviation gasoline engines and the widespread availability of diesel fuel, it can be concluded that water-in-diesel emulsions can be a viable alternative towards the goal of

improving fuel consumption rates, lowering emissions, and reducing costs when optimised for specific operating conditions of diesel-powered aerial vehicles.

Keywords

Pollution, fossil fuels, internal combustion engine, diesel engine, emulsified fuels, water-in-diesel emulsion, aviation fuels, performance, emissions

Table of Contents

List of Figures

List of Tables

List of Acronyms

CI	Compression-Ignition
C-MAST	Centre for Mechanical and Aerospace Science and Technologies
ET	Engine Block Temperature
ECB	Eddy Current Brake
FAME	Fatty Acid Methyl Esters
FCT	Foundation for Science and Technology
F-T	Fischer-Tropsch
GHG	Greenhouse Gas
HC	Hydrocarbons
HHV	Higher Heating Value
HLB	Hydrophilic-Lipophilic Balance
HLD	Hydrophilic-Lipophilic Difference
HV	Heating Value
HVO	Hydrotreated Vegetable Oil
ICE	Internal Combustion Engine
IR	Infrared
LHV	Lower Heating Value
LNG	Liquified Natural Gas
OPE	Opposed Piston Engine
O/W	Oil-in-Water
O/W/O	Oil-in-Water-in-Oil
PC	Percent Change
PDI	Polydispersity Index
PM	Particulate Matter
PS	Particle Size
SAF	Sustainable Aviation Fuel
SEC	Specific Energy Consumption
SFC	Specific Fuel Consumption
SI	Spark-Ignition
TDC	Top Dead Centre
TE	Thermal Efficiency
UAV	Unmanned Aerial Vehicle
UBI	University of Beira Interior
WFE	Water-in-Fuel Emulsion
WiDE	Water-in-Diesel Emulsion
W/O	Water-in-Oil
W/O/W	Water-in-Oil-in-Water

Nomenclature

Latin letters	Description	Unit
a	Distance from the Axis of Rotation	[m]
AFR	Air-Fuel Ratio	[-]
AFR_{sto}	Stochiometric Air-Fuel Ratio	[-]
BMEP	Brake Mean Effective Pressure	[bar]
BP	Brake Power	[kW]
BSFC	Brake Specific Fuel Consumption	[g kW^{-1} h^{-1}]
BT	Brake Torque	[N m]
BTE	Brake Thermal Efficiency	[%]
CO	Carbon Monoxide	[%]
CO_2	Carbon Dioxide	[%]
D_i	Cook's Distance for the i^{th} Observation	[-]
$Diesel_p$	Diesel Fuel Parameter	[-]
F	Force Applied	[N]
H_{cv}	Hydrogen-to-Carbon Atomic Ratio	[-]
HHV_v	Higher Heating Value at Constant Volume	[MJ kg^{-1}]
L	Length of the Pipe	[m]
LHV	Lower Heating Value	[MJ kg^{-1}]
LHV_p	Lower Heating Value at Constant Pressure	[MJ kg^{-1}]
LHV_v	Lower Heating Value at Constant Volume	[MJ kg^{-1}]
MEP	Mean Effective Pressure	[bar]
MSE	Mean Squared Error	[-]
$\dot{m}_{air}$	Air Mass Flow Rate	[g h^{-1}]
$\dot{m}_{fuel}$	Fuel Mass Flow Rate	[g h^{-1}]
n	Number of Mols	[mol]
N	Rotational Speed	[rpm]
NO	Nitric Oxide	[ppm]
NO_x	Nitrogen Oxides	[ppm]
NO_2	Nitric Dioxide	[ppm]
N_2O	Nitrous Oxide	[ppm]
nR	Crank Cycles per Power Stroke per Cylinder	[-]
O_{cv}	Oxygen-to-Carbon Atomic Ratio	[-]
O_2	Oxygen	[%]
O_3	Ozone	[%]
p	Number of Parameters of the Model	[-]
P	Power	[kW]
P_{gas}	Pressure of the gas	[Pa]
PC	Percent Change	[%]
Q	Volumetric Flow Rate	[m^3 s^{-1}]
r	Radius of the Pipe	[m]
R	Ideal Gas Constant	[J mol^{-1} K^{-1}]
SFC	Specific Fuel Consumption	[g kW^{-1} h^{-1}]
T	Temperature	[K]
V	Volume	[m^3]
V_d	Swept Volume	[dm^3]
W_h	Molar Weight of Hydrogen	[g mol^{-1}]
W_o	Molar Weight of Oxygen	[g mol^{-1}]
W_r	Molar Weight of Reagent	[g mol^{-1}]
$WiDE_p$	Water-in-Diesel Emulsion Parameter	[-]

Y_h	Mass Fraction of Hydrogen	[-]
$Y_{h.d}$	Mass Fraction of Hydrogen of Diesel	[-]
$Y_{h.e}$	Mass Fraction of Hydrogen of the Emulsion	[-]
$Y_{h.w}$	Mass Fraction of Hydrogen of Water	[-]
$Y_{h.EH}$	Mass Fraction of Hydrogen of the Hydrophilic Surfactant	[-]
$Y_{h.EL}$	Mass Fraction of Hydrogen of the Lipophilic Surfactant	[-]
Y_o	Mass Fraction of Oxygen	[-]
$Y_{o.d}$	Mass Fraction of Oxygen of Diesel	[-]
$Y_{o.e}$	Mass Fraction of Oxygen of the Emulsion	[-]
$Y_{o.w}$	Mass Fraction of Oxygen of Water	[-]
$Y_{o.EH}$	Mass Fraction of Oxygen of the Hydrophilic Surfactant	[-]
$Y_{o.EL}$	Mass Fraction of Oxygen of the Lipophilic Surfactant	[-]
$\hat{y}_j$	j^{th} Fitted Value from the Model	[-]
$\hat{y}_{j(i)}$	j^{th} Fitted Value from the Model Excluding the i^{th} Observation	[-]
$\%_{m/m}$	Percent by Mass	[%]

Greek letters	**Description**	**Unit**
$\Delta H_{vap.water}$	Enthalpy of Vaporisation of Water	[MJ kg^{-1}]
ΔP	Pressure Difference	[Pa]
η	Dynamic Viscosity	[Pa s]
λ	Air-Fuel Ratio Coefficient	[-]
ρ	Density	[g cm^{-3}]
τ	Torque	[N m]
Φ	Fuel-Air Equivalence Ratio	[-]

Chapter 1. Introduction

1.1 Motivation

For many years, pollution and its harmful effects on the environment have been neglected by Governments all over the World, despite being one of the main causes of health problems and the planet's degradation in the last decades. One of the worst forms of pollution is air pollution, which the World Health Organization estimates to cause over 4.2 million deaths every year [1]. Not only is it harming human health, but also the environment in which we live, with effects such as acid rain, haze, ozone (O_3), and global climate change. The six major air pollutants are particulate matter (PM), ground-level O_3, carbon monoxide (CO), sulfur oxides (SO_x), nitrogen oxides (NO_x), and lead [2]. Fossil fuels are one of the main responsible for these emissions, accounting for over 84.3% of all primary energy sources, followed by hydro, renewables, and nuclear [3], [4]. Oil, gas, and coal are the main types of fossil fuels available, and their global distribution in 2024 can be found in Figure 1.1.

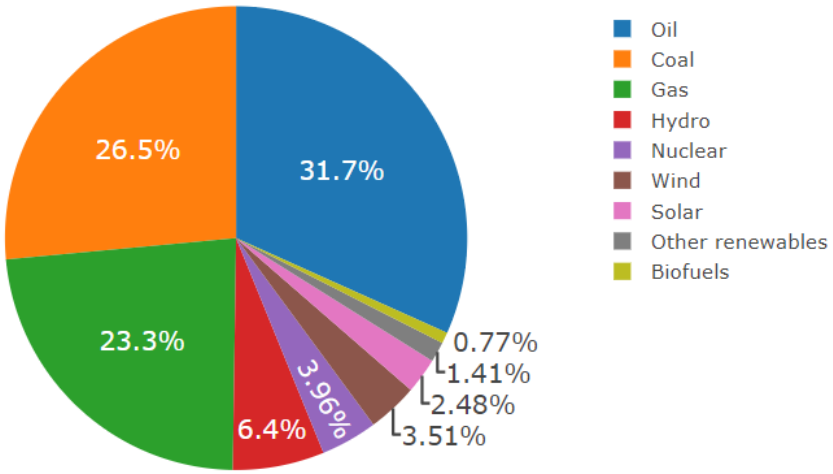

Figure 1.1. Energy sources distribution (adapted from [5]).

The transport sector represents over 15,0% of global fossil fuel emissions, and in Europe, oil represents over 93% of the total energy consumption in the sector, followed by low amounts of biofuels and natural gas [6], [7], [8]. Carbon dioxide (CO_2) accounts for about 76% of total greenhouse gases (GHGs) emissions (excluding water vapour), and in Figures 1.2 and 1.3, it is possible to observe how each mode of transportation contributes to it, at a global level.

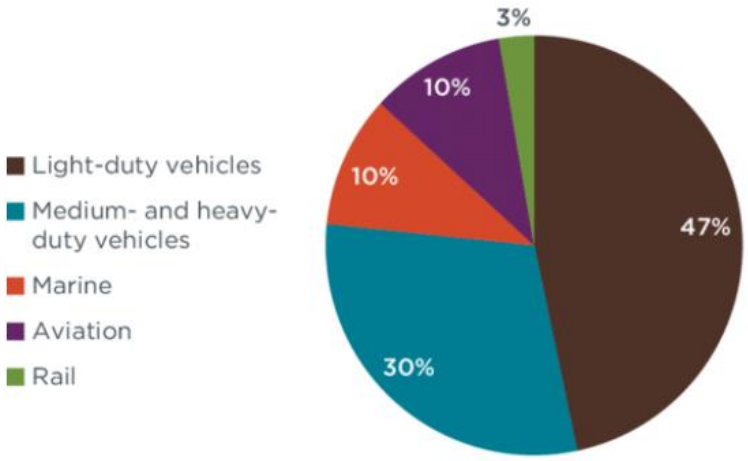

Figure 1.2. Greenhouse gas emissions by transportation mode [9].

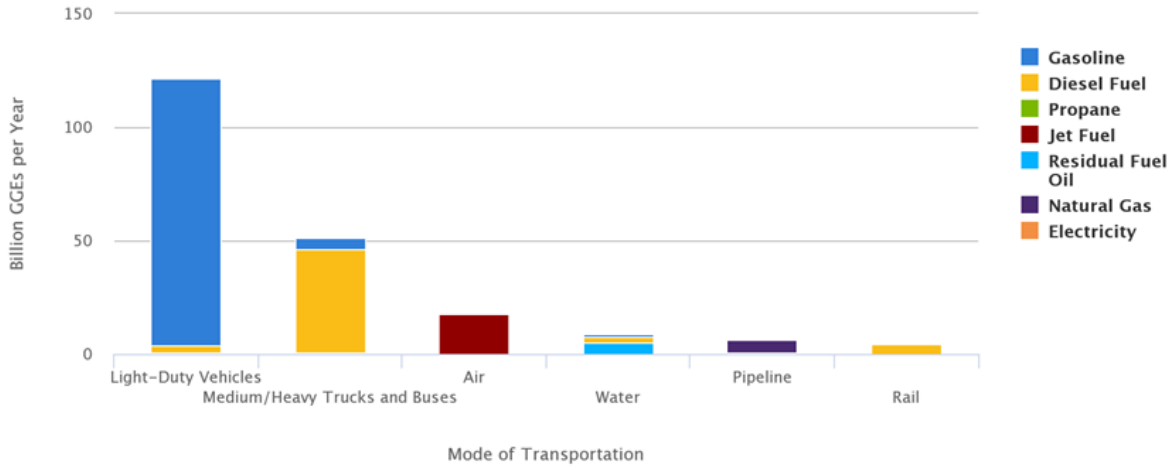

Figure 1.3. Energy use by transportation mode by fuel type [10].

Compared to ground vehicles, air transportation accounts for a smaller share of emissions, which explains why the focus on aircraft engine emissions has not been as intense in recent years. The two main sources of aircraft emissions are the jet engines and the auxiliary power unit. Since most jet fuel is burned in flight, most of the emissions (over 90%) occur at altitude, however, recent studies show that they can affect local air quality at ground-level [11].

The aviation sector, and as can be seen in Figure 1.3, primarily uses jet fuel combustion as an energy source. This choice is not an accident and is based on petroleum's recognised advantages. Liquid fuels have higher energy contents per unit volume than gases, and liquid hydrocarbons (HC) offer the best combination of energy content, availability, and price [12]. The most common and utilised types of jet fuel are Jet A, Jet A-1, Jet B, and TS-1. Despite jet fuel being the main choice for civil aviation, due to its lower freezing point and higher flash point, offering higher octane ratings and thus greater power and efficiency, many aircraft with alternative engines can also utilise diesel and avgas (aviation gasoline). Unlike gas fossil fuels that are primarily composed of a single hydrocarbon isomer, liquid fossil fuels are a compilation of hydrocarbon isomers. Depending on how many hydrogen and carbon atoms there are, the molecules behave differently.

While C_6 to C_{10} range makes gasoline, jet fuel is derived from much heavier chains, in the C_8 to C_{16} range, and diesel even heavier [12].

Over the past years, a lot of effort has been put into the search for alternative solutions capable of reducing the use of carbon-based fuels and their emissions. Legislations and projects to reduce these emissions have been and are being created by governments all around the world to significantly contribute to the prevention of global warming. At the moment, plentiful different technologies are available that offer reduced emissions, like alternative and cleaner fuels (electricity, hydrogen, biofuels, natural gas, etc.), despite having known disadvantages. Another method that can contribute to the reduction of fossil fuels' associated pollution, and with significant advances in recent years, is the application of emulsion techniques, which is the focus of this work. This improvement in efficiency is mostly related to microexplosion effects in emulsion droplets. Emulsions are dispersions containing two immiscible phases which are mixed using mechanical shear and surfactant [13]. In an emulsion, droplets of one liquid (dispersed phase) are dispersed in the other (continuous phase) [14].

Many studies about emulsions with different kinds of fuels have been performed throughout the years, mainly directed to road transportation, with hydrophobic formulations optimised for storage stability. However, for aviation where the laws are much stricter and where safety always stands up as the most important factor, there aren't many. With the difficulty of further optimising engines running on avgas, a transition to diesel-powered aerial vehicles seems a reasonable path to take to improve efficiency and reduce costs in general aviation. To address this, and acknowledging the widespread availability of diesel fuel as well as engine compatibility with future sustainable fuels, this work was initiated with the main purpose of checking the viability of utilising water-emulsified diesel fuels in a diesel engine using a hydrophilic formulation optimised for operating conditions and analyse its risks and potential utilization in aeronautical applications as a way to improve specific fuel consumption, reduce the emissions of some Green House Gases (GHGs) and lower operating costs.

1.2 Objectives

The main objective of the work is to evaluate an alternative way to improve performance and reduce fossil fuels consumption and emissions in aerial vehicles equipped with diesel engines (small aircraft and unmanned aerial vehicles (UAVs)), by analysing and verifying the possibility of utilising emulsified diesel fuels in a compression-ignition (CI) engine, and to measure its performance in comparison with traditional diesel. Therefore, it is expected to:

i) Understand the concerns regarding the consumption of fossil fuels, the operating process of aeronautical internal combustion engines (ICEs), the importance of fuel quality in their performance and viability, and the principles of the different types of emulsions.
ii) Gather and analyse information about the different kinds of aeronautical fuels, alternative fuels, and emulsified fuels.

iii) Prepare the emulsified fuels, optimising their properties at the engine's operating temperature.
iv) Select and measure the performance of the engine with diesel fuel and emulsified diesel fuels under different test conditions.
v) Analyse the results, more specifically in the power/torque output, the specific fuel consumption (SFC), thermal efficiency (TE), and emissions.
vi) Draw conclusions and verify the viability of the emulsified fuels in aeronautical CI engines, as well as the influence of their properties and parameters on engine performance.

In addition, this work aims to provide valuable insights and experimental statistical data in the field of emulsified fuels by following an alternative approach of focusing on performance over storage stability. Furthermore, and in contrast with the literature (adopting hydrophobic formulations to enhance storage stability), a hydrophilic emulsion formulation was adopted to ensure stability at higher fuel temperatures commonly found in diesel engines during operation.

1.3 Methodology

In the first stage of the work (State of the Art), there will be a research, analysis, and a literature review in order to understand the concerns regarding the consumption of fossil fuels and their hazardous effects on the planet, the operating process of ICEs, specifically CI engines, on the factors and the importance of the fuel quality in their performance and reliability. The different types of aeronautical fuels, alternative fuels, and emulsified fuels will be studied, regarding their different properties, as well as the parameters that affect their performance. There will be a literature review on the different types of emulsions, techniques, composition, and the importance of their particle size (PS) and polydispersity index (PDI) in their stability and properties. Some key variables regarding engine performance and emissions will also be reviewed.

After analysing the existing and available information on the different topics, in the Case Study, the best combinations of water, diesel, and surfactant for the emulsions will be selected and prepared in the university laboratories by mechanical homogenization, a cheaper method when compared to ultrasonication [15]. The chemical properties of each fuel will also be examined. There will be a selection of an engine and the most adequate fuels for testing. The engine will be a diesel engine and the fuels: diesel and two mixtures of water-emulsified diesel. A specific type of certified diesel fuel will be selected. The main parameters to be measured in the engine are speed, torque, power, SFC, TE, and emissions for the different tested fuels. Regarding the emulsified fuels, the tests will be performed for different percentages of water and surfactant, and at different engine loads, engine speeds, and fuel temperatures for all fuels. The measurements will be performed in a test-bench composed of a home-built eddy current dynamometer with suitable sensors, dedicated material, and its corresponding test protocol. Raw data from the tests will be presented at the end of this section.

The next step is to analyse and refine some of the results obtained from the experiments. These results will be divided into two sections: performance analysis and emission analysis. The relationship between the different engine parameters will be studied for each case. This data analysis will be performed using the programming language R (a free software environment for statistical computing and graphics). A correlation between engine load and different flight phases of an aerial vehicle will be traced, and a comparative analysis between the fuels will be performed for each condition. After collecting the required information from the results analysis, the viability of utilising water-emulsified diesel fuels in a CI engine will be evaluated, taking into consideration some restrictions and safety requirements applied to aircraft fuel and aerial vehicles.

In the final section of this work, the necessary conclusions will be drawn, some limitations found during the experimental part will be discussed, and potential future work on the subject will be analysed.

Figure 1.4 highlights the structure of the thesis, organised into four main chapters in addition to the Introduction chapter. Each chapter is broken down into its corresponding specific topics.

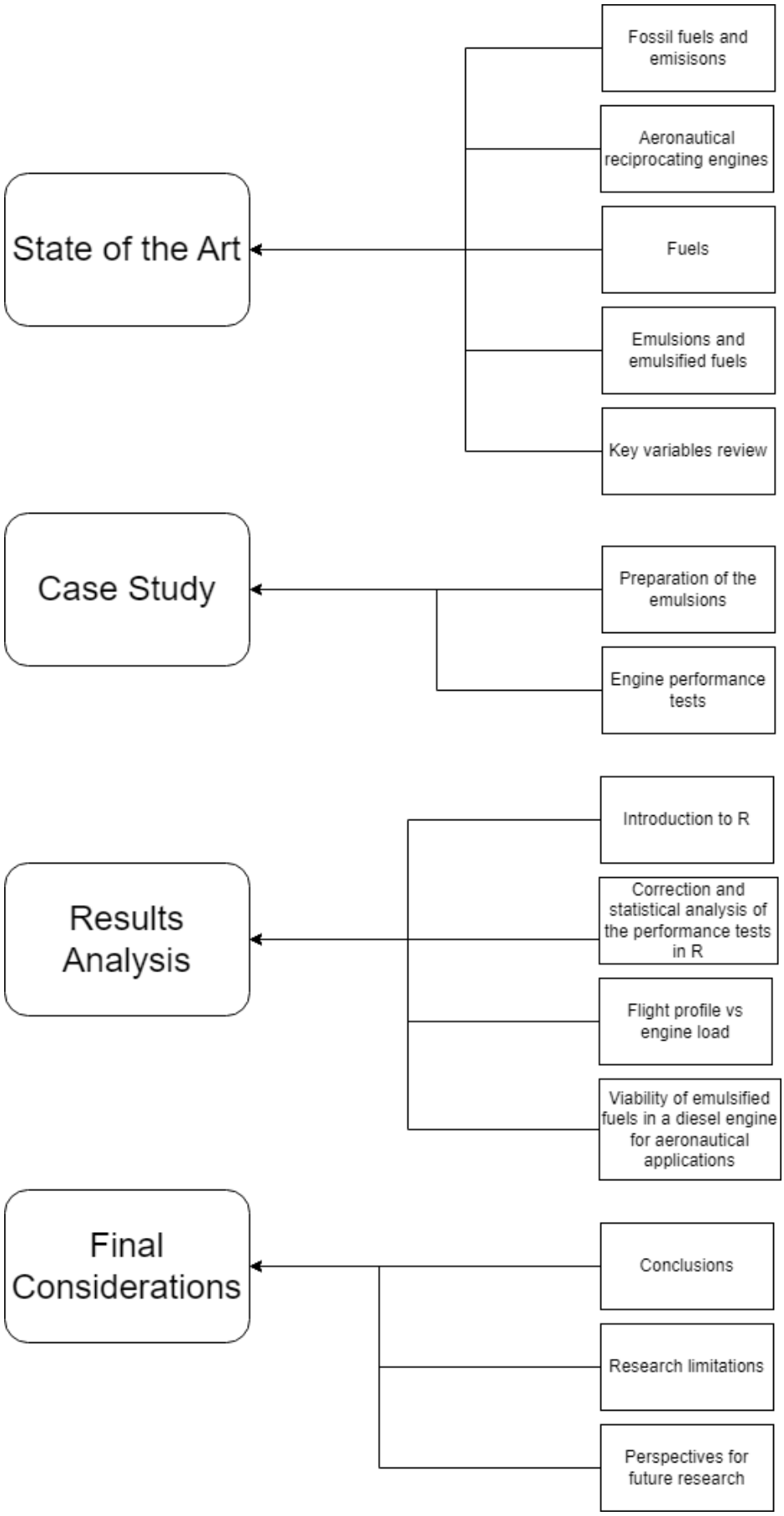

Figure 1.4. Methodology diagram.

Chapter 2. State of the Art

2.1 Fossil fuels and emissions

Since the beginning of the industrial era, the hazardous effects of burning fossil fuels have been addressed. When fossil fuels are burned, large amounts of GHGs, especially CO_2 are released into the air. These gases trap heat in the atmosphere (the solar energy absorbed at the Earth's surface is radiated back into the atmosphere as heat, and a big percentage of this heat is absorbed by GHGs when it makes its way through the atmosphere and back out to space), increasing the average global temperature, and causing global warming which can lead to sea level rise, extreme weather, extinction of species, and many other concerning problems [16], [17]. Water vapour is the largest contributor to the Earth's greenhouse effect, accounting for about 85% to 90% of the greenhouse effect (it emits and absorbs infrared (IR) radiation at many more wavelengths than any of the other GHGs). However, its concentration is not directly affected by human activity. It is a consequence of the temperature increase (caused by man-made emissions of CO_2 and other GHGs), increasing the amount of water vapour in the air by boosting the rate of evaporation [18].

For many years, large amounts of GHGs, such as CO_2, methane (CH_4), nitrous oxide (N_2O), NO_x, water vapour, and other radiatively active gases have been emitted into the atmosphere by humankind, leading to an increase of the global-mean temperature of over 0.8ºC since 1880 [19], [20]. The usage of fossil fuels as an energy source has significantly increased over the past century, reaching values that should be worrying enough to take action against it immediately. ICEs represent the big share of fossil fuels consumption, being responsible for the high concentrations of GHGs in the atmosphere [21]. When compared to gasoline engines, CI engines represent the main percentage of the worst exhaust emissions gases. While CO and CO_2 emissions from gasoline engines are generally higher (because CI engines are more efficient and normally operate leaner) [15], [22], the higher NO_x and PM emissions from CI engines are very worrying [23].

Over the past decades, a lot of effort has been put into reducing the pollution associated with the burning of fossil fuels, especially in the road transport sector. In the case of Europe, since 1992, regulations have been imposed on new cars, with the aim of improving air quality by reducing emissions. These regulations, known as the European emissions standards, are still being updated to the present date, as seen in Table 2.1.

Table 2.1. European emissions standards in diesel exhaust (adapted from [24]).

Stage	Date	CO	HC	HC+NOx	NOx	PM
		g/km				
Euro 1‡	1992.07	2.72 (3.16)	-	0.97 (1.13)	-	0.14 (0.18)
Euro 2, IDI	1996.01	1.0	-	0.7	-	0.08
Euro 2, DI	1996.01[a]	1.0	-	0.9	-	0.10
Euro 3	2000.01	0.64	-	0.56	0.50	0.05
Euro 4	2005.01	0.50	-	0.30	0.25	0.025
Euro 5a	2009.09[b]	0.50	-	0.23	0.18	0.005[f]
Euro 5b	2011.09[c]	0.50	-	0.23	0.18	0.005[f]
Euro 6	2014.09	0.50	-	0.17	0.08	0.005[f]
Euro 7	2026.11.29	0.50	-	0.17	0.08	0.0045

† Euro 5-6: particles > 23 nm; Euro 7: particles > 10 nm
‡ Values in brackets are conformity of production (COP) limits
a. until 1999.09.30 (after that date DI engines must meet the IDI limits)
b. 2011.01 for all models
c. 2013.01 for all models
f. 0.0045 g/km using the PMP measurement procedure

From Euro 3 to Euro 6, NO_x limits from diesel cars were reduced by 84%. From the last Euro to the present Euro 6, those limits were reduced by 55.5%. Euro 7, scheduled for 2026, will demand emissions to be even lower making many brands believe it will significantly increase ICEs costs as many engine modifications would have to be made to keep up with the established emissions limits [25], [26]. Even the European Commission has acknowledged that Euro 7 could be the last rules for conventional vehicles before moving to zero and low emission alternatives. As we reflect upon the issue of high emissions, particularly from diesel engines, it is also important to address that one of the main causes for this problem lies in the ageing fleet of vehicles and their engines. These less efficient systems, having been in operation for many years, are significantly more polluting compared to the modern engines of today. The global emissions data, and because it is compiled over the decades, highlights this contribution from older vehicles, that just like the ones produced today, have and are still going to be on the road with a median operating life of twenty or more years.

In aviation, GHGs emissions are much lower when compared to the ground transport sector, including rail transport (over 10% and 80%, respectively). General aviation is estimated to contribute less than 1% of all GHGs emissions, and piston-powered general aviation aircraft around 0.1%. Despite only being the second most polluting transport source, aviation emissions have been increasing over the past years, being much more relevant today when compared to a few decades ago. Between 1990 and 2016, CO_2 emissions from European flights increased by over 95%. NO_x emissions have followed a steeper upward trend with an increase of over 123%. The fleet renewal contributed to a stabilisation of HC, CO, and PM emissions between 2005 and 2014, even though PM emissions are expected to increase in the next decades if engine technology does not change [27].

Figure 2.1 represents the overall increase in the emissions of CO_2 (the most responsible human-emitted GHG for altering global temperatures) from global aviation over the last decades. As can

be observed, and in line with the aviation industry's projected growth, the expectations are for these numbers to keep increasing in future years.

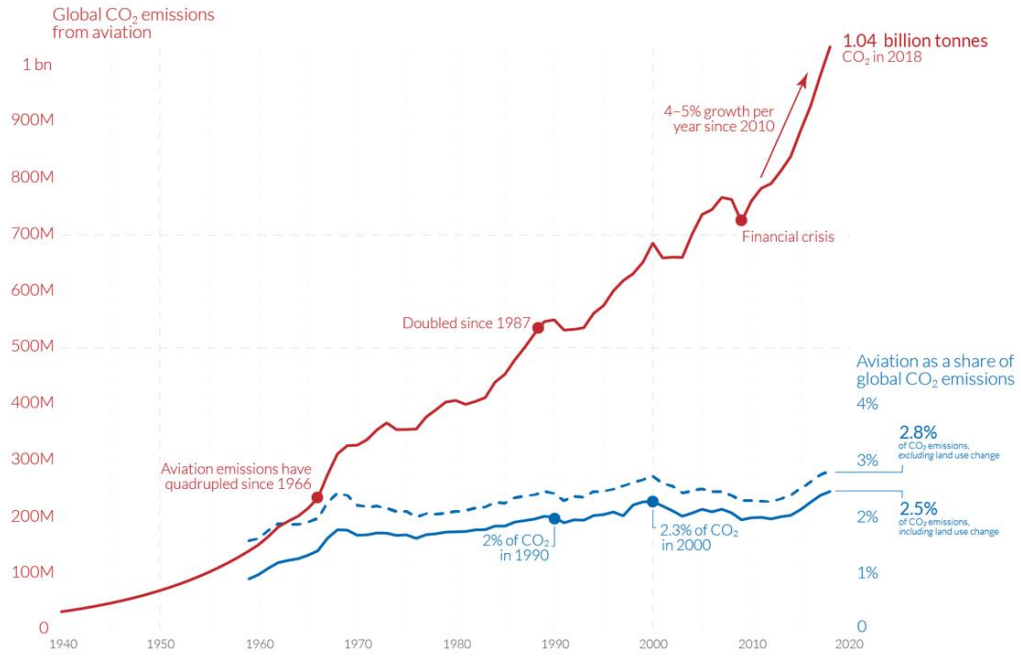

Figure 2.1. Global CO2 emissions from aviation [28].

2.2 Aeronautical reciprocating engines

An aircraft engine is the component of the propulsion system for an aircraft that produces mechanical power. Aircraft engines can be classified into gas turbines (usually called jet engines) or lightweight piston ICE [29]. Jet engines can still be divided into turbojet, turboprop, turboshaft, turbofan, ramjet, pulsejet, and scramjet [30].

In the first forty years of the 20th century, the gasoline ICE engine, driving a propeller, was the best propulsion mechanism at the time, with significant advances until the birth of the jet engine, in the last years of World War II. Even though jet engines seemed to be, at the time, the excellent propulsion mean, it did not stop the progress already verified in the conventional and hence alternative engines [31].

2.2.1 Internal combustion engine

In the 1860s, many people claimed the invention of the ICE, however, only in 1862, Alphonse Beau de Rochas, a French engineer, had a patent on the four-stroke operating sequence. In 1876, Nikolaus August Otto, a German engineer, developed the four-stroke “Otto” cycle, widely used in transportation even in the current days [32]. A brief outline of the history and development of the ICE over the years can be seen in Table 2.2.

Table 2.2. History of the ICE [32].

Year	*Inventor*	*Contributions*
1680	Christian Huygens	Invented an ICE to be fuelled with gunpowder.
1807	Francois Isaac de Rivaz	Invented an ICE that used a mixture of hydrogen and oxygen (O_2) for fuel. Designed the first, however unsuccessful, ICE-powered automobile.
1824	Samuel Brown	Developed an old Newcomen steam engine adapted to burn gas.
1858	Jean Joseph Étienne Lenoir	Invented and patented a double-acting, electric SI ICE fuelled by coal gas.
1862	Alphonse Beau de Rochas	Patented but didn't build a four-stroke engine.
1864	Siegfried Marcus	Built a one-cylinder engine with a crude carburettor.
1866	Eugen Langen and Nikolaus August Otto	Improved on Lenoir's and de Rochas' designs and invented a more efficient gas engine.
1873	George Brayton	Developed a two-stroke kerosene engine that used two external cylinders and was considered the first safe and practical oil engine, but was unsuccessful.
1876	Nikolaus August Otto Sir Dougald Clerk	Invented and later patented a successful four-stroke engine, known as the "Otto cycle". Invented the first successful two-stroke engine.
1883	Edouard Delamare-Debouteville	Built a single-cylinder four-stroke engine that ran on stove gas.
1885	Gottlieb Daimler	Invented the prototype of the modern gas engine, with a vertical cylinder and with gasoline injected through the carburettor.
1886	Karl Benz	Received the first patent for a gas-fuelled car.
1889	Gottlieb Daimler	Built an improved four-stroke engine, with mushroom-shaped valves and two V-slant cylinders.
1890	Wilhelm Maybach	Built the first four-cylinder four-stroke engine.

ICEs are the most common form of heat engines, a device that transforms the chemical energy of a fuel into thermal energy, utilising this thermal energy to perform useful work. In ICEs, the thermal energy is converted to mechanical energy, and combustion takes place within the engine. The fuel and air mixture is then emitted as exhaust, commonly done using a piston, but many times with a turbine [33].

There are many different types of piston ICEs that can be classified according to different parameters, such as [34]:

- Application – Automobile, marine, aircraft, truck, locomotive, power generation, portable power system.
- Basic engine design – Reciprocating engines (in-line, V, radial, opposed), rotary engines (Wankel, etc.).
- Working cycle – Four-stroke cycle: naturally aspirated, supercharged, and turbocharged. Two-stroke cycle: crankcase scavenged, supercharged, and turbocharged.
- Valve or port design and location – Overhead (or I-head) valves, underhead (or L-head) valves, rotary valves, cross-scavenged porting, loop-scavenged porting, through- or uniflow-scavenged.
- Fuel – Gasoline, diesel, natural gas, liquid petroleum gas, alcohols (methanol, ethanol), hydrogen, dual fuel.
- Method of mixture preparation – Carburetion, fuel injection into the intake ports or intake manifold, fuel injection into the engine cylinder.
- Method of ignition – Spark-ignition (SI), compression-ignition (CI).
- Combustion chamber design – Open chamber (disc, wedge, hemisphere, bowl-in-piston), divided chamber (small and large auxiliary chambers). Many designs (swirl chambers, pre-chambers).
- Method of load control – Throttling of fuel and air flow together (mixture composition basically remains unchanged), control of fuel flow alone, or a combination of both.
- Method of cooling – Water cooled, air cooled, uncooled.

Commonly, ICEs are differentiated according to the method of ignition: SI engines and CI engines. Since they have much in common, a detailed comparison of the two is shown in Table 2.3.

Table 2.3. A comparison between SI and CI engines [33].

Description	*SI Engine*	*CI Engine*
Basic Cycle	Works on Otto cycle or constant volume heat addition cycle.	Works on Diesel cycle or constant pressure heat addition cycle.
Fuel	Gasoline, a highly volatile fuel. Self-ignition temperature is high.	Diesel oil, a non-volatile fuel. Self-ignition temperature is comparatively low.
Introduction of Fuel	A gaseous mixture of fuel-air is introduced during the suction stroke. A carburettor or an injection system, and an ignition system are necessary.	Fuel is injected into the combustion chamber at high pressure at the end of the compression stroke. A fuel pump and injector are necessary.
Load Control	The throttle controls the quantity of the fuel-air mixture introduced.	The quantity of fuel is regulated. Air quantity is not controlled.
Ignition	Requires an ignition system with a spark plug in the combustion chamber. Primary voltage is provided by either a battery or a magneto.	Self-ignition occurs due to the high temperature of air because of the high compression. An ignition system and spark plug are not necessary.
Compression Ratio	10 to 13. The upper limit is fixed by the antiknock quality of the fuel.	16 to 20. The upper limit is limited by the weight increase of the engine.
Speed	Due to their light weight and homogeneous combustion, they are high-speed engines.	Due to their heavy weight and heterogeneous combustion, they are low-speed engines.
Thermal Efficiency	Because of the lower compression ratio, the maximum value of TE that can be obtained is lower.	Because of the higher compression ratio, the maximum value of TE that can be obtained is higher.
Weight	Lighter due to lower peak pressures.	Heavier due to higher peak pressures.

2.2.1.1 Diesel engine

The genesis of the more efficient ICE can be linked to an inspiring lecture. As a student, Rudolf Diesel was intrigued when his professor, Carl Linde (a German scientist), explained Carnot's theorem and the low efficiency of existing engines, pointing out that an engine working under isothermal conditions would convert all heat into work. Because at the time, and in practical terms, this statement was not considered possible, Diesel set himself to the task of realising the ideal Carnot cycle, after writing the statement in the margin of his college notebook. This wish ended up dominating his existence. After beginning his work on the project in 1890, Diesel eventually found it impossible to construct this nearly isothermal (constant temperature) engine,

having to settle for a design with combustion under constant pressure, which still produced an engine of unprecedented efficiency, ruggedness, and reliability [35].

The SI engine, following the Otto cycle, had some inconveniences and limitations, resulting in lower TE. The need for a special quality fuel (vaporisable), being limited to a maximum value of compression ratio, and the existence of tight limits for air-fuel mixing, led Diesel to conceive a cycle in which its practical application can solve these limitations, despite bringing some other disadvantages. The components of the CI (diesel) engine are very similar to the common Otto engine (gasoline), although it works under different operating principles [36]. An example of the cross section of a turbocharged four-stroke direct-injection CI engine and its components can be found in Figure 2.2. Older and less efficient indirect-injection diesel engines are also composed of a swirl chamber (precombustion chamber), located at the engine's head, where the fuel is injected and rapidly mixed with air, leading to autoignition and combustion that then spreads into the cylinder beneath it, acting on the piston [37].

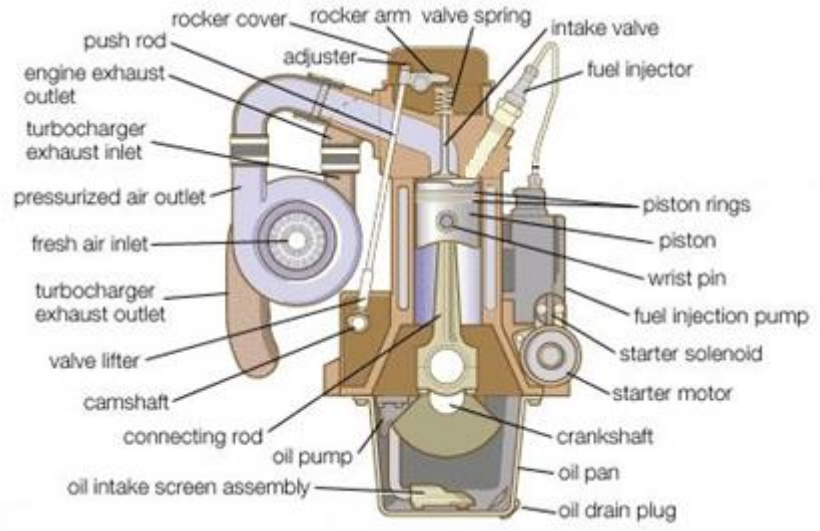

Figure 2.2. Direct-injection diesel engine components (adapted from [38]).

The four-stroke CI engine is similar to the four-stroke SI engine. The operating cycle is the same, only differing in the ignition method. However, it operates at a much higher compression ratio (16 to 20), almost double the ratio of SI engines. An ideal four-stroke cycle of a diesel engine can be observed in Figure 2.3.

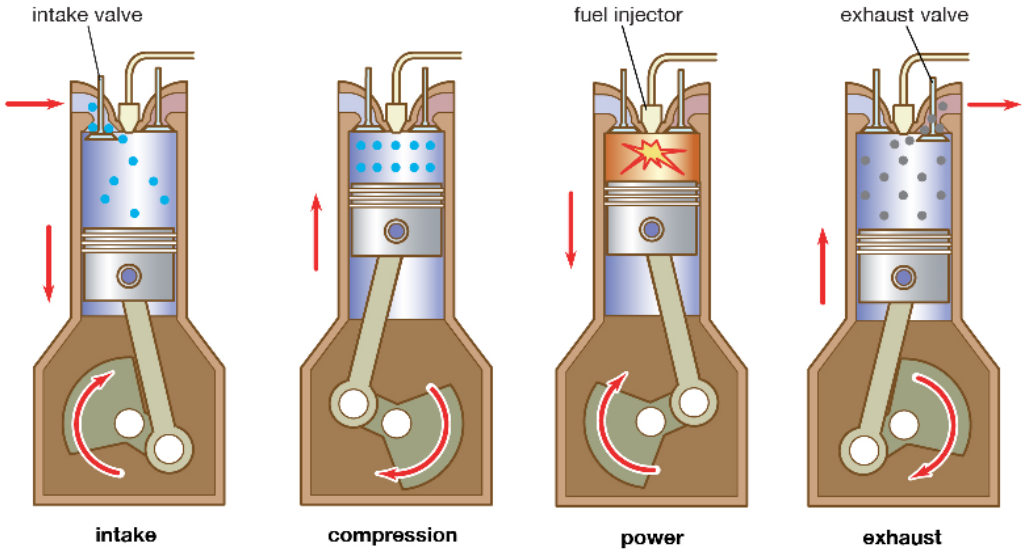

Figure 2.3. The four-strokes of a direct-injection diesel engine [38].

A detailed description of what happens in each stroke of the cycle is given next [36]:

- Intake stroke – Starts with the piston at top dead centre (TDC) and ends with the piston at bottom dead centre. The intake valve is open, drawing fresh air into the cylinder.
- Compression stroke – With both valves closed, the piston moves to TDC, compressing the fresh air in the cylinder.
- Explosion-expansion (power) stroke – Starts with the piston at TDC or before. The fuel is injected into the hot air, spontaneously igniting when in contact with it. The injection (and combustion) continues during the piston descent such that the pressure does not exceed a limiting value, corresponding to this engine stroke.
- Exhaust stroke – With the piston in TDC, the exhaust valve opens, allowing burnt gases to be released into the atmosphere through the exhaust system during the piston ascent.

As said before, the main difference between Diesel and Otto cycles lies in the heat-supplying phase. In the Diesel cycle, it is supplied at constant pressure. The P-V and T-S diagrams for the ideal cycle are represented in Figure 2.4.

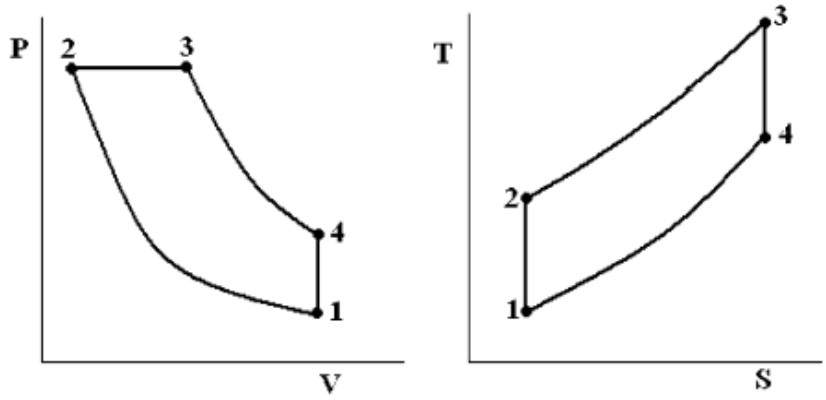

Figure 2.4. P-V and T-S diagram for the ideal diesel cycle [39].

The different stages of the cycle represented in the diagram are explained next [36]:

- From 1 to 2, isentropic compression occurs. The air is compressed and the work is supplied to increase the internal energy (area below the 1-2 line of the P-V diagram).
- From 2 to 3, isobaric heat addition occurs. The fuel is injected and burned while the volume increases (not instantaneous combustion).
- From 3 to 4, isentropic expansion occurs. The fluid is expanded, doing work due to its internal energy (area of the polygon in the P-V diagram).
- From 4 to 1, isochoric heat rejection occurs, completing the cycle.

However, this analysis uses an ideal "air-standard" assumption, where air is the working fluid that behaves as an ideal gas, all the processes are internally reversible, the heat addition process replaces the combustion process, and the heat rejection process replaces the exhaust process by returning the working fluid to its original state [37]. The ideal gas law is given by:

$$P_{gas}\mathrm{V} = \mathrm{nRT}, \tag{2.1}$$

where P_{gas} is the pressure of the gas (Pa), V is the volume (m^3), n is the number of mols (mol), R is the ideal gas constant (m^3Pa/molK), and T is the temperature (K).

Because ICEs operate on a real cycle, and not on an ideal cycle [37], a more realistic PV phase diagram is significantly different from an ideal one (due to the existence of friction and heat losses), as shown in Figure 2.5.

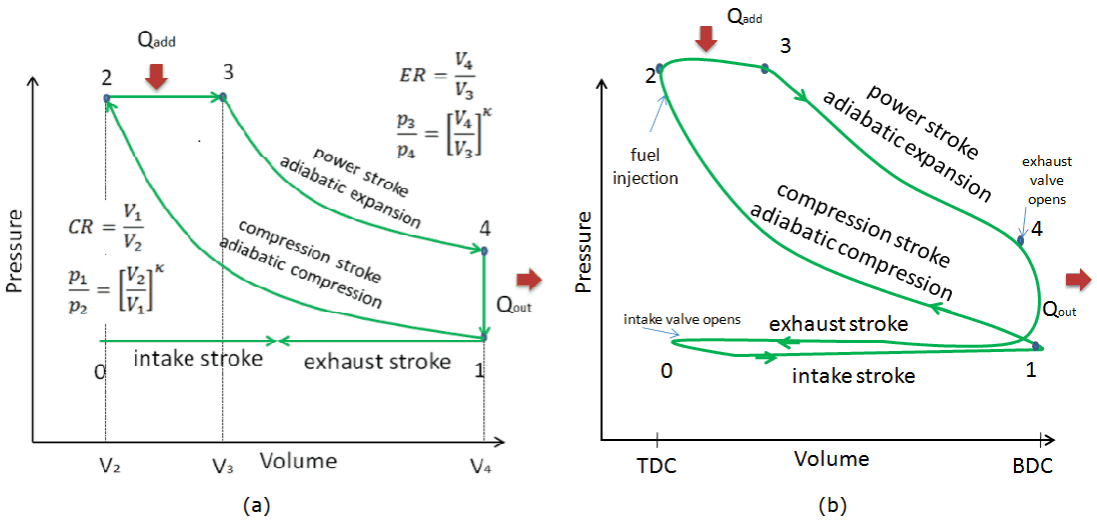

Figure 2.5. (a) Ideal and (b) real diesel engine cycle [40].

For aviation, four-stroke engines are preferred and more advantageous than two-stroke engines. Two-stroke SI engines have less efficiency, and fresh mixture losses through the exhaust are inevitable. Despite its mechanical simplicity, the mutual dependence on the same operations, causing less efficiency, disproportionate emissions, and the lack of proper lubrication and cooling, makes the use of two-stroke SI engines on aircraft much more restricted [31], [41]. Currently, two-stroke CI engines are also rarely used in aviation due to the need for robust components to achieve higher compression ratios, as well as the same lubrication and cooling challenges, increasing their total weight and making them less favourable.

The first successful flight, performed by the Wright Brothers, Wilbur and Orville, dates December 17th of 1903, after inventing their first powered aircraft with SI combustion mechanisms. A few years later, in the 1920s and 1930s, diesel engines have been considered, tested, and used in aircraft. Junkers Jumo was the most famous, and for a lot of time, the only successful 2-stroke aviation diesel powerplant. Despite their sporadic interest in the post-war period, they were not widely adopted beyond this. One of the major objections to diesel-powered aircraft was the heavier weight of a diesel engine when compared to the other options, which would lead to lower power-to-weight ratios, a very important parameter when designing an aircraft. Fuels like diesel also have higher freezing points, and the solidification of paraffin in very cold weather could eventually block the fuel lines [42], [43]. Since the fuel to be used in piston aircraft rarely experiences the lower temperatures commonly found at higher altitudes by turbine-powered aircraft, additives and proper heating can overcome this concern [44]. At these extremely low temperatures, and because diesels are CI engines (where ignition is obtained without the use of spark plugs), they can also be difficult to cold start. Another reason is the violent torque pulses commonly encountered in diesel non-homogeneous combustion. The uneven torque distribution causes vibrations that eventually fatigue the propeller, reducing its lifespan and increasing the risk of failure. The propeller design must be carefully matched to the type of engine.

Today, and with all the technological advances, it is possible to design light diesel engines feasible enough to be used in piston aircraft. The advantages of utilising a diesel-powered airplane can also possibly outweigh the negative aspects previously listed. Some of the benefits include [45]:

- Running on fuels with higher energy density allows a longer flight range.
- Simpler technology (no ignition system, carburettors, or reduction gear needed), leading to easier maintenance, higher reliability, and longer lifespan.
- Better efficiency, allowing up to 30% reduced fuel consumption.
- High torques in take-off and at low propeller speeds.
- Fuels with high flash points and therefore safer in case of an accident.
- Fuels act as a lubricant for the engine components.
- Wide availability of diesel fuel and less expensive than avgas, especially in Europe.

Figures 2.6 to 2.8 show an example of different diesel aviation power plants and how they differ from the other types in terms of power, weight, and fuel consumption.

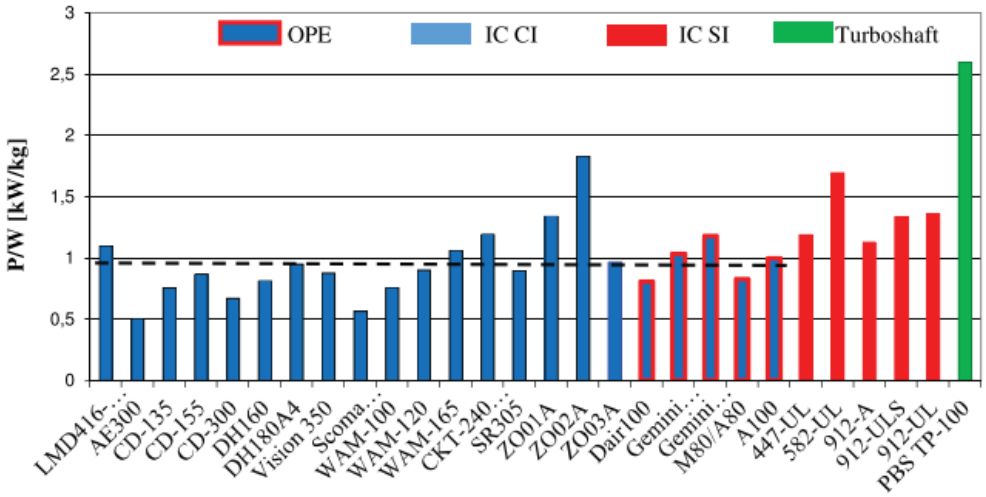

Figure 2.6. Power-to-weight ratio of some aircraft engines [46].

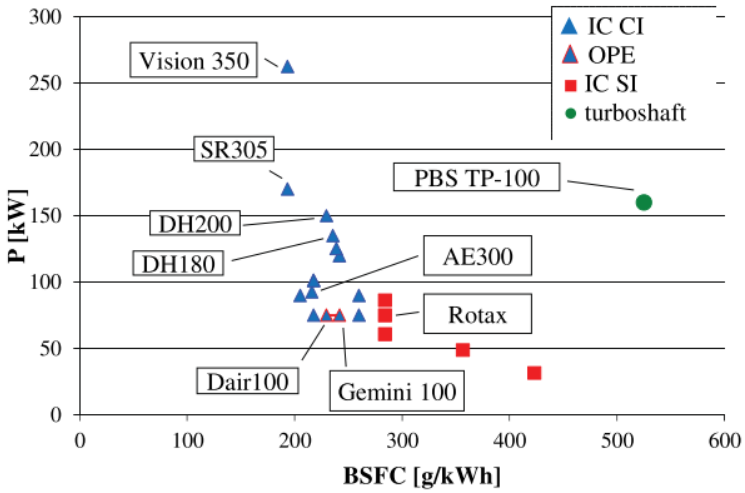

Figure 2.7. Power vs BSFC of some aircraft engines [46].

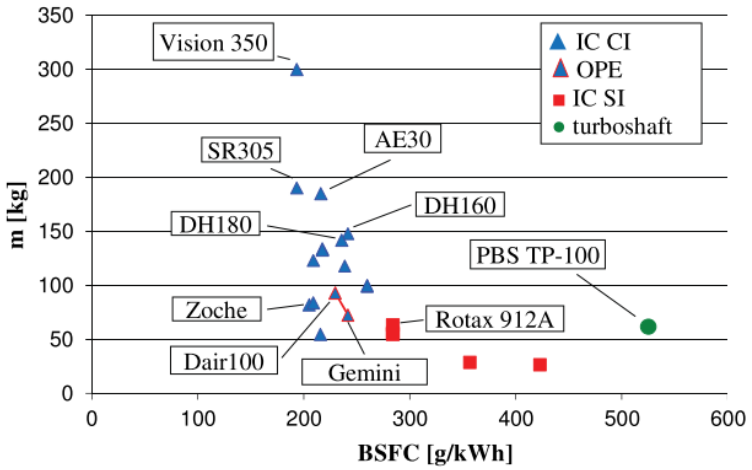

Figure 2.8. Weight vs BSFC of some aircraft engines [46].

So as can be seen, and even though gasoline engines running on avgas are much more common in general aviation applications, having a proved track record of reliability and performance for over a century, while still being optimised throughout the years, it has reached a point where further optimisation in its technology is very hard to be accomplished, and if the goal is to reach better efficiency levels, the next step could be a transition to diesel engines, which are becoming increasingly popular for use in light aircraft and UAVs, in an effort to reduce operating costs, simplify design, and improve reliability. For these reasons, several engine manufacturers are turning to CI engines as a viable alternative [41].

2.2.1.1.1 Combustion characteristics

Combustion can be described as a chain of chemical reactions in which certain elements of a fuel (often hydrogen and carbon) combine with O_2, releasing heat energy and causing an increase in the temperature and pressure of the gases. This energy can be converted, via a heat engine, into useful work [33].

The combustion in a diesel engine is quite different from that in a SI engine. It is an unsteady process occurring simultaneously at many regions in a very non-homogeneous mixture, where its rate is controlled by fuel injection. Because of the non-homogeneous mixture, more air needs to enter the cylinder, and the overall air-fuel ratio (AFR) on which CI engines operate is quite lean ($\Phi < 1$). The amount of fuel injected per cycle determines the engine torque and power output. The higher compression ratios of CI engines (where only the unthrottled air is contained in the cylinder during the compression stroke) allow higher thermal efficiencies and therefore, better fuel economy. Near the end of the compression stroke, the injector injects fuel at high pressures, allowing a high injection velocity and assuring a good atomization [37], [47].

After the fuel injection phase, a series of events ensures the proper combustion process of the fuel [47]:

- Atomisation – Fuel drops break into very small droplets. The high velocity fuel jet from the injector that breaks up into droplets leads to a quicker and more efficient atomisation process.
- Vaporisation – Due to the hot air temperatures (created by the high compression ratios), the smaller droplets of liquid fuel evaporate to vapour. Within 0.001 seconds, about 90% of the fuel injected has been vaporised.
- Mixing – After vaporisation, and due to the high fuel injection velocity added to the swirl and turbulence in the cylinder, the fuel vapour mixes with the air forming a combustible mixture, within the AFR for combustion.
- Self-Ignition – Subsequently, the air-fuel mixture starts to self-ignite. The combustion is proceeded by secondary reactions and the breakdown of large HC molecules into smaller species and some oxidation.
- Combustion – Starts from simultaneous self-ignition at many locations in the slightly rich spot of the fuel jet. Multiple flame fronts spreading from the different self-ignition locations quickly consume all the gas mixture, even when self-ignition would not occur. The temperature and pressure within the cylinder rise, reducing the vaporisation and ignition delay time for additional fuel particles, causing more ignition points to further increase the combustion process. Fuel injection is still occurring after the first fuel is already burning. After the air-fuel mixture is consumed, the rest of the combustion process is controlled by the rate at which fuel can be injected, vaporised, and mixed in the correct AFR. The burning rate increases with engine speed. Figure 2.9 represents the variation of cylinder pressure as a function of the crank angle, from the start to the end of the fuel injection process.

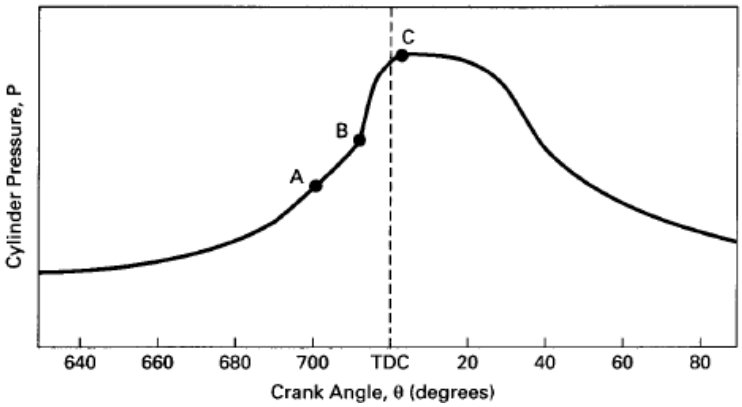

Figure 2.9. Pressure diagram for a CI engine [47].

Fuel injection starts at point A. When the air-fuel mixture is in a combustible AFR and the temperature is hot enough for self-ignition, the ignition delay (from A to B) will be in the range of 0.4 to 3 milliseconds. This time can be shortened by increases in temperature, pressure, engine speed, and/or compression ratio. Point C represents the end of fuel injection. To measure the ignition delay, the cetane number is used. Cetane influences cold startability. A low cetane number will lead to a longer ignition delay, and a more-than-desirable amount of fuel will be

injected before the combustion starts. A high cetane number will lead to an early combustion (before TDC), resulting in a loss of engine power [47].

2.3 Fuels

A fuel can be defined as any material that can react with other substances, by burning, releasing energy in a controlled manner in the form of heat and/or work [48]. The energy released can be converted into mechanical energy via a heat engine. Fuels can be found as solids, liquids, or gases, and their most common form is HC (hydrophobic organic compounds consisting entirely of hydrogen and carbon). By carrying out some processing steps on a fuel before it is burned, it is possible to improve its performance during combustion and to mitigate potential environmental problems resulting from its consumption [48], [49].

Fossil fuels (coal, petroleum, natural gas, oil shales, bitumens, tar sands, and heavy oils) represent fossilised biomass, which stores carbon out of the natural carbon cycle in sediments for a very long time [48]. They were formed as a result of geologic processes acting on the remains of organic matter produced by photosynthesis, which release energy in combustion, many years ago (2.5 billion to 4 billion). Most of the fossil fuel material we use today comes from algae, bacteria, and plants from more than 250 million years ago [50]. An illustration of the process can be seen in Figure 2.10.

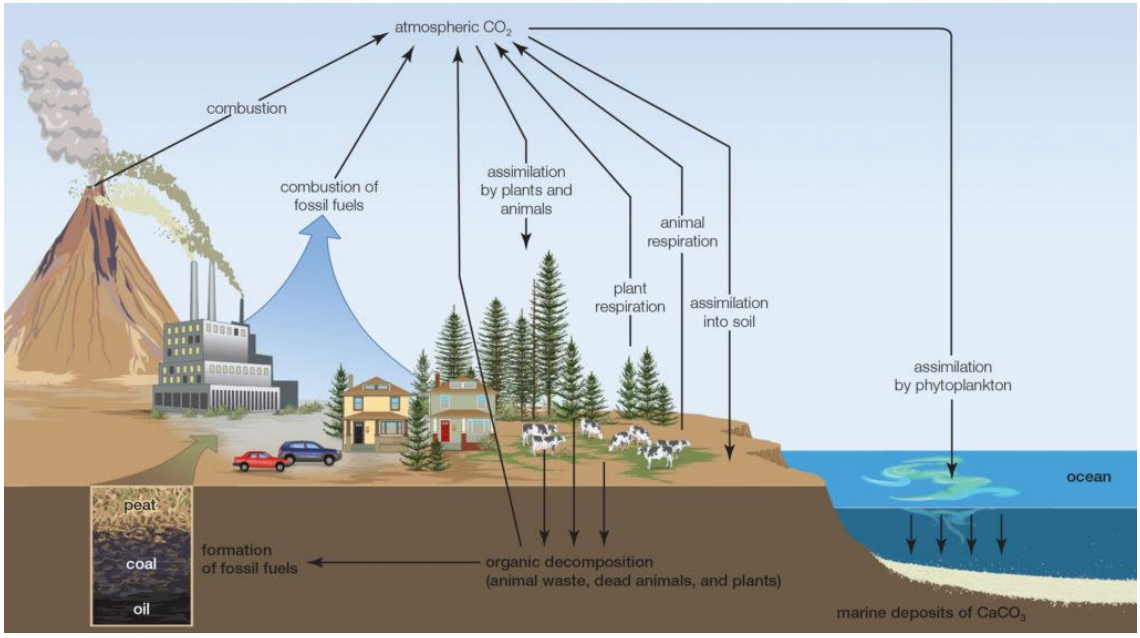

Figure 2.10. Formation and use of fossil fuels [50].

2.3.1 Aeronautical fuels

Fuel for aircraft is usually divided into two different categories, considering the engine type (gas turbines or piston engines) and application (civil, military, or general aviation). While piston engine aircraft usually run on avgas, turbine engines use jet fuel as an energy source. Although not very common, some aircraft equipped with diesel engines can also run on diesel fuel, with jet

fuel being the main preference [41]. Specifications of the different aviation fuels and their variations are shown in the next subsection.

2.3.1.1 Different types and compositions

Today, avgas is mainly used by light aircraft and piston engine helicopters, although a significant number of military and civil transports powered by large piston engines also utilise avgas. The most common and used grades of avgas today are [12], [51], [52]:

- Avgas 100 – This high lead content grade, dyed green, was the standard high-octane fuel for aviation piston engines. Today, it has low market demand and is only produced in very few locations in the world.
- Avgas 100LL – This is the main grade of avgas used worldwide. This grade, dyed blue, is the lower lead version of avgas 100, even though it still carries up to 0.56 g/L of lead. avgas 100VLL is the very low lead version of avgas 100LL with a maximum lead concentration of 0.45 g/L. In similarity to the other grades of avgas, it has a freezing point of -58°C and a flash point lower than -40°C, which makes this fuel an extremely flammable liquid.
- Avgas UL91 and UL94 – Avgas UL91 is similar to avgas 100LL but with zero-lead content, resulting in a lower octane rating. Avgas UL94 includes some more exotic high-octane HC, improving the octane rating. Both are undyed grades and cleaner for the environment in the general aviation network.

For jet fuel, it can be divided according to different purposes. The main jet fuel grades for civil use are [12], [51], [52]:

- Jet A-1 – This kerosene grade of fuel is suitable for most turbine-engine aircraft. It has a flash point minimum of 38°C and a freeze point maximum of -47°C. It is widely used and available outside the U.S.A.
- Jet A – This grade of fuel is similar to jet A-1. It has the same flash point, a higher freeze point maximum (-40°C), and is normally only available in the U.S.A, used by domestic and international airlines.
- Jet B – This grade of fuel can be used as an alternative to jet A-1. The higher flammability makes it more difficult to handle, leading to minimal demand and availability for this grade of fuel. It is desired for use in very cold climates, where better cold weather performance is preferred.
- TS-1 – This is the main grade available in Russia and the Commonwealth of Independent States. This grade has a slightly higher volatility (flash point of 28°C minimum) and a lower freeze point (less than -50°C) compared to jet A-1.

Jet fuels for military use basically offer similar properties. The main difference is attributed to the lower freezing points, because of the higher altitudes where military aircraft fly. The main jet fuel grades for military use are [51]:

- JP-4 – This grade is the military equivalent of jet B with the addition of some additives. This was the primary jet fuel for the US Air Force. It was phased out in the 1990s because of safety concerns. Despite its very low production, a few air forces around the world still use it.
- JP-5 – This grade has a high flash point and is the primary jet fuel for use in aircraft carriers.
- JP-8 – This grade is the military equivalent of Jet A-1 with the addition of some additives. It is the dominant military jet fuel grade for NATO air forces.

Diesel fuel for aircraft is not very commonly used, but when it is, it needs to follow special specifications and certifications to ensure maximum safety during flight [41]. Fuel specifications are set on a more local level, varying significantly in content. In Europe, EN590 is a standard describing the physical properties that all automotive diesel fuel must meet to be sold in European countries. It allows up to 7% blending of Fatty Acid Methyl Esters (FAME) (biodiesel) with diesel [53].

The absence of diesel fuel in aircraft can be explained by the variable content and quality of diesel fuel over the globe; the blending of FAME in diesel can present risks to low-temperature properties and affect fuel stability, and, at low temperatures, the risk of freezing or form wax crystals blocking filters and stalling engines [54], [55], [44]. Diesel fuel has a flash point of 55°C, and a Cold Filter Plugging Point (CFPP) of -10°C in winter. The main grade of certified diesel fuel for use in aircraft, and that some companies manufacturing diesel engines for aviation (Continental, Lycoming, TAE, SMA) are certified to run is Diesel EN590 [41]. For small aircraft and UAVs, heavy fuels like diesel provide some benefits due to their higher density, higher flash point, and enhanced safety during storage and transportation [56].

From a chemical and physical perspective on the properties of the different liquid fossil fuels, avgas (gasoline) is the lighter fuel, formed from the C_6 to C_{10} chains, jet fuel (kerosene) is derived from much heavier chains, in the C_8 to C_{16} range, and diesel even heavier [12]. An example of how crude oil is treated and how each treatment contributes to the formation of the different aeronautical fuels can be seen in Figure 2.11, illustrating a modern refinery. Generally, four major stages of refining to separate crude oil into usable substances can be defined [57]:

- Physical separation of the different types of HC through distillation.
- Purification of intermediate products in pre-treatment facilities.
- Chemical processing of lower value fractions into lighter products.

- Treatment and mixing of intermediates by removing undesirable elements for integration into final products.

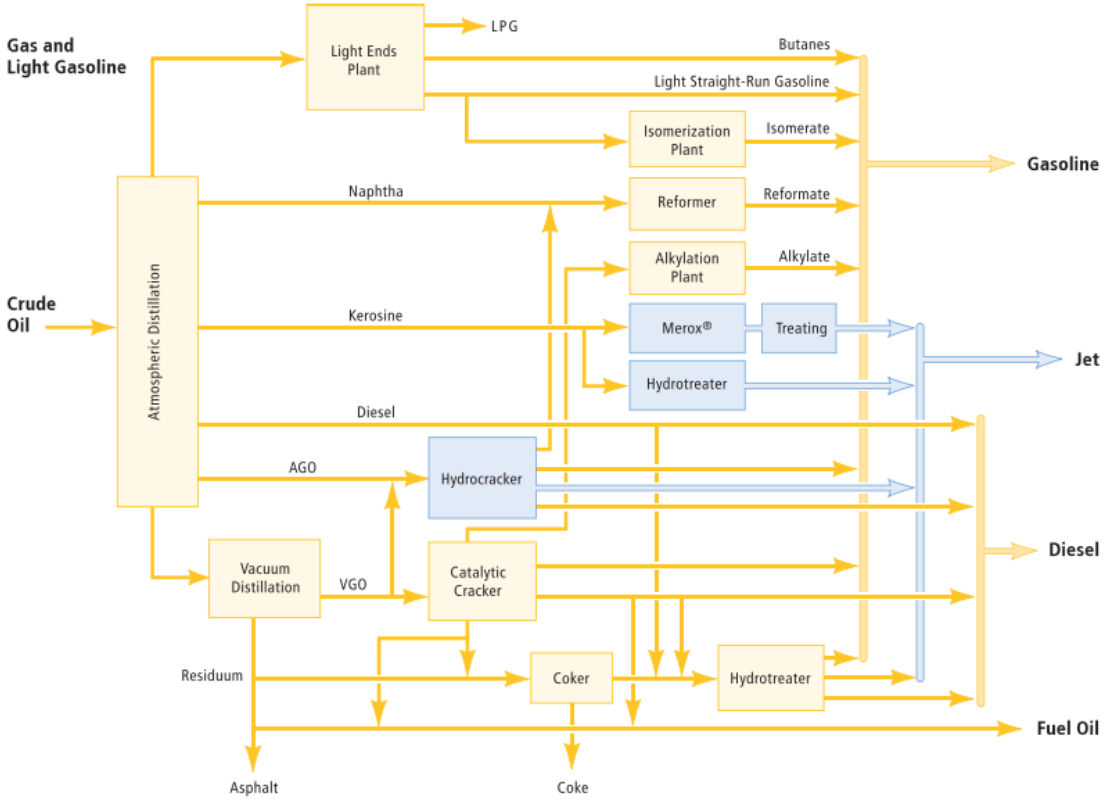

Figure 2.11. The modern refinery [12].

After crude oil is fed to the distillation column, gasoline, kerosene, and diesel are separated at atmospheric pressure, as shown in Figure 2.12. Jet fuel can be viewed as a highly refined kerosene, processed at a higher temperature to remove more of the volatile compounds. It is the middle distillate (with a hydrocarbon length between that of gasoline and diesel), making up to 10% of the crude oil fraction [58].

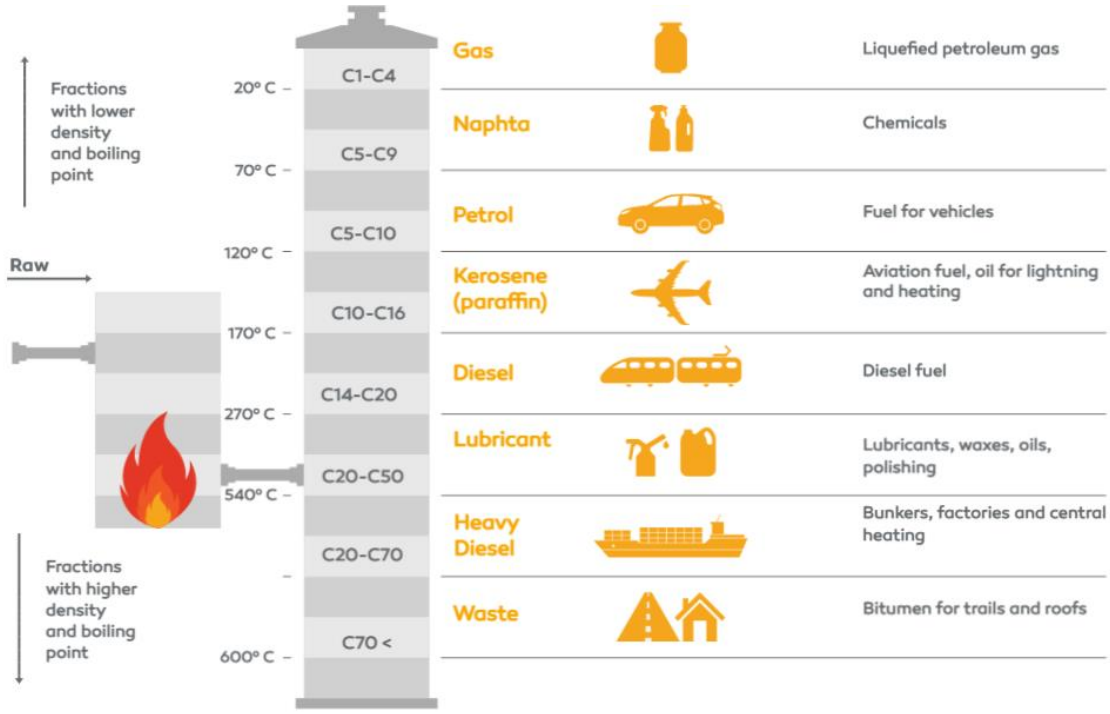

Figure 2.12. Distillation column [57].

This process, known as fractional distillation, starts with the heating of crude oil. The vapour formed rises through a fractionation column with compartments of different heights. The most volatile components rise to the top of this column. The highest boiling point components remain in the lower layers. This is the starting point of the petroleum refining process [57].

As seen, the fuel utilised in aeronautical applications is obtained by this process, and for each application, a different type of fuel is selected. Table 2.4 represents the different properties of some fuels used in aviation.

Table 2.4. Basic physical and chemical properties of different aeronautical fuels [12], [59], [60], [61], [62], [63].

Fuel	*Diesel (EN590)*	*Jet Fuel (Jet-A1)*	*Avgas (100LL)*
Typical Density [g/cm³] at 15°C	820-845	775-840	715
Specific Energy [MJ/kg]	42.7	43.28	43.71
Energy Density [MJ/L]	35.7	35.06	31
Viscosity [mm²/s] at 40°C	2-4.5	1.4	0.5-0.75
Flash Point [°C]	55	38	-58
Freezing Point [°C]	-10 (winter)	-47	-40

Fuels differ in density, and therefore, in energy content per unit volume. More dense fuels, such as diesel, have a higher energy content per unit volume. For aircraft, a high volumetric energy content fuel provides the longest flight range. On the other hand, a fuel with a higher gravimetric energy content (specific energy, or heating value (HV)) will allow more passengers and cargo on the same given route [64]. Higher flash point fuels are usually safer to operate (less volatile) and

more suited for storage conditions (stable for longer periods of time). Lower freezing point fuels offer better cold weather performance and the ability to be used in extreme conditions.

2.3.1.2 Safety precautions

Fuels for aviation need to respect certain properties and measures: on-board, arising from the environmental conditions existing at higher altitudes, and in-land, in the handling services. Basic requirements that an aviation fuel must fulfill are high energy contents (to make up for flight's relatively long distances) and that they must not be too volatile (which is the case of high energy HC), to make sure the fuel will not evaporate and form the ignitable vapour needed for combustion, decreasing the chances of fire during plane crashes. Fuels with higher flash points are a safer choice because they do not vaporise quite so easily.

Another of the main parameters for making sure a certain fuel is safe and operational to use on-flight is its freezing point. Lowering the temperature of the fuel will cause it to reach its cloud point (wax starts to form a cloudy appearance). Lowering this temperature even more will lead to the fuel's pour point (the lowest temperature at which fuel continues to flow). If the temperature is low enough, the whole fuel will crystallise and solidify, changing its state of matter and reaching its freezing point. At very low temperatures, aviation fuels can develop solid hydrocarbon crystals, impeding fuel flow, which can have catastrophic effects on aircraft, such as interfering with the atomisation of the fuel. Frozen fuel can clog up the fuel lines, decrease the engine output, or even let the engine flame out, leading to incidents and possibly a crash. For this reason, aviation fuels must retain their fluidity at low temperatures to properly flow from the storage tanks in the wings to the engine, while also lubricating some engine parts. Another aspect that can influence the performance of fuels is the presence of water as a separate liquid phase, or "free water". This is dangerous because although it is inevitable to have very low percentages of dissolved water (which isn't harmful), fuel contaminated with free water can also lead to its freezing (water freezing point of 0^{o}C), putting safety at risk. Aviation fuels also need to be non-corrosive and must not react with the material used to make the storage tanks. In addition to their primary function as a source of energy, they are used to absorb excess heat, and as a hydraulic operating fluid in engine control systems, serving as a lubricant for the engine control systems and pumps [64].

When it comes to handling aviation fuels, it can be hazardous if not done properly. They are easy to ignite and burn rapidly (jet fuel) and explosively (avgas). Exposure to liquid or vapour can be unhealthy and should be limited. It is also important to keep in mind that only the vapour burns (not always), the liquid does not [12].

2.3.2 Alternative fuels

As previously seen, petroleum products have always been the main choice for transportation fuels because they offer the best combination of energy content, performance, availability, ease of handling, and price [64]. However, due to the scarce petroleum resources, deteriorating global environment, and energy management issues, the development and application of Sustainable

Aviation Fuels (SAF) have received particular attention from people in the aviation industry over the past years [65]. Recently, biofuel was used in aviation in 2008, blended with conventional jet fuel [66]. Currently, blends up to 50% of certified SAF with kerosene are allowed to be used in commercial flights. In march 2021 (A350), October 2021 (A319neo), and march 2022 (A380), Airbus have performed different and successful flight tests powered by 100% SAF [67], [68]. Despite its known advantages, the current consumption of SAF is very low compared to the overall aviation fuel consumption [69]. In Europe, it only represented 0.05% of aviation fuel consumption in 2017 and nearly 1% in 2018 [66]. Worldwide, it only corresponded to 0.004% of total jet fuel used by commercial operators in 2017 [70].

More recently, hydrogen is also being considered to be used in turbine commercial aircraft [71]. The advantages are linked to the fact that it is one of the most abundant elements in the world, and does not emit CO_2 into the atmosphere, only water and NO_x due to the high temperatures registered in the combustion chamber [72], [73] (AFR of 34:1, which requires more O_2 availability to burn the same mass of fuel compared to other fuel sources). The disadvantages are linked to the fact that currently, only a small fraction of hydrogen (~4%) is obtained from renewable sources (the so-called green hydrogen), and around 96% is obtained from natural gas (blue and grey hydrogen), composed essentially of CH_4 [74]. Not only that, extremely low temperatures (- 253ºC boiling point at atmospheric pressure) and very high pressures are needed to maintain it in a liquid form to be stored in heavy engine tanks, which increases vehicle mass and the risk of explosion. Transport and handling are also not very easy, since long and special pipelines are needed [75].

Today, a variety of cleaner and alternative fuels are being developed, targeting the reduction of emissions and pollution from the exhaust gases of engines. Some of the advantages of using alternative fuels are linked to [76]:

- The reduction of GHGs, especially CO_2, and the reduction of atmospheric pollution (sulphur oxides, NO_x, and CO). Explained by the cleaner and more efficient burning of biofuels when compared to petroleum products.
- Increased energy security. More energy sources lead to market stability, reducing the risk of scarcity.
- A more developed bioenergy industry (generating more jobs).
- A decreased dependence on oil, a limited natural resource.

It is, however, important to note that, similarly to aeronautical fuels, alternative fuels to be used in aviation must be compatible with existing fuel systems, storage conditions, and fuel transfer processes [77]. For SAF, high heat content, good atomisation, rapid evaporation, good burning characteristics, low explosion risk, being free from contaminants, minimum carbon formation, low viscosity, good thermal stability, and good storage should be obtained. Only after passing laboratory, storage, and flight tests for operational purposes of the regulating entities, aviation

fuels can be certified for use [77], [78]. Fuels to be used in diesel engines should also have a short ignition delay, be sufficiently volatile, allow good starting characteristics, not have a very high viscosity, and possess high flash and fire points [33].

2.3.2.1 Different types and compositions

According to some literature review, alternative fuels to be used in aviation can be from fossil sources, the Fischer-Tropsch (F-T) process, cryogenic fuels, or bio-derived fuels [64]. Fossil fuels from fossil sources generally consist of replacing petroleum (or crude oil, where most of the fuels are manufactured) with other sources (natural gas, shale oil, and coal) [64], [79].

The F-T synthesis was developed in Germany during World War II [64], and it is a conversion technology that was developed with the goal of converting any carbon-based material into an oil product that can be refined into conventional transportation fuels and petrochemical products. In order to make use of biomass as feed material and produce aviation fuels as products, the technology has to follow three process steps: conversion of biomass to synthesis gas, conversion of synthesis gas to oil, and oil refining to aviation fuels [80].

Cryogenic fuels are gases at normal ambient conditions that require storage at extremely low temperatures to maintain them in a liquid state [64]. These fuels are used in machinery that operates in space (rocket ships and satellites) where ordinary fuel cannot be used, due to the very cold temperatures often encountered in space and the absence of an environment that supports combustion. For that reason, liquid hydrogen is one of the fuels used in space exploration [81]. Another example of a cryogenic fuel is liquified natural gas (LNG), widely used for heating, generating electricity, and sometimes even as a transportation fuel for vehicles (not to confuse with liquified petroleum gas, composed mainly of propane and butane, as opposed to the lighter CH_4 and ethane existing in LNG).

Biofuels represent the main branch of all the alternative and sustainable fuels to be used in transportation, and they can be divided into different categories based on the production methods, as shown in Figure 2.13.

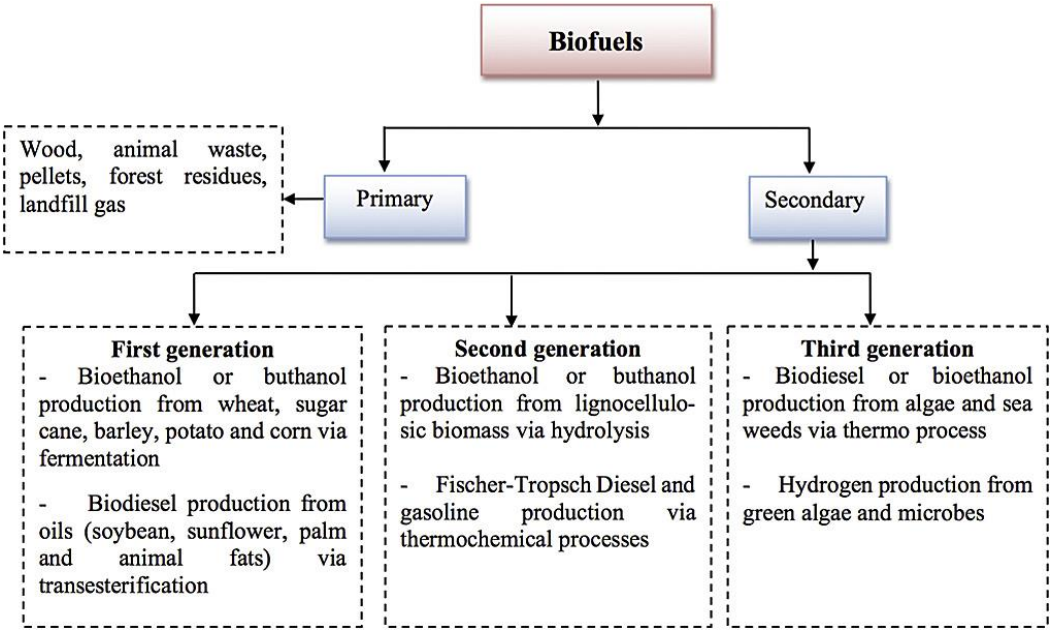

Figure 2.13. Biofuels based on production methods [78].

Biofuels can be produced from organic matter such as crops, agricultural waste, and even sewage. Unlike fossil fuels (created from ancient organic matter that has been buried for millions of years), biofuels are made from living organisms that have recently absorbed CO_2 from the atmosphere by photosynthesis. Therefore, when biofuels are burned, the CO_2 is released back into the atmosphere, which is balanced out by the fact that the biomass used to make the biofuels absorbed an equivalent amount of CO_2 during their growth. For that reason, they are also usually called carbon-neutral fuels, since the net amount of CO_2 released into the atmosphere from their burning is zero [82], [83]. However, it is important to note that the production of biofuels can still have negative environmental impacts, especially when it involves the destruction of forests or other natural habitats, or if it requires large amounts of energy and water to produce. An example of the carbon cycle for fossil and biofuels is shown in Figure 2.14.

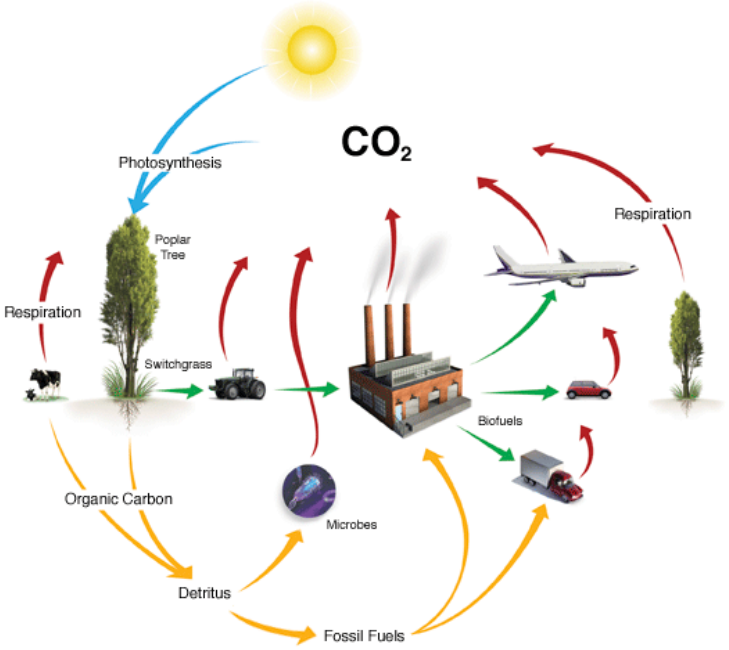

Figure 2.14. Carbon cycle [84].

For ICEs, and specifically CI engines, the most popular alternative is biodiesel. Just like other biofuels, and because they are produced from the same raw materials, they have similar fuel properties and characteristics. It is one of the most used fuels in road transportation, mainly mixed with diesel [85]. For instance, in diesel engines, ethanol or butanol can be added to diesel fuel/biodiesel blends. In addition, diesel/butanol blends have shown similar engine characteristics and emissions as diesel/biodiesel blends in diesel engines. Therefore, those fuels can be seen and used in the same engine in the form of various combinations of blends [78].

Biodiesel (also known as FAME) is a liquid fuel, and a relatively complex mixture of esters of fatty acids with short molecular chain alcohol, created by chemically processing vegetable oil (by esterification or transesterification), and by altering its properties to match the performance of petroleum diesel [85]. When compared to diesel, biodiesel presents higher density (870-895 kg/m^3 at 15ºC), viscosity (3.5-5.5 mm^2/s at 40ºC), higher cetane number (45-65) and a lower heating value (LHV) (36.5-38 MJ/Kg) [65], [86]. Its main advantage lies in the reduction of emissions, even though compensated by a lower engine performance (because of its lower LHV). However, the shorter ignition delay or the higher density and viscosity led some authors to report an increase in power and torque for engines running on biodiesel or biodiesel blends [87].

An arguably better alternative process to esterification to produce diesel from biomass (biodiesel) is hydrotreating. Hydrotreated vegetable oils (HVO), or hydroprocessed esters and fatty acids, are commonly referred to as renewable diesel or green diesel. They are one of the main contributors to SAF. In this process, hydrogenation is used to remove the O_2 from the vegetable oils, resulting in the absence of glycerol as a side product (as opposed to esterification). One of the main advantages of HVO is the better cold properties with a lower CFPP that can be adjusted to meet the local requirements, by adjusting the severity of the process or by additional catalytic

processing [88]. This characteristic is important because it also enables the production of renewable jet fuel, which has been approved for use in jet fuel blends of up to 50% [89]. Figure 2.15 shows a comparison between renewable diesel and biodiesel processes and CO_2 emissions with both fuels originating from the same feedstock.

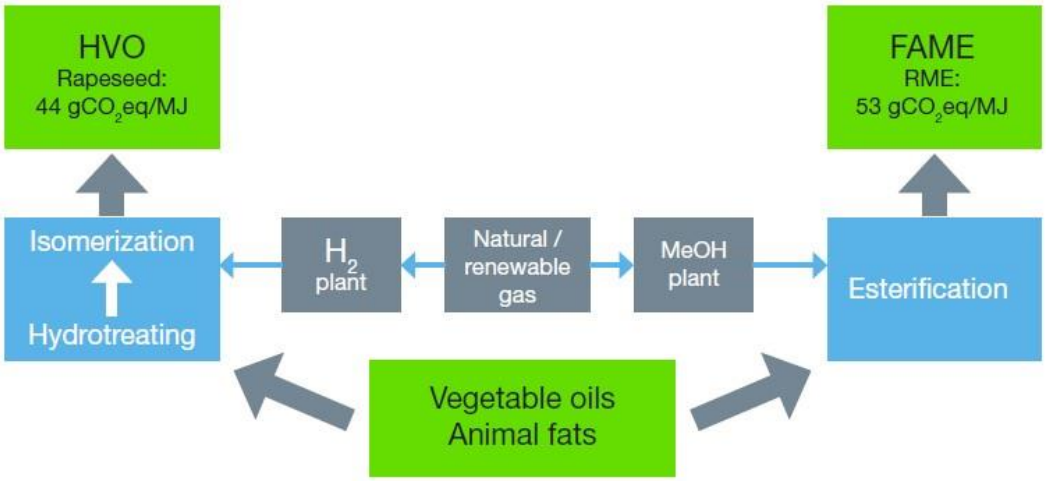

Figure 2.15. Differences in the production processes of renewable diesel and biodiesel [88].

HVO is a paraffinic diesel fuel, free from sulfur, O_2, and aromatic HC, which covers the HVO and F-T GTL (gas-to-liquid) fuel products up to 7% (v/m) of FAME. High blending ratios of HVO meet the diesel fuel standards, such as EN590 and ASTM D975. The chemical properties are similar to the fossil-based diesel, despite having a lower density, lower energy content, and a higher cetane number. The storage stability is also improved [90]. One of the main drawbacks regarding the adoption of HVO as a sustainable fuel is related to its increased production price due to the high cost of bio-based feedstocks, the complexity of its production process, and the infrastructure needed [91].

Table 2.5 represents information regarding some different types of biofuels for aviation [91].

Table 2.5. Biofuels for aviation.

Type of Biofuel	Production Process	Benefits	Challenges	Technological Aspects
Hydrotreated Vegetable Oils	Hydroprocessing of vegetable oils or animal fats.	Direct drop-in replacement; up to 80% reduction in lifecycle GHGs emissions; no sulfur content; reduced	Higher production costs; economic viability depends on policy support and technological advancements.	Improving yield and cold flow properties; exploring a wider variety of feedstocks.

		particulate emissions.		
Synthetic Iso-Paraffin	F-T process or hydroprocessing of renewable fats and oils.	Reduction in particulate and GHGs emissions; compatible with existing engines and infrastructure.	Higher production costs; scalability and sustainability of feedstock supply chains.	High-quality fuel with no sulfur; excellent combustion properties.
Fischer–Tropsch	Conversion of syngas (from coal, natural gas, or biomass) into liquid HC.	Sulfur-free; lower GHGs emissions; high performance in engines.	Capital-intensive production plants; variability in feedstock costs.	Advances in catalysis and process engineering; integration of carbon capture and utilisation technologies.
Alcohol-to-Jet	Conversion of alcohols (ethanol, isobutanol) into synthetic paraffinic kerosene.	Uses renewable feedstocks; significant GHGs emissions reduction.	High initial capital investment; economic viability depends on feedstock costs and fermentation efficiency.	Established catalytic processes for dehydration and oligomerisation.
Oil from Algae	Cultivation of algae, lipid extraction, and refining into biofuel.	High oil yields per area; can be cultivated in diverse environments without competing with agricultural resources.	Economic costs of large-scale production; energy-intensive cultivation and harvesting processes.	Optimisation of growth conditions; integration with waste management systems.

In addition to these, some other options are also emerging and showing promise as new biofuels for the aviation industry [91]:

- Lignin-based biofuels: Lignin is a complex polymer and an abundant major component of plant biomass that can be converted into simpler hydrocarbon chains to be used as drop-in fuels in aviation, as a promising route to high energy density jet fuels.
- Solar fuels: Produced through the conversion of solar energy into chemical energy, mimicking natural photosynthesis, potentially providing limitless carbon-neutral energy from sunlight and air. Integrating these solar energy systems with catalytic processes to produce liquid HC could reduce the carbon footprint of aviation fuels.
- Electrofuels: A class of synthetic fuels produced from CO_2 and water (split to obtain hydrogen) using electrical energy (often sourced from renewable sources). The CO_2 can be captured from ambient air, point sources, such as power plants, or biomass. Its potential for high energy density and compatibility with existing fuel infrastructures make it an attractive technology for the aviation industry. They can also be synthesised through various pathways, including the electrochemical reduction of CO_2, reducing the reliance on fossil fuels.

2.4 Emulsions and emulsified fuels

2.4.1 Principles and different types of emulsions

An emulsion can be defined as a mixture of two immiscible liquids, formed by various mechanical or chemical processes. Emulsions are classified as a dispersion system, where the disperse phase (droplets of one liquid) is dispersed in a continuous flow [14]. Commonly, water and oil emulsions can be distinguished into four different types, based on their morphology: water-in-oil (W/O), oil-in-water (O/W), water-in-oil-in-water (W/O/W) or oil-in-water-in-oil (O/W/O) [13]. W/O emulsions consist of oil as the continuous phase and water as the dispersed phase. The opposite happens for O/W emulsions. For the more complex W/O/W emulsion, oil droplets enclosing water droplets are dispersed in water. The opposite happens for O/W/O emulsions. W/O emulsions (or water-in-fuel, for this case) are going to be the focus of this work. These types of emulsions can still be divided into macro, nano, or micro, according to different parameters [13], as shown in Table 2.6.

Macroemulsions are distinguished from the others due to their very low stability properties. Nanoemulsions are kinetically stable (the dispersed droplets are held in suspension by Brownian motion, the random motion of particles suspended in a medium [92], [93]), and microemulsions are thermodynamically stable (the system is in its lowest energy state, in chemical equilibrium with its environment). Despite being named nanoemulsions, their PS may be similar when compared to microemulsions (1-100nm) [92]. The reason for this confusing terminology is due to the development of the field of colloid science. One of the first articles that used the term "microemulsion" was published in 1961, whereas the first article using the term "nanoemulsion" is more recent (1996). This led to a well-established term of "microemulsion" well before the term

"nanoemulsion" was introduced, among researchers in the field [94]. In sum, microemulsions (also known as lyotropic liquid crystalline phases) and metastable nanoemulsions are significantly different. While nanoemulsions are dispersions of nanoscale droplets formed by mechanical shear (rupturing), microemulsions are nanoscale equilibrium phases formed by self-assembly, in which surface tension does not play a significant role [92].

Table 2.6. Different properties of macro, nano, and microemulsions [95].

Properties	Macro	Nano	Micro
Particle Size (vol.)	1-20mm	1-200nm	1-100nm
Polydispersity Index	>0.30	0.05-0.10	<0.10
Stability	Unstable	Kinetically stable	Thermodynamically stable
Shelf-Life	Very low/Low	Medium/High	Very high
Phases	Biphasic	Monophasic	Monophasic
Aspect	Turbid	Translucent or semi-transparent	Semi-transparent or transparent
Viscosity	High	Low	Low
Energy Required to Emulsify	High/Very high	Low/Medium	Ultra-low/Low
Preparation Cost	High	Low/Medium	Low/Medium
Interfacial Tension	High	Ultra-low/Low	Ultra-low
Optical Isotropy	Anisotropic	Isotropic	Isotropic
Concentration of Surfactant	Low/Medium	Medium	High/Very high

Figure 2.16 illustrates an example of how stability can be measured as a function of Gibbs free energy across the different types of emulsions. A thermodynamically stable system will tend towards minimising this energy.

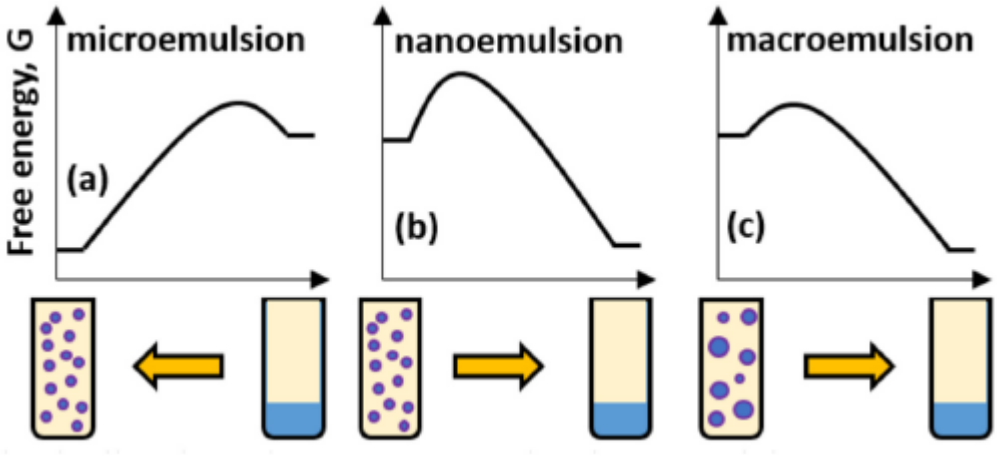

Figure 2.16. Evolution of Gibbs free energy in micro, nano, and macroemulsions [96].

Microemulsions can also be classified into four different types, according to their phase equilibria. Initially, the oil and water phases are separate. Type I and Type II emulsions can be formed by the addition of a surfactant/co-surfactant system [97], [98]. An illustration of the different phases can be seen in Figure 2.17:

Winsor Type I: the surfactant is preferentially soluble in water, and O/W microemulsions form. The surfactant-rich water phase coexists with the oil phase, and the surfactant exists as a monomer at a small concentration.

Winsor Type II: the surfactant is mainly in the oil phase, and W/O microemulsions form. The surfactant-loaded oil phase coexists with the surfactant-poor aqueous phase.

Winsor Type III: the surfactant-rich middle-phase coexists with excess water and oil, surfactant-poor phases.

Winsor Type IV: a single-phase (isotropic) micellar solution, formed after the addition of a sufficient quantity of amphiphile. An extension of a Winsor Type III at higher surfactant concentrations. Further addition of the surfactant system will result in phase separation, described as the cloud point.

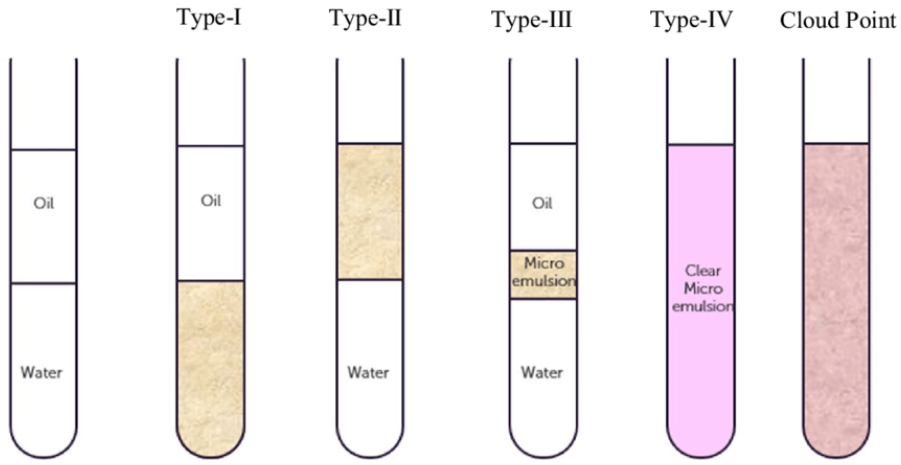

Figure 2.17. Winsor's classification of microemulsions [98].

2.4.2 Surfactants

To secure the stabilisation of an emulsion, another component is often added to the system: a surfactant. The primary goal of a surfactant (or surface-active agent) is to lower the interfacial tension between the two surfaces (e.g., oil and water), reducing the repellent force between the two liquids and diminishing the attraction between the molecules of the same liquid. This results in lower energy required to increase the surface area, leading to a spontaneous dispersion of water or oil droplets and possibly to a thermodynamically stable system [97]. The secondary role is to maintain the stability of the emulsion while reducing the coagulation effect in the water phase [99]. A surfactant is an amphiphilic molecule that has hydrophobic and hydrophilic parts. The hydrophobic part within the molecule is commonly referred to as the tail (usually a hydrocarbon),

and the hydrophilic part is commonly referred to as the head. Because of the similarity between the hydrophobic (non-polar) tails, surfactants are typically classified based on their polar head.

An ionic surfactant has an electric charge. There are three types of ionic surfactants:

- Anionic (negatively charged).
- Cationic (positively charged).
- Amphoteric or Zwitterionic (can contain positive, negative, or no charge).

For ionic surfactants, the most popular and widely used are the anionic surfactants, which can be found in practically every type of detergent and cleaning product. The most commonly used hydrophilic groups are carboxylates, sulphates, sulphonates, and phosphates. Cationic and amphoteric surfactants are used much less frequently. Cationic surfactants are usually found in fabric softeners and disinfectants since they are more effective at killing microorganisms. Their head groups are generally molecules derived from substituted ammonium compounds. Amphoteric surfactants have excellent dermatological properties and are most commonly found in shampoos, body washes, and hand washes. The most used amphoteric surfactants are the N-alkyl betaines [100].

Another type of surfactant is the non-ionic surfactant, which contains no charge. They are the second most widely used surfactants after anionic with various applications in different fields, one of which and very important for this work is the field of W/O emulsions [101]. Their ability not to dissociate into ions prevents the worsening of exhaust emissions by substances added to the fuel [102]. The most common non-ionic surfactants are ethoxylated. Non-ionic surfactants are famous for their non-toxicity when compared to other kinds [100]. Figures 2.18 and 2.19 show the different types of surfactants and how they interact with the different phases.

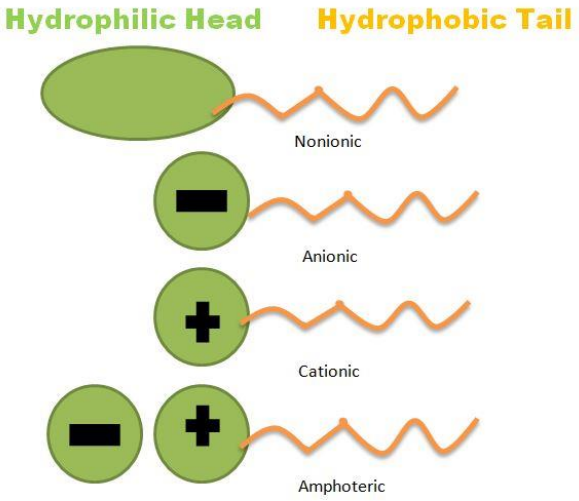

Figure 2.18. Ionic and non-ionic surfactants [103].

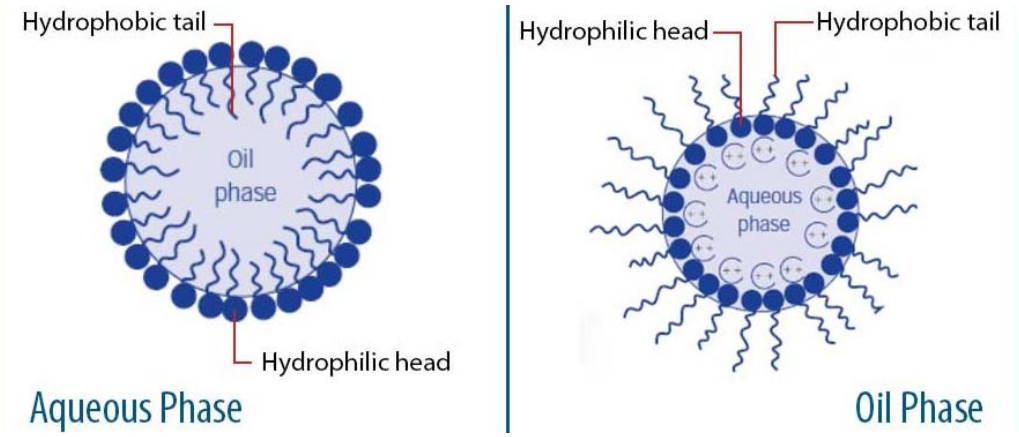

Figure 2.19. Surfactant interaction with oil and water phases [104].

As seen before, each type of surfactant has its own application. For a better understanding of how to choose between the different types of surfactants, a hydrophilic-lipophilic balance (HLB) score was conceived. HLB can vary from 1 to 20, and it measures the affinity of a surfactant for water or oil. Low HLB values are usually preferred for W/O emulsions, while surfactants with high HLB values (more hydrophilic) are usually preferred to make O/W emulsions. [105]. Hydrophilic surfactants may also become lipophilic at higher temperatures due to the dehydration of their hydrophilic groups. This can lead to improved stability by using higher HLB surfactants in W/O emulsions, as was manifested [106]. Despite its simplicity, the HLB scale has generated some controversy over the years. One of the biggest criticisms is that HLB is reserved for a fundamentally flawed idea. Because it is a property of the surfactant, it must be wrong when physical quantities like temperature change.

For this reason, a different term, hydrophilic-lipophilic difference (HLD), is emerging, which ascribes the balance of the system. It conveys a similar sentiment, without the connotations of the discredited HLB system. An optimal formulation (when the different properties of the system are balanced) should have an HLD equal to zero [107], the end of the journey for those who want type III microemulsions. The numbers from the HLD will tell us immediately if the system is O/W, W/O, or in an intermediate state. HLD is generally used in describing the balance between oil, salinity, temperature, and surfactant, a scientifically meaningful approach to surfactant formulation [107], [108]. Figure 2.20 shows the variables used for the balance of the surfactants, i.e., the HLB + temperature and salinity.

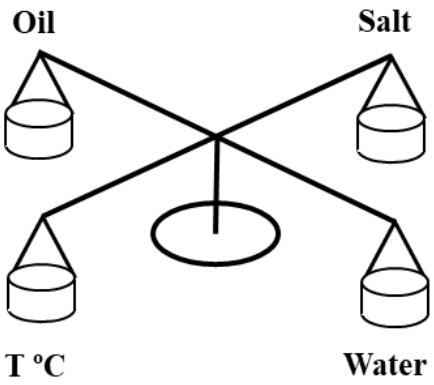

Figure 2.20. Surfactants balance [107].

The fish-cut tail is also a good visualisation method and is mostly used in surfactant theory. Plots can be made in terms of temperature (T), salinity (Sa), effective alkane carbon number (EACN), and characteristic curvature (Cc) of the net average curvature [109].

Figure 2.21 shows (a) a two-dimensional planar cut of temperature (T) vs surfactant-oil-water (SOW) phase (3D prism) diagram at a constant water-to-oil ratio (WOR) and (b) a fishtail diagram of temperature (T) vs surfactant concentration (CS) showing Winsor type emulsions and HLD for a system with 50% water and 50% oil ratio (WOR = 1), with a very pure non-ionic surfactant; critical microemulsion concentration (CmC) and surfactant concentration (CS) [107], [110].

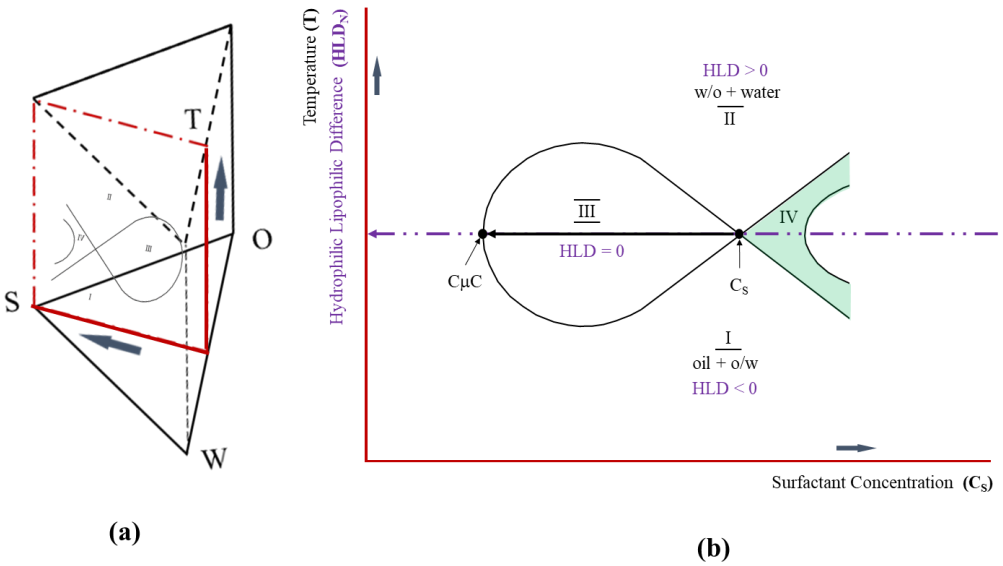

Figure 2.21. (a) Temperature (T) vs surfactant-oil-water (SOW) phase diagram at constant water-to-oil ratio (WOR) and (b) fishtail diagram of temperature (T) vs surfactant concentration (CS) showing Winsor type emulsions and HLD for a system with 50% water and 50% oil (WOR = 1), with a very pure non-ionic surfactant [95], [107], [110], [111].

2.4.3 Emulsions breakdown mechanisms

Phase separation can occur in unstable emulsions by a variety of different processes, such as creaming and sedimentation, flocculation, coalescence, and Ostwald ripening. These processes often occur simultaneously, interacting with each other [112]. The addition of heat can lead to the destabilisation of an emulsion (changes in viscosity and density), gravity separation, retention time (related to gravity), agitation (breaking surface tension of liquids), coalescing (related to agitation process), and chemical demulsification (demulsifiers) [107], [113].

2.4.3.1 Creaming and sedimentation

When external forces (gravitational or centrifugal) exceed the thermal or Brownian motion of the dispersed phase (droplets), creaming and sedimentation can occur. A concentration builds up in the system, and depending on the density of the droplets (higher or lower than the continuous phase), the larger droplets move to the bottom or to the top, respectively. The droplet concentration gradient produced by those two mechanisms in the emulsion increases with time until the emulsion droplets are contained in a close-packed configuration together with a separated continuous solvent [107], [113], [114].

2.4.3.2 Flocculation

Flocculation is the process where flocs, flakes, or clusters are formed by individual droplets in the continuous phase of the emulsion, enabling them to bind together, creating larger aggregates, easier to separate. Since the flocs retain their individual properties, the system may be redispersed if enough force is applied. The pH and ionic strength of the aqueous environment affect the rate of flocculation [107], [113], [115].

2.4.3.3 Coalescence

Coalescence is an irreversible process and consists of breaking the interfacial film. The coalescence stability of an emulsion is affected by the solubility of the surfactants, pH, salts, surfactant concentrations, phase volume ratio, temperature, and properties of the film. Extensive droplet coalescence may lead to the formation of a separate layer of oil on top of the emulsion (oiling off) [107], [113], [116].

2.4.3.4 Ostwald ripening

Ostwald ripening is a well-known phenomenon that was first systematically investigated in 1900 by Willhelm Ostwald and is the process where a disappearance of small particles or droplets occurs by dissolution and deposition as larger particles or droplets. The driving force for this mechanism is the difference in solubility between small and large particles. At low interfacial energy, Ostwald ripening stops, bringing the formulation close to HLD = 0 with greater stability [107], [117].

2.4.4 Water-in-fuel emulsions

A major application field of emulsions is the fuel industry. Water can be added and occurs in fuels in three different forms: dissolved in the fuel, as a separate liquid phase (free water), and as a fuel-water emulsion, which is the focus of this work [12]. Free water can be portentously hazardous and should be avoided.

Water-in-fuel emulsions (WFE) as an alternative fuel are becoming more and more an option to fight existing and upcoming emissions restrictions. The main advantage of using emulsion fuels is a more complete combustion, which can lead to a better fuel economy (lower fuel consumption), better engine performance, and lower emissions [105]. On top of that, it is a technology that does not require engine modification, and hence more practical and appellative to companies who do not want to invest in new engine designs.

The cleaner combustion of WFE can be attributed to the puffing and microexplosion phenomena in emulsion droplets. When the emulsion is sprayed into a hot combustion chamber, heat is transferred to the surface of the fuel droplets by convection and radiation. A rapid break-up of the parent droplets due to the different volatility of the fuel and water (the water molecules reach their superheated stage faster than the fuel, creating vapour expansions breakup and splitting the fuel droplets) promotes a secondary atomisation that reduces the combustion duration [15], [118]. At this stage, the two phenomena prevail [105], [119]. Puffing is the partial ejection of some dispersed water out of an emulsion droplet. Micro-explosion is the complete break-up of the parent droplet. These two occurrences improve the combustion process by enhancing the effective fuel droplet size distribution, increasing the surface area of the particles with the intake air, leading to better air-fuel mixing and therefore better fuel efficiency and fewer emissions [119], [96]. The sudden expansion of the vapour phase in the droplets may also exert an additional force on the piston, leading to enhanced benefits in engine torque and fuel consumption [96]. Figure 2.22 shows a schematic diagram of the puffing and microexplosion process. A simplified example of the mechanism of microexplosion in WFE is also shown in Figure 2.23.

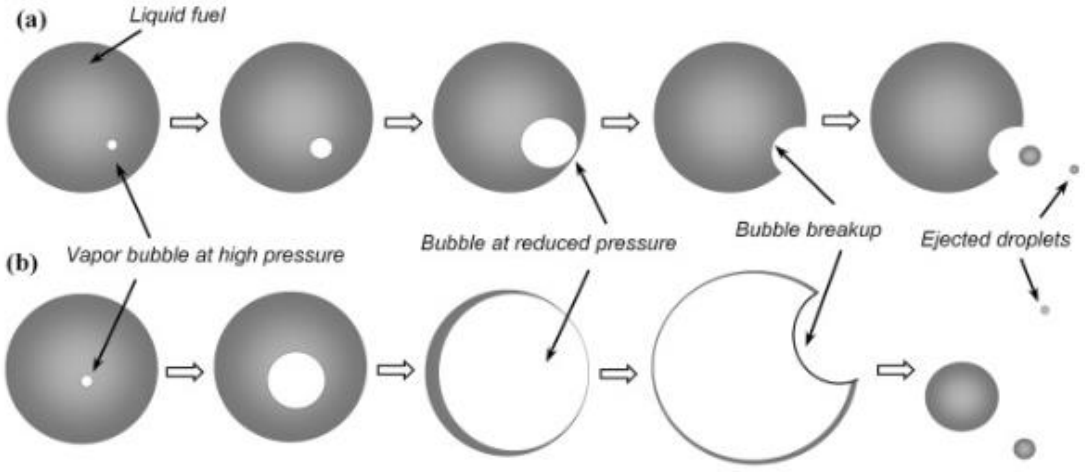

Figure 2.22. Sequence diagram of (a) puffing and (b) microexplosion phenomena [120], [121].

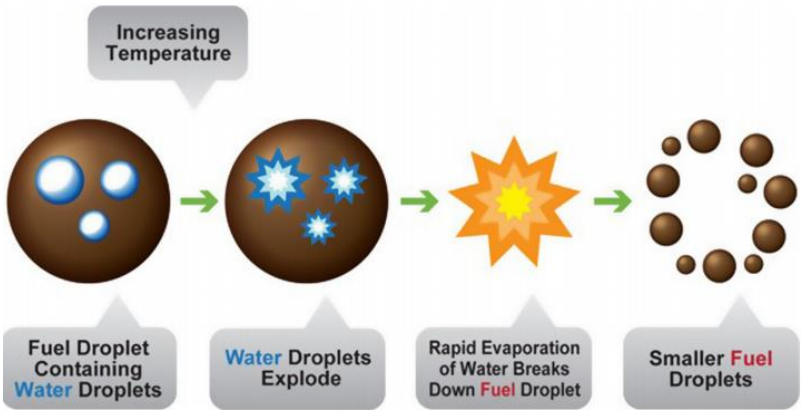

Figure 2.23. Microexplosion mechanism in WFE [122].

The evaporation of water present in the emulsion also leads to a significant reduction in the combustion chamber temperature. The evaporation of water droplets absorbs heat instead of releasing it (heat sink effect), indicating an endothermic process, hence why water does not have a calorific value [123]. This leads to a reduction in NO_x emissions. From the longer ignition delay due to the heat sink effect results more fuel combustion in premixed mode [15], [124]. The AFR becomes higher, ensuring a sufficient amount of O_2 availability, which can help to reduce soot, PM, CO, and HC formation [125].

The most explored type of WFE is water-in-diesel emulsions (WiDE). One of the major reasons is the simplicity of emulsifying water in diesel fuel when compared to petrol (gasoline) or other energy sources, which are much harder to mix. This simplicity can also be explained by the higher hygroscopicity (the phenomenon of attracting and holding water molecules via absorption or adsorption from the surrounding environment) of diesel over the other remaining fuels. Another reason can be due to the more effective occurrence of puffing and microexplosions mechanisms when utilising diesel as a fuel compared to the other options. The higher combustion temperatures and higher pressures existent on diesel engines can also explain this preference. In the next subsection, the WiDE process is explained, and an extensive literature review of the findings and results obtained from different authors over the years in this field will be performed.

2.4.4.1 Water-in-diesel emulsions

Adding water to fuel dates back to the early 1900s, but only recently, in the last two decades, commercial attempts took place by major entities using diesel-emulsified fuels, on a macro-level. This is known as “white diesel”. Currently, hundreds of patents have been made for WFE, with a lot of companies attempting to take advantage in the field.

WiDE can be classified as W/O (oil-based), where diesel is the continuous phase and water is the dispersed phase. They are generally formed by a hydrocarbon, water, and one or more surfactants, generally non-ionic, as the emulsifier agent, as shown in Figure 2.24.

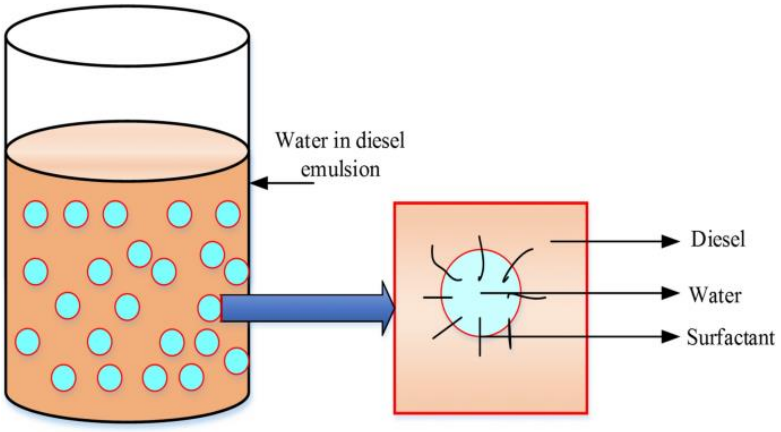

Figure 2.24. WiDE schematic [126].

Surfactants are used to stabilise the emulsions, and they should easily burn with no soot, free of sulfur and nitrogen, while having no impact on the physiochemical properties of the fuel [105], [127]. These emulsions can also be characterised as macro (the most common type, or white diesel), nano, and microemulsions, according to their morphology, and defined by PS, PDI, and stability (kinematic or dynamic). An example diagram of the process of the production of WiDE can be seen in Figure 2.25.

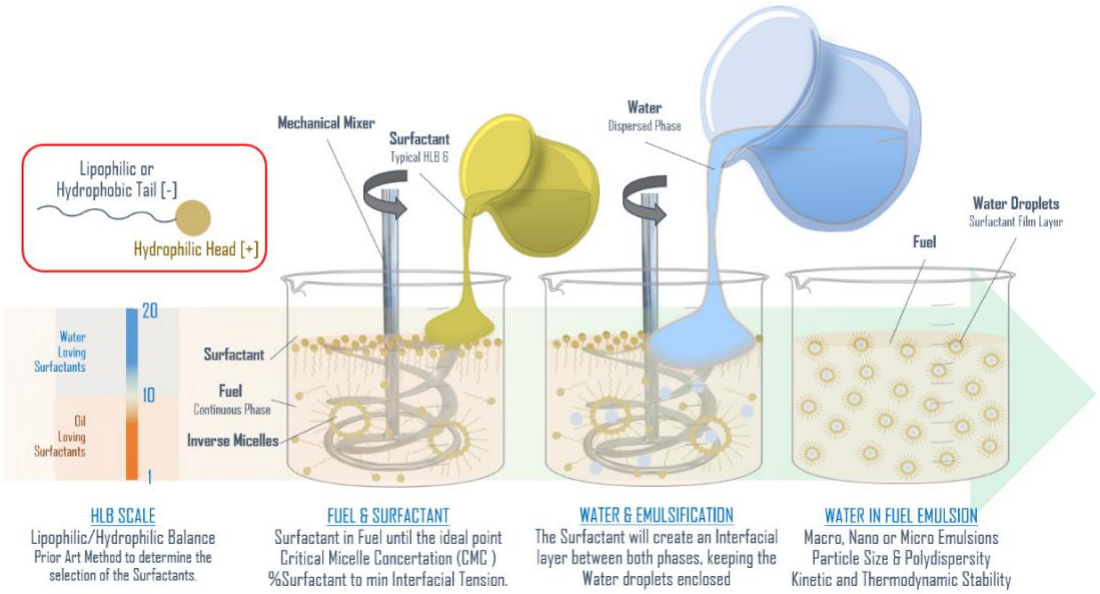

Figure 2.25. Typical water-in-diesel emulsification process [95].

In this process, the HLB scale is used to select the most appropriate surfactants, which are then added to the fuel until an ideal point. With the addition of water, the surfactant will create an interfacial layer between both phases, keeping the water droplets enclosed and dispersed in the fuel, forming the emulsion.

A lot of researchers have been utilising a wide variety of techniques, developing many studies in the field of WiDE. However, there are still many uncertainties about the ideal properties and composition that the emulsified fuel should have (water percentage, surfactant percentage, temperature, oil, etc.) [107]. Although most studies are consensual on the reduction of NO_x and PM, the results for CO, CO_2, and HC differ widely. The same happens for torque, fuel consumption, and TE. It is also important to address that the conditions in which the tests were performed in the various researches are very different (engine type, load conditions, diesel fuel properties, water properties, surfactants used, ratio of the mixture, mixing methods, mixing speed, mixing time, equipment used, ambient conditions, etc.). A relationship between the increase or decrease of one or more reactants in the emulsion fuel and its effects on the different engine parameters is hard to assess, because results are not consensual, and often rely upon specific conditions, even in the same research study. Kapadia et al. [99], Sartomo et al. [128], Mostafa et al. [129], and Gowrishankar et al. [96] effectively separate the results of some of the different research based on the different conditions they were achieved. The studies described next are based on general findings, listed in chronological order, and results may vary depending on specific conditions in the same study.

Park, Kwak, and Oh [130], Nadeem et al. [131], Selim and Ghannam [132], Fahd et al. [133], Hoseini and Sobati [134], Mondal and Mandal [15], Okumus, Kaya, and Kökkülünk [135], and Patel and Dhiman [136] have reported a decrease in torque and power of WiDE compared to diesel fuel. Abu-Zaid [137], [138], Kannan and Udayakumar [139], Alahmer et al. [140], Alahmer [141], Seifi et al. [142], Hosseinzadeh-Bandbafha et al. [143], and Khathri et al. [144] have reported in their studies an increase in torque and power of WiDE. Mondal and Mandal [145] reported similar results of torque and power for the different fuels.

When it comes to fuel consumption, different results can also be observed. Some authors consider only the energy portion of the fuel (diesel) and calculate the specific energy consumption (SEC) and other authors consider the emulsion as a whole fuel, calculating the SFC. Bernaud, Schmelzle, and Schulz [146], Park, Huh, and Lee [147], Kannan and Udayakumar [139], Alahmer [141], Zhang et al. [148], Singh and Bharj [149], Ramlan et al. [150], Ithnin et al. [151], Ramalingam et al. [152], Rahman et al. [153], Tamam et al. [154], and Anil, Hemadri, and Swamy [101] reported a decrease in the SFC of WiDE. Holt [155], Suresh and Amirthagadeswaran [156], Ithnin et al. [157], Ogunkoya et al. [158], Mazlan et al. [159], Mondal and Mandal [15], and Vellaiyan, Subbiah, and Chockalingam [160] only considered the energy portion of the emulsion and reported a decreased SEC of WiDE. Abu-Zaid [137], Lin and Wang [161], Lin and Chen [162], Tzirakis et al. [163], Ghojel, Honnery, and Al-Khaleefi [164], Nadeem et al. [131], Alahmer et al. [165], Maiboom and Tauzia [166], Fahd et al. [133], Mondal and Mandal [15], Venkatesan et al. [167], Rosid et al. [168], Hassan et al. [169], Patel and Dhiman [136], and Gautam et al. [170] reported increased SFC of WiDE. Park, Kwak, and Oh [130] only considered the energy portion of the emulsion and still reported an increased SEC.

Regarding TE, Armas et al. [171], Fahd et al. [133], Venkatesan et al., [167], Hosseinzadeh-Bandbafha et al. [143], Mondal and Mandal [15], Hassan et al. [169], and Gautam et al. [170] reported decreased values of TE of WiDE. The majority of the studies reported an increase in this engine parameter: Abu-Zaid [137], Ghojel, Honnery, and Al-Khaleefi [164], Kannan and Udayakumar [139], Alahmer et al. [165], Badran et al. [172], Basha and Anand [173], Alahmer [141], Fahd et al. [133], Syu et al. [174], Singh and Bharj [149], Attia and Kulchitskiy [175], Ogunkoya et al. [158], Suresh and Amirthagadeswaran [156], Baskar and Kumar [176], Mondal and Mandal [145], Ithnin et al. [151], Mondal and Mandal [177], Ramalingam et al. [152], Patel and Dhiman [136], Tamam et al. [154], Rahman et al. [153], and Anil, Hemadri, and Swamy [101].

In the matter of exhaust emissions, similar to the engine performance parameters, a lot of variety is also found. Subramanian and Ramesh [178], Nadeem et al. [131], Singh and Bharj [149], Venkatesan et al. [167], Patel and Dhiman [136], and Anil, Hemadri, and Swamy [101] reported a decrease in CO emissions in WiDE. A wider range of authors reported increased emissions of CO: Nazha, Rajakaruna, and Wagstaff [179], Park, Kwak, and Oh [130], Lin and Wang [161], Holt [155], Lif and Holmberg [180], Lin and Chen [162], Basha and Anand [173], Fahd et al. [133], Syu et al. [174], Ithnin et al. [157], Ramlan et al. [150], Ahmad et al. [181], Mondal and Mandal [145], Mazlan et al. [159], Sugeng et al. [182], Hosseinzadeh-Bandbafha et al. [143], Rosid et al. [168], Mondal and Mandal [15], and Hassan et al. [169].

With respect to CO_2 emissions, Saravanan, Anbarasu, and Gnanasekaran [183], Ithnin et al. [157], Ramlan et al. [150], Abdurahman et al. [184], Mazlan et al. [159], Hosseinzadeh-Bandbafha et al. [143], and Basha and Al Balushi [185] obtained a reduction in CO_2 emissions in WiDE. Lin and Wang [161], Alahmer et al. [165], Al-Sabagh et al. [186], Singh and Bharj [149], Hoseini and Sobati [134], and Rahman et al. [153] obtained an increase in CO_2 emissions. Lin and Chen [162] found no difference in the CO_2 emissions for the different fuels.

Regarding HC emissions, Barnaud, Schmelzle, and Schulz [146], Samec, Kegl, and Dibble [187], Armas et al. [171], Ghojel, Honnery, and Al-Khaleefi [164], Kannan and Udayakumar [139], Attia and Kulchitskiy [175], Singh and Bharj [149], Mondal and Mandal [177], Venkatesan et al. [167], Patel and Dhiman [136], and Anil, Hemadri, and Swamy [101] reported a decrease of these emissions in their studies. Nazha, Rajakaruna, and Wagstaff [179], Holt [155], Park, Kwag, and Oh [130], Lif and Holmberg [180], Alahmer et al. [140], Basha and Anand [173], Syu et al. [174], Emberson et al. [188], Vellaiyan and Amirthagadeswaran [189], Mondal and Mandal [145], Sugeng et al. [182], Hosseinzadeh-Bandbafha et al. [143], Rosid et al. [168], Hassan et al. [169], Gautam, Vishnoi, and Gupta [170], and Rahman et al. [153] reported an increase of HC emissions in WiDE.

As for NO_x emissions, almost every author reported a decrease of these values: Barnaud, Schmelzle, and Schulz [146], Nazha, Rajakaruna, and Wagstaff [179], Park, Huh, and Lee [147], Samec, Kegl, and Dibble [187], Holt [155], Lin and Wang [161], Park, Kwak, and Oh [130], Armas et al. [171], Lif and Holmberg [180], Nadeem et al. [131], Ghojel, Honnery, and Al-khaleefi [164],

Lin and Chen [162], Kannan and Udayakumar [139], Rajasekar et al. [190], Subramanian [191], Maiboom and Tauzia [166], Basha and Anand [173], Al-Sabagh et al. [186], Zhang et al. [148], Scarpete [192], Alahmer [141], Fahd et al. [133], Singh and Bharj [149], Attia and Kulchitskiy [175], Syu et al. [174], Ithnin et al. [157], Emberson et al. [188], Vellaiyan and Amirthagadeswaran [189], Ramlan et al. [193], Mondal and Mandal [145], Sugeng et al. [182], Ahmad et al. [181], Mazlan et al. [159], Ithnin et al. [151], Mondal and Mandal [15], [177], Hosseinzadeh-Bandbafha et al. [143], Vellaiyan, Subbiah, and Chockalingam [160], Hassan et al. [169], Gautam, Vishnoi, and Gupta [170], Tamam et al. [154], Rahman et al. [153], and Anil, Hemadri, and Swamy [101]. Only Venkatesan et al. [167] reported an increase in NO_x emissions.

Finally, and concerning PM or smoke emissions, Barnaud, Schmelzle, and Schulz [146], Park, Huh, and Lee [147], Kadota and Yamasaki [194], Lin and Wang [161], Armas et al. [171], Nadeem et al. [131], Tzirakis et al. [163], Lif and Holmberg [180], Lin and Chen [162], Alahmer et al. [140], Rajasekar et al. [190], Basha and Anand [173], Subramanian [191], Maiboom and Tauzia [166], Zhang et al. [148], Attia and Kulchitskiy [175], Ithnin et al. [157], Emberson et al. [188], Mondal and Mandal [145], Sugeng et al. [182], Ahmad et al. [181], Mazlan et al. [159], Ithnin et al. [151], Wang et al. [195], Rosid et al. [168], Mondal and Mandal [15], [177], Hassan et al. [169], Patel and Dhiman [136], Gautam, Vishnoi, and Gupta [170], Tamam et al. [154], Rahman et al. [153], and Anil, Hemadri, and Swamy [101] reported a decrease of these emissions. Only Saravanan, Anbarasu, and Gnanasekaran [183] and Ramlan et al. [193] reported increased values for these emissions.

After carefully analysing the different research and the specific conditions in which they were performed and the obtained results, it is possible to draw some conclusions and recommendations as shown in Tables 2.7 and 2.8.

Table 2.7. Effects of WiDE on engine performance: findings and possible solutions (adapted from [96]).

Occurrences	Effects	Possible Solutions
Lower Calorific Value	Reduced power/torque.	Reduce water content.
Puffing and Microexplosion	Improved TE.	-
Additional Force on the Piston due to Water Expansion	Increased power/torque.	-
Increased Injection Duration	Increased SFC.	Increase injection pressure.
Increased Spray Penetration	Increased SFC.	-
Increased Burning Rate	Reduced SFC.	-

Table 2.8. Effects of WiDE on engine emissions: findings and possible solutions (adapted from [96]).

Occurrences	Effects	Possible Solutions
Lower Cylinder Pressure	Decreased NO_x. Increased HC and CO.	Reduce water content.
Increased Premixed Combustion	Increased NO_x.	Retard injection timing.
Puffing and Microexplosion	Decreased CO, HC, and PM/smoke.	-
Formation of OH Radicals	Decreased CO, HC, and PM/smoke.	-
Increased Ignition Delay	Decreased PM/smoke. Increased NO_x.	Retard injection timing.
Increased Injection Duration	Increased PM/smoke.	Increase injection pressure.
Increased Spray Penetration	Increased HC (spray wall wetting).	Retard injection timing.
Deteriorated Combustion	Increased CO.	Adjust operating parameters.

As can be observed from the previous information, the fuel spray characteristics of WiDE have a predominant role in determining how combustion will occur inside the cylinder. Figure 2.26 illustrates a basic example of a fuel spray and its parameters.

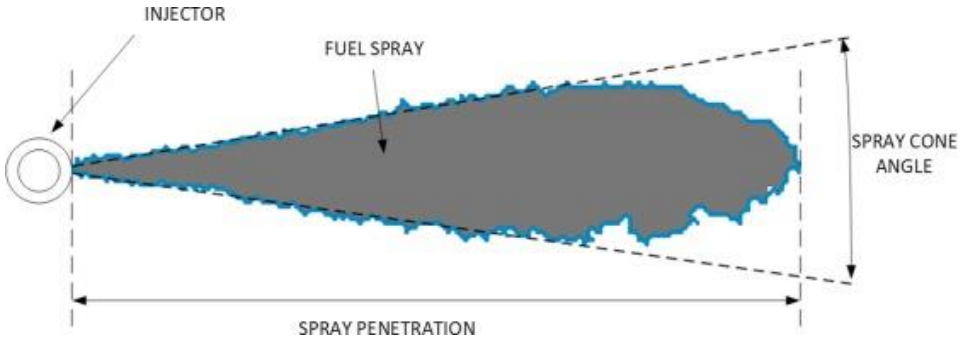

Figure 2.26. Fuel spray [196].

After analysing the different studies, some conclusions can be drawn [96], [197]:

- A longer spray penetration length (distance travelled by the fuel spray in the axial direction) is obtained by increasing the density and viscosity of the emulsion and decreasing the volatility of the fuel, by increasing water content.
- The spray cone angle (divergence of the fuel spray as it exits the injector nozzle, measured from the centreline of the injector) for the emulsion is reduced during fuel injection due

to the increased density and viscosity, lowering the air entrainment into the spray. After a short period, and due to microexplosions, this angle is expanded, improving atomisation and better mixing, especially at higher water concentrations.

- The hotspots corresponding to higher temperature regions during combustion are significantly reduced when using emulsion fuels.
- A higher spray momentum (direction and velocity of the fuel spray, containing the kinetic energy carried by the fuel droplets and the direction in which they are propelled) and air entrainment into the spray zone were obtained, helping to achieve proper atomisation and mixing.

2.5 Key variables review

2.5.1 Engine parameters

2.5.1.1 Torque and power

An engine specification is usually expressed by the maximum power and torque values and their respective curves [36]. Torque represents an engine's ability to do work and can be measured with a dynamometer. The engine is clamped on a test bed with the shaft connected to the dynamometer rotor. The rotor is coupled to a stator, electromagnetically, hydraulically, or by mechanical friction. The torque exerted on the stator with the rotor turning is measured by balancing the stator with weights, springs, or pneumatic means [34]. A simplified mechanism is shown in Figure 2.27.

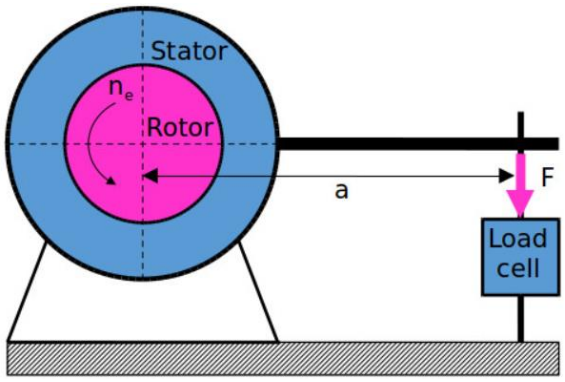

Figure 2.27. Operational principle of a dynamometer [198].

Torque is calculated by multiplying the force and distance and expressed in newton meters (Nm). For this example:

$$\tau = Fa, \tag{2.2}$$

where F is the force applied in newtons (N) and a is the distance from the axis of rotation in meters (m).

Whilst torque refers to the capacity of an engine to do work, power is the rate at which work is done [34]. It is calculated by multiplying torque and angular speed and expressed in Watts (W):

$$P = N\tau, \tag{2.3}$$

where N is the rotational speed in radians per second (rad/s) and τ is torque in Nm.

The engine parameters brake torque (BT) and brake power (BP) contain the keyword "brake" because a dynamometer (brake) is used to measure them. This is the usable power or torque delivered by the engine to the load [34].

2.5.1.2 Load

The engine load can be defined as the amount of effort the engine needs to generate to respond to imposed external forces and accomplish a required task. It represents the capacity of the engine to produce power and overcome these forces. Power and torque curves are published by manufacturers at full load, highlighting the maximum torque and power distribution at all engine speeds. However, in real-life situations, engines rarely operate in this condition and run on partial load. In CI engines, this load can be controlled with fuel injection [36].

2.5.1.3 Specific fuel consumption

The efficiency of an engine at using the fuel supplied to produce work is measured by the SFC parameter, expressed in $\frac{g}{kWh}$. It is inversely proportional to the TE of the engine [33]:

$$SFC = \frac{\dot{m}_{fuel}}{P}, \tag{2.4}$$

where $\dot{m}_{\text{fuel}}$ is the fuel mass flow rate ($\frac{g}{h}$) and P is the power produced in kW. BP gives brake specific fuel consumption (BSFC). Lower values of SFC are desirable and represent a better fuel economy.

2.5.1.4 Thermal efficiency

This parameter represents how well an engine converts the chemical energy released from the fuel into mechanical energy. The amount of heat released during the combustion of a certain fuel is called HV. There are two types of HV: higher heating value (HHV) and LHV. The first includes the energy released in condensing water. LHV doesn't include this energy. Brake thermal efficiency (BTE) is calculated using BP, and is expressed in % [47]:

$$BTE = \frac{360000}{\text{BSFC.LHV}}, \tag{2.5}$$

where BSFC is the brake specific fuel consumption ($\frac{g}{kWh}$) and LHV is the lower heating value of the fuel ($\frac{MJ}{Kg}$). LHV is preferred because water vapour in combustion products is often not condensed, and the energy released during its condensation is not considered.

2.5.1.5 Air-fuel ratio

The proportions of air and fuel in an engine are very important when it comes to combustion and efficiency. It is expressed as a ratio of the mass of air to that of the fuel [33]:

$$AFR = \frac{\dot{m}_{air}}{\dot{m}_{fuel}}, \tag{2.6}$$

where $\dot{m}_{air}$ and $\dot{m}_{fuel}$ are the mass flow rates of air and fuel, respectively.

In a CI engine at a given speed, the fuel flow varies with the load [33]. When the relationship between air and fuel is such that the entire fuel is (or can be) burned, the mixture is called stoichiometric. The fuel-air equivalence ratio compares the stoichiometric AFR (AFR_{sto}) to the actual AFR, using the following equation [36]:

$$\Phi = \frac{AFR_{sto}}{AFR}. \tag{2.7}$$

A mixture having more fuel than that in a stoichiometric mixture is called a rich mixture and has $\Phi > 1$ [36]. Lean mixtures have $\Phi < 1$. The AFR_{sto} for diesel is 14.5:1. Diesel engines are usually operated at leaner mixtures when compared to gasoline engines, which, in par with the higher temperatures and compression ratios, lead to higher emissions of NO_x, formed at higher combustion temperatures, characteristic of diesel engines' operation.

2.5.1.6 Mean effective pressure

Torque is a valuable measure of expressing a specific engine's ability to do work. However, engines with larger sizes will often have higher values of torque. By dividing the work per cycle by the cylinder volume displaced per cycle, we can obtain the mean effective pressure (MEP), expressed in bar, which is useful to compare engines with different displacements and identify which one is more efficient at producing work [34], [36]:

$$MEP = \frac{\text{PnR x 10 x 60}}{V_d N}, \tag{2.8}$$

where P is power (kW), nR is the number of crank revolutions for each power stroke per cylinder (2 for four-stroke cycles), V_d is the volume displaced (dm^3), and N is the rotational speed (rpm). BP will give the brake mean effective pressure (BMEP).

2.5.2 Engine emissions

During the combustion process, IC engines produce undesirable emissions that pollute the atmosphere. The composition of exhaust gases emissions is approximately 67% of di-nitrogen, 12% CO_2, 11% water, and 9% O_2. The remaining 1% is composed of CO, HC, NO_x, sulphur dioxide (SO_2), and PM [199], [200]. Major causes of the pollutant emissions are non-stochiometric combustion, dissociation of nitrogen, and impurities in the fuel and air [33].

The lambda value (excess of air) can be estimated from the composition of the exhaust gases by the Brettschneider equation:

$$\lambda = \frac{CO_2+\frac{CO}{2}+O_2+\left(\frac{H_{cv}}{4}.\frac{3.5}{3.5+\frac{CO}{CO_2}}-\frac{O_{cv}}{2}\right).(CO_2+CO)}{(1+\frac{H_{cv}}{4}-\frac{O_{cv}}{2})(CO_2+CO+6.\frac{HC}{10000})}, \tag{2.9}$$

where H_{cv} is the hydrogen-to-carbon atomic ratio and O_{cv} is the oxygen-to-carbon atomic ratio.

It is important to address that a change in the type of fuel, which translates to different constant values in the equation (different carbon-to-hydrogen ratios and chain lengths) while maintaining the same exhaust gases concentration, has a trivial effect on the final value of lambda. This is important because most gas analysers (similar to the one used in this work) are usually meant to be operated on gasoline engines. However, the lambda value calculated for gasoline fuel, while keeping the exhaust gases concentration constant, would not be very different from the real one using diesel fuel. Gas analysers for diesel exhaust are usually more expensive, and opacimeters are used to measure smoke and PM emissions. Some of the exhaust gases and their formation mechanisms are explained next.

2.5.2.1 Carbon dioxide

CO_2 is a non-toxic gas responsible for most of the greenhouse effect on the planet. It results from the complete combustion of the HC in the fuel molecules [201]. A complete combustion of a hydrocarbon with O_2 produces CO_2 and water vapour (Equation 2.10). It represents how well the air/fuel mixture is burned in the engine. Because diesel engines are more thermodynamically efficient, they have lower fuel consumption and therefore overall lower CO_2 emissions.

$$C_xH_y + \left(x+\frac{y}{4}\right)O_2 \rightarrow xCO_2 + \frac{y}{2}H_2O. \tag{2.10}$$

2.5.2.2 Carbon monoxide

CO is a colourless, odourless, poisonous gas, and a product of incomplete combustion due to rich fuel/air ratios, lower combustion chamber temperatures, or insufficient time in the cycle for completion of combustion. When the O_2 available is not enough to convert all carbon to CO_2, the unburned carbon ends up as CO [36], [47].

2.5.2.3 Hydrocarbons

HC emissions correspond to the unburned portion of the fuel and are the result of incomplete combustion. They can also originate from engine oil or pressure leaks in the exhaust valves [36]. The effect of AFR on HC emissions is nearly the same as found in CO emissions. At near stoichiometric fuel/air mixtures, both HC and CO emissions are higher, and lower at lean fuel mixtures [33]. In diesel engines, the main source of HC emissions is the fuel withheld in the injection nozzle. Other sources can be wall deposit absorption, oil film absorption, and crevice volume. [47].

2.5.2.4 Nitrogen oxides

NO_x is a combination of nitric oxide (NO), nitric dioxide (NO_2), and N_2O, the first with the highest concentration of the three [36], [47]. They are formed due to the high combustion temperatures, leading to the dissociation of nitrogen molecules and their reaction with O_2 in the air (thermal NO_x), contributing to the formation of acid rain. Therefore, higher peak combustion temperatures and wide availability of O_2 lead to higher emissions of NO_x, which only occur in the engine exhaust [33], [36]. In diesel engines, these emissions are even higher, not only because the higher compression ratios allow higher combustion temperatures but also because they often operate with excess O_2 in the air/fuel mixture. Besides thermal NO_x, there can also occur fuel NO_x and prompt NO_x. The first one refers to NO_x formed from the nitrogen present in the fuel itself. The latter refers to NO_x formed through the rapid reaction of atmospheric nitrogen with HC radicals in the flame front, occurring early in the combustion process, even at lower temperatures [202].

2.5.2.5 Sulfur oxides

These gases are generated from the sulfur present in diesel fuel. The concentration is heavily correlated with the amount of sulfur present in the fuel. Sulfur dioxide is a colourless, toxic gas with an irritating odour. Similar to NO_x emissions, they are also one of the contributors to the formation of acid rain, however, due to regulations, the requirement of low sulfur content of modern diesel fuels has greatly reduced these emissions from diesel exhaust [203].

2.5.2.6 Particulate matter

PM majorly corresponds to the solid carbon soot particles, generated in the fuel-rich zones within the cylinder during combustion, often found in the exhaust of CI engines (smoke). It refers to inhalable particles, usually with a diameter inferior to 2.5 microns, composed of sulphate, nitrates, ammonia, sodium chloride, black carbon, mineral dust, or water [95]. This value is maximum at high load conditions, where fuel is injected to obtain maximum power. Rich mixtures favour the formation of these very small particles in the exhaust gases that obstruct, reflect, or diffuse the light [36], [47]. Black smoke resulting from the excess fuel injection is one of the different types of smoke produced by this soot that is limited and regulated by law [36].

Chapter 3. Case Study

3.1 Preparation of the emulsions

In order to achieve the best possible formulation, different trials had to be performed with different percent by mass ($\%_{m/m}$) of water, diesel, and surfactants. The ultimate goal was to produce an emulsion that would be optimised for engine performance and emissions and stable at a temperature close to 40°C, which is similar to the temperature of the fuel in the tank of a high performance diesel engine during operating conditions.

3.1.1 Equipment, material, and methods

En590 diesel fuel, deionised water, a hydrophilic surfactant, and a lipophilic surfactant were acquired to be used as reagents to produce WiDE. An analytic balance (RADWAG AS 310/C/2), a magnetic stirrer (Stuart Scientific SM3), a thermometer (Enviro-Safe), beakers, pipettes, and flasks were the materials and equipment used to accurately weigh, measure, and mix the different reagents. Figure 3.1 shows the equipment and material used for laboratory testing.

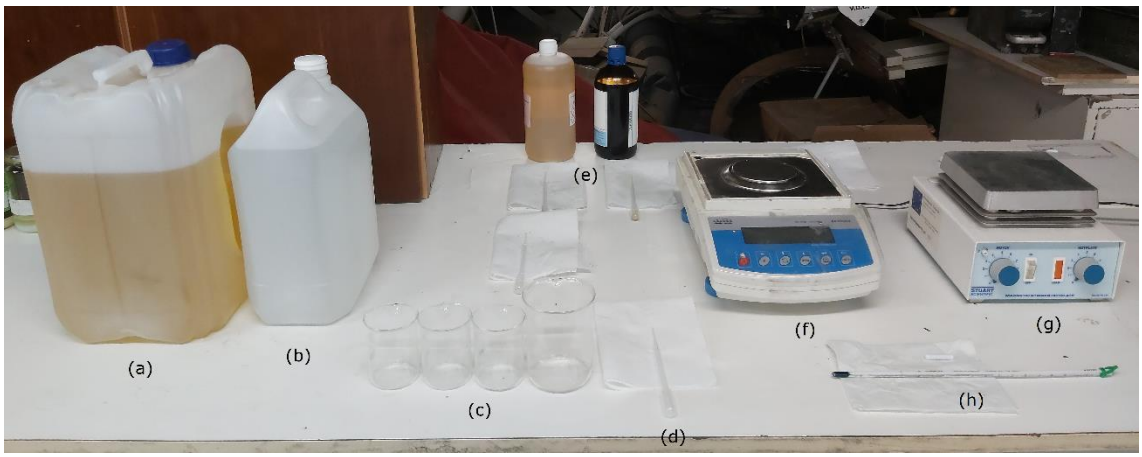

Figure 3.1. Laboratory equipment and material – (a) diesel fuel, (b) deionised water, (c) beakers, (d) pipettes, (e) surfactants, (f) analytic balance, (g) magnetic stirrer, and (h) thermometer.

3.1.2 Laboratory protocol

Initially, for the WiDE composed of 8% water (8% WiDE), the water content $\%_{m/m}$ was set at 8%, and the surfactants content $\%_{m/m}$ at 3%. For the WiDE composed of 16% water (16% WiDE), the water content $\%_{m/m}$ was set at 16%, and the surfactants content $\%_{m/m}$ at 6%. Taking into account these initial parameters, the next step was to test various percentages between the two surfactants. Multiple emulsions were developed, heated, and their properties were observed between 15°C and 60°C. It was observed that a temperature between 40°C and 50°C with a specific surfactant formulation would make the most transparent emulsions, translated in the lowest dispersed water PS, observed by pointing a flashlight on one side of the flask containing the emulsion and watching its light on the opposite side.

After some trials, it was concluded that a mix of 91% and 9% for the hydrophilic and lipophilic surfactants was ideal for 8% WiDE, and a mix of 95% and 5% for the hydrophilic and lipophilic surfactants was ideal for 16% WiDE. It was also found that the higher the water content, the more hydrophilic surfactant was needed. The following protocol was used during the trials for preparing the emulsions:

- Place a beaker in the analytic balance. Tare the balance.
- With a pipette, add the corresponding weight of lipophilic surfactant to the beaker. Tare the balance.
- With a pipette, add the corresponding weight of hydrophilic surfactant to the beaker.
- In another beaker, with a pipette, weigh the corresponding amount of deionised water.
- In another beaker, with a pipette, weigh the corresponding amount of diesel fuel.
- Place the beaker containing the two surfactants in the magnetic stirrer and introduce the stirrer's magnet into the beaker.
- Gradually add the diesel fuel into the beaker in the magnetic stirrer and let it stir for 2 minutes.
- With a pipette, add the deionised water to the beaker, droplet by droplet for 4 minutes.
- For 2 more minutes, leave the beaker in the magnetic stirrer to mix the solution.
- In a thermostatic bath, watch the behaviour of the different emulsions in the temperature range of 15ºC to 60ºC and select the best ones.

3.1.3 Results

After analysing the different samples, the stability of the emulsions was verified. The most stable emulsions at the temperature of 40ºC were selected and chosen to perform different laboratory tests regarding their properties, in addition to diesel. Figure 3.2 shows the emulsions obtained and how water and surfactant percentages affect the visual appearance of the fuels, from translucid (a) to less translucid (c). Even though (b) and (c) may appear opaque, light can still travel through, as was verified with a flashlight, which was also a fundamental property to differentiate between the different emulsion samples, as it is an indication of small PS and low PDI of the dispersed phase, suggesting enhanced stability.

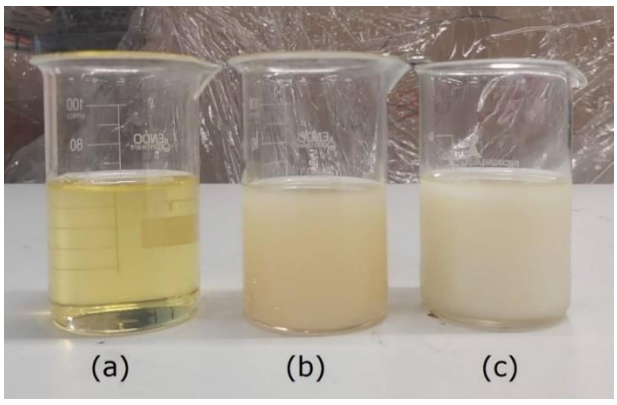

Figure 3.2. (a) Diesel fuel, (b) 8% WiDE, and (c) 16% WiDE at ambient temperature (T = 15ºC).

3.1.3.1 Fuel properties

The density, viscosity, and calorific value, among other properties of the fuels, can affect the spray, mixing, and energy release rate during the engine combustion processes [118]. For this reason, different tests were performed in the original fuel and in the emulsions to observe the variation of these properties between them.

3.1.3.1.1 Density

Density is easily defined as the mass of an object divided by its volume, given by the expression $\rho = m/v$, in g/cm^3. It shows how compact or heavy a fuel is in relation to its volume. It is a key fuel property, directly influencing engine performance. Parameters like cetane number and HV are also related to a fuel's density [204]. The density of the different fuels was tested with a hydrometer at different temperatures (Figure 3.3), and its results are shown in Figure 3.4.

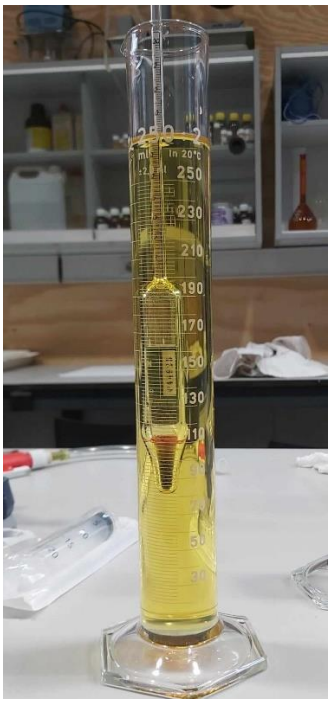

Figure 3.3. Hydrometer.

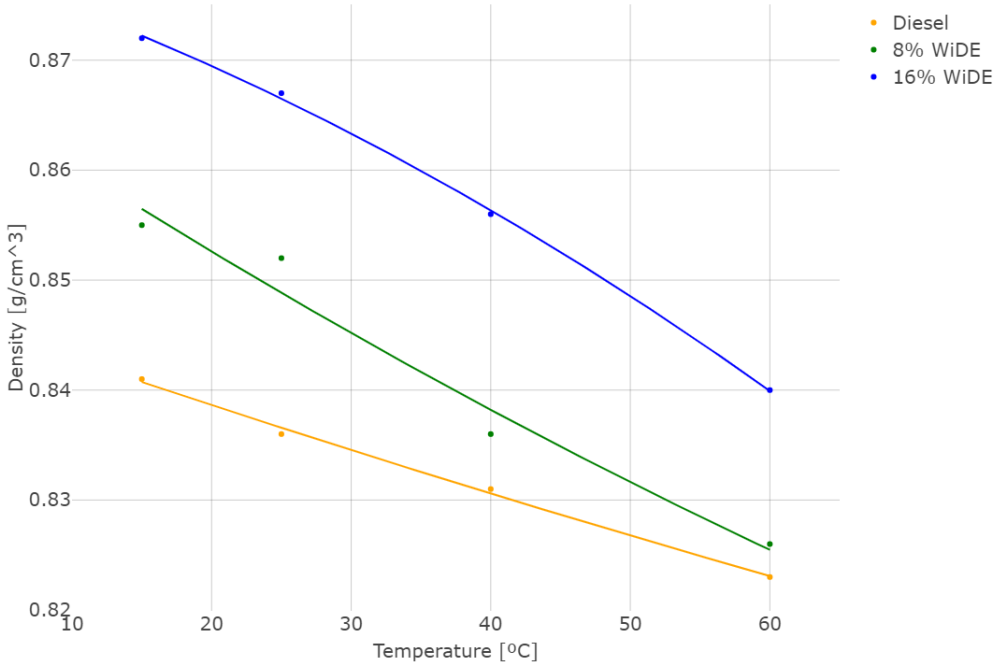

Figure 3.4. Density of the different fuels.

3.1.3.1.2 Viscosity

Viscosity is a measure of a fluid's resistance to flow, to a change in shape, or movement of neighbouring portions to one another [205] and is expressed in Pa.s. It may be thought of as internal friction between the molecules, which opposes the development of velocity gradients within a fluid. There are two types of viscosity: dynamic (measures a fluid's internal resistance to flow) and kinematic (measures how fast a fluid flows under gravity). Fluidity is the opposite of viscosity and is a measure of the ease of flow [206]. Fluids can also be divided into two major groups according to their viscosity behaviour: Newtonian and non-Newtonian. Newtonian fluids (like water and diesel) follow a fundamental law where the shear stress is directly proportional to the rate of shear. The viscosity of such fluids is only influenced by changes in temperature and pressure, and it can be quantified using a viscometer. The Navier-Stokes equations serve as a mathematical model to describe a Newtonian fluid's behaviour. In non-Newtonian fluids (like WiDEs), the viscosity does not remain constant under different shear rates. The relationship between the shear stress and the rate of shear is not linear, and depending on the forces applied to the fluid, its viscosity can change [207]. The viscosity of non-Newtonian fluids should be measured with a rheometer. Figure 3.5 shows the viscosity differences between the fluids. While shear stress is the force that causes deformation or displacement of a material parallel to a surface, shear rate describes how quickly that deformation occurs.

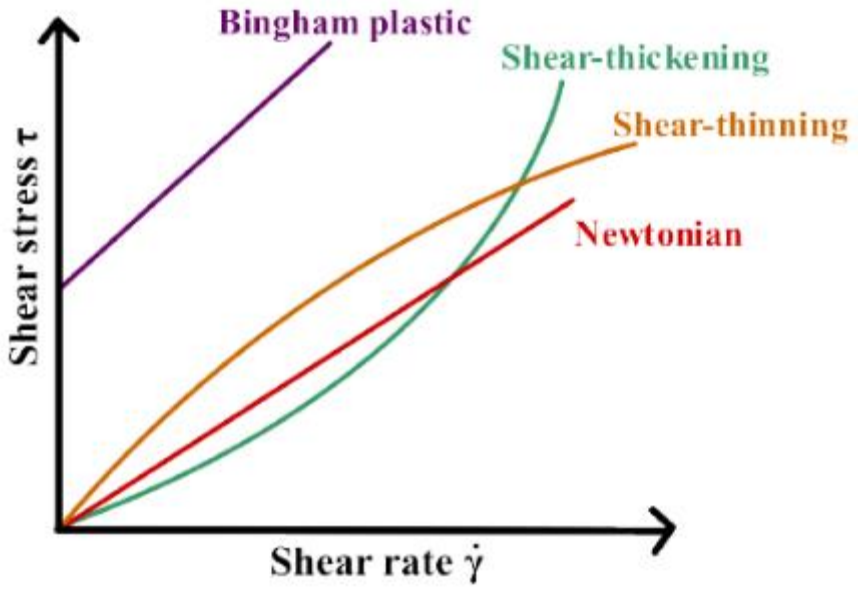

Figure 3.5. Apparent viscosity of Newtonian and non-Newtonian fluids [208].

In general, an increase in the surface tension, and indirectly in the viscosity of a diesel fuel, will result in a corresponding increase in the ignition delay. This is because a more viscous fuel will be more resistant to flow and will take longer to vaporise and mix with the O_2 in the combustion chamber. As a result, it will take longer for the fuel to ignite and start the combustion process. It is worth noting that the effect of viscosity on ignition delay may not be the same for all diesel fuels. The specific relationship between viscosity and ignition delay can vary depending on the chemical composition and physical properties of the fuel, as well as the operating conditions of the engine. The same Ostwald viscometer with a constant of 0.01332 at 100°F (suitable for the expected range of viscosities) was used to measure viscosity during the tests (Figure 3.6). The change in the kinematic viscosity with the increase of temperature for the different fuels was tested and is shown in Figure 3.7.

Figure 3.6. Ostwald viscometer in a thermostatic bath.

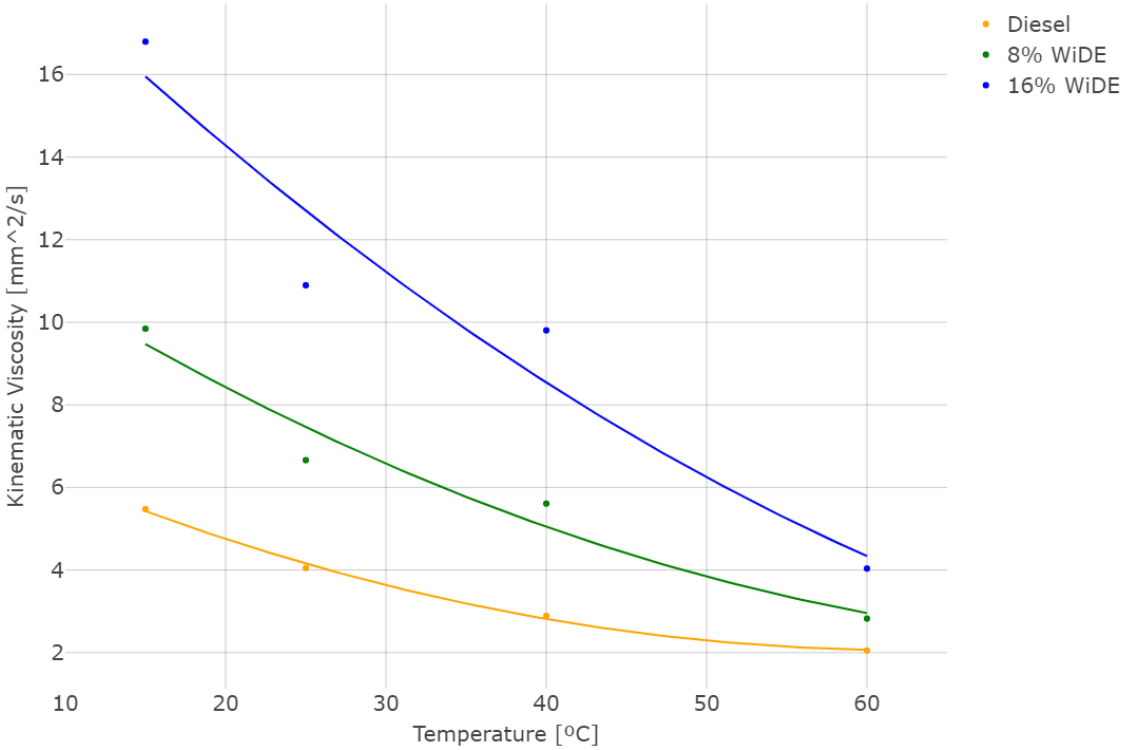

Figure 3.7. Kinematic viscosity of the different fuels.

As can be seen, higher fuel temperatures will translate into similar viscosities between the emulsified fuels and the viscosity of diesel fuel. Since the mass flow rate of a fuel is heavily correlated with its kinematic viscosity (Poiseuille's law, Equation 3.1), because it incorporates

fluid density as a part of its measurement, and therefore is a measure of velocity (as opposed to dynamic viscosity which is a measure of force), to achieve more similar injection delays, during engine tests the emulsions in the fuel tank were heated in a thermostatic bath, while diesel fuel was at the temperature reached during engine operation (20-25°C):

$$Q = \frac{\pi r^4 \Delta P}{(8\eta L)}, \tag{3.1}$$

where Q is the volumetric flow rate in m^3/s, r is the radius of the pipe in m, ΔP is the pressure difference between the two ends of the pipe in Pa, η is the dynamic viscosity of the fluid in Pa.s, and L is the length of the pipe in m.

3.1.3.1.3 Heating value

As stated before, the HV of a fuel is related to the amount of heat released during its stoichiometric combustion, where the reagents and products remain in the same pressure and temperature conditions or the same volume and temperature conditions [209]. This value can be calculated by using a calorimeter, which is a device used to measure the amount of heat exchanged in a chemical or physical reaction. For this case, it was utilised a bomb calorimeter, model 6050 from Parr, as seen in Figures 3.8 and 3.9.

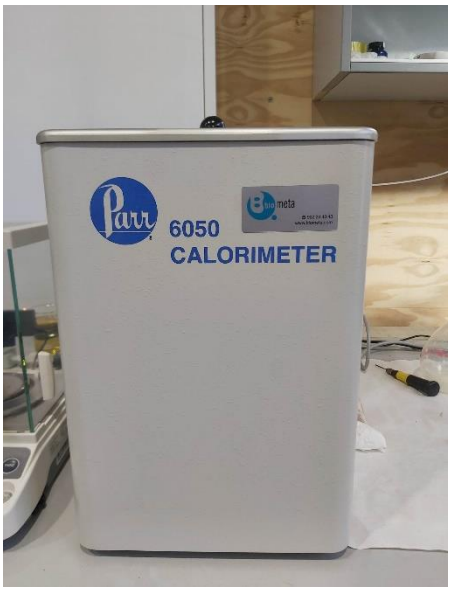

Figure 3.8. Parr 6050 calorimeter.

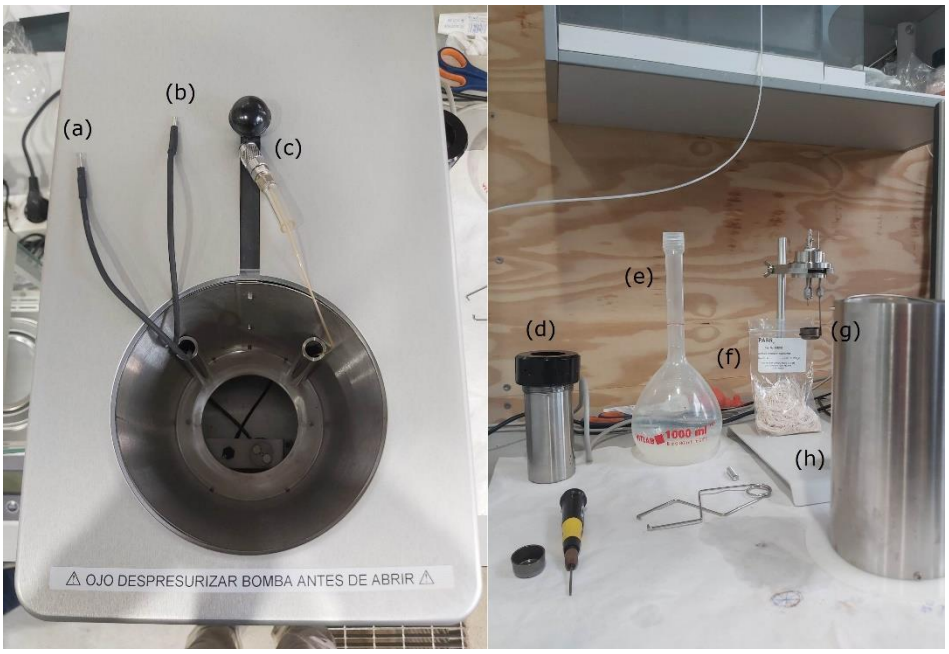

Figure 3.9. (a) positive electrode, (b) negative electrode, (c) O_2 valve, (d) bomb, (e) water supply, (f) ignition thread, (g) fuel sample, and (h) jacket.

By maintaining a constant temperature in the jacket, the heat generated at constant volume and an initial pressure of 30 bar in the combustion of the sample fuel will lead to a rise in the water temperature. By knowing the sample weight and the water temperature variation, the equipment will give us the HHV, where water is present in a liquid phase in the combustion products. To calculate the LHV, where water is not condensed and exists in a vapour form (characteristic of diesel engine combustion) [210], the following equation is given [209]:

$$LHV_v = HHV_v - 9\Delta H_{vap.water} Y_h, \tag{3.2}$$

where LHV_v is the LHV at constant volume, HHV_v is the HHV at constant volume, $\Delta H_{vap.water}$ is the enthalpy of vaporisation of water, and Y_h is the mass fraction of hydrogen. At standard conditions, for a temperature of 25ºC and ambient pressure of 1 bar, the $\Delta H_{vap.water}$ is 2.3051 MJ/kg [209].

On top of that, and because the heat addition phase in the diesel cycle is performed at constant pressure, another expression is given to calculate LHV_p [209]:

$$LHV_p = LHV_v - 0.61942 Y_h - 0.07743 Y_o, \tag{3.3}$$

where LHV_p is the LHV at constant pressure and Y_o is the mass fraction of oxygen.

In order to calculate the mass fraction of hydrogen and oxygen in the different fuels, an elementary analysis needs to be performed on the diesel fuel, surfactants, and deionised water. For the diesel fuel, the mass fraction of hydrogen was estimated from [209], since similarly to the

one utilised in this thesis, it follows the norm EN590 for diesel fuels commercialised in Europe. For the surfactants and deionised water, the mass fractions of hydrogen and oxygen were estimated from their corresponding formulas, as shown in Table 3.1. Equations 3.4 and 3.5 give the mass fraction of hydrogen and oxygen for each of the reagents:

$$Y_h = \frac{W_h}{W_r}, \tag{3.4}$$

$$Y_o = \frac{W_o}{W_r}, \tag{3.5}$$

where W_h is the molar weight of hydrogen, W_o is the molar weight of oxygen, and W_r is the total weight of the reagent.

Table 3.1. Psychochemical properties of the reagents.

	Chemical Formula	Molecular Weight [g/mol]	Hydrogen [% m/m]	Oxygen [% m/m]
Diesel Fuel	$C_{15.18}H_{29.13}$	211.70	13.87	-
Deionised Water	H_2O	18.02	11.19	88.81
Hydrophilic Surfactant	$CH_3(CH_2)_nC(=O)N(CH_2CH_2OH)_2$*	299.45	11.11	16.03
Hydrophobic Surfactant	$C_{24}H_{44}O_6$	428.61	10.35	22.40

* n can vary from 8 to 12. The mean value of 10 was considered for calculation procedures.

To now calculate the hydrogen and oxygen mass fraction for each of the emulsions, we need to multiply the mass fraction of each component by its corresponding weight in the total fuel. The ratio of surfactant/water for both emulsions is 0.375. Only the percentage of the hydrophilic surfactant compared to the hydrophobic one is changed (plus 4% for 16% WiDE). The remaining is diesel fuel. This gives a final composition of 89% diesel fuel, 8% water, and 3% formulation for 8% WiDE and 78% diesel fuel, 16% water, and 6% formulation for 16% WiDE. The mass fractions of hydrogen and oxygen for each of the emulsions are given by Equations 3.6 and 3.7:

$$Y_{h.e} = \%_{diesel}.Y_{h.d} + \%_{water}.Y_{h.w} + \%_{formulation}.\%_{EH}.Y_{h.EH} + \%_{formulation}.\%_{EL}.Y_{h.EL}, \tag{3.6}$$

$$Y_{o.e} = \%_{diesel}.Y_{o.d} + \%_{water}.Y_{o.w} + \%_{formulation}.\%_{EH}.Y_{o.EH} + \%_{formulation}.\%_{EL}.Y_{o.EL}, \tag{3.7}$$

where $Y_{h.e}$ is the mass fraction of hydrogen of the emulsion, $Y_{o.e}$ is the mass fraction of oxygen of the emulsion, $Y_{h.d}$ is the mass fraction of hydrogen in diesel, $Y_{h.w}$ is the mass fraction of hydrogen in deionised water, $Y_{h.EH}$ is the hydrogen mass fraction of the hydrophilic surfactant, $Y_{h.EL}$ is the hydrogen mass fraction of the lipophilic (hydrophobic) surfactant, $Y_{o.d}$ is the mass fraction of

oxygen in diesel, $Y_{o.w}$ is the mass fraction of oxygen in deionised water, $Y_{o.EH}$ is the oxygen mass fraction of the hydrophilic surfactant, and $Y_{o.EL}$ is the oxygen mass fraction of the lipophilic surfactant.

For 8% WiDE:

$Y_{h.e}$ = 0.89 x 13.87 + 0.08 x 11.19 + 0.03 x 0.91 x 11.11 + 0.03 x 0.09 x 10.35 = 13.57%.

$Y_{o.e}$ = 0.08 x 88.81 + 0.03 x 0.91 x 16.03 + 0.03 x 0.09 x 22.40 = 7.60%.

For 16% WiDE:

$Y_{h.e}$ = 0.78 x 13.87 + 0.16 x 11.19 + 0.06 x 0.95 x 11.11 + 0.06 x 0.05 x 10.35 = 13.27%.

$Y_{o.e}$ = 0.16 x 88.81 + 0.06 + 0.95 x 16.03 + 0.06 x 0.05 x 22.40 = 14.28%.

Finally, it is now possible to use Equation 3.2 to calculate the $LHV_{v,}$ and from this value, use Equation 3.3 to calculate the real LHV of the fuels in diesel engine combustion, as shown in Table 3.2. By multiplying the specific energy (MJ/kg) and the fuel's density at 15ºC, we can also obtain the energy density (MJ/L) for each of the fuels.

Table 3.2. HV of the different fuels.

Fuel	HHV_v (MJ/kg)	HHV_v (MJ/L)	LHV_p (MJ/kg)	LHV_p (MJ/L)
Diesel	45.49	38.26	42.53	35.77
8% WiDE	41.68	35.64	38.77	33.15
16% WiDE	38.27	33.37	35.42	30.89

3.2 Engine performance tests

3.2.1 Equipment, material, and methods

3.2.1.1 Engine

The engine selected for testing the different fuels was a Hatz 1B40 (Figure 3.10), a four-stroke, single-cylinder, naturally aspirated, Euro 5, direct injection diesel engine. Its specifications are shown in Table 3.3.

Figure 3.10. Hatz 1B40 engine.

Table 3.3. Engine specifications.

Specifications	Hatz 1B40
Operation Cycle	4-stroke
Cylinders	1
Valves per Cylinder	2
Bore (mm)	88
Stroke (mm)	76
Engine Displacement (cm^3)	462
Injection System	Direct injection
Injection Pressure (bar)	200
Compression Ratio	20.5:1
Empty Weight (kg)	48
Cooling System	Air cooling
Maximum Torque (Nm)	23.4
Maximum Power (kW)	7.3

Even though it's not an engine designed to be used in aerospace applications, given its heavy weight and very low power-to-weight ratio, similar principles apply when compared to other CI engines. By testing it in load conditions often encountered in aerial vehicles, it is possible to have a good idea of how the fuels will perform between them and verify the efficiency of the fuels in the different scenarios. Ideally, an aircraft diesel engine, mostly commercialised as a jet-A/A1 engine,

would be utilised. However, the operational ones are very expensive, impractical to carry out experiments due to aviation regulations, and could not be acquired.

3.2.1.2 Engine test-bench

To test and characterise the performance of an engine, it is necessary a test-bench, often composed of a dynamometer, which absorbs the energy of the engine and measures the force produced. The test-bench used can be seen in Figures 3.11 and 3.12.

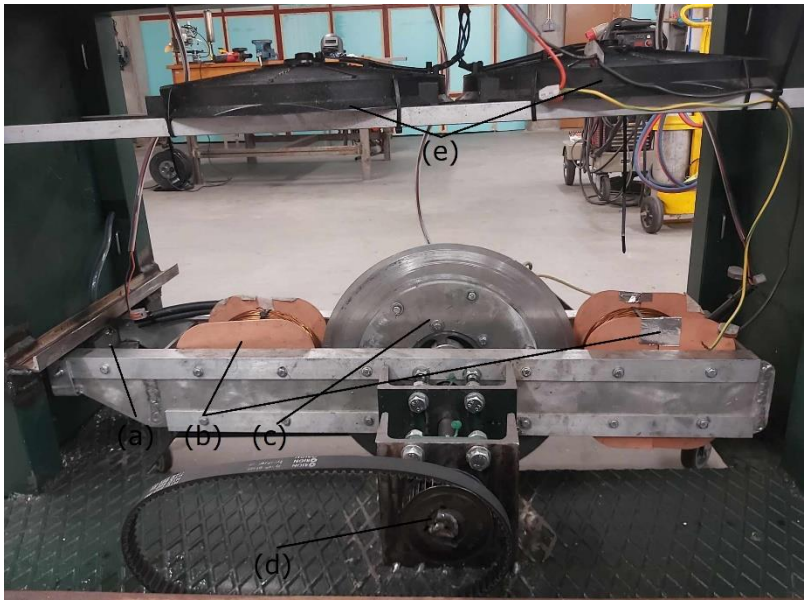

Figure 3.11. Engine test-bench (front-view) – (a) load cell, (b) copper coils, (c) rotating aluminium disk, (d) driveshaft, and (e) cooling fans.

Figure 3.12. Engine test-bench (rear-view) – (a) starter motor, (b) hall sensor, and (c) dynamometer controller.

It is composed of an electromagnetic brake acting as a dynamometer that was dimensioned to dissipate a power of 30 kW at 3000 rpm. A common configuration of an eddy current brake (ECB) and its cross section can be seen in Figure 3.13.

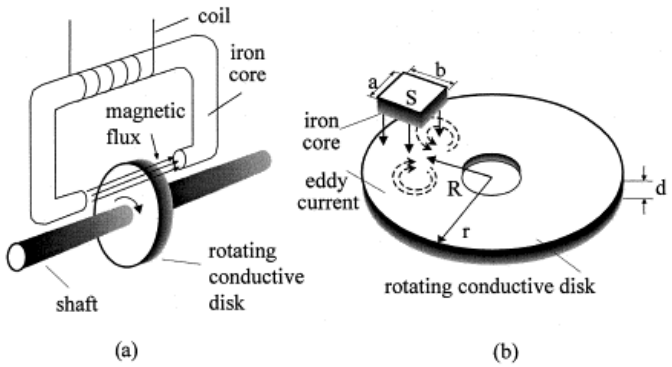

Figure 3.13. (a) ECB configuration and (b) cross section of the iron core and disk [211].

An electric conductive disk rotates through a magnetic field that induces eddy currents opposing the original magnetic field and producing a braking torque. Ferro-magnetic materials in the rotating disk are usually avoided since they reduce the effectiveness of the currents induced in the disk. In the engine bench, two opposed C-shaped electromagnets induced the eddy currents on a single rotating disk, producing a magnetic field, as seen in Figure 3.14. Nunes and Brójo [211] wrote a paper that gives a detailed explanation of how the ECB was designed and the mathematical model utilised.

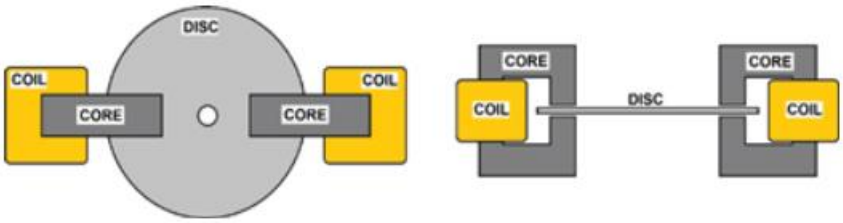

Figure 3.14. Illustration of the ECB utilised [211].

At first, the eddy current dynamometer was projected to be operated with stainless steel, which would induce enough current to completely stall small engines and allow better control of the load supplied to the coils and later to the disk. However, these induced currents weren't enough to stop the diesel engine, since its maximum torque was higher than the one able to be produced in the dynamometer. For this reason, different aluminum disks were dimensioned (around 20 times more conductive than stainless steel) with different thicknesses until reaching the ideal point where the disk, together with reinforcements of the same material in both faces would allow to stall the engine while keeping the disk from warping (which happened to other disks of similar material, given its lower density and toughness, when compared to stainless steel). It is also important to address that given the very high electrical conductivity of aluminum (3.8×10^7 $ohm^{-1}m^{-1}$), the current supplied to the coils and the consequential eddy current braking

is basically instantaneous, which requires a very sensitive approach by supplying current softly and in a balanced manner for both coils avoiding excessive heating on the rotating disk, which could lead to warping.

3.2.1.3 Emission gas analyser and opacimeter

The selected emission gas analyser was an AVL DiTest gas 1000 model 2301, by AVL (Figure 3.15). It was designed to measure emissions gases from ICEs, specifically CO, CO_2, HC, O_2, and NO. Complementary, an opacimeter was also used to measure the smoke opacity in the exhaust, an AVL DiSmoke 480, also from AVL (Figure 3.16). Both instruments were connected to each other to deliver synchronised values for the emission data. Their specifications and measurement tolerances are shown in Table 3.4.

Figure 3.15. Emission gas analyser.

Figure 3.16. Opacimeter.

Table 3.4. Emission gas analyser and opacimeter specifications.

Measuring Ranges	*Accuracy*
CO: 0-15% vol.	+/- 0.03% vol.
CO_2: 0-20% vol.	+/- 0.5% vol.
HC: 0-30000 ppm vol.	+/- 10 ppm vol.
O_2: 0-25% vol.	+/- 5% o. M.
NO: 0-5000 ppm vol.	+/- 50 ppm vol.
Lambda: 0-9.999	Calculated from CO, CO_2, HC, and O_2
Opacity: 0-100%	+/- 0.1%
Absorption (k-value): 0-99.99 m^{-1}	+/- 0.01 m^{-1}

The exhaust gas analyser uses the non-dispersive IR method to measure CO and CO_2 by detecting the amount of IR light absorbed by the gases. CO and CO_2 molecules absorb IR radiation at specific wavelengths. The analyser passes an IR beam through the sample, measuring its intensity before and after passing through the gases. The difference in intensity is proportional to the concentration of the gases. HC emissions are measured by the flame ionisation detector, by burning the sample gas in a hydrogen flame. This produces ions, which are collected by electrodes, generating a current proportional to the concentration of HC in the sample. O_2 is measured by an electrochemical sensor, which contains an electrolyte and electrodes leading to a redox reaction when O_2 is present. This generates a current proportional to the O_2 concentration. NO is measured by the chemiluminescence method by reacting it with O_3, producing excited NO_2. When returning to its ground state, it emits light with intensity directly proportional to the concentration of NO [212]. The opacimeter measures smoke opacity by shining a light through the exhaust smoke, which gets blocked or absorbed by the smoke particles. A sensor on the opposite side measures how much light makes it through the smoke, and by comparing it with the original light, it tells how opaque the smoke is [213].

3.2.1.4 Sensors

In order to measure the different parameters during engine testing, different sensors had to be installed. These sensors rely on electronic components and therefore on voltage differences and can be digital or analog.

3.2.1.4.1 Load cell and amplifier

A load cell is used to measure force. It is an aluminium piece composed of a strain gauge that changes its resistance when subjected to a load. The load cell's metal structure deforms when weight is being applied, causing the strain gauge to change its resistance and convert it into an electrical signal read by an amplifier to display the force produced. Two S-Type load cells were utilised (DYLY-103), as well as two HX711 amplifiers to decode the signal received, as shown in Figures 3.17 and 3.18.

Figure 3.17. S-Type load cell.

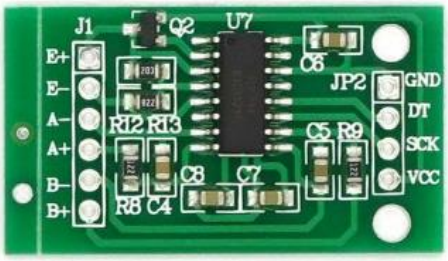

Figure 3.18. HX711 amplifier.

The first load cell is a 20 kg load cell connected to the aluminium structure in the test-bench, which supports the copper coils. When the engine is operating and current is being supplied to the coils, it produces a force in the structure. By multiplying this force by the distance to the rotor axis, it is able to give results for the torque output of the engine. By also using the results from the speed sensor, it is possible to calculate the power output as well. The second load cell is a 10 kg load cell and is used in a balance with the fuel tank of the engine on top of it, as seen in Figure 3.19. By recording the loss in weight in the fuel tank and dividing it by the corresponding time interval, we can have results for the mass flow rate of the different fuels. Both cells were calibrated accordingly.

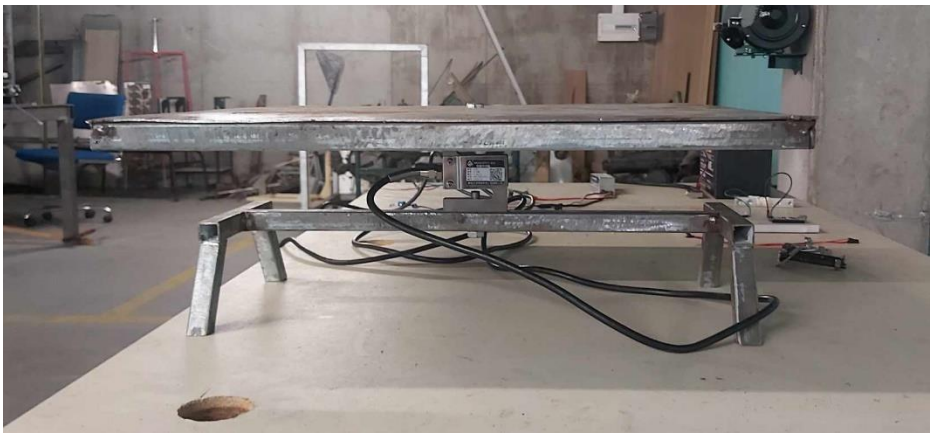

Figure 3.19. Balance for the fuel tank.

3.2.1.4.2 Speed sensor

The speed sensor can be found in the testing bench and Figure 3.20. It was used a hall effect sensor, which is a transducer that responds to a magnetic field. When a magnetic field is applied perpendicularly to a current-carrying conductor, the voltage difference generated can be used to determine its presence and direction, allowing the monitoring of the engine speed by generating pulses.

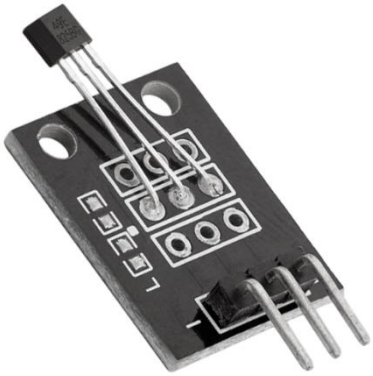

Figure 3.20. Hall sensor.

3.2.1.4.3 Type K thermocouple and amplifier

A type K thermocouple, as shown in Figure 3.21, was utilised to monitor the temperature at the engine's block. It is composed of two different metal alloys where voltage is generated due to temperature differences between the two junctions. The two metals intersect in the hot junction, which is exposed to the temperature being measured. The cold junction is maintained at a controlled temperature.

Figure 3.21. Type K thermocouple.

To digitise the signal from the thermocouple, a MAX6675 amplifier is used, as shown in Figure 3.22. It performs the cold-junction compensation and provides a digital output that can be easily interfaced with a microcontroller.

Figure 3.22. MAX6675 amplifier.

3.2.1.5 Sensors, Arduino, and LabVIEW hookup

In order to read the output from the sensors, a microcontroller is necessary. The ones utilised in this thesis were arduinos nano, as shown in Figure 3.23.

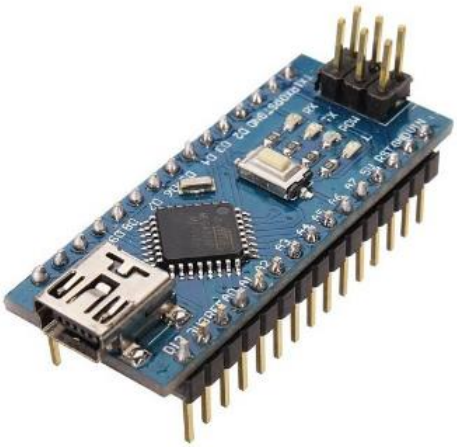

Figure 3.23. Arduino nano.

In Arduino 1, inside the test bench, the load cell for measuring the engine torque and the hall effect sensor for measuring the engine speed are connected. In Arduino 2, the load cell for monitoring the weight loss of the fuel tank and the type k thermocouple to measure the engine's block temperature were connected. The two arduinos were connected to the computer via two different USB ports. The LabVIEW software 2019, from NI instruments, was used to synchronise the response of both arduinos and to export synchronous data from the sensors in a desired time interval. The data was exported to different CSV files to be later imported into the R programming software. Regarding the exhaust emissions test, the AVL analyser and AVL opacimeter were connected together to display synchronous data. VSPEmulator software was used to create a virtual serial port since the equipment was not ready for data logging. RealTerm software was used to read and save the data points into CSV format. The block diagram designed to acquire the data in LabVIEW is shown in Figure 3.24. The interface for real-time monitoring of the engine

data is shown in Figure 3.25. The programming code for arduino 1 and arduino 2 is shown in annexes B.1 and B.2. The code for the test-bench arduino, as well as the LabVIEW block diagram, were adapted from Nunes [211], who developed the ECB.

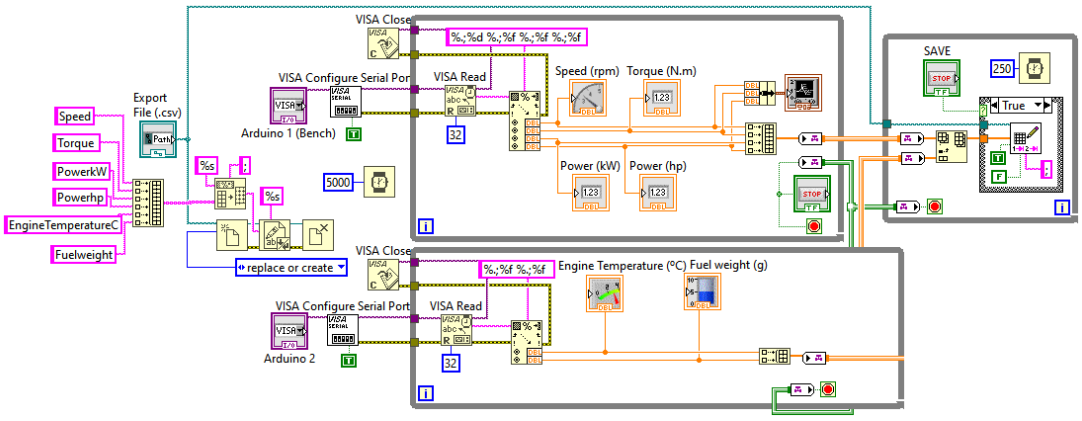

Figure 3.24. LabVIEW block diagram.

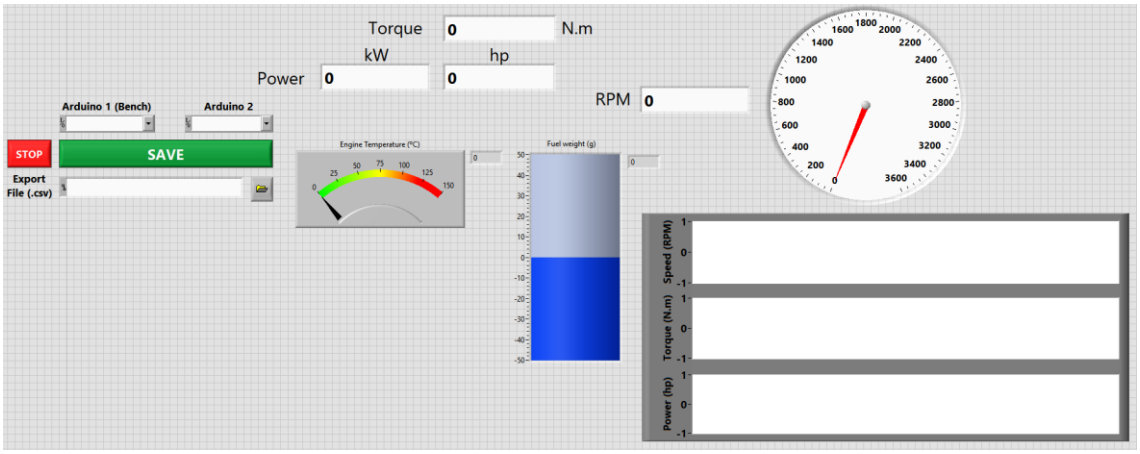

Figure 3.25. LabVIEW user interface.

3.2.1.6 Assembly scheme

The engine was coupled to the test bench through a pulley and belt arrangement. Taper lock bush 1108 was used for both pulleys (22.4mm inner diameter for the dynamometer shaft and the engine shaft) to allow the connection between the engine and the bench (Figure 3.26).

Figure 3.26. Pulley and taper lock bush in engine shaft.

The engine's power take-off was machined from 25.4mm to 22.4mm to fit the taper lock bush. The 1108 pulleys were also similar, with the same number of teeth to allow the same gear ratio between the parts. The sensors were connected to microcontrollers that were connected to a PC, via a USB cable, to allow the monitoring and a synchronous display of results during the time sequence. Figures 3.27 and 3.28 show the scheme used for the engine and fuels testing.

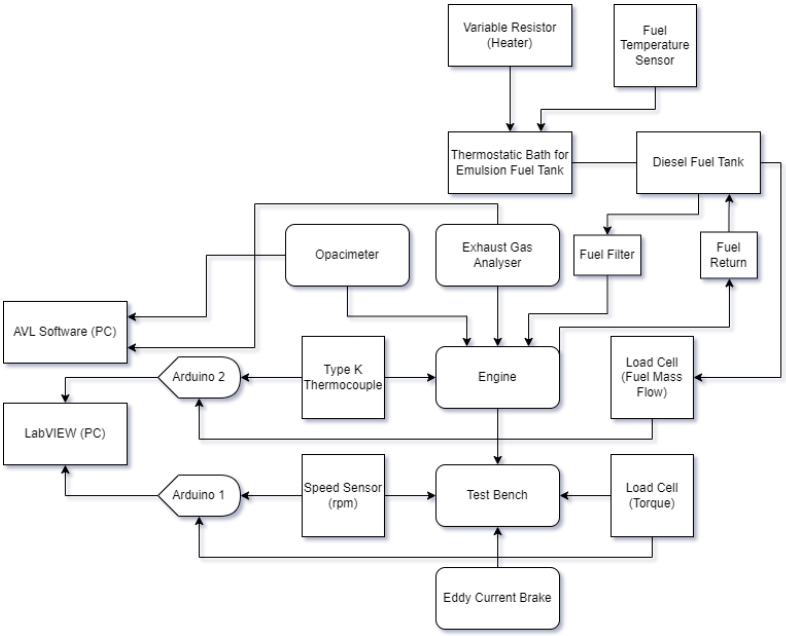

Figure 3.27. Test-bench diagram.

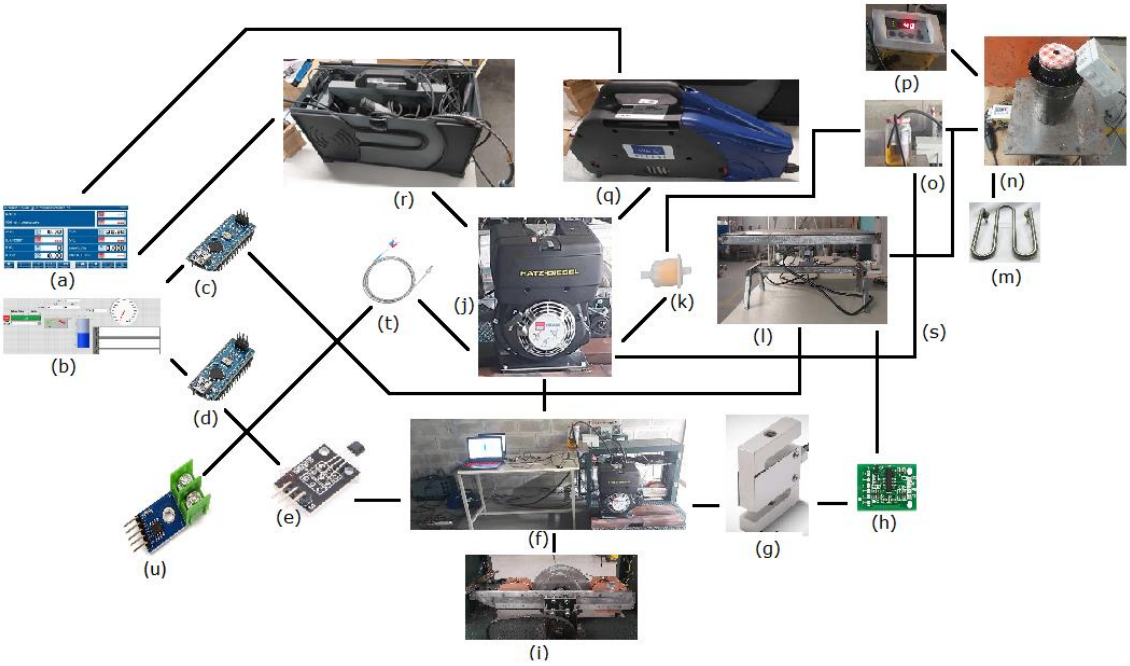

Figure 3.28. Test-bench layout - (a) emission data acquisition, (b) performance data acquisition, (c) arduino 1, (d) arduino 2, (e) hall sensor (speed), (f) test-bench, (g) load cell for torque measurement, (h) HX711 load cell amplifier, (i) eddy current dynamometer, (j) diesel engine, (k) fuel filter, (l) load cell and fuel tank balance for fuel consumption measurement, (m) heating unit (variable resistor), (n) thermostatic bath for emulsion fuel tank, (o) diesel fuel tank, (p) fuel temperature sensor, (q) opacimeter, (r) exhaust gas analyser, (s) fuel return, (t) type K thermocouple, and (u) MAX6675 thermocouple amplifier.

Figure 3.29 shows the engine in the test-bench. Figure 3.30 shows the mixing process and 8% WiDE at T = 40°C and Figure 3.31 shows the 16% WiDE in a thermostatic bath.

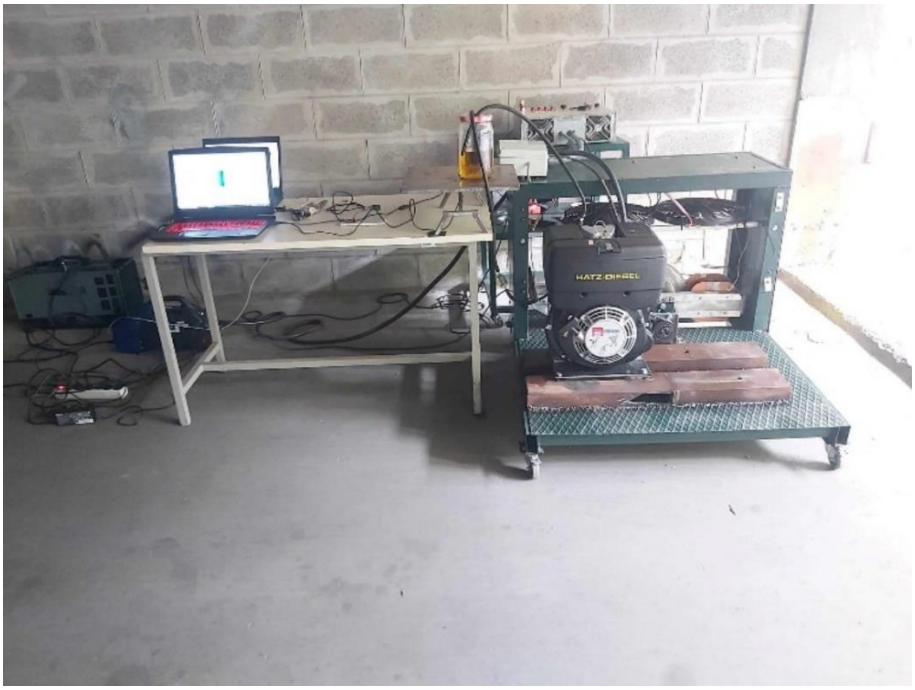

Figure 3.29. Bench-test of diesel fuel.

Figure 3.30. Low-energy mixing method and 8% WiDE at T = 40ºC.

Figure 3.31. 16% WiDE in a thermostatic bath.

The evaporation of water occurred at temperatures below its boiling point of 100ºC on the liquid's surface due to the addition of localised heat from the resistance in the thermostatic bath. When heating the water to 45ºC and 55ºC for both emulsions, the weight loss on the balance would be higher and not consistent between both emulsions due to this evaporation. An average value could be calculated in grams per minute of water loss, and added to the final weight to calculate the real fuel consumption, however, heating cycle durations were not constant. For this reason, polyethylene glycol 400 was used as the thermostatic bath liquid as it would not evaporate, leading to more precise fuel consumption results, while also maintaining a constant temperature in the oil bath where the flask was inserted during engine testing.

3.2.2 Bench-test protocol

In order to obtain the most optimal and accurate results when testing the different fuels, some precautions had to be taken. The first one was to record the ambient conditions when testing the different fuels, which were very similar. The air temperature, pressure, and relative humidity for the different tests are shown in Table 3.5.

Table 3.5. Ambient conditions during engine tests.

Environmental Conditions	Diesel, 8% WiDE, and 16% WiDE
Temperature [°C]	15.9 – 16.1
Relative Humidity [%]	67 - 73
Pressure [hPa]	937 - 942

The second precaution was to measure the different fuels' viscosities and try to match them by heating the emulsified fuels (more viscous than diesel at the same temperature) so that the different fuel flows (expressed in g/s) could be more similar (according to Poiseuille's law), as well as no changes to the injection timing had to be made (an increase in the kinematic viscosity due to the water content in the fuel may decrease its lubricity and delay the injection timing).

The following protocol was followed during engine tests:

- Perform a manual cold-start on the engine and leave it in idle position for 10 minutes to reach its operating temperature.
- Monitor ambient temperature, pressure, and relative humidity conditions.
- After the warm-up phase, insert the exhaust gas analyser and opacimeter probes simultaneously in the engine's exhaust system.
- Accelerate the engine to 3000 rpm.
- Supply voltage and current to energise the dynamometer's coils as a way to load and brake the engine.
- Adjust the voltage and the current settings in both coils to achieve a combined electrical power output of 25W, which will be constant for the different speeds. If the increase to the desired load leads to a slight decrease in the engine speed, accelerate it back to 3000 rpm.
- Once the engine is stable, record the results for performance and emissions over 1.5 minutes.
- Decelerate the engine to 2500 rpm.
- Once the engine is stable, record the results for performance and emissions over 1.5 minutes.
- Decelerate the engine to 2000 rpm.
- Once the engine is stable, record the results for performance and emissions over 1.5 minutes.
- Decelerate the engine to 1500 rpm.
- Once the engine is stable, record the results for performance and emissions over 1.5 minutes.
- Remove the exhaust gas analyser and opacimeter probes, and the load applied.
- Shut-down the engine.
- Repeat the procedure for 50W, 75W and 100W.

- Repeat the procedure for all the fuels. In addition to diesel fuel testing, use a thermostatic oil bath to heat both emulsified fuels to a targeted temperature of 45°C and 55°C with the goal of attaining comparable viscosities to diesel.

3.2.3 Raw results

The tables and figures shown in Annex C represent the raw results obtained from the sensors by directly measuring the different variables, excluding some extreme data points due to signal interference. As torque and speed are not equal between the different fuels as they should have been, these results should not be used as a representation of the real difference between the fuels tested. They should serve as a comparison to observe how the posterior statistical corrected results deviate from the original ones. For each load condition, the mean value of each parameter was calculated and used as a representation in the plots. Fuel consumption data points are not represented since it was calculated based on the slope of a linear regression, and not at every time interval. BSFC and TE values are also not represented as they depend on fuel consumption data points. Exhaust gases data points are not represented as they were calculated individually, at different time stamps, and not fully synchronised with engine speed values.

Chapter 4. Results Analysis

4.1 Introduction to R

R is an open-source programming language directed towards data manipulation and statistical analysis. This software, along with RStudio (an integrated development environment), fits the needs of this project, because it allows to visualise and manipulate gathered data, perform the best possible analysis, by choosing the most adequate statistical models, and plot results in an interactive way while maintaining good precision during the whole process of the data analysis. The wide variety of different packages that are publicly available and that can be utilised at will was also a major reason that led to the selection of this software. Over 8000 lines of code were written during the whole data processing to produce the different dataframes, equations, models, tables, and figures shown in this work. However, only small chunks of code related to some data analysis are shown in this chapter for clarification.

4.2 Correction and statistical analysis of the performance and emissions tests in R

Values from variables such as speed, torque, and therefore power, which is related to the previous ones, should be the same for any fuel. For a constant dynamometer load, constant speed, constant ambient conditions, and constant disk temperature, the same eddy currents should be induced in the disk producing an equal braking force, which multiplied by the distance to the load cell (arm) would produce an equal braking torque at a given speed for any fuel. A good example of similarity would be a propeller, which always produces the same torque at a given speed. Despite ambient conditions being very similar, the speed and especially the torque obtained for the different fuels were significantly different, mainly due to differences in disk temperatures and unstable current supply to the coils during tests. Increasing temperatures reduce the conductivity of an aluminium disk due to increased thermal vibrations of the atoms within the material. This leads to greater scattering of electrons moving through the lattice, which impedes the flow of electrons, resulting in higher electrical resistance and reduced conductivity. Therefore, for a constant dynamometer load, fewer currents would be induced in a hotter disk, which would lead to a reduced braking torque being recorded in the dynamometer. In addition, the power supply from the dynamometer to the coils did not remain constant during the tests, especially at lower loads, leading to variations in the force measured. Both these aspects are very significant because less torque means less power at a given speed. If the engine is consuming a certain mass of fuel every second to sustain a given power, higher power means a reduced BSFC. Even though an increase in engine power should also lead to a slight increase in the mass flow rate of fuel, increasing engine power presents a much more significant contribution towards decreasing BSFC.

4.2.1 Performance

4.2.1.1 Outlier treatment

After filtering out very few and extreme data entry errors due to sensors interference during data logging, the next step was to observe the relationship between the loss of weight in the fuel tank and the corresponding time interval, so that fuel consumption could be calculated for each case. A linear regression was conducted to determine the slope, corresponding to the fuel consumption of the engine in g/s. As fuel consumption can not be negative (it only is because the balance is losing weight over time), the coefficient was multiplied by -1. In the following chunks of code and for each case, FuelType is replaced by diesel, 8% WiDE, and 16% WiDE, Load is replaced by 25W, 50W, 75W, and 100W, and Speed is replaced by 1500 rpm, 2000 rpm, 2500 rpm, and 3000 rpm.

```
model_FuelConsumption_FuelType_Load_Speed <- lm( FuelWeight_FuelType_Load_Speed ~ TimeSequence_FuelType_Load_Speed,
                                                 data = dataframe_FuelConsumption_FuelType_Load_Speed )

coefficients( model_FuelConsumption_FuelType_Load_Speed )[ 2 ]*( -1 )
```

Figure 4.1. Linear regression model for fuel consumption determination.

Cook's distance was the method applied to identify influential data points affecting the estimated regression coefficients. The threshold was set to 4 (a typical value) so that no significant number of points would be removed. For every case, Equation 4.1 was used.

$$D_i = \sum_{j=1}^{n} \frac{(\hat{y}_j - \hat{y}_{j(i)})^2}{p.MSE}, \tag{4.1}$$

where D_i is Cook's distance for the ith observation, $\hat{y}_j$ is the jth fitted value from the regression model, $\hat{y}_{j(i)}$ is the jth fitted value from the model when the ith observation is excluded, p is the number of parameters in the model, and MSE is the mean squared error of the regression model. For this analysis, an observation with $D_i > 4$ was considered highly influential.

```
cooksd <- cooks.distance( model_FuelConsumption_FuelType_Load_Speed )

influential <- as.numeric( names( cooksd )[ ( cooksd > ( 4/length( FuelWeight_FuelType_Load_Speed ) ) ) ] )

model_FuelConsumption_FuelType_Load_Speed <- lm( FuelWeight_FuelType_Load_Speed ~ TimeSequence_FuelType_Load_Speed,
                                                 data = dataframe_FuelConsumption_FuelType_Load_Speed[ -influential, ] )
```

Figure 4.2. Outlier detection and removal from the linear regression model.

Figures 4.3 to 4.14 show the fuel consumption of the different fuels at different engine speeds and load conditions.

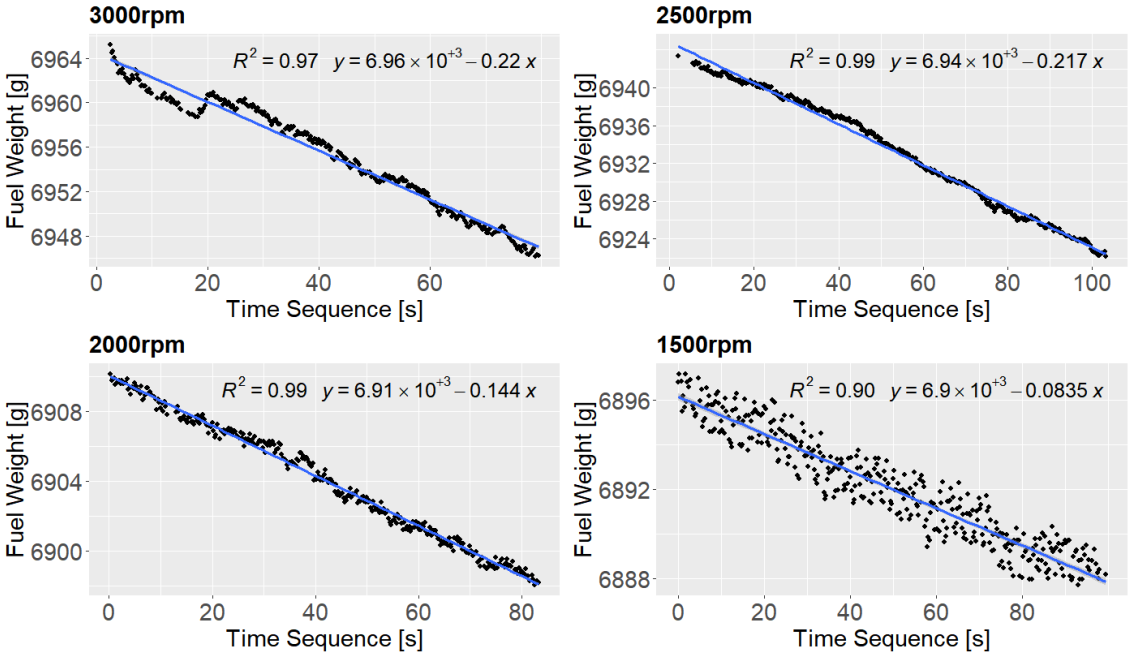

Figure 4.3. Mass flow rate of diesel fuel at different speeds at 25W load.

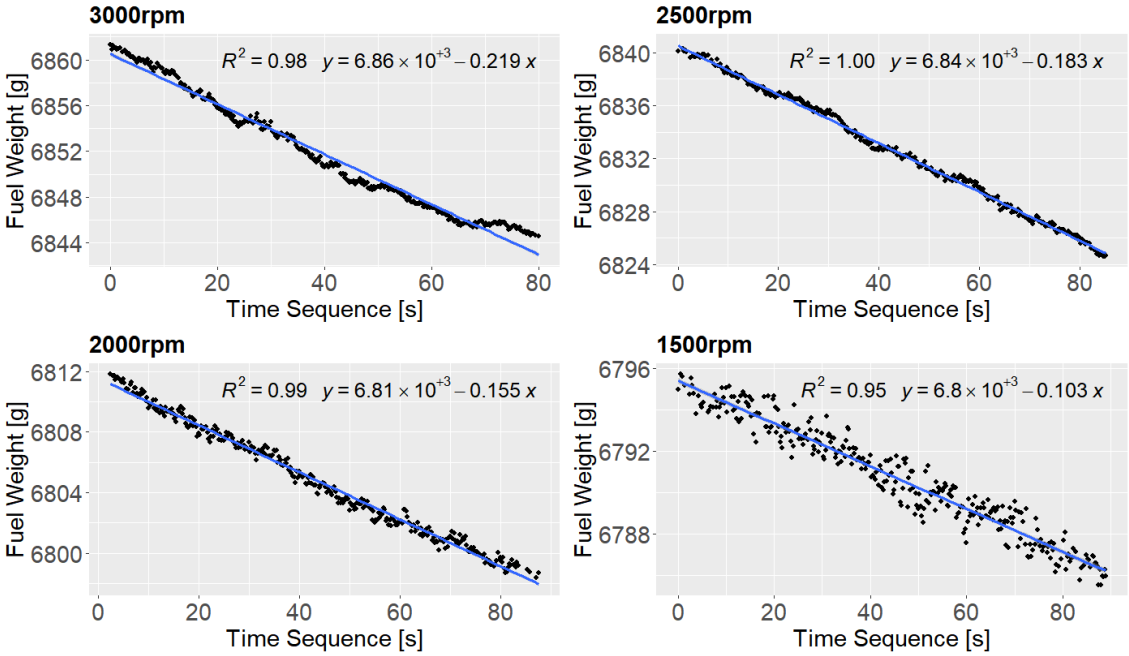

Figure 4.4. Mass flow rate of diesel fuel at different speeds at 50W load.

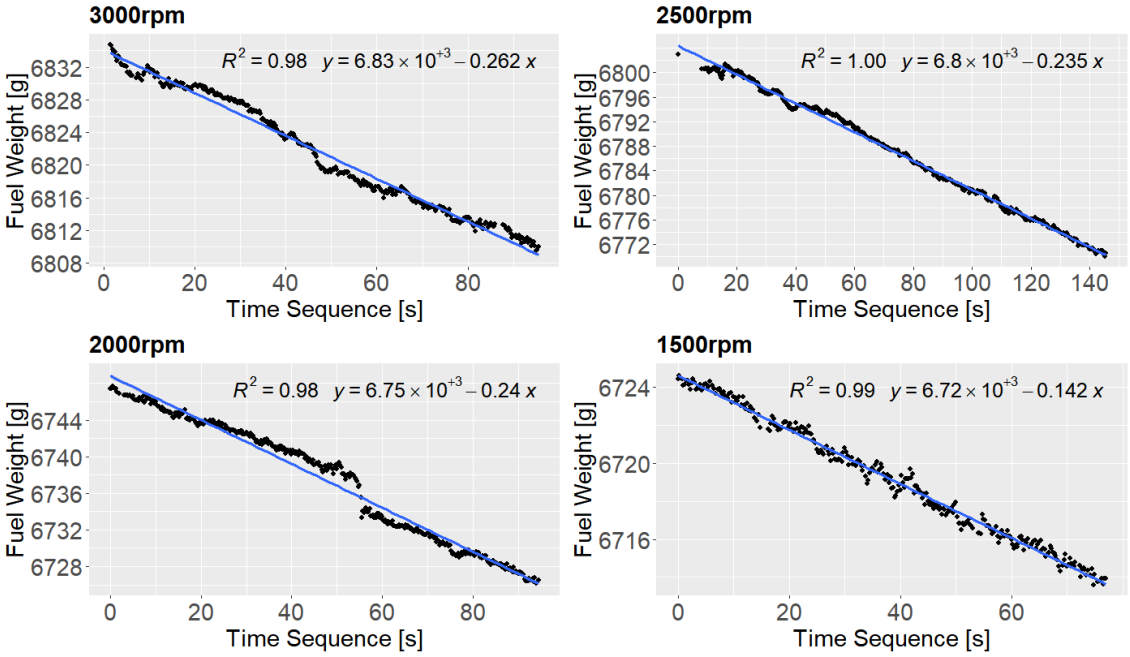

Figure 4.5. Mass flow rate of diesel fuel at different speeds at 75W load.

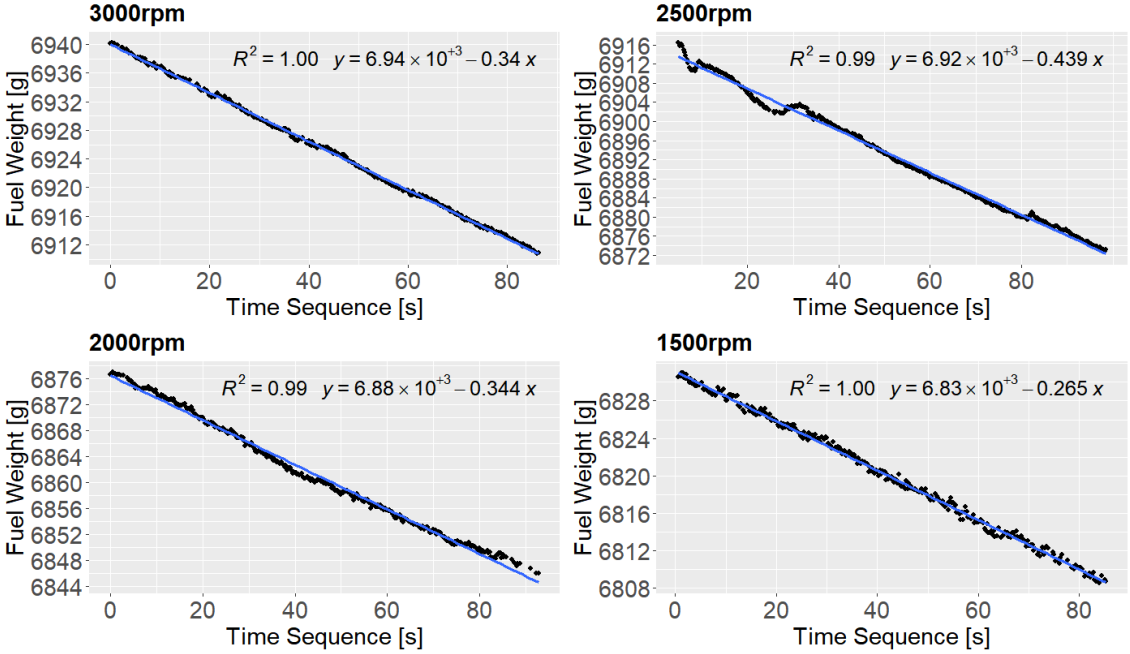

Figure 4.6. Mass flow rate of diesel fuel at different speeds at 100W load.

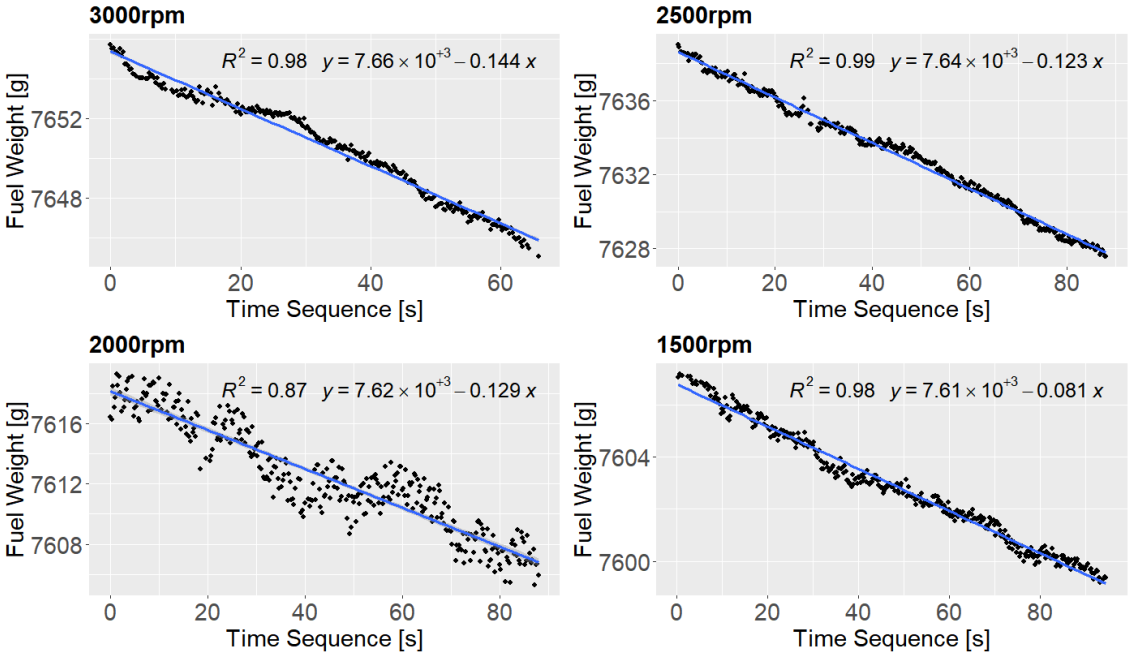

Figure 4.7. Mass flow rate of 8% WiDE at different speeds at 25W load.

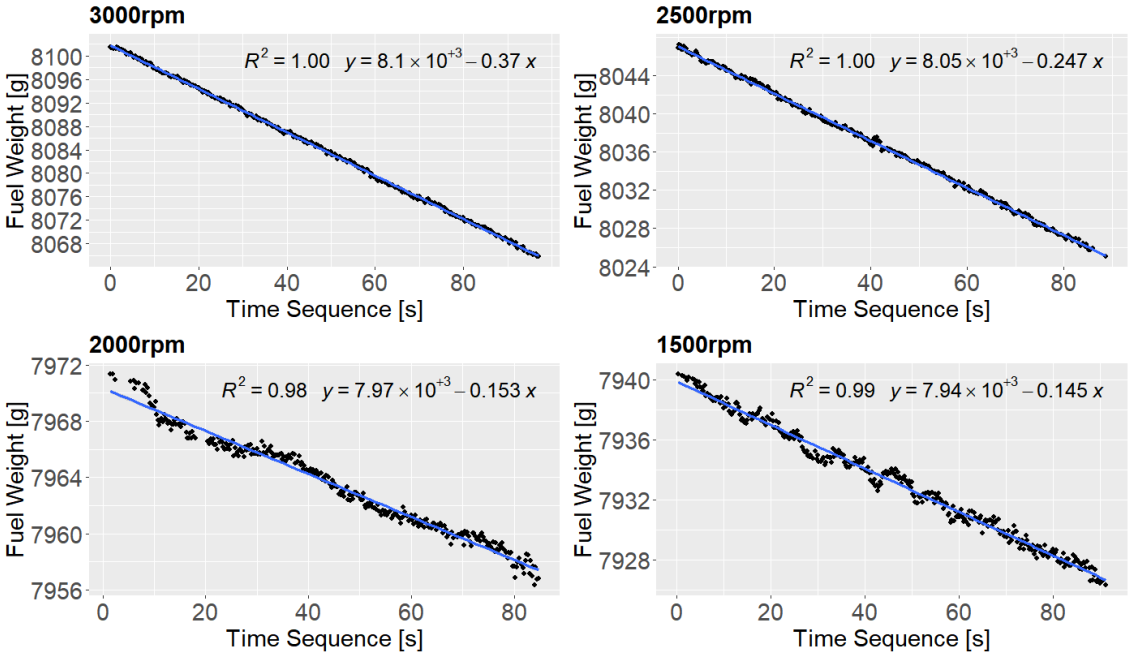

Figure 4.8. Mass flow rate 8% WiDE at different speeds at 50W load.

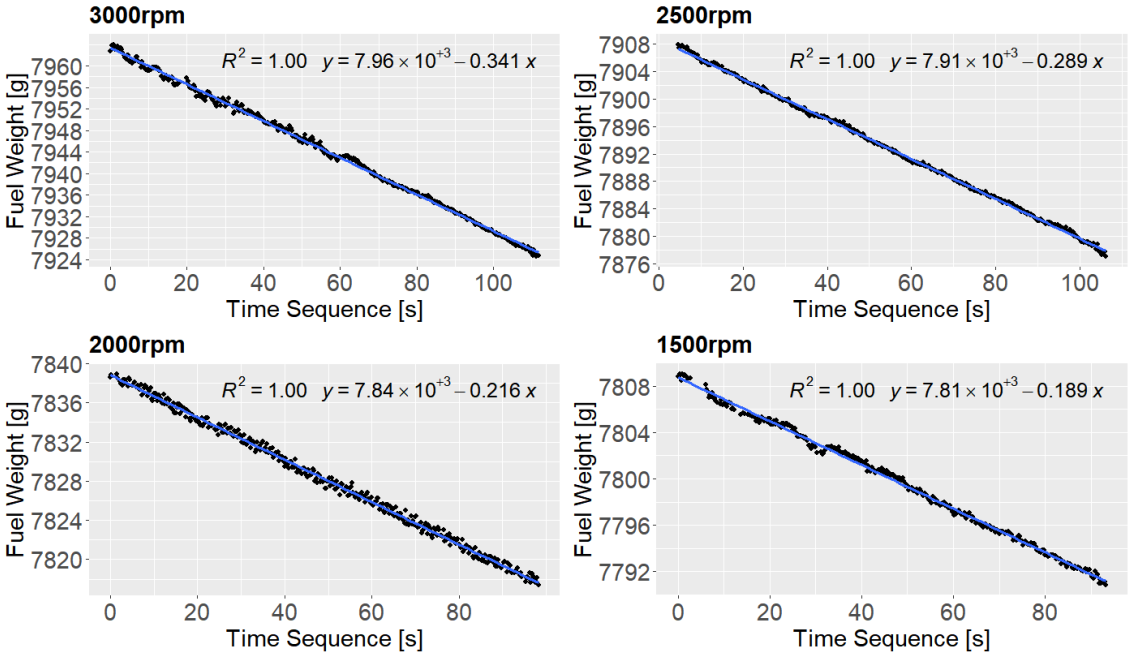

Figure 4.9. Mass flow rate of 8% WiDE at different speeds at 75W load.

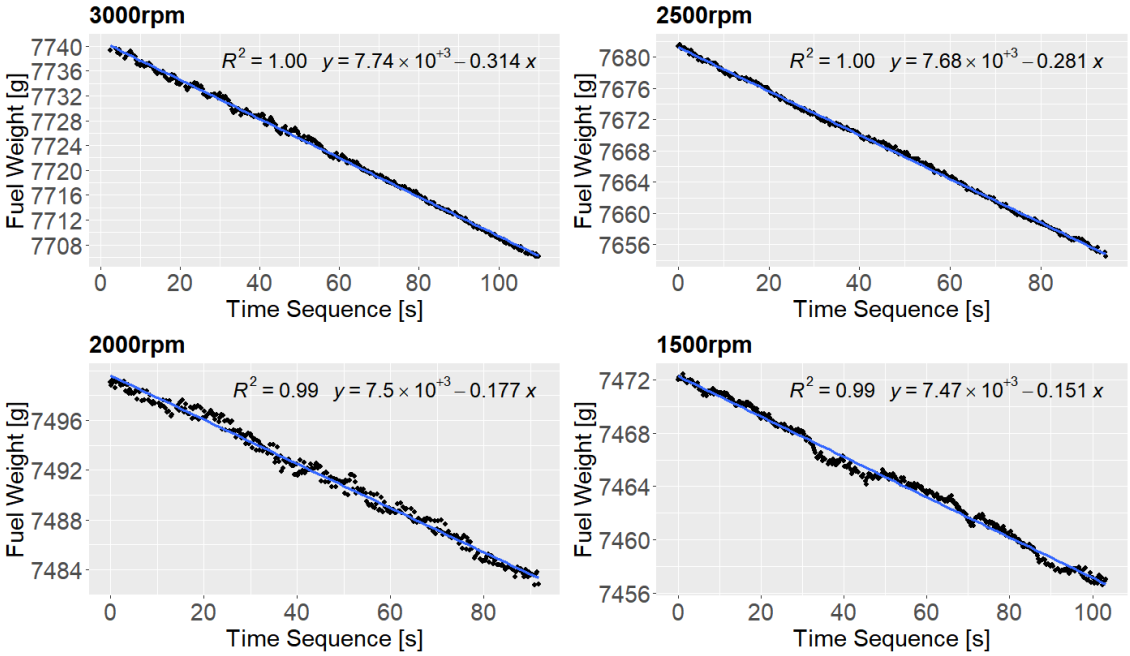

Figure 4.10. Mass flow rate of 8% WiDE at different speeds at 100W load.

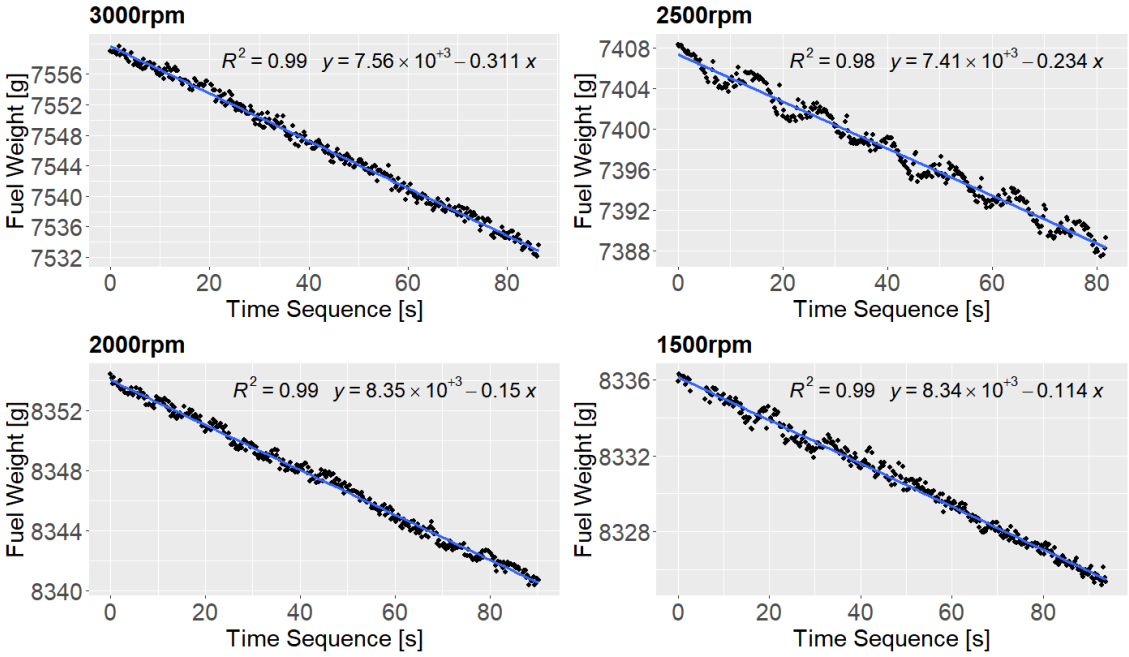

Figure 4.11. Mass flow rate of 16% WiDE at different speeds at 25W load.

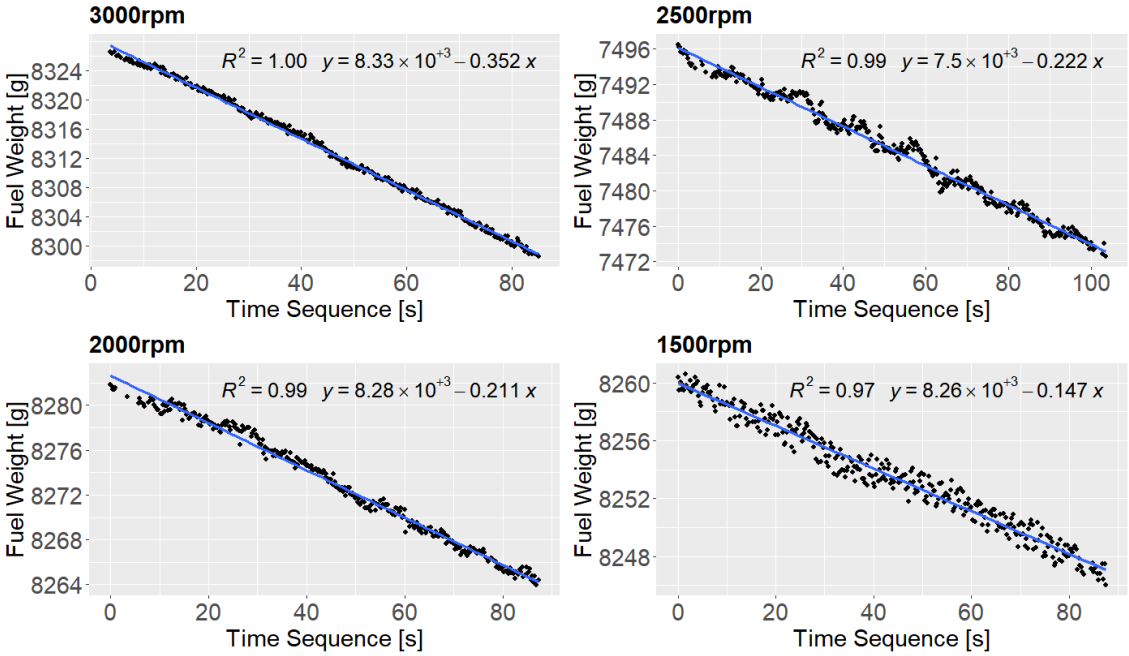

Figure 4.12. Mass flow rate of 16% WiDE at different speeds at 50W load.

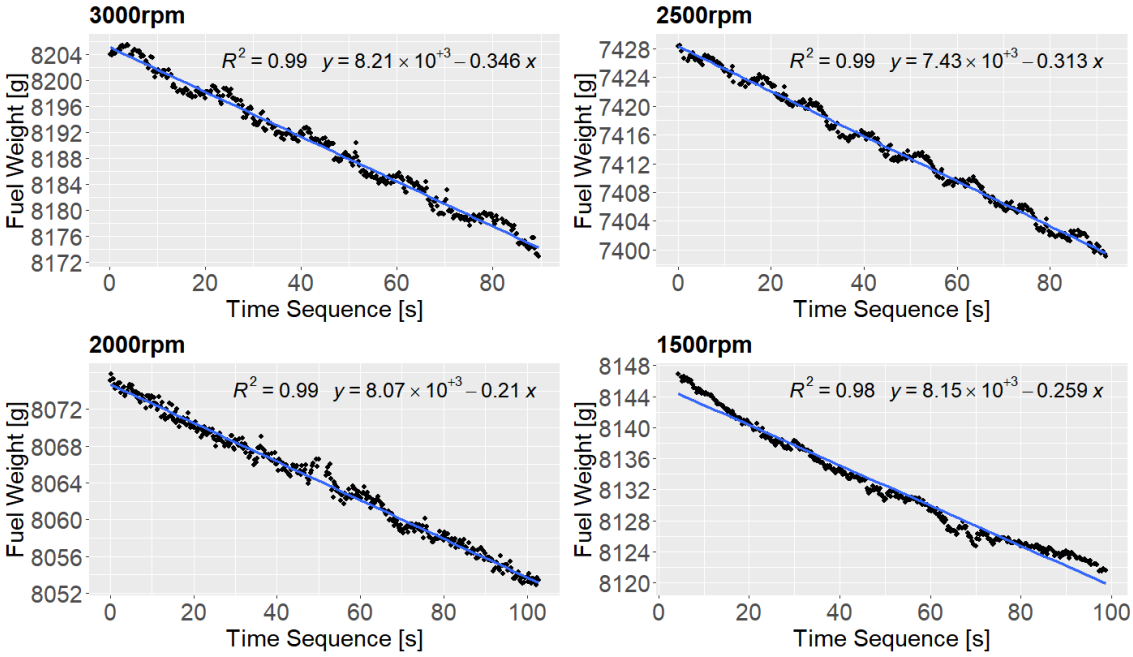

Figure 4.13. Mass flow rate of 16% WiDE at different speeds at 75W load.

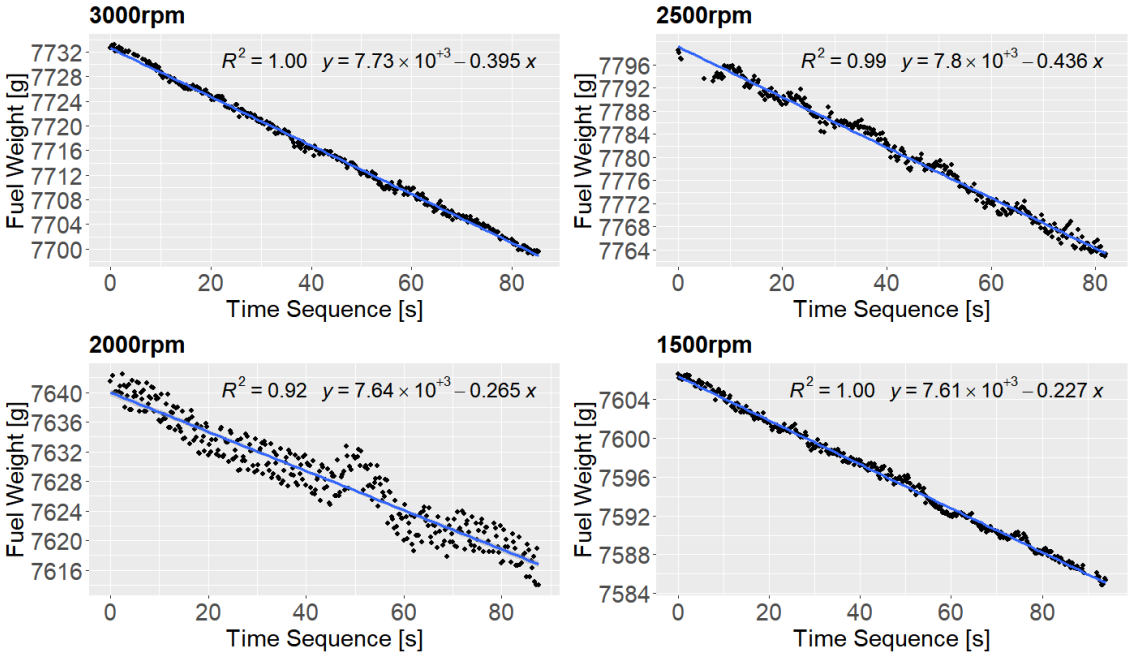

Figure 4.14. Mass flow rate of 16% WiDE at different speeds at 100W load.

Higher dispersions of points along the line are a consequence of engine vibrations transmitted through the fuel lines to the fuel tank, which were more intense at specific operating speeds and conditions, where the engine was more unstable. Even though various experiments were done to reduce those vibrations and the noise associated, difficulties in doing so were encountered.

4.2.1.2 Speed and torque relationship

To use the same speed values for every case, a linear regression was applied between torque and speed for each fuel (Figures 4.16, 4.17, and 4.18). The torque values to be predicted were at constant speed values of 1500 rpm, 2000 rpm, 2500 rpm, and 3000 rpm.

```
model_Torque_FuelType_Load <- lm( Torque_FuelType_Load ~ Speed_FuelType_Load, data = Mean_FuelType_Load )
model_Torque_FuelType_Load_xvalues <- data.frame( Speed = c( 3000, 2500, 2000, 1500 ) )
model_Torque_FuelType_Load.predict <- predict( model_Torque_FuelType_Load, newdata = model_Torque_FuelType_Load_xvalues )
model_Torque_FuelType_Load.predict <- data.frame( model_Torque_FuelType_Load.predict )
model_Torque_FuelType_Load.predict <- cbind( model_Torque_FuelType_Load_xvalues, model_Torque_FuelType_Load.predict )
```

Figure 4.15. Prediction of BT values for fixed engine speeds.

Despite that an increase in engine speed should theoretically lead to an increase in fuel consumption, by increasing engine speed, the braking torque is also reduced, which would in turn reduce the fuel consumption. Due to opposite tendencies of these two variables, the fuel consumption was kept constant when predicting the new engine torques for fixed speeds.

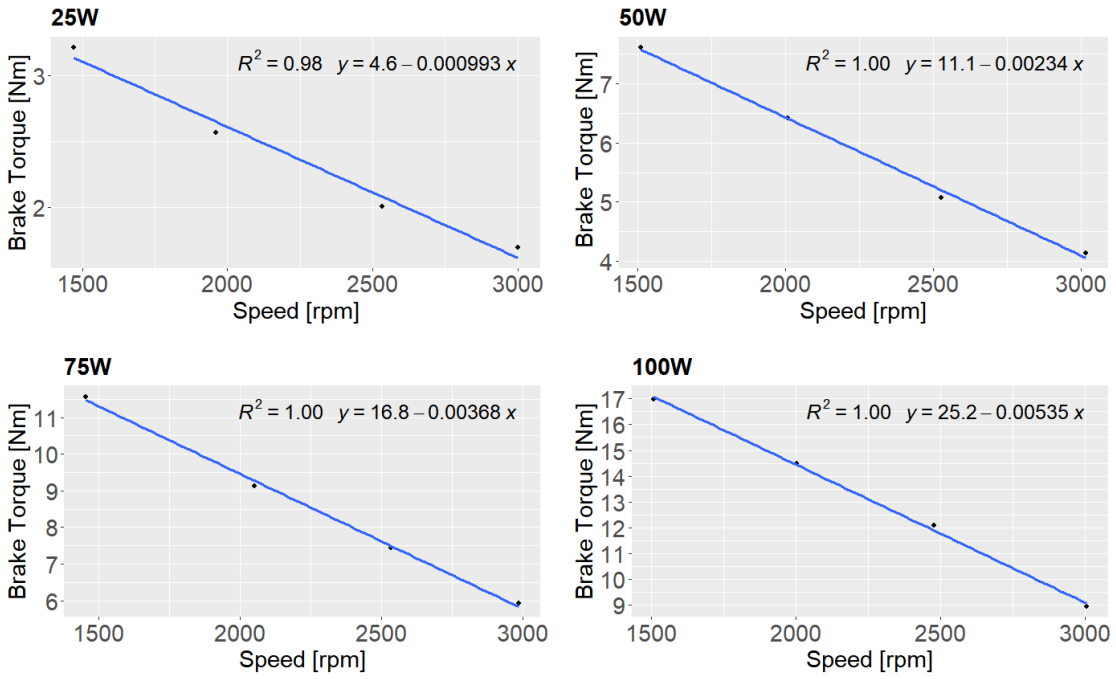

Figure 4.16. Speed vs BT relationship of diesel fuel.

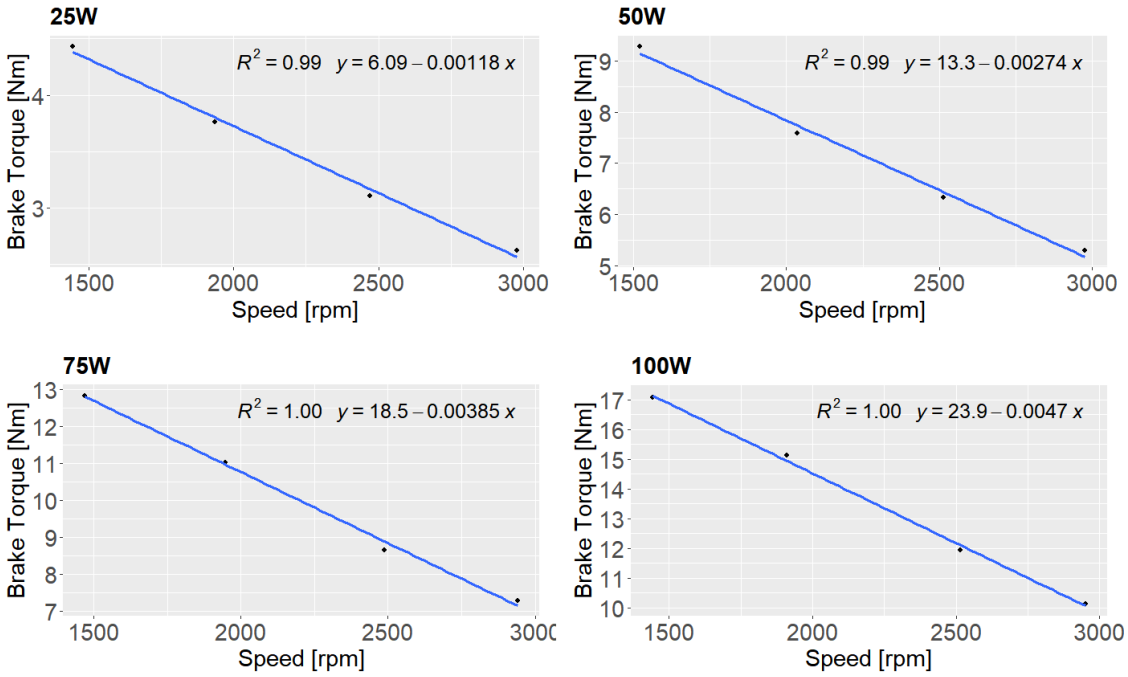

Figure 4.17. Speed vs BT relationship of 8% WiDE.

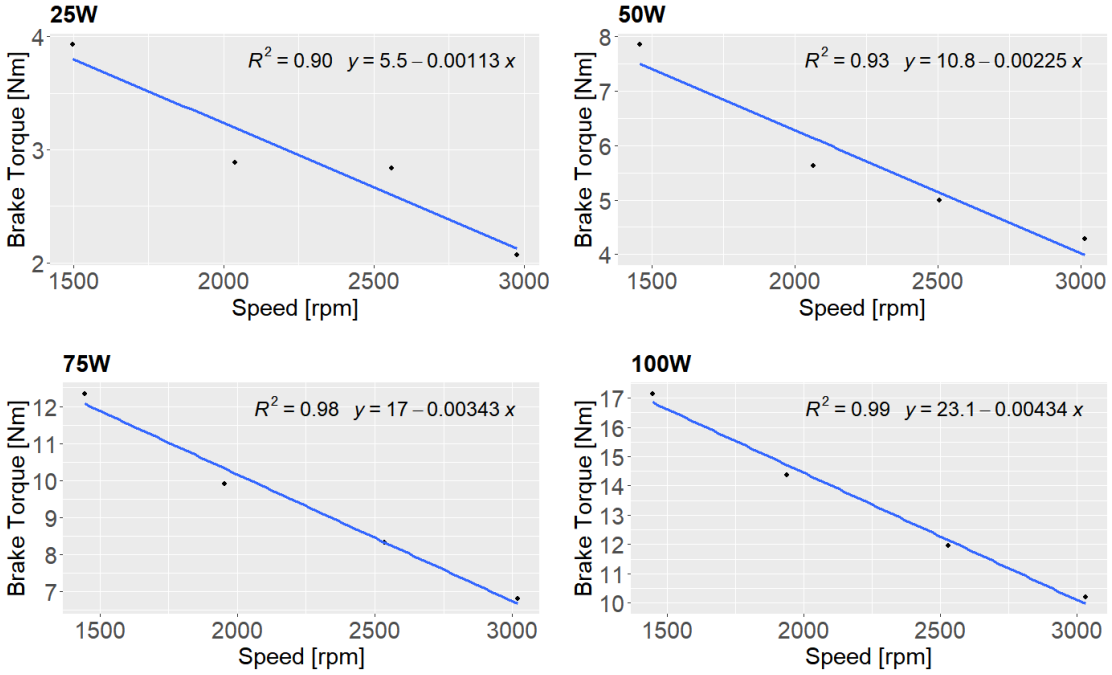

Figure 4.18. Speed vs BT relationship of 16% WiDE.

4.2.1.3 Torque and power

After predicting the new torque values for the speeds of 1500 rpm, 2000 rpm, 2500 rpm, and 3000 rpm by applying the different linear equations, new power values were also calculated for each fuel, load, and speed condition by applying Equation 2.3. To choose and select constant power values for every fuel at each condition, the mean value between the fuels was calculated, using Equation 4.2.

$$BP = \frac{BP_{diesel\,(x,y)} + BP_{8WiDE\,(x,y)} + BP_{16WiDE\,(x,y)}}{3}, \quad (4.2)$$

where BP is brake power in kW, x is load (25W, 50W, 75W, and 100W), and y is speed (1500 rpm, 2000 rpm, 2500 rpm, and 3000 rpm).

```
MeanPower_Load_3000rpm <- mean( c( MeanDiesel_Load$Power[ 1 ], MeanWiDE8_Load$Power[ 1 ], MeanWiDE16_Load$Power[ 1 ] ) )
MeanPower_Load_2500rpm <- mean( c( MeanDiesel_Load$Power[ 2 ], MeanWiDE8_Load$Power[ 2 ], MeanWiDE16_Load$Power[ 2 ] ) )
MeanPower_Load_2000rpm <- mean( c( MeanDiesel_Load$Power[ 3 ], MeanWiDE8_Load$Power[ 3 ], MeanWiDE16_Load$Power[ 3 ] ) )
MeanPower_Load_1500rpm <- mean( c( MeanDiesel_Load$Power[ 4 ], MeanWiDE8_Load$Power[ 4 ], MeanWiDE16_Load$Power[ 4 ] ) )
```

Figure 4.19. Determination of mean BP between the fuels to achieve a unique value at each speed and load.

After obtaining the different values for power, torque was also calculated for each condition using Equation 2.2. Figures 4.20, 4.21, 4.22, and 4.23 show the new torque and power values at each engine speed.

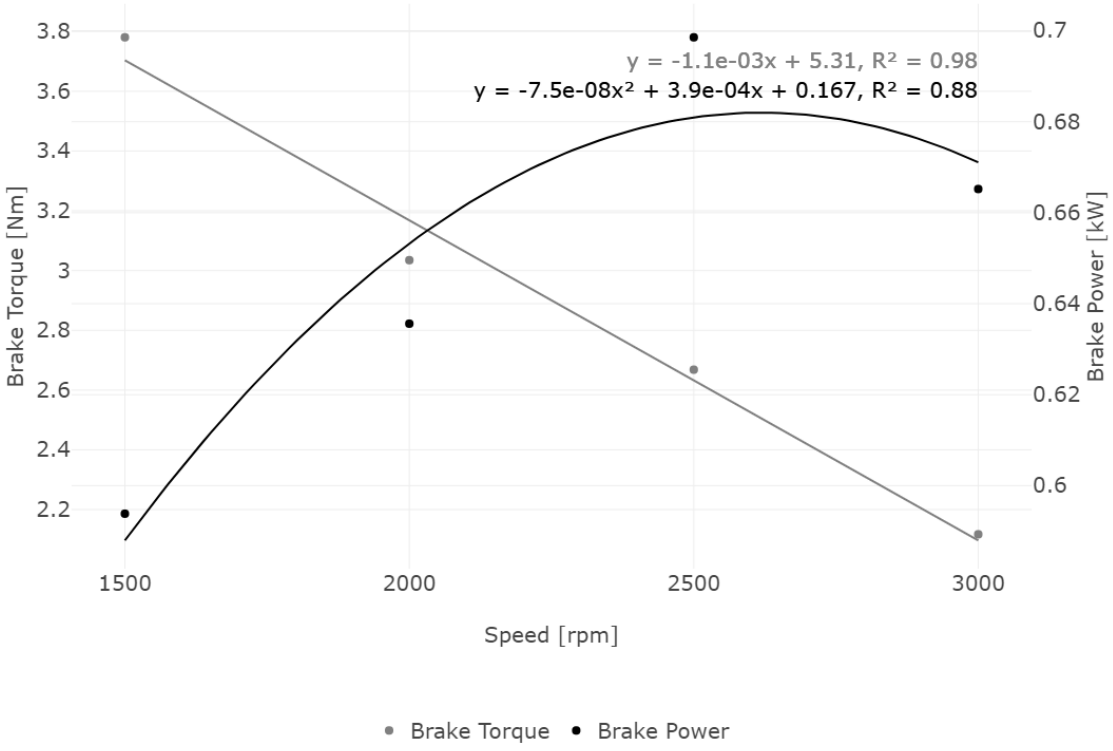

Figure 4.20. BT and BP at 25W load.

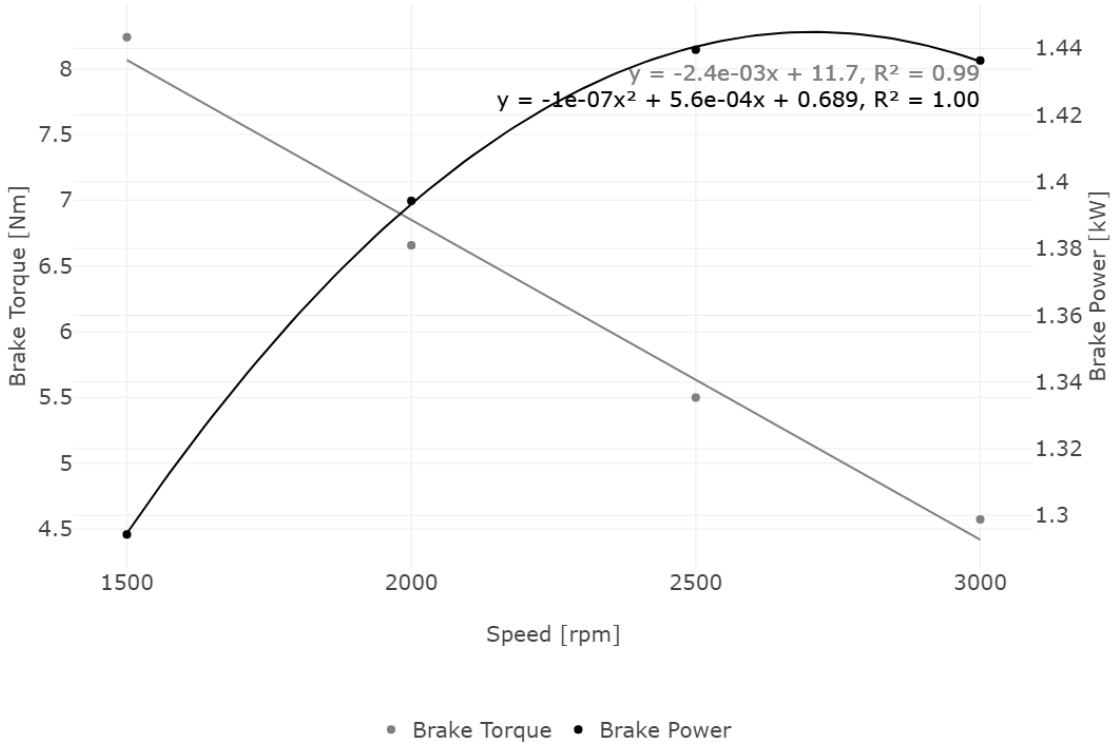

Figure 4.21. BT and BP at 50W load.

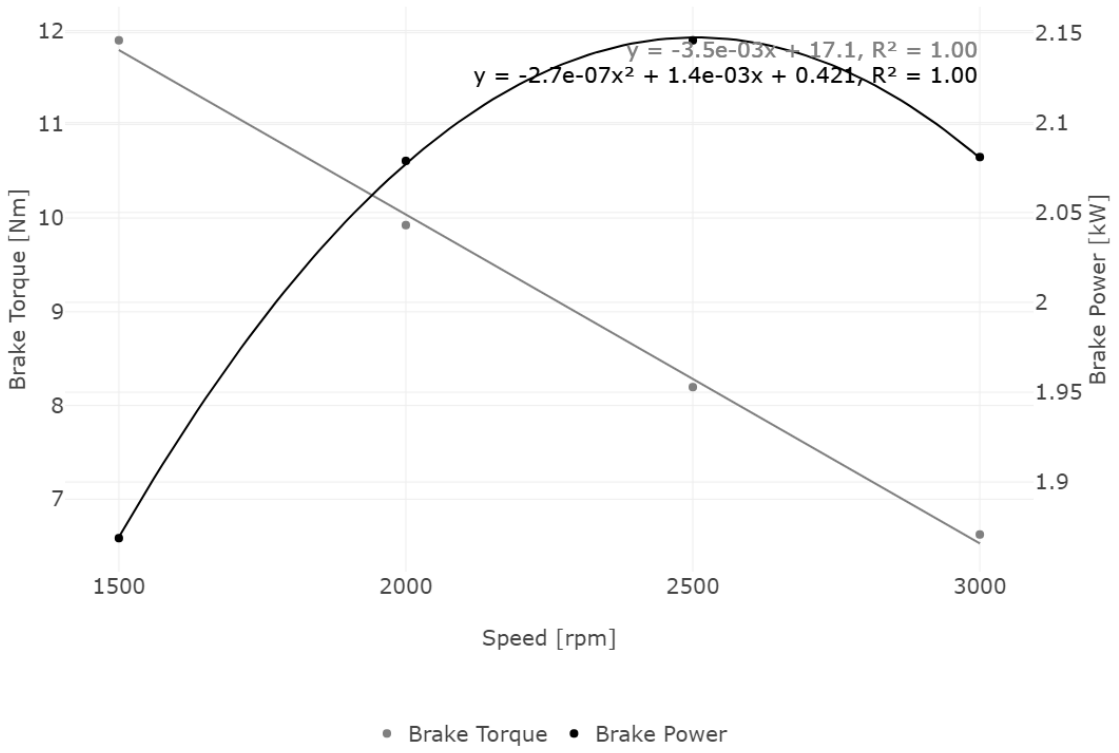

Figure 4.22. BT and BP at 75W load.

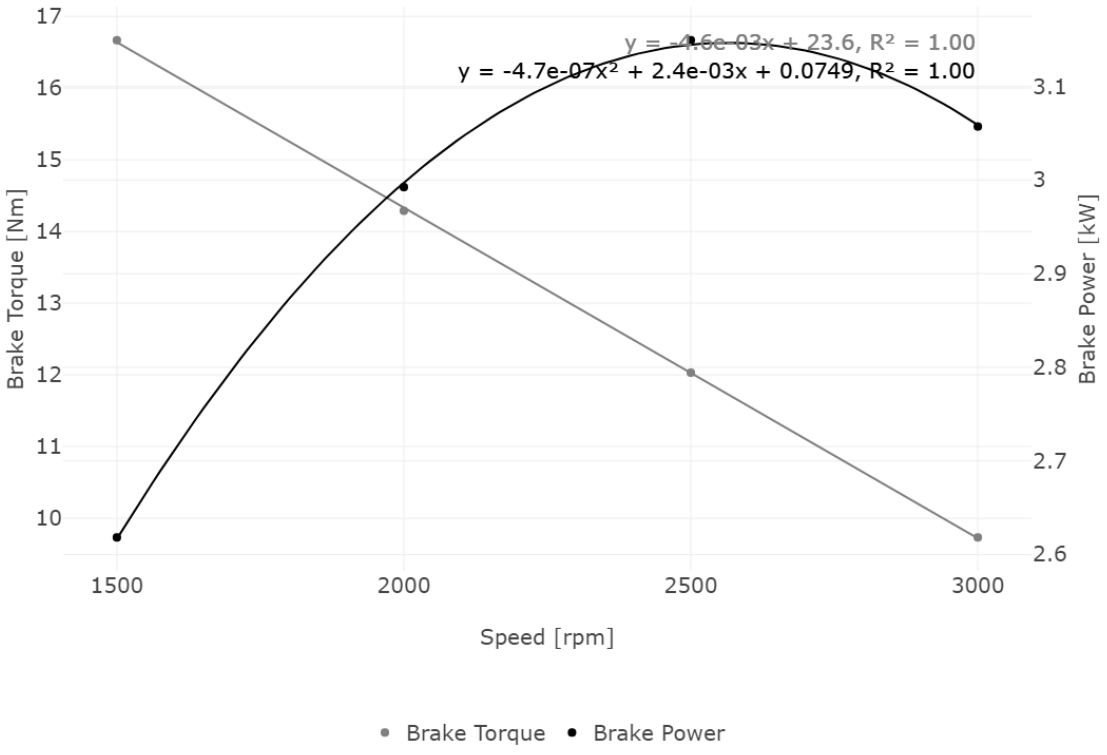

Figure 4.23. BT and BP at 100W load.

As seen in Figures 4.20 to 4.23, at every engine load, the BT linearly increases with the decrease of engine speed. This linearity is a consequence of the testing conditions. For this electromagnetic brake under constant load conditions, a decrease in engine speed leads to an increase in the braking torque, as more force is being applied in the coils structure where the load cell is placed due to the increased braking effect. By decreasing the speed even further, an engine stall would occur right after a peak torque value for that load condition, as the engine would not be able to produce enough torque or power to counteract the applied load. Torque and power are directly proportional to each other. The BP of the engine is calculated from BT and speed. At all engine loads, the power increases from 1500 rpm to 2500 rpm due to the increase in engine speed and then starts decreasing until 3000 rpm. From 2500 rpm to 3000 rpm, as the ECB is reducing the BT linearly with rotational speed, for these values, the rotational speed is no longer increasing as much as the ECB torque is, leading to a decrease in BP.

4.2.1.4 Power and fuel consumption relationship

After obtaining similar power values for all the fuels, the next step was to check how each fuel relates its power with fuel consumption, so it is possible to predict new mass flow rates for each case.

```
model_FuelConsumption_FuelType_Speed <- lm( FuelConsumption ~ I( Power^2 ) + Power, data = Mean_FuelType_Speed )

model_FuelConsumption_FuelType_Speed_xvalues <- data.frame( Power = c( MeanPower_25W_Speed, MeanPower_50W_Speed,
                                                                       MeanPower_75W_Speed, MeanPower_100W_Speed ) )

model_FuelConsumption_FuelType_Speed.predict <- predict( model_FuelConsumption_FuelType_Speed,
                                                         newdata = model_FuelConsumption_FuelType_Speed_xvalues )

model_FuelConsumption_FuelType_Speed.predict <- data.frame( model_FuelConsumption_FuelType_Speed.predict )

model_FuelConsumption_FuelType_Speed.predict <- cbind( model_FuelConsumption_FuelType_Speed_xvalues,
                                                       model_FuelConsumption_FuelType_Speed.predict )
```

Figure 4.24. Prediction of fuel consumption values for fixed engine BP.

This relationship is shown in Figures 4.25, 4.26, and 4.27.

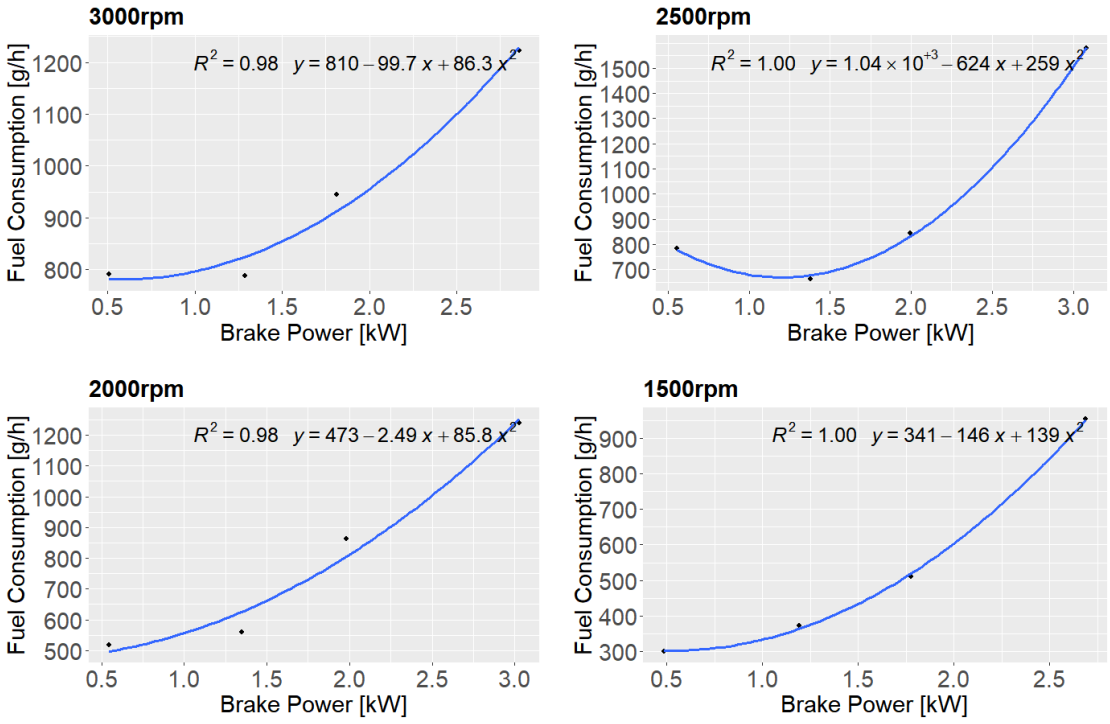

Figure 4.25. BP vs fuel consumption relationship of diesel fuel.

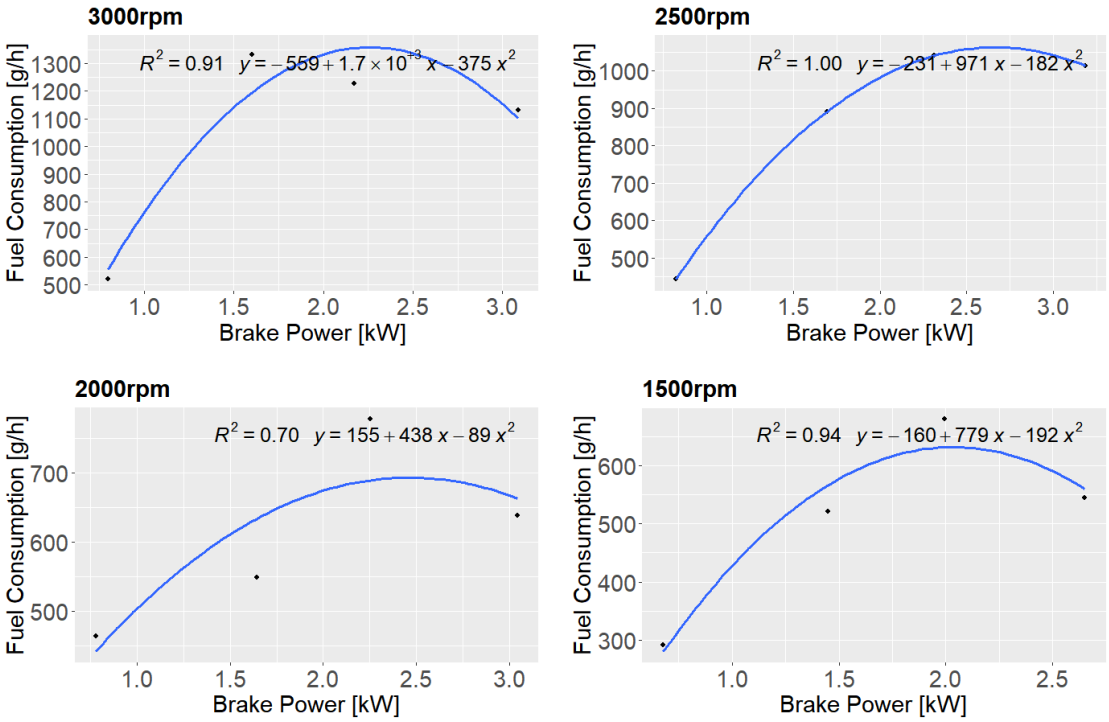

Figure 4.26. BP vs fuel consumption relationship of 8% WiDE.

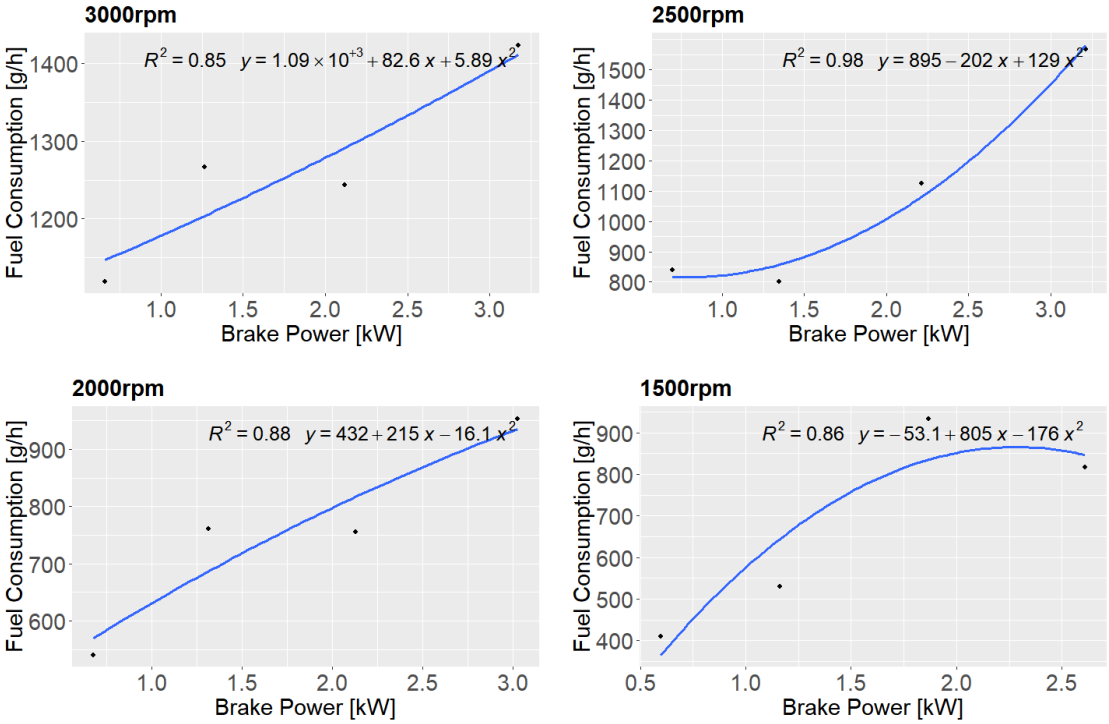

Figure 4.27. BP vs fuel consumption relationship of 16% WiDE.

4.2.1.5 Specific fuel consumption

After predicting the new fuel consumption values by applying the different quadratic equations for each case, new SFC values can also be calculated (Figures 4.28 to 4.31) for the new power values by using Equation 2.4.

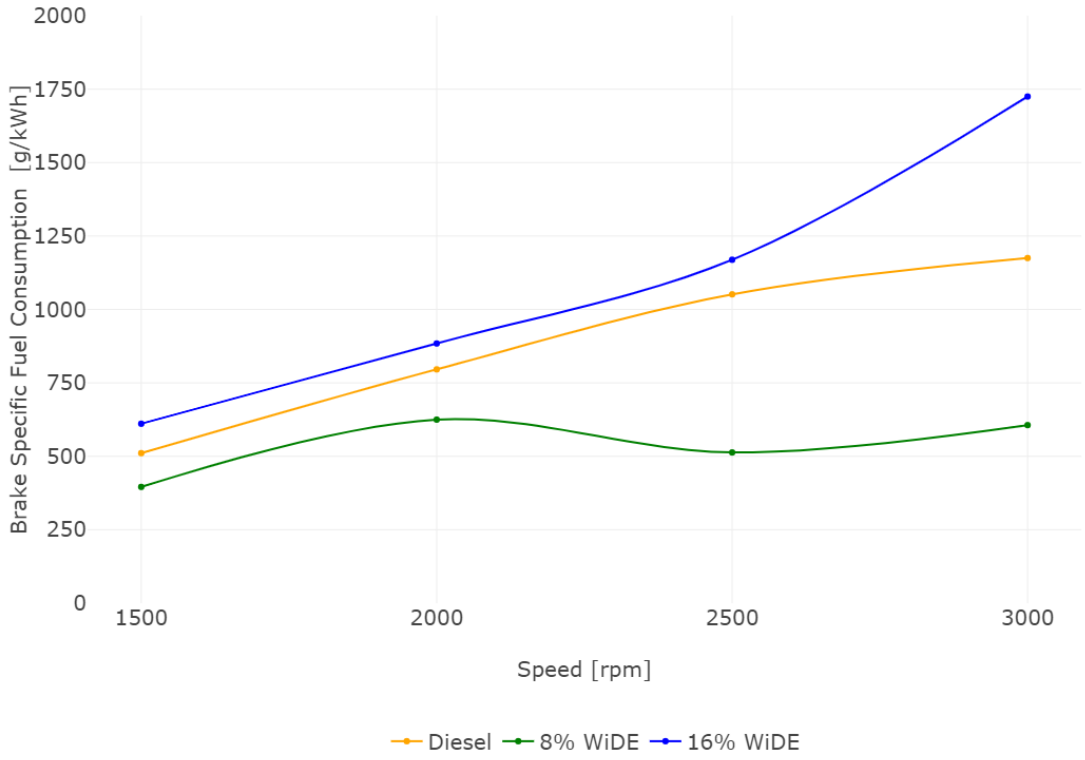

Figure 4.28. Engine BSFC at 25W load.

Figure 4.29. Engine BSFC at 50W load.

Figure 4.30. Engine BSFC at 75W load.

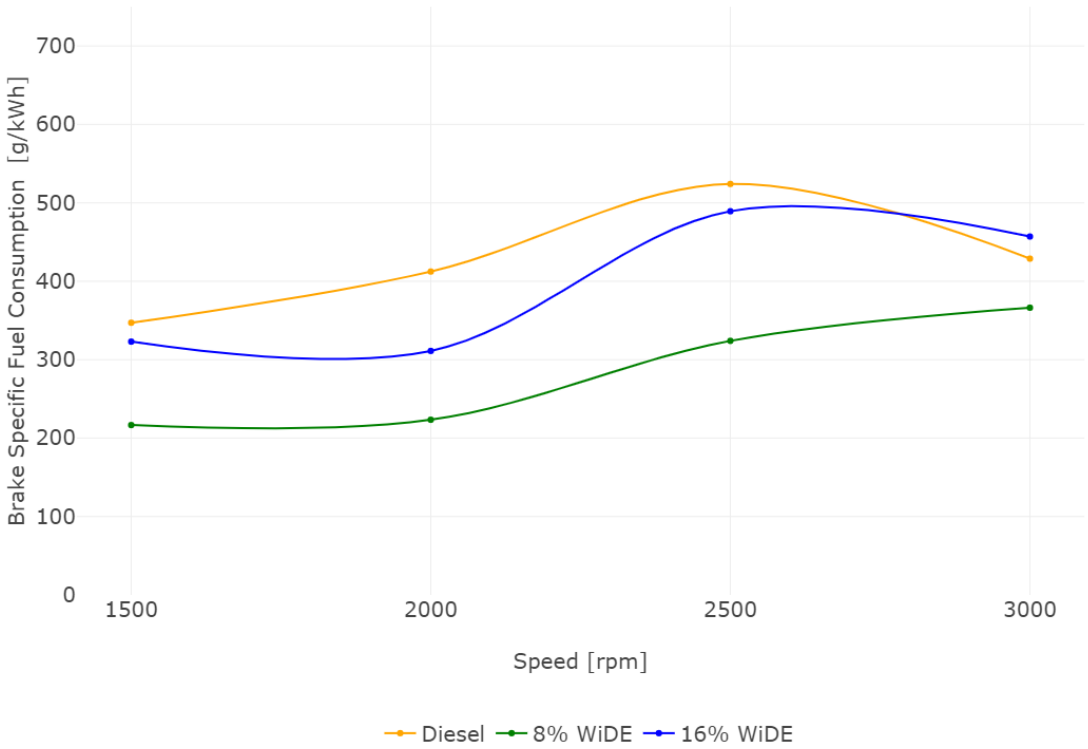

Figure 4.31. Engine BSFC at 100W load.

At 25W load condition, the BSFC of 8% WiDE is lower than diesel at every engine speed. The BSFC of diesel is also lower than 16% WiDE at every engine speed. In general, the BSFC increases with the increase of engine speed, with the exception of 8% WiDE where it increases from 1500 rpm to 2000 rpm, followed by a decrease from 2000 rpm to 2500 rpm, further increasing until 3000 rpm. At 50W load, the BSFC of 16% WiDE is higher than the other fuels at every engine speed. The BSFC of 8% WiDE is higher than diesel fuel, except at 2500 rpm, which is lower. For diesel fuel and 8% WiDE, the BSFC increases with engine speed. For 16% WiDE, the BSFC decreases from 1500 rpm to 2000 rpm and then increases until 3000 rpm. At 75W load, the BSFC of diesel is lower than the emulsions at all engine speeds except at 2000 rpm where it is higher. The BSFC of 8% WiDE is lower than 16% WiDE at every engine speed except at 3000 rpm where it is higher. For diesel fuel, the BSFC increases with engine speed. For both emulsions, it decreases from 1500 rpm to 2000 rpm and then increases until 3000 rpm. At 100W load, the BSFC of 8% WiDE is the lowest of all the fuels at every engine speed. The BSFC of 16% WiDE is also lower than diesel at every speed except 3000 rpm where it is slightly higher. The BSFC for 8% WiDE increases with the increase in engine speed. The BSFC of 16% WiDE decreases from 1500 rpm to 2000 rpm, followed by an increase to 2500 rpm and then decreasing until 3000 rpm. The BSFC of diesel increases until 2500 rpm, further decreasing until 3000 rpm.

4.2.1.6 Thermal efficiency

By using Equation 2.5, new TE values were also calculated for each case, as shown in Figures 4.32 to 4.35.

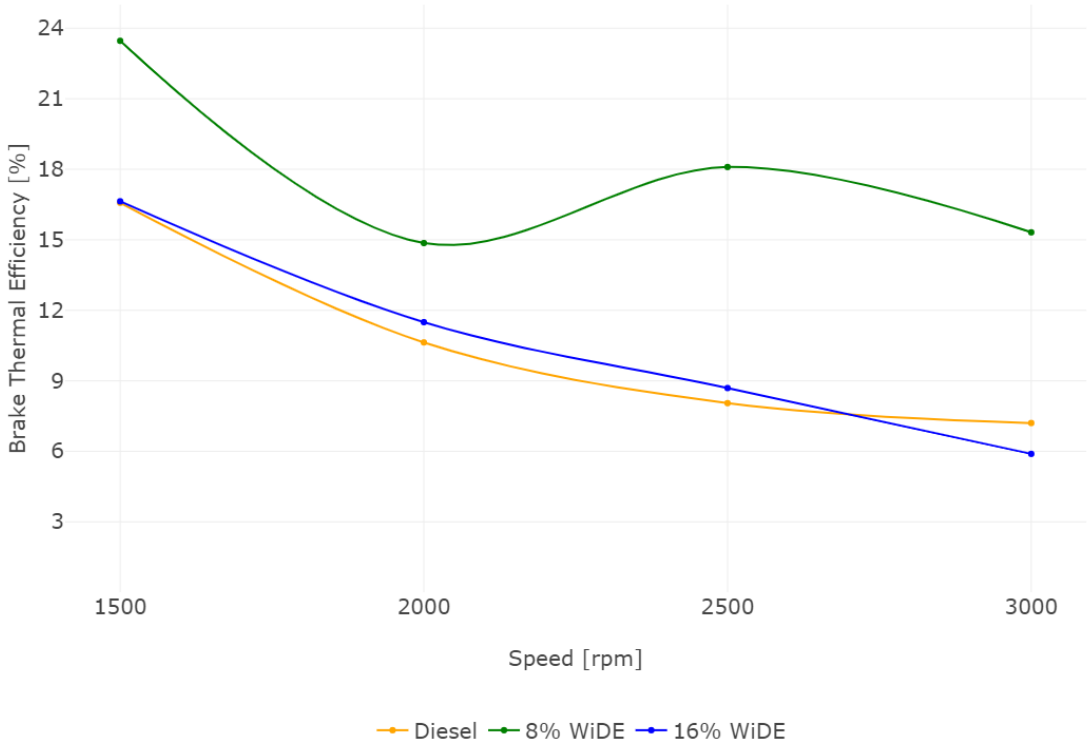

Figure 4.32. Engine BTE at 25W load.

Figure 4.33. Engine BTE at 50W load.

Figure 4.34. Engine BTE at 75W load.

Figure 4.35. Engine BTE at 100W load.

BTE is inversional proportional to BSFC and LHV (Equation 2.5). Therefore, the trends observed for BSFC plots are going to be opposite for BTE. At 25W load condition, 8% WiDE presents the highest BTE of all fuels at every engine speed. 16% WiDE presents similar BTE compared to diesel at 1500 rpm, worse at 3000 rpm, and higher at 2000 rpm and 2500 rpm. For diesel and 16% WiDE, BTE increases with the decrease in engine speed (increasing BT). For 8% WiDE, BTE increases from 3000 rpm to 2500 rpm, followed by a decrease from 2500 rpm to 2000 rpm, followed by another increase until 1500 rpm. For the 50W load condition, diesel fuel shows better BTE at every engine speed except at 2000 rpm, where it is lower. 8% WiDE also presents better BTE than 16% WiDE at 1500 rpm and 2000 rpm, and similar BTE at 2500 rpm and 3000 rpm. For all fuels, the BTE generally increases with the decrease in engine speed, except for 16% WiDE, which decreases from 2000 rpm to 1500 rpm. At 75W load, diesel fuel presents better BTE at 1500 rpm and 3000 rpm when compared to the emulsions, worse at 2000 rpm and similar at 2500 rpm. For all fuels, BTE also increases with the decrease in speed, except at both emulsions, where it decreases from 2000 rpm to 1500 rpm. At 100W load, the differences are more significative between all the fuels. The BTE of 8% WiDE is higher at every engine speed when compared to the other fuels. This is followed by the BTE of 16% WiDE, which is higher than diesel fuel at every engine speed. The BTE of 8% WiDE increases with the decrease in engine speed. The BTE of 16% WiDE decreases from 3000 rpm to 2500 rpm, followed by an increase until 2000 rpm, and then decreases until 1500 rpm. For diesel fuel, BTE decreases from 3000 rpm to 2500 rpm and then increases until 1500 rpm.

4.2.2 Emissions

Similar to power and fuel consumption, the relationship between power and exhaust emissions was also checked individually for each fuel. In this case, Emissions is replaced by CO, CO_2, HC, NO, O_2, and smoke.

```
model_Emissions_FuelType_Speed <- lm( Emissions ~ I( Power^2 ) + Power, data = Mean_FuelType_Speed )

model_Emissions_FuelType_Speed_xvalues <- data.frame( Power = c( MeanPower_25W_Speed, MeanPower_50W_Speed,
                                                                 MeanPower_75W_Speed, MeanPower_100W_Speed ) )

model_Emissions_FuelType_Speed.predict <- predict( model_Emissions_FuelType_Speed,
                                                   newdata = model_Emissions_FuelType_Speed_xvalues )

model_Emissions_FuelType_Speed.predict <- data.frame( model_Emissions_FuelType_Speed.predict )

model_Emissions_FuelType_Speed.predict <- cbind( model_Emissions_FuelType_Speed_xvalues,
                                                 model_Emissions_FuelType_Speed.predict )
```

Figure 4.36. Prediction of exhaust emissions for fixed engine BP.

4.2.2.1 Power and CO relationship

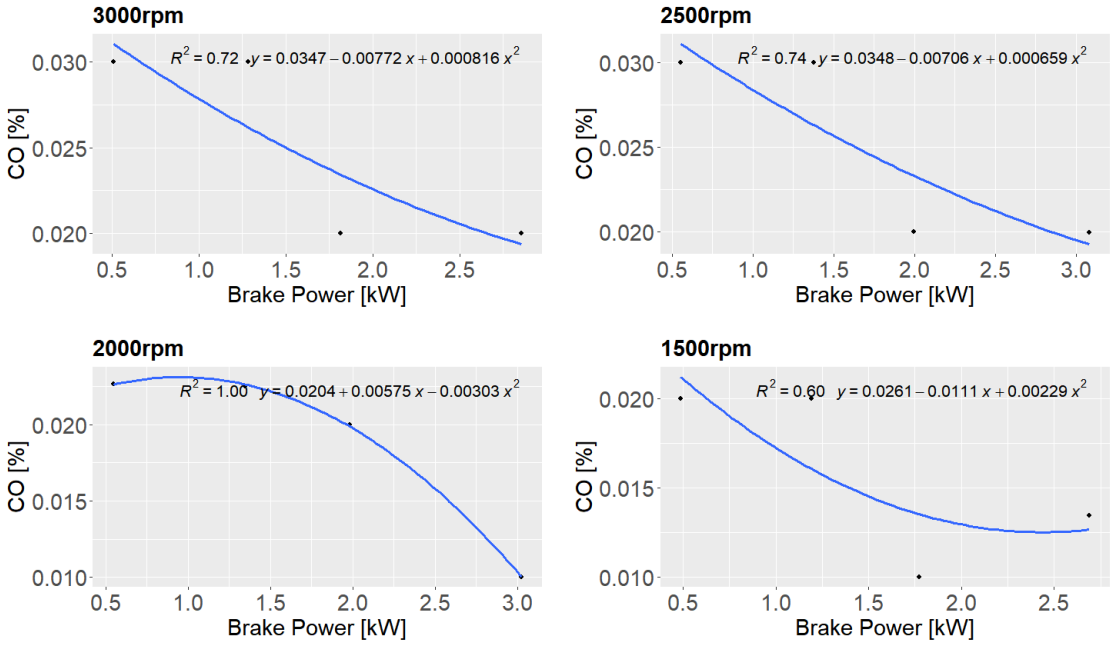

Figure 4.37. BP vs CO relationship of diesel fuel.

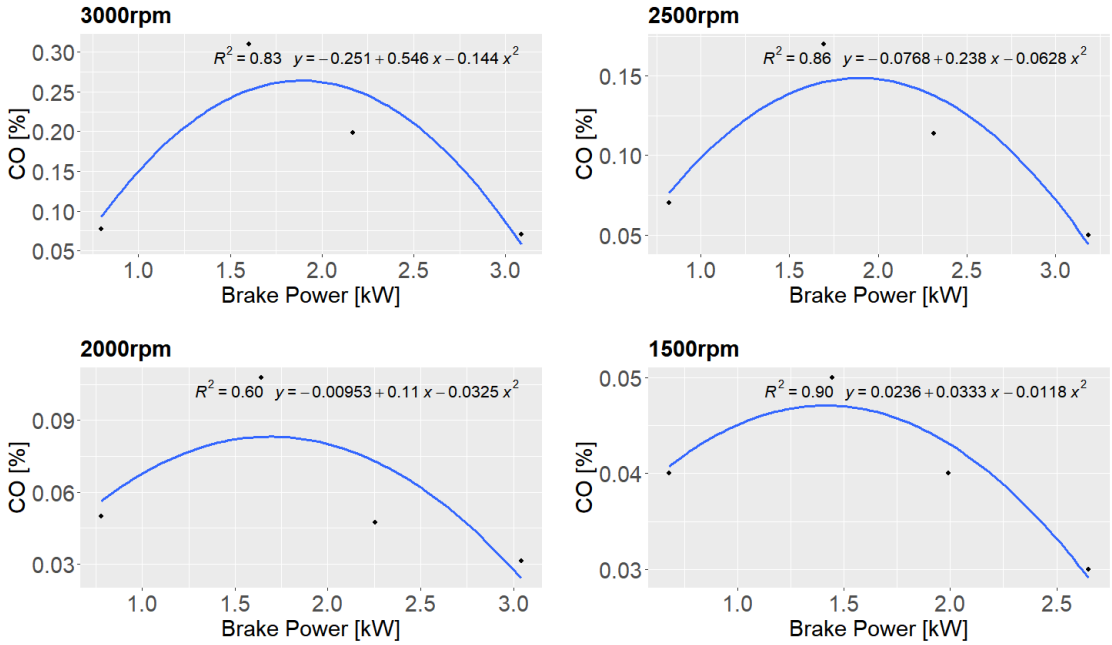

Figure 4.38. BP vs CO relationship of 8% WiDE.

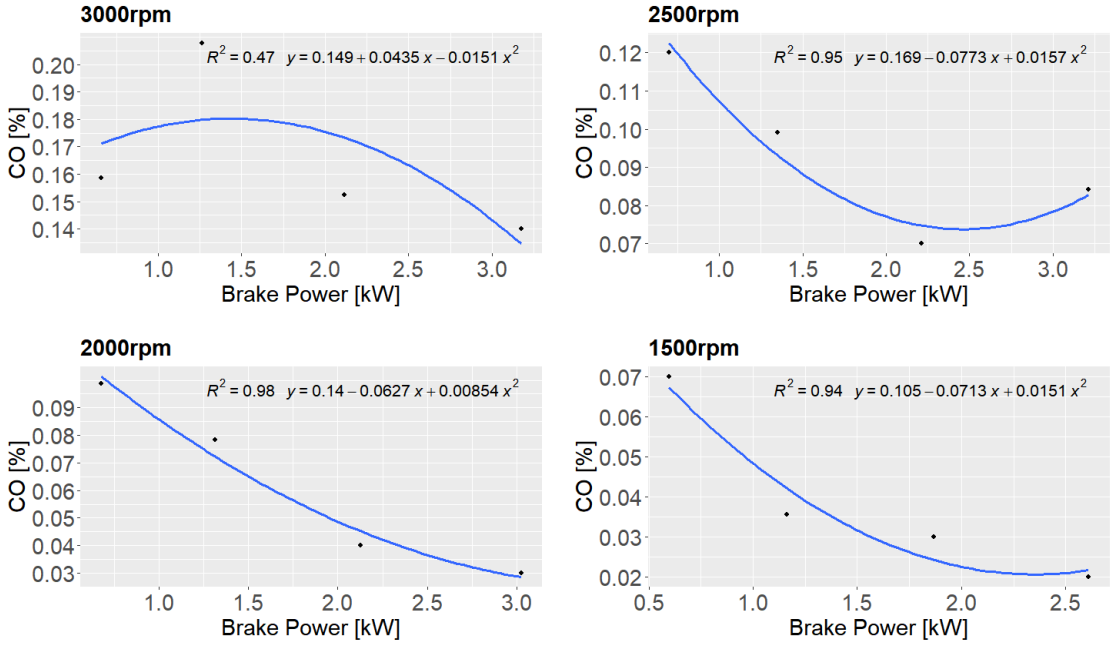

Figure 4.39. BP vs CO relationship of 16% WiDE.

As can be seen in Figures 4.37 to 4.39, a correlation is hard to achieve between CO emissions and brake engine power, which can be verified by the overall low R-squared of the second-degree polynomial models. Third-degree polynomial models weren't utilised as they would lead to an r-squared of 1 (due to only 4 data points in the regression) and possibly conduct to overfitting of the model, where the regression line would be fitting the residuals instead of describing the relationship between the variables, leading to future rash predictions. This is common when the model used is too complex for the data in question.

Due to these reasons, it was decided that for these cases, the raw data values, obtained through the mean of around 2000 different data points at different engine conditions, would be used instead.

4.2.2.2 CO emissions

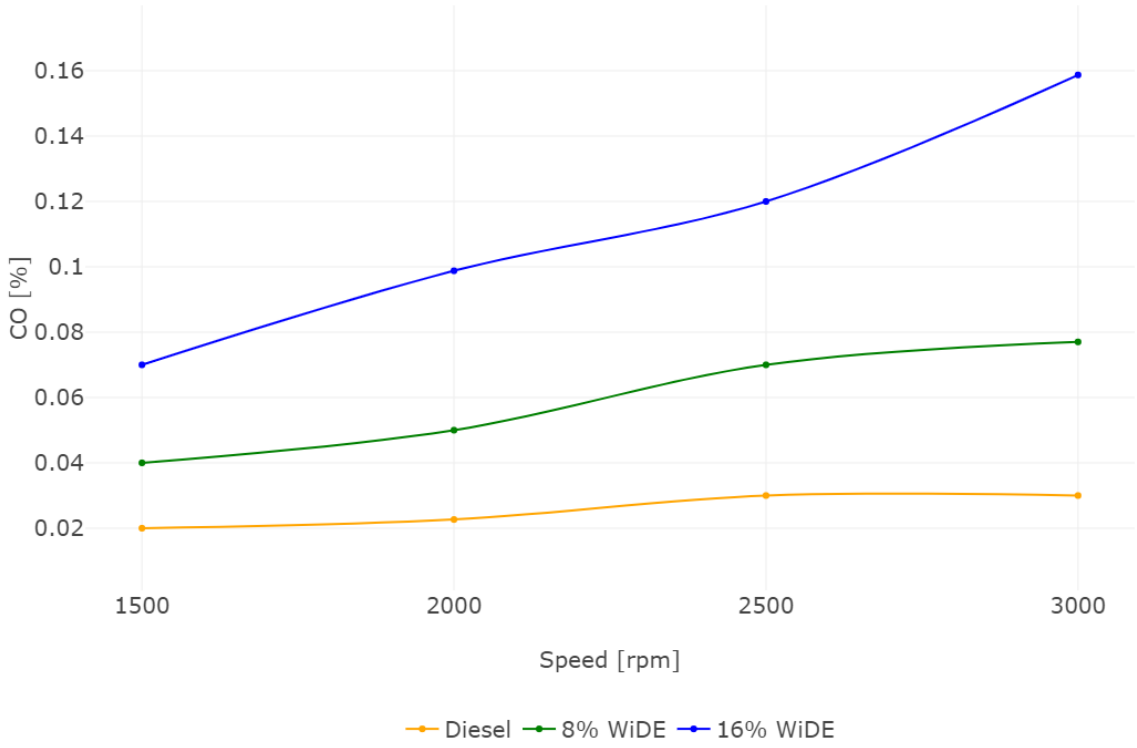

Figure 4.40. CO emissions at 25W load.

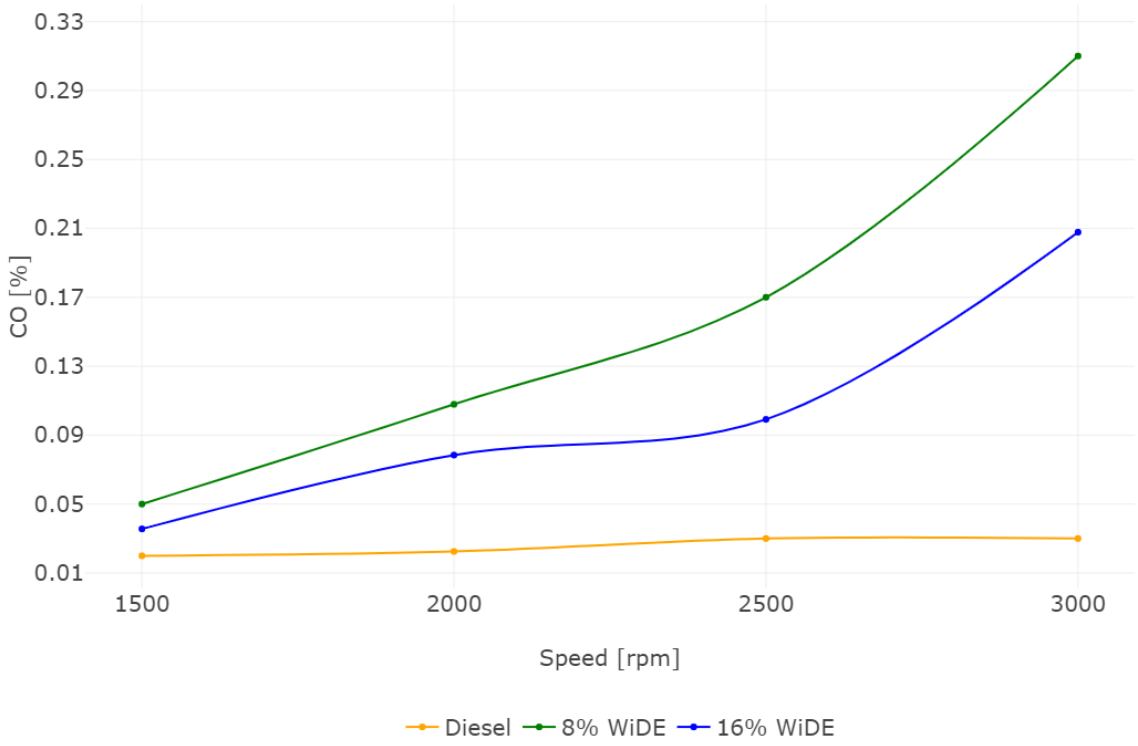

Figure 4.41. CO emissions at 50W load.

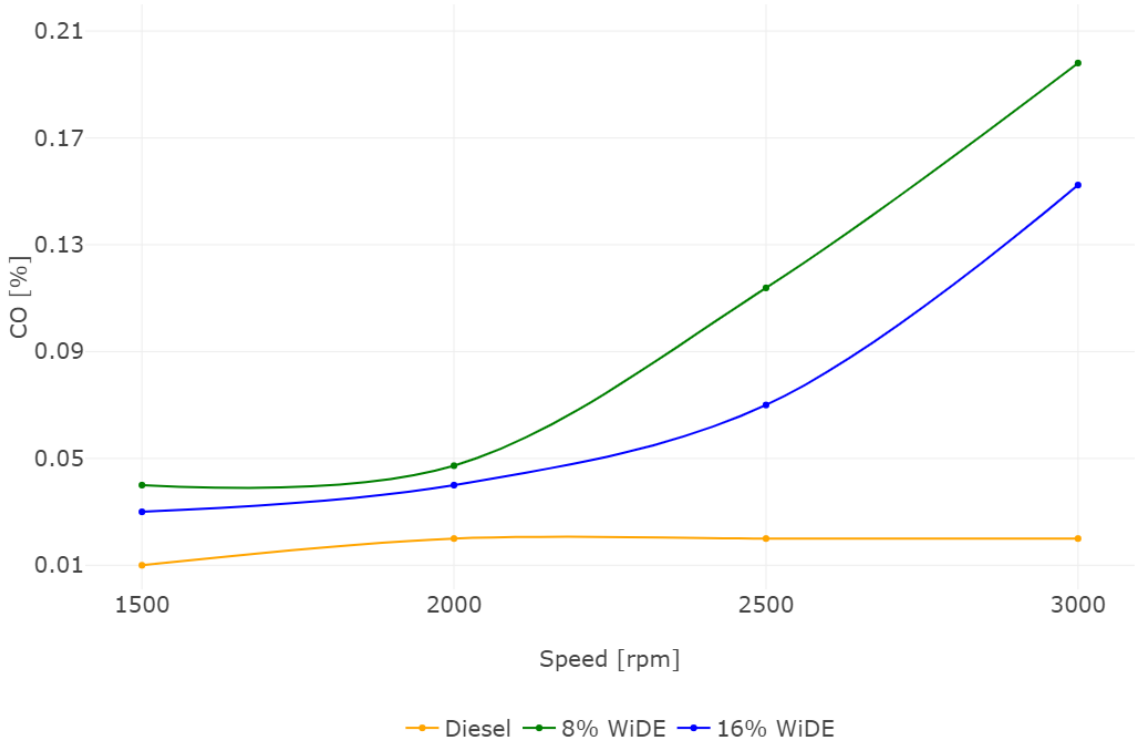

Figure 4.42. CO emissions at 75W load.

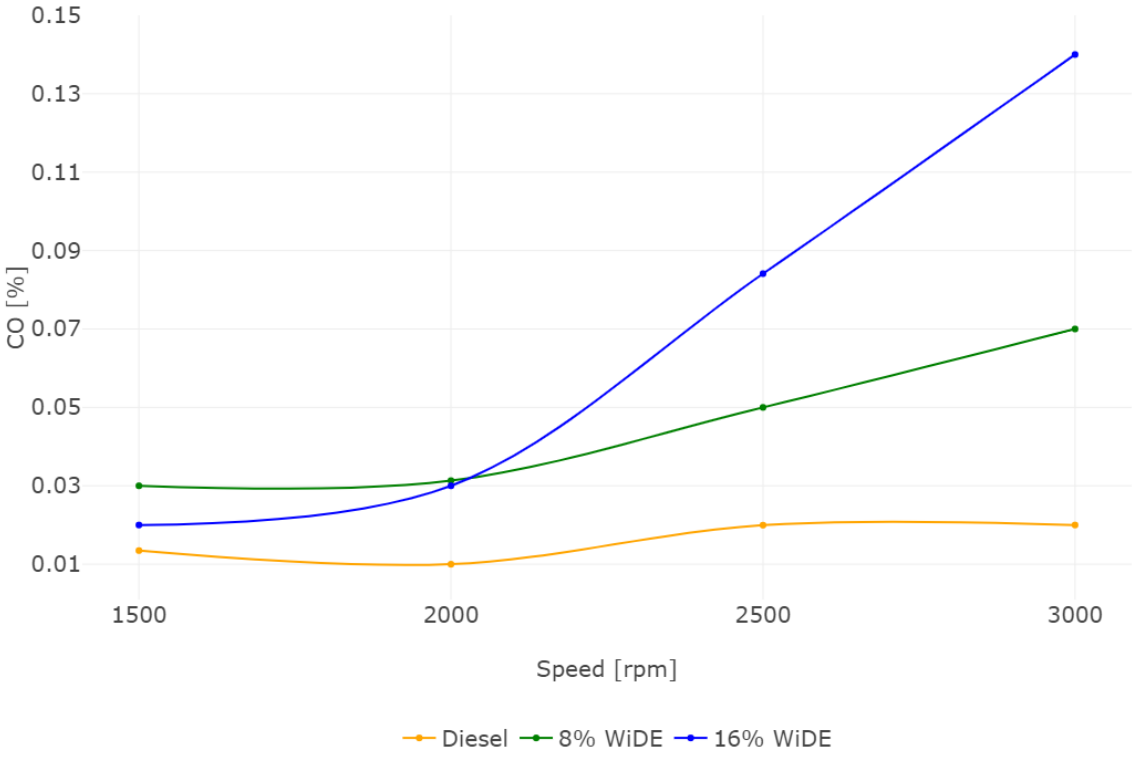

Figure 4.43. CO emissions at 100W load.

At every engine load, CO emissions of diesel are always lower than the emulsions. For this fuel at 25W load, they increase from 1500 rpm to 2500 rpm, remaining constant until 3000 rpm. CO emissions of 8% WiDE are always lower than 16% WiDE, and for both emulsions, these emissions increase from 1500 rpm to 3000 rpm. At 50W load, CO emissions of diesel increase from 1500 rpm to 2500 rpm, remaining constant until 3000 rpm. CO emissions of 16% WiDE are always lower than 8% WiDE, and for both emulsions, these emissions increase from 1500 rpm to 3000 rpm. At 75W load, CO emissions of diesel increase from 1500 rpm to 2000 rpm, remaining constant until 3000 rpm. CO emissions of 16% WiDE are always lower than 8% WiDE, and for both emulsions, these emissions increase from 1500 rpm to 3000 rpm. At 100W load, CO emissions of diesel decrease from 1500 rpm to 2000 rpm, increase until 2500 rpm, remaining constant until 3000 rpm. CO emissions of 16% WiDE are lower than 8% WiDE at 1500 rpm, similar at 2000 rpm, and higher from 2000 rpm to 3000 rpm. For 16% WiDE, they increase from 1500 rpm to 3000 rpm. For 8% WiDE, they remain constant from 1500 rpm to 2000 rpm and then increase until 3000 rpm.

4.2.2.3 Power and CO_2 relationship

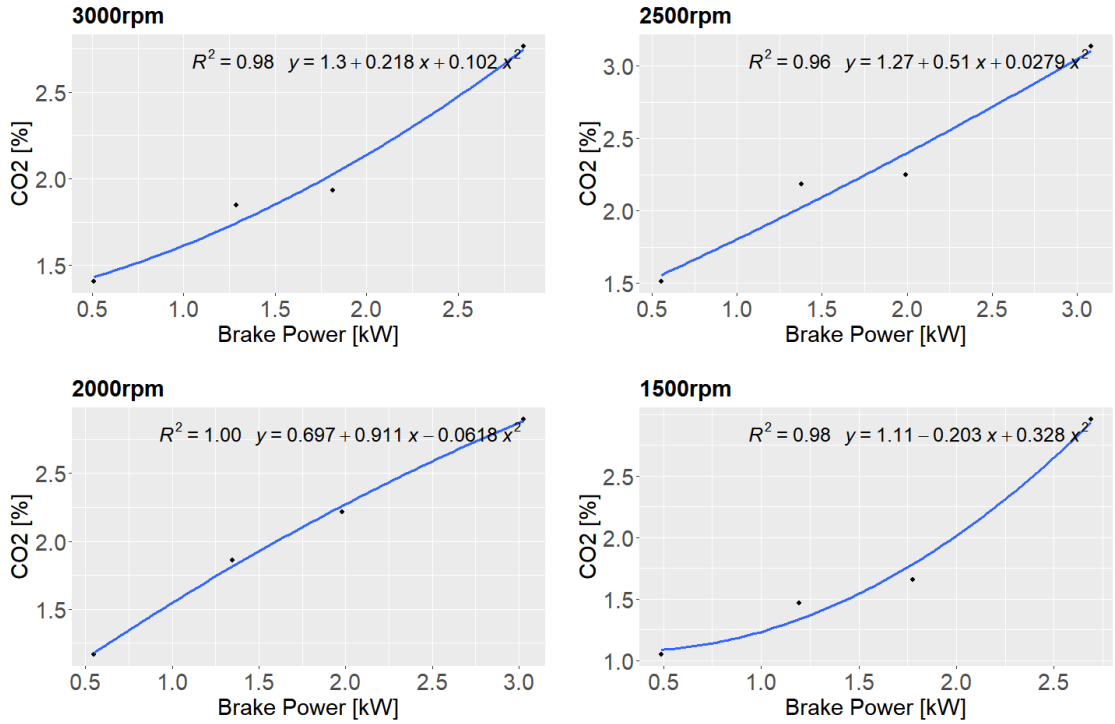

Figure 4.44. BP vs CO_2 relationship of diesel fuel.

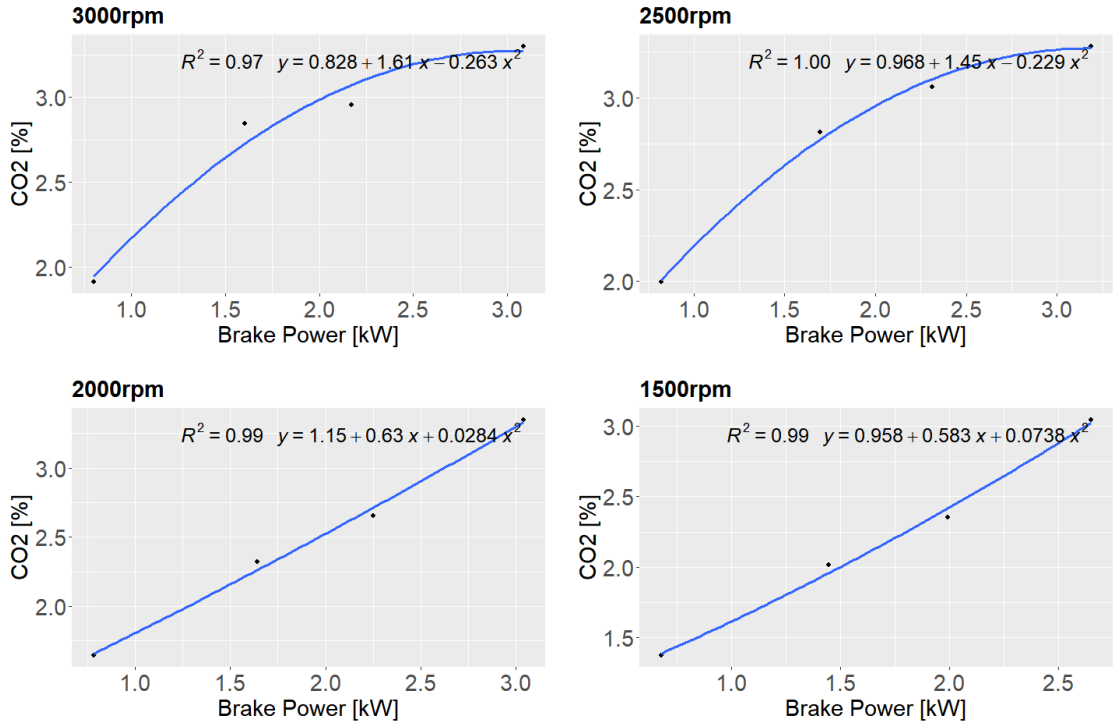

Figure 4.45. BP vs CO_2 relationship of 8% WiDE.

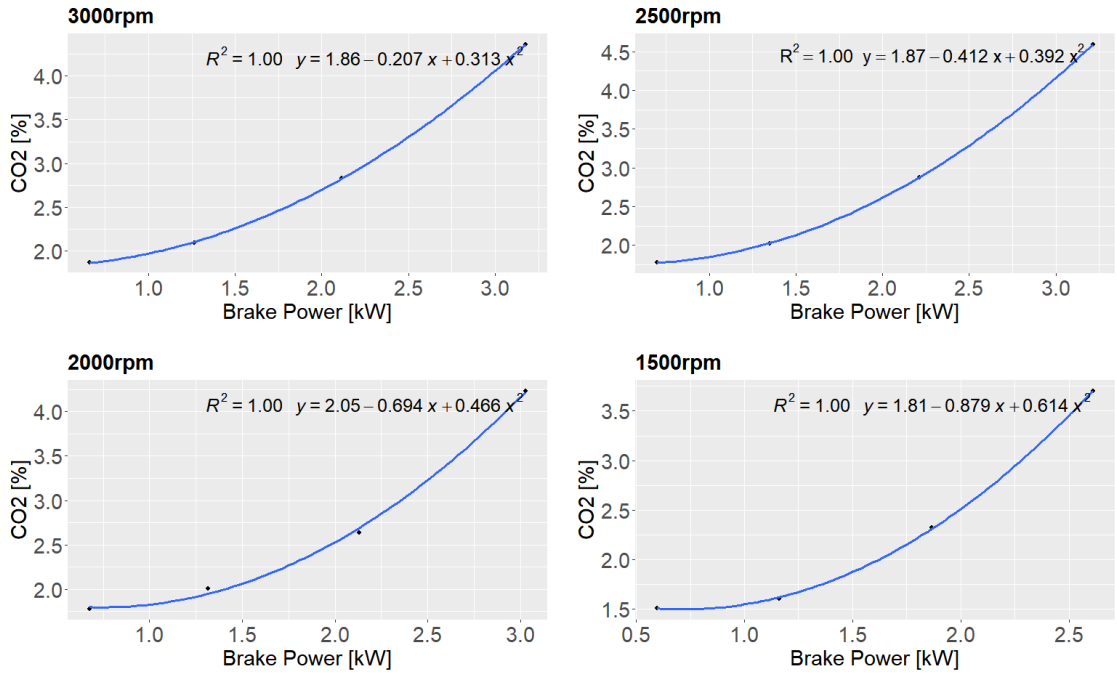

Figure 4.46. BP vs CO_2 relationship of 16% WiDE.

4.2.2.4 CO_2 emissions

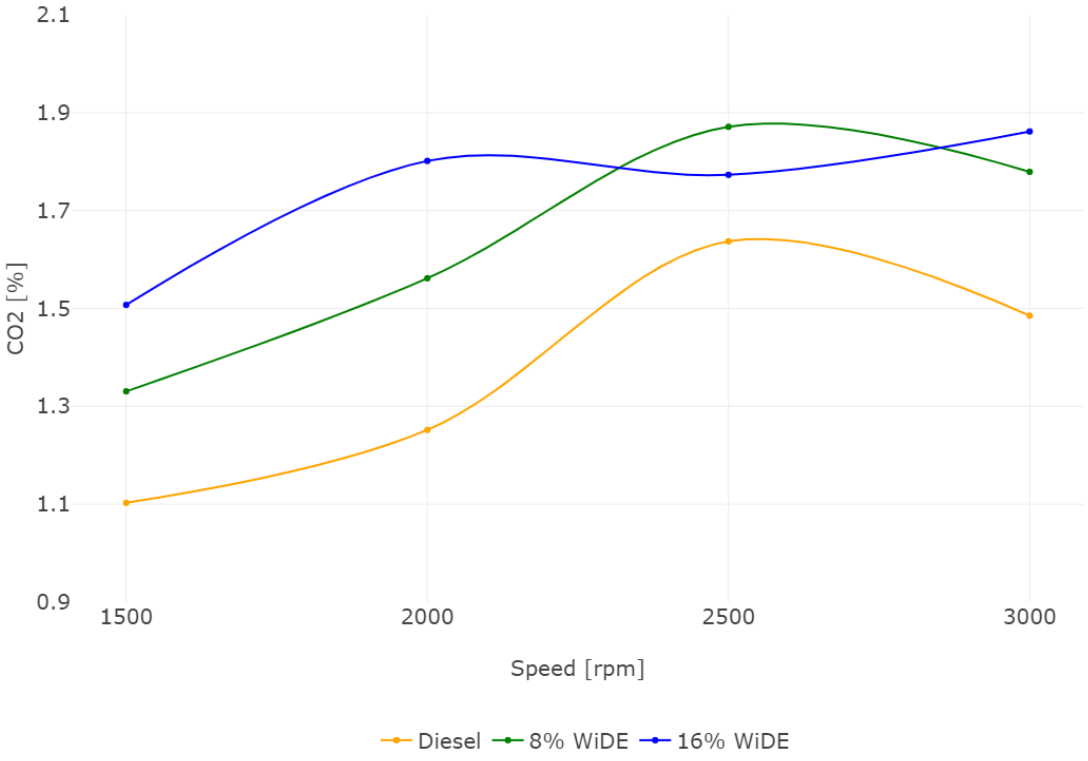

Figure 4.47. CO_2 emissions at 25W load.

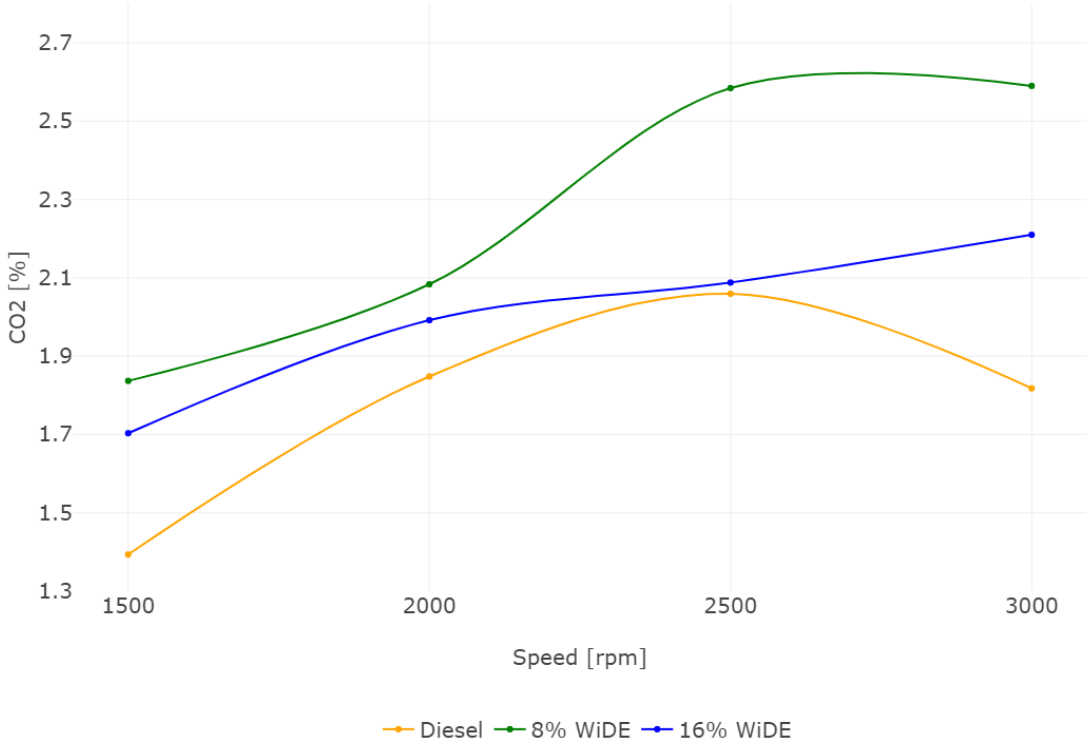

Figure 4.48. CO_2 emissions at 50W load.

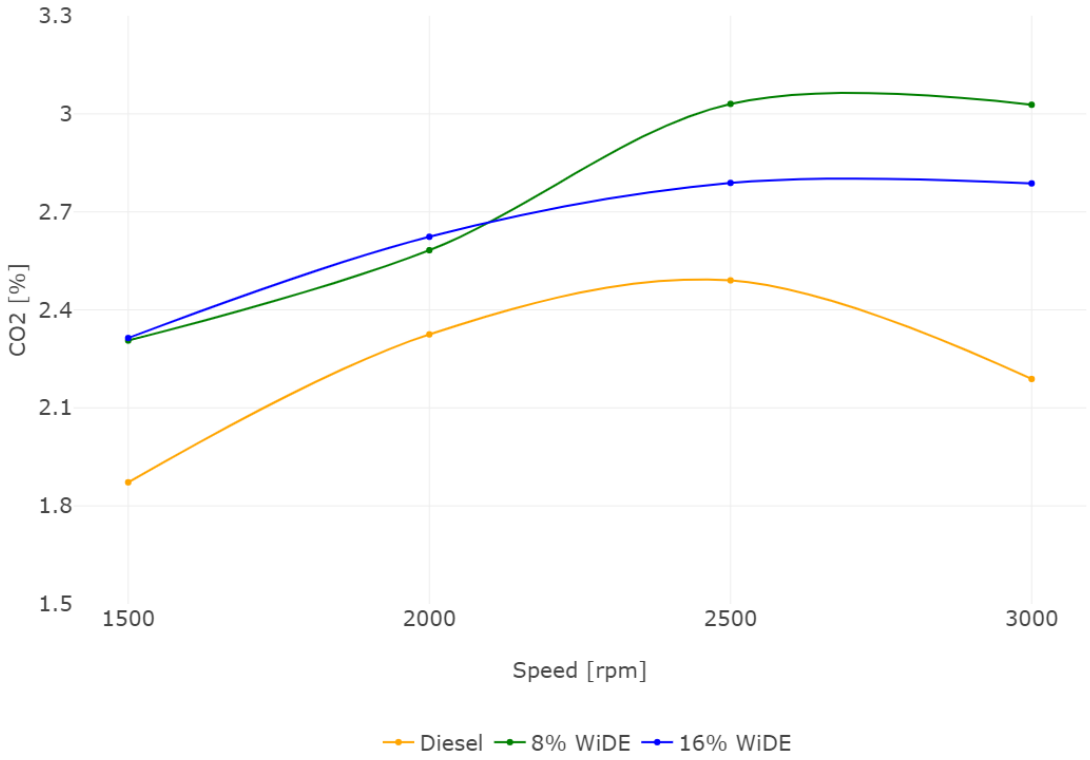

Figure 4.49. CO_2 emissions at 75W load.

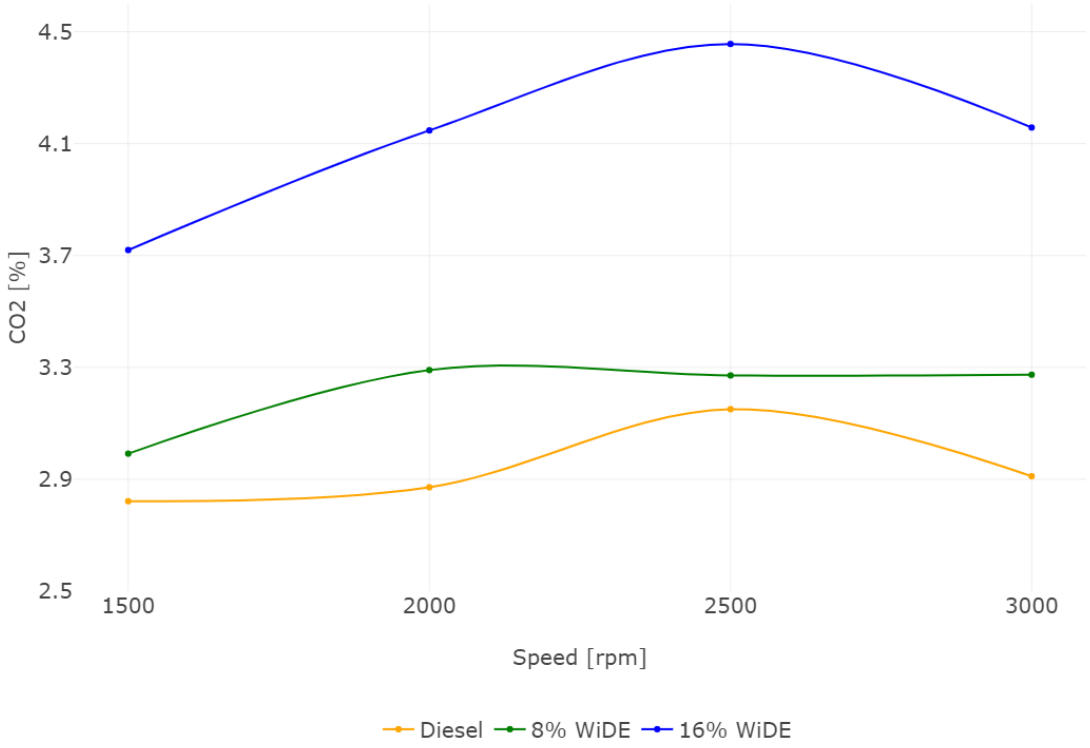

Figure 4.50. CO_2 emissions at 100W load.

At every engine load, the CO_2 emissions of diesel are always lower than the emulsions. For this fuel, at every load, they also increase from 1500 rpm to 2500 rpm and decrease from 2500 rpm to 3000 rpm. At 25W load, CO_2 emissions of 8% WiDE are lower than 16% WiDE except at 2500 rpm. For 8% WiDE, the emissions increase from 1500 rpm to 2500 rpm followed by a decrease until 3000 rpm. For 16% WiDE, the emissions increase from 1500 rpm to 2000 rpm, followed by a decrease until 2500 rpm, followed by another increase until 3000 rpm. At 50W load, CO_2 emissions of 8% WiDE were higher than 16% WiDE at every engine speed, and for both emulsions, they also increased with engine speed. At 75W load, the emissions of CO_2 were similar for both emulsions at 1500 rpm, lower for 8% WiDE at 2000 rpm, and higher for 8% WiDE at 2500 rpm and 3000 rpm. For both emulsions, the emissions increased from 1500 rpm to 2500 rpm and remained constant until 3000 rpm. At 100W load, CO_2 emissions of 16% WiDE were much higher than 8% WiDE at every engine speed, increasing from 1500 rpm to 2500 rpm, and decreasing until 3000 rpm. For 8% WiDE, CO_2 emissions increased from 1500 rpm to 2000 rpm and remained constant until 3000 rpm.

4.2.2.5 Power and HC relationship

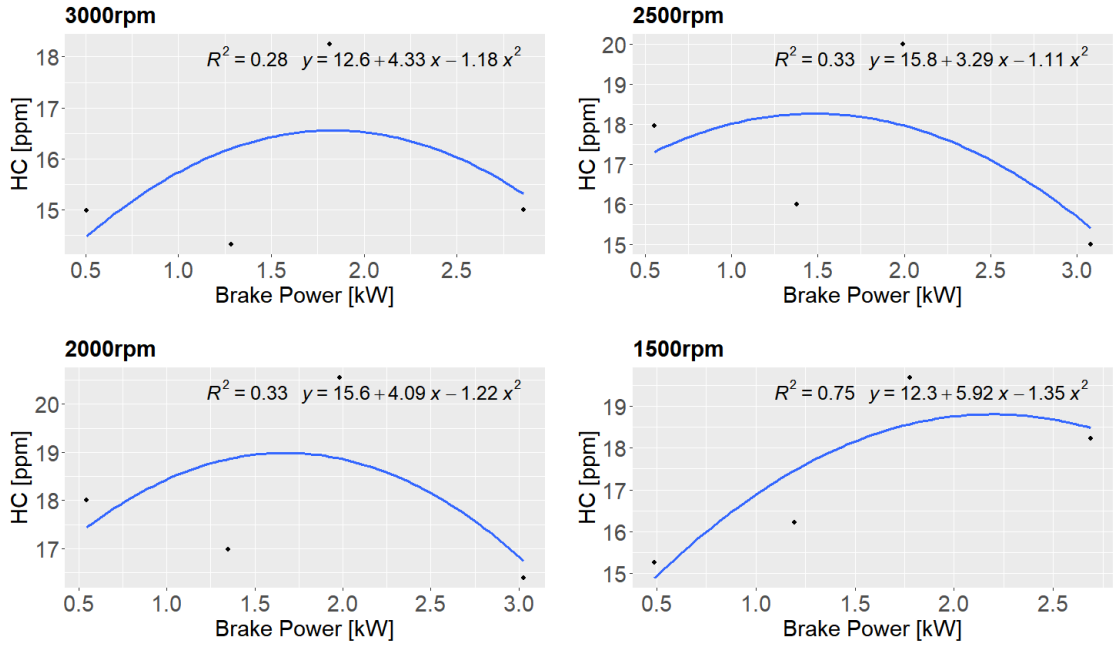

Figure 4.51. BP vs HC relationship of diesel fuel.

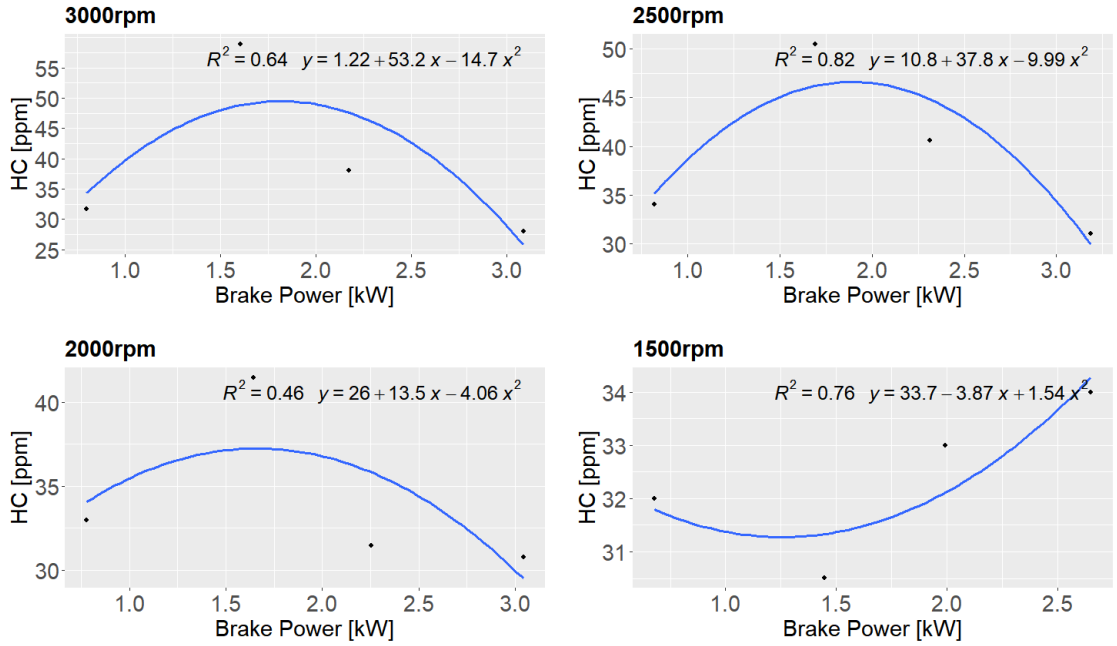

Figure 4.52. BP vs HC relationship of 8% WiDE.

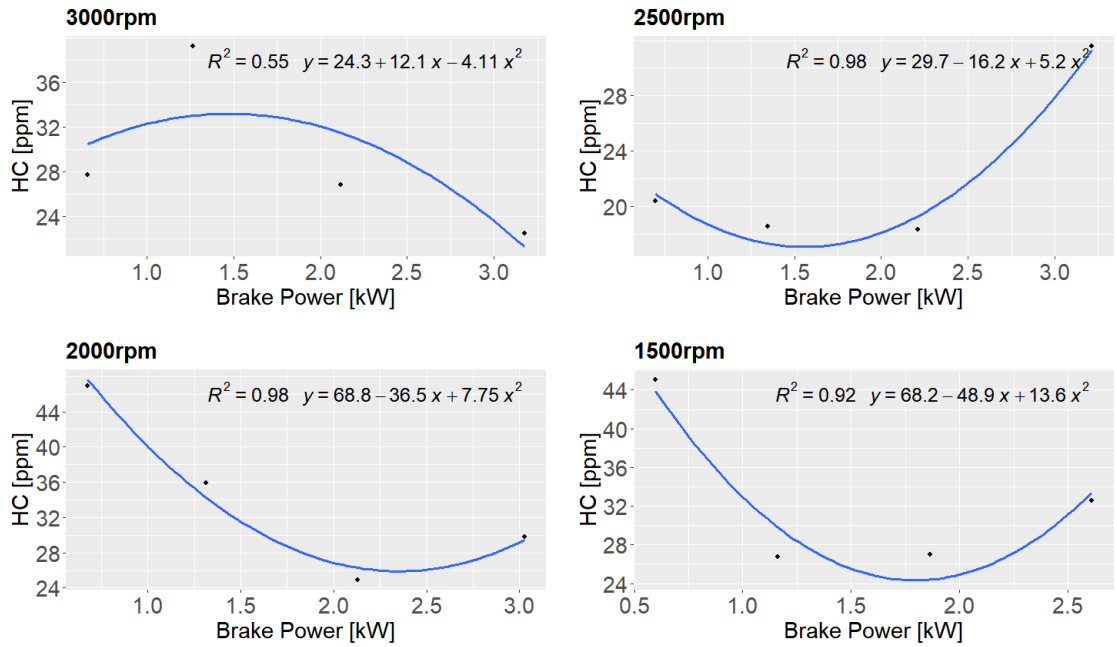

Figure 4.53. BP vs HC relationship of 16% WiDE.

As seen in Figures 4.51 to 4.53 and similar to CO emissions, a precise correlation can't be defined for HC emissions. The raw data for these emissions was also utilised instead.

4.2.2.6 HC emissions

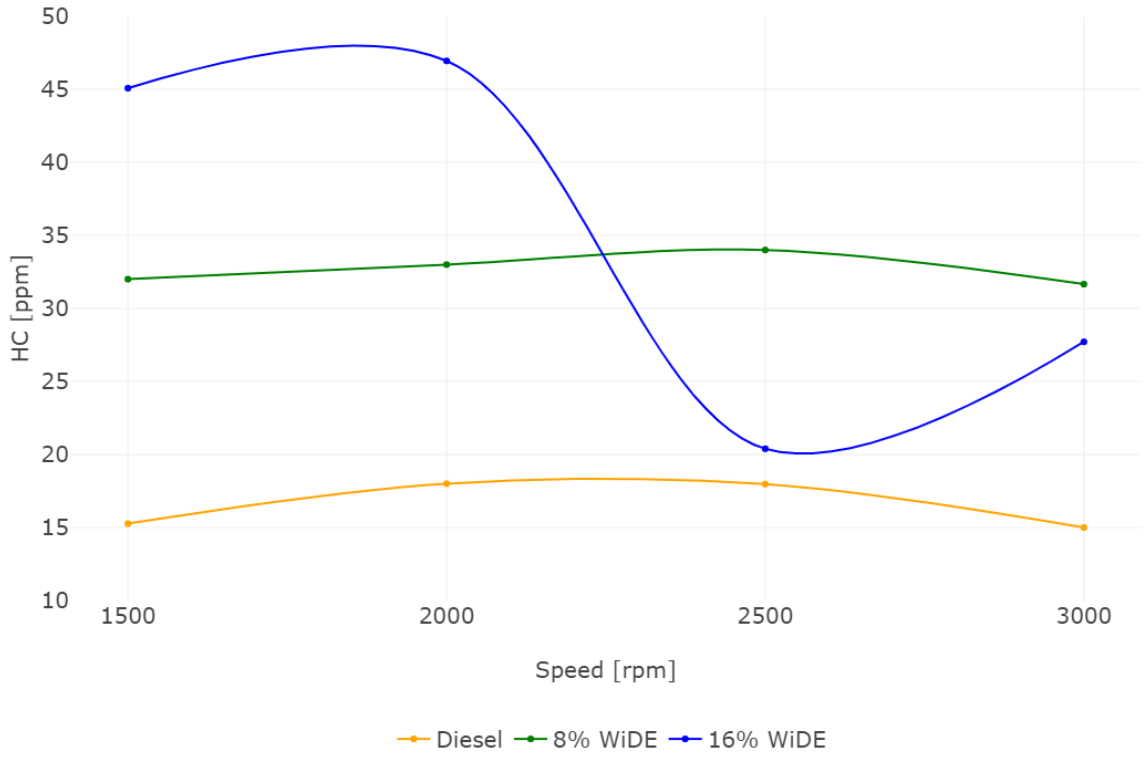

Figure 4.54. HC emissions at 25W load.

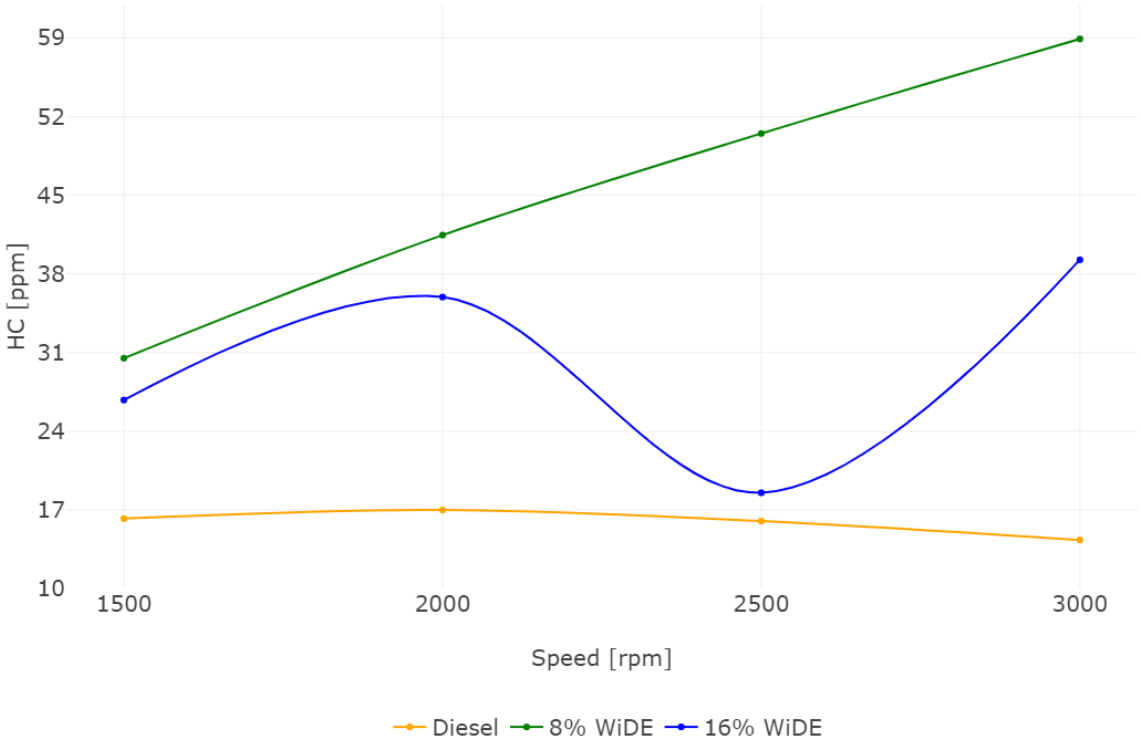

Figure 4.55. HC emissions at 50W load.

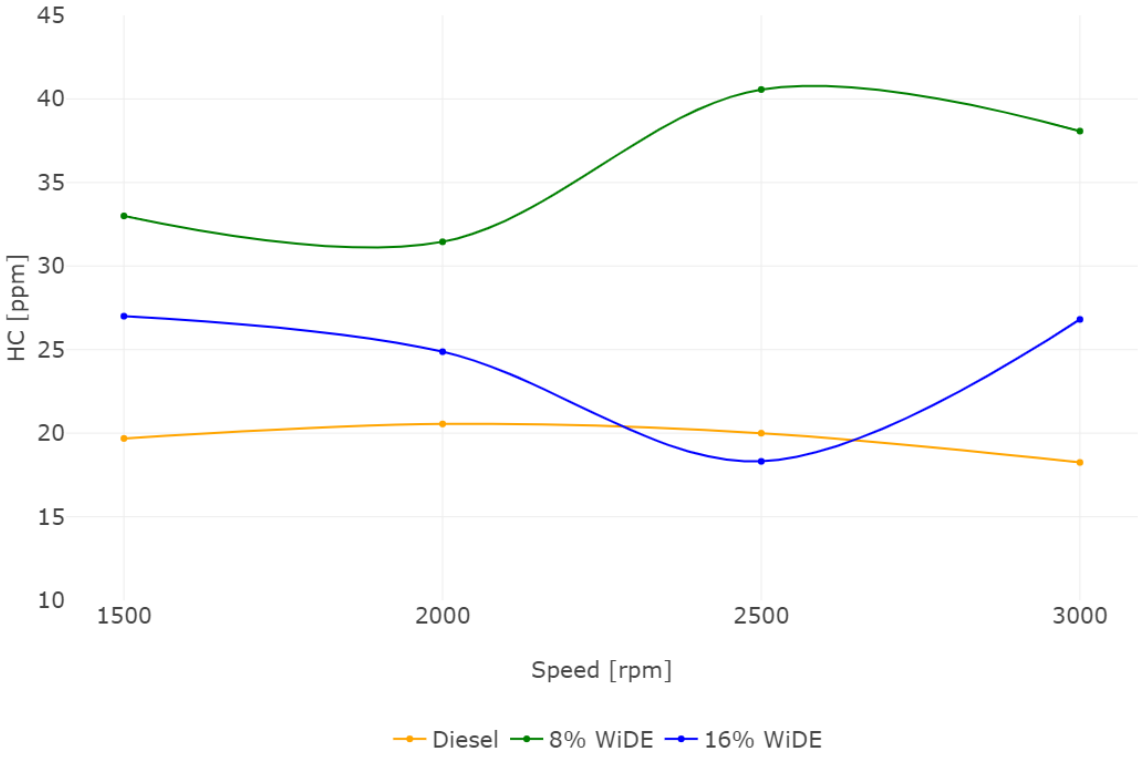

Figure 4.56. HC emissions at 75W load.

Figure 4.57. HC emissions at 100W load.

At every load, HC emissions of diesel are always lower than the emulsions, except at 75W load at 2500 rpm, where HC emissions of 16% WiDE are lower. At 25W load, HC emissions of diesel increase from 1500 rpm to 2000 rpm, remain constant until 2500 rpm, and then decrease until 3000 rpm. For 16% WiDE, HC emissions are higher than 8% WiDE from 1500 rpm to 2000 rpm, and lower from 2500 rpm to 3000 rpm. For 16% WiDE, these emissions increase from 1500 rpm to 2000 rpm, decrease until 2500 rpm, and increase again until 3000 rpm. For 8% WiDE, HC emissions increase from 1500 rpm to 2500 rpm, decreasing until 3000 rpm. At 50W load, HC emissions of 8% WiDE are always higher than 16% WiDE. For 8% WiDE, they increase from 1500 rpm to 3000 rpm. For 16% WiDE, they increase from 1500 rpm to 2000 rpm, decrease until 2500 rpm, and increase until 3000 rpm. For diesel, these emissions remain similar from 1500 rpm to 2500 rpm and decrease until 3000 rpm. At 75W load, HC emissions of 8% WiDE are higher than 16% WiDE. For 8% WiDE, they decrease from 1500 rpm to 2000 rpm, increase until 2500 rpm, and decrease until 3000 rpm. For 16% WiDE, these emissions decrease from 1500 rpm to 2500 rpm and increase until 3000 rpm. For diesel, HC emissions remain constant from 1500 rpm to 2500 rpm, decreasing until 3000 rpm. At 100W load, HC emissions of diesel decrease from 1500 rpm to 2500 rpm, and remain constant until 3000 rpm. These emissions are lower for 16% WiDE at all speeds except 2500 rpm, where 8% WiDE emissions are lower. For 8% WiDE, HC emissions decrease from 1500 rpm to 2000 rpm, remain similar until 2500 rpm, and decrease until 3000 rpm. For 16% WiDE, these emissions decrease from 1500 rpm to 2000 rpm, increase until 2500 rpm, and decrease until 3000 rpm.

4.2.2.7 Power and NO relationship

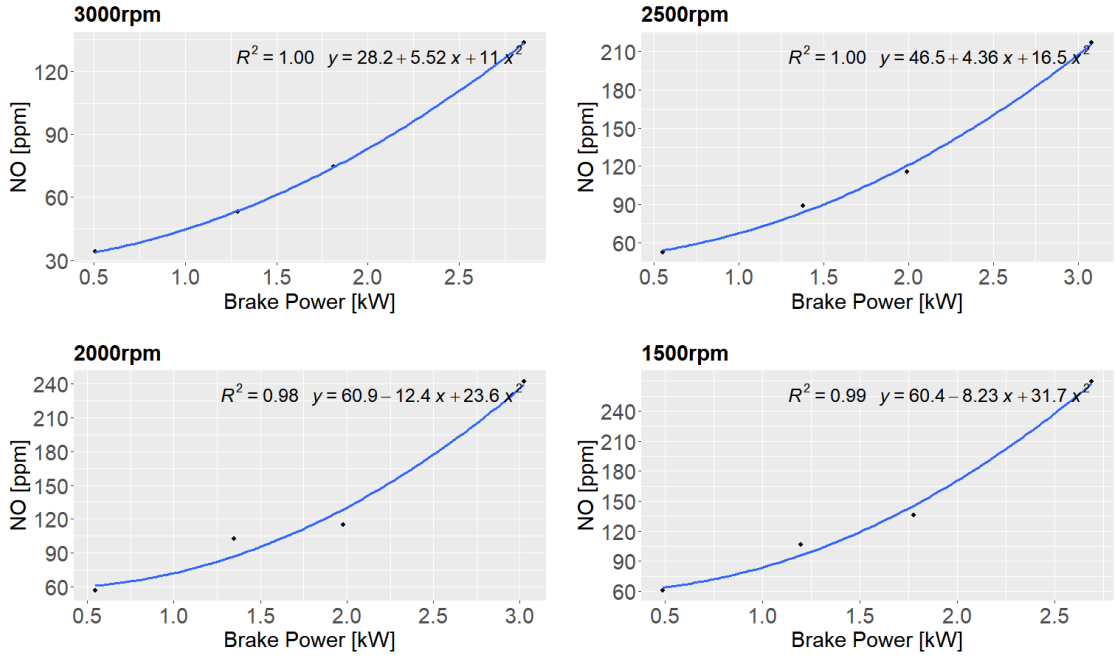

Figure 4.58. BP vs NO relationship of diesel fuel.

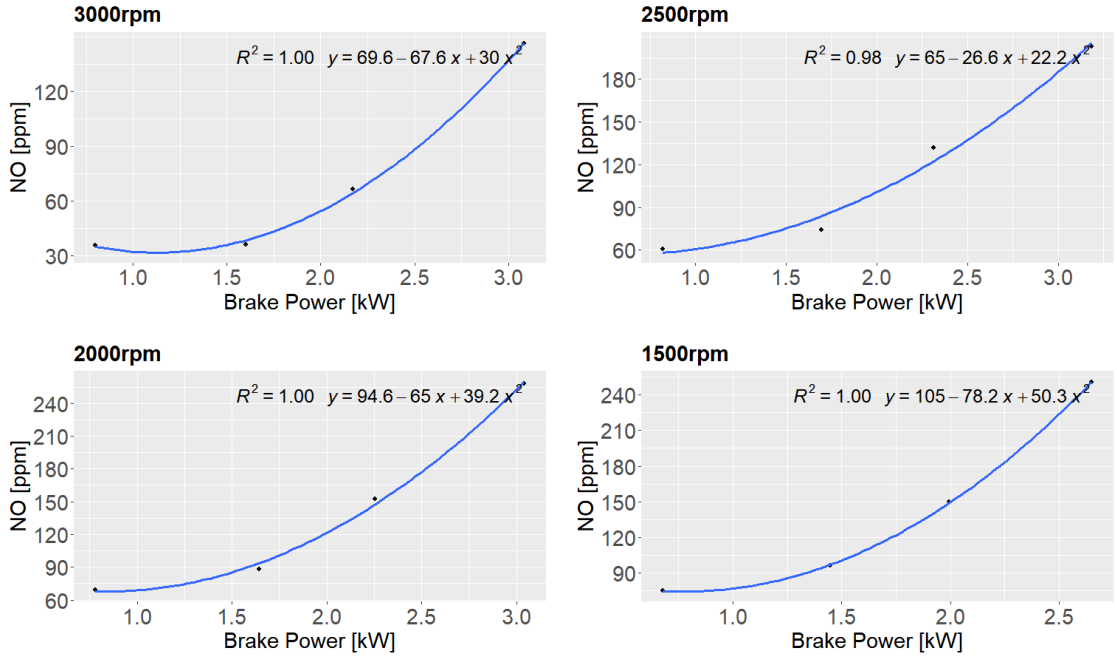

Figure 4.59. BP vs NO relationship of 8% WiDE.

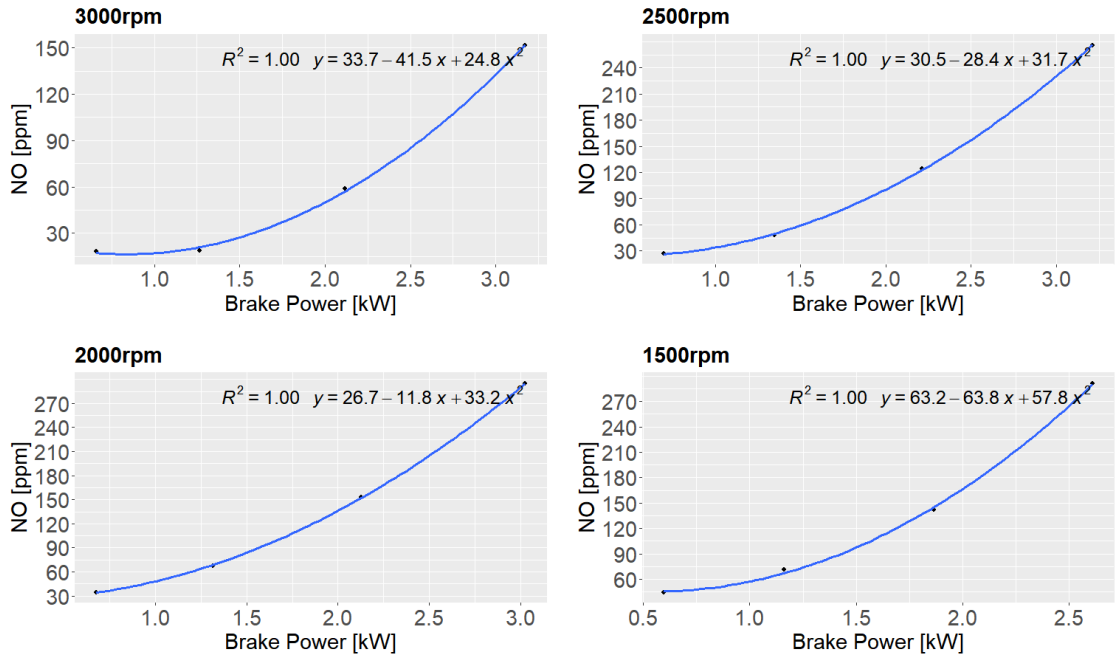

Figure 4.60. BP vs NO relationship of 16% WiDE.

4.2.2.8 NO emissions

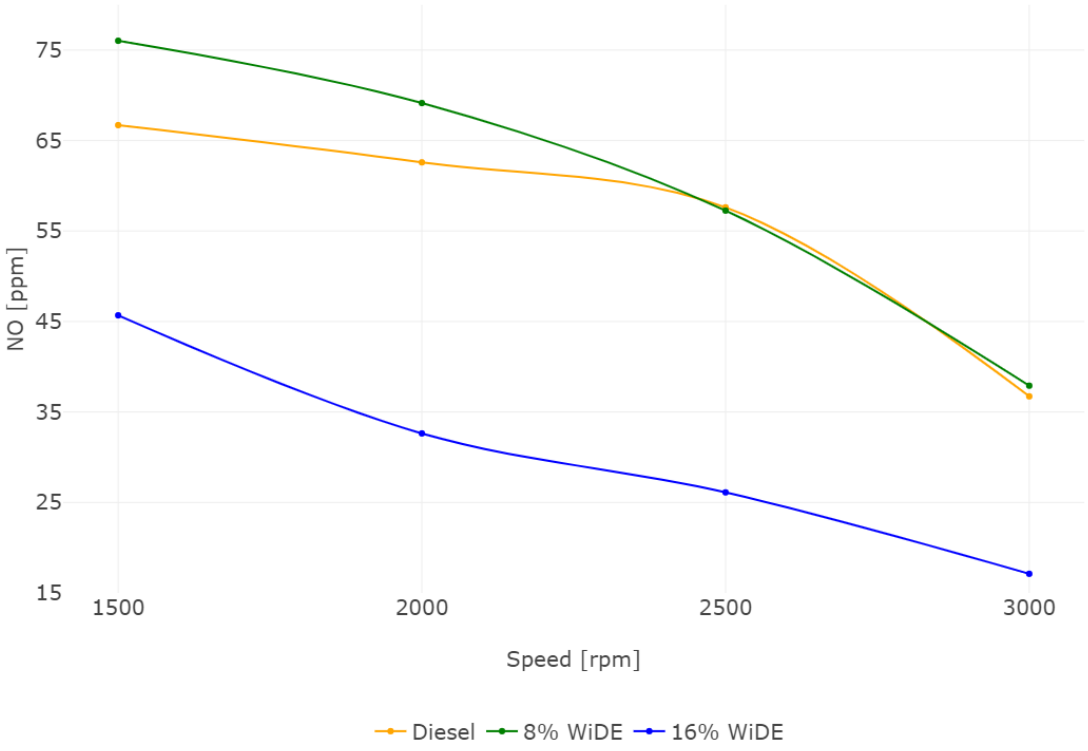

Figure 4.61. NO emissions at 25W load.

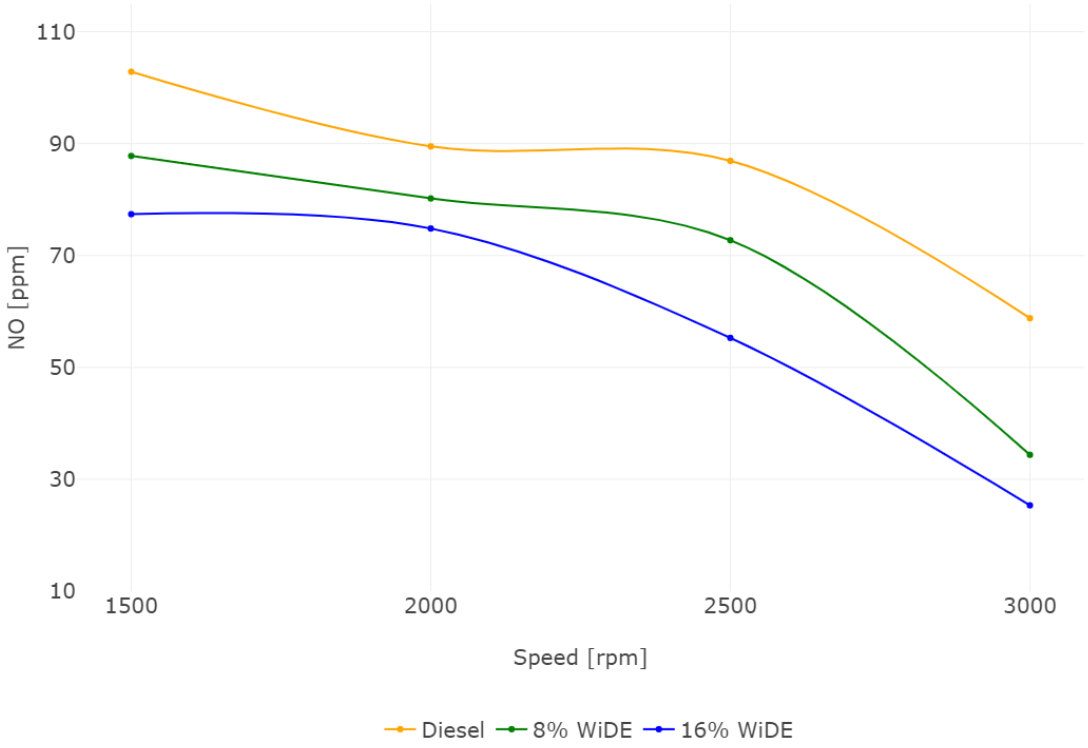

Figure 4.62. NO emissions at 50W load.

Figure 4.63. NO emissions at 75W load.

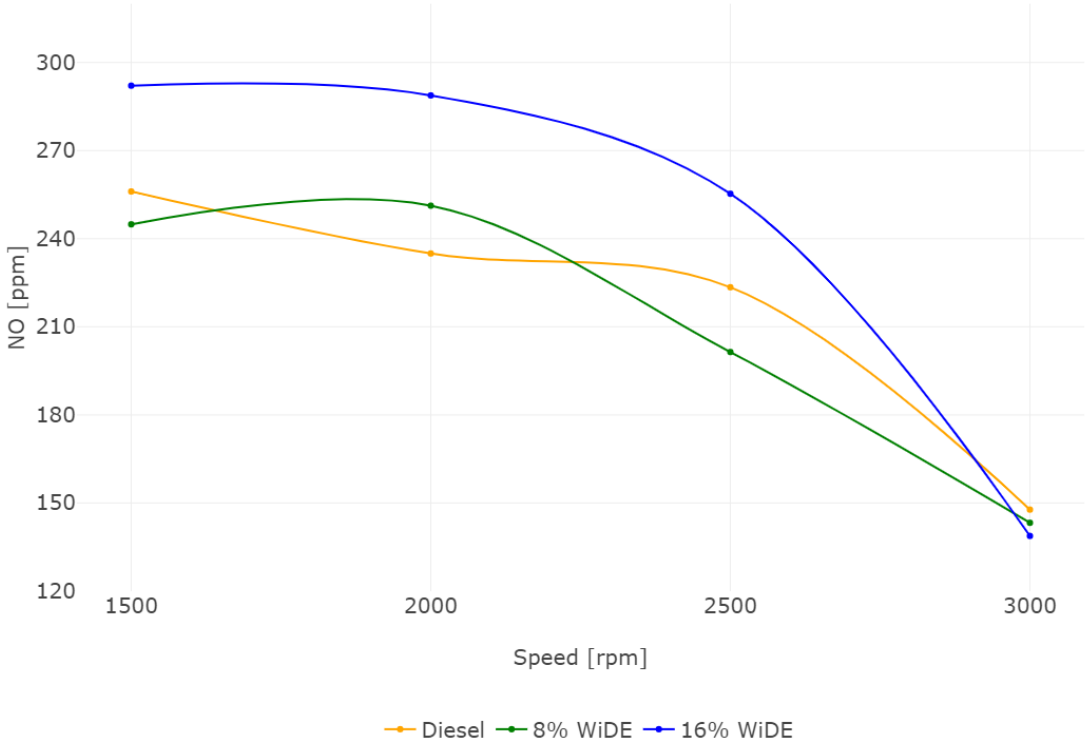

Figure 4.64. NO emissions at 100W load.

At 25W load, the NO emissions of 16% WiDE are lower than the other fuels at every engine speed. NO emissions of 8% WiDE are higher than diesel at 1500 rpm, 2000 rpm, and 3000 rpm, and similar at 2500 rpm. For all fuels, these emissions increase with the decrease in engine speed (increasing engine torque). At 50W load, NO emissions also increase with decreasing engine speed. They are lower for 16% WiDE, followed by 8% WiDE, followed by diesel fuel, at every engine speed. At 75W load, NO emissions also increase with decreasing engine speed, except for 16% WiDE from 1500 rpm to 2000 rpm, where they remain constant. For 8% WiDE, they are lower than the other fuels, except at 3000 rpm where they are higher than 16% WiDE. 16% WiDE also has lower emissions of NO at every engine speed when compared to diesel, except at 2000 rpm where they are higher. At 100W load, NO emissions of 16% WiDE are higher than the other fuels at every engine speed except 3000 rpm where they are lower. NO emissions of 8% WiDE are lower than diesel at every engine speed except at 2000 rpm where they are higher. For diesel fuel and 16% WiDE, NO emissions increase with decreasing engine speed. For 8% WiDE, they increase from 1500 rpm to 2000 rpm and then decrease until 3000 rpm.

4.2.2.9 Power and O_2 relationship

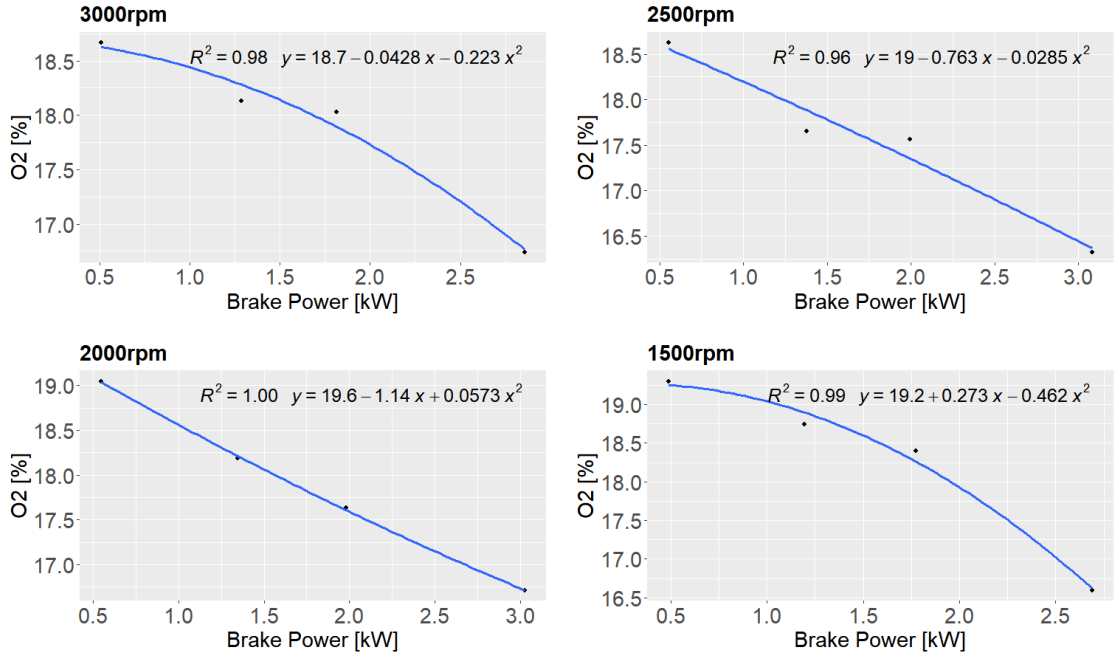

Figure 4.65. BP vs O_2 relationship of diesel fuel.

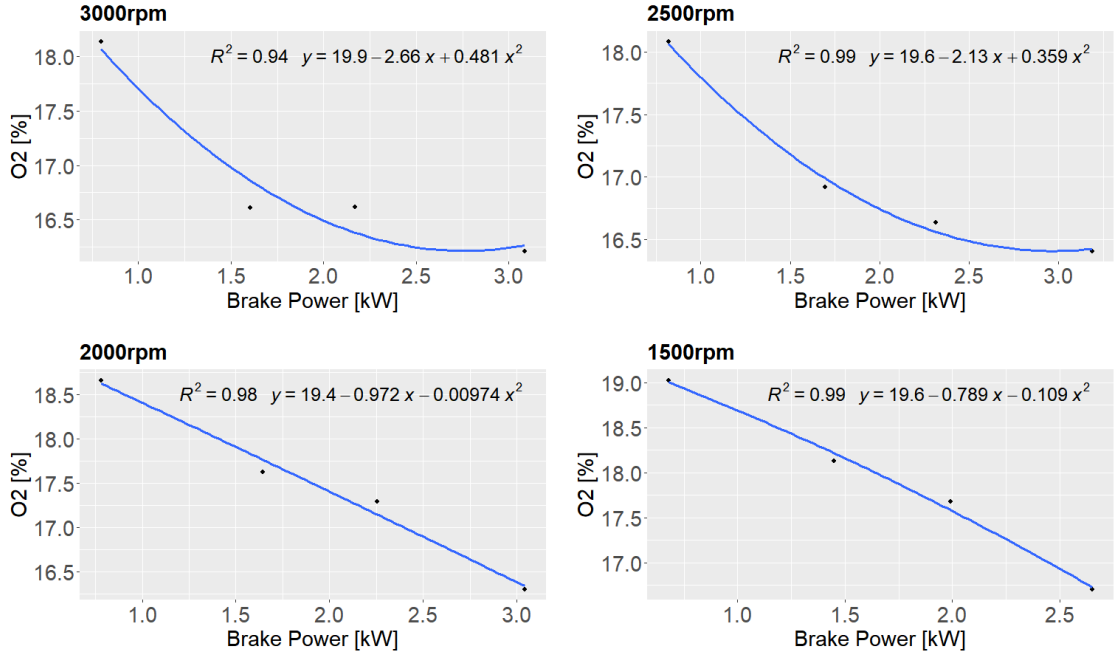

Figure 4.66. BP vs O_2 relationship of 8% WiDE.

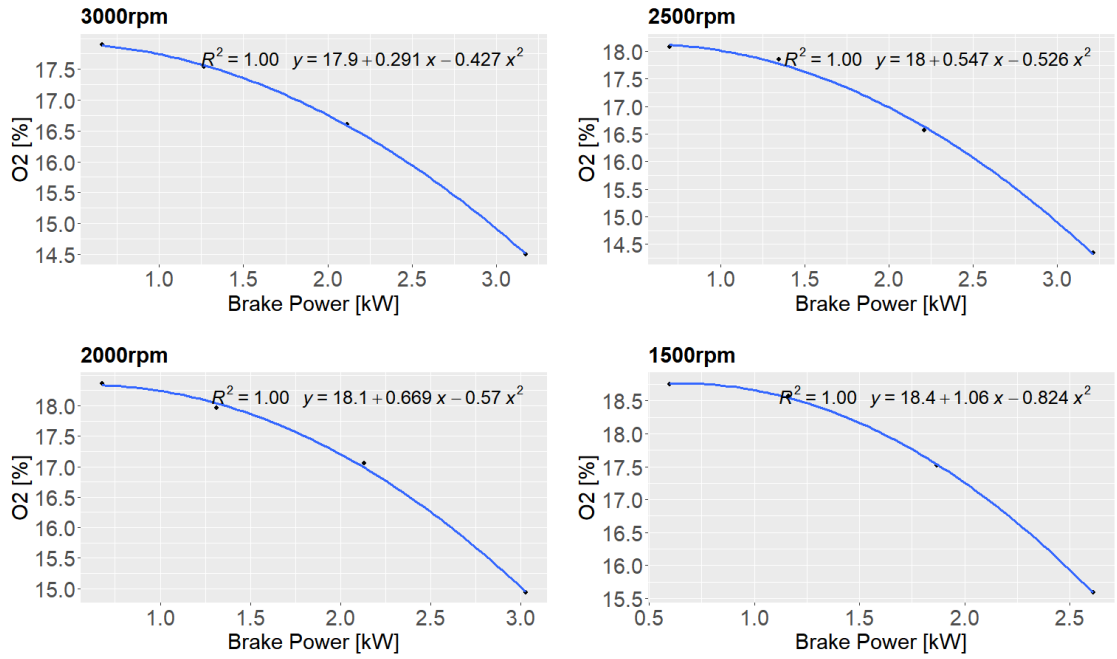

Figure 4.67. BP vs O_2 relationship of 16% WiDE.

4.2.2.10 O_2 emissions

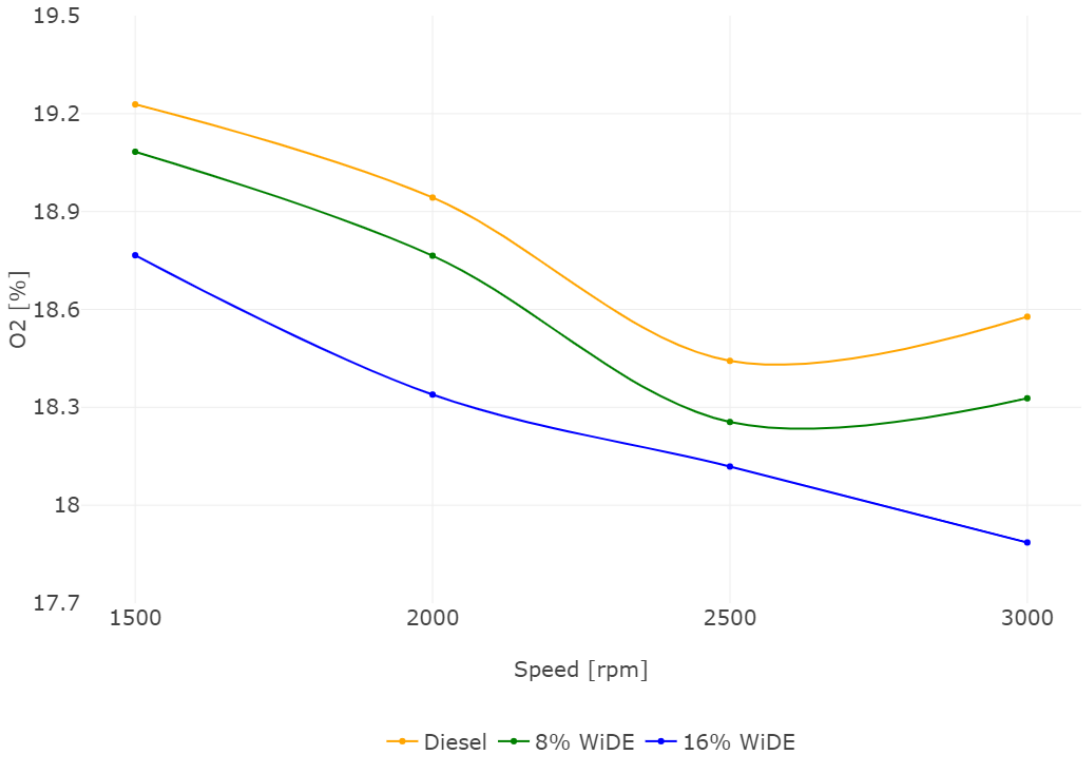

Figure 4.68. O_2 emissions at 25W load.

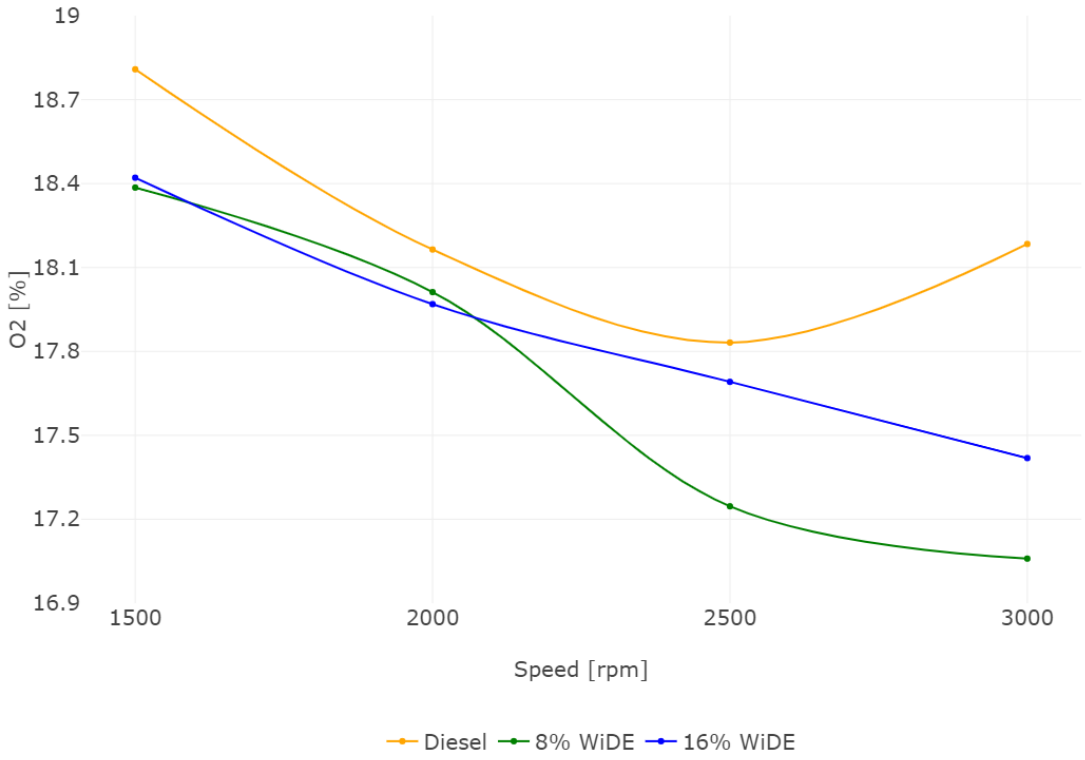

Figure 4.69. O_2 emissions at 50W load.

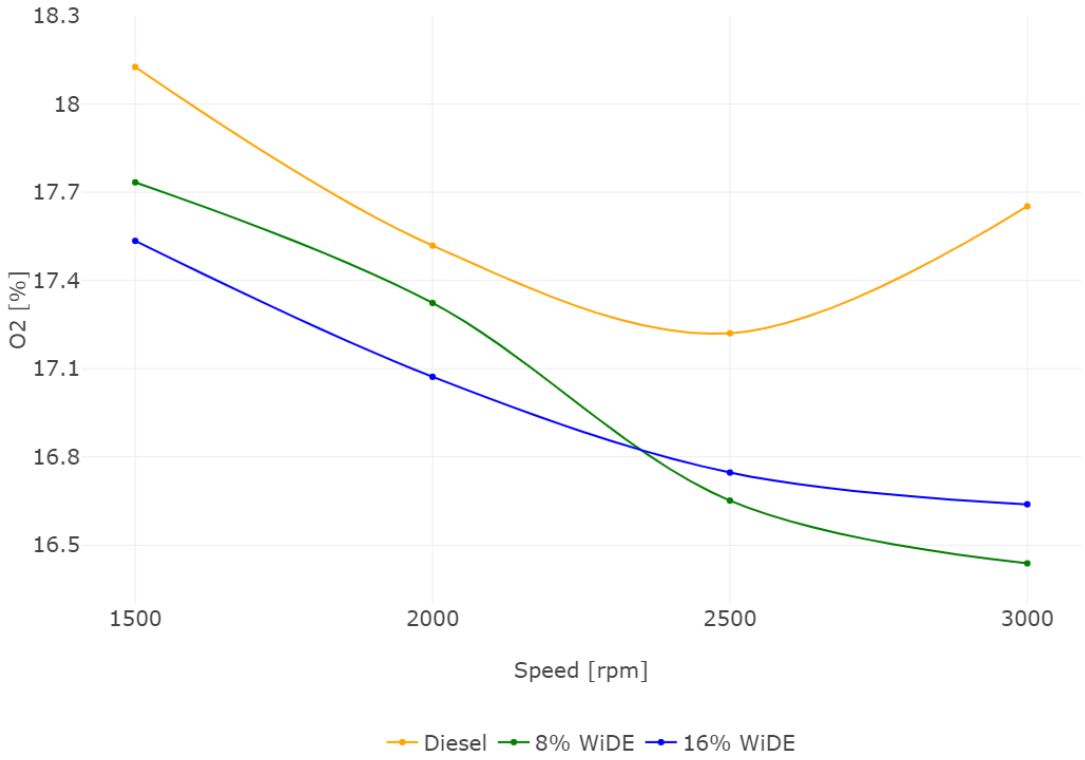

Figure 4.70. O_2 emissions at 75W load.

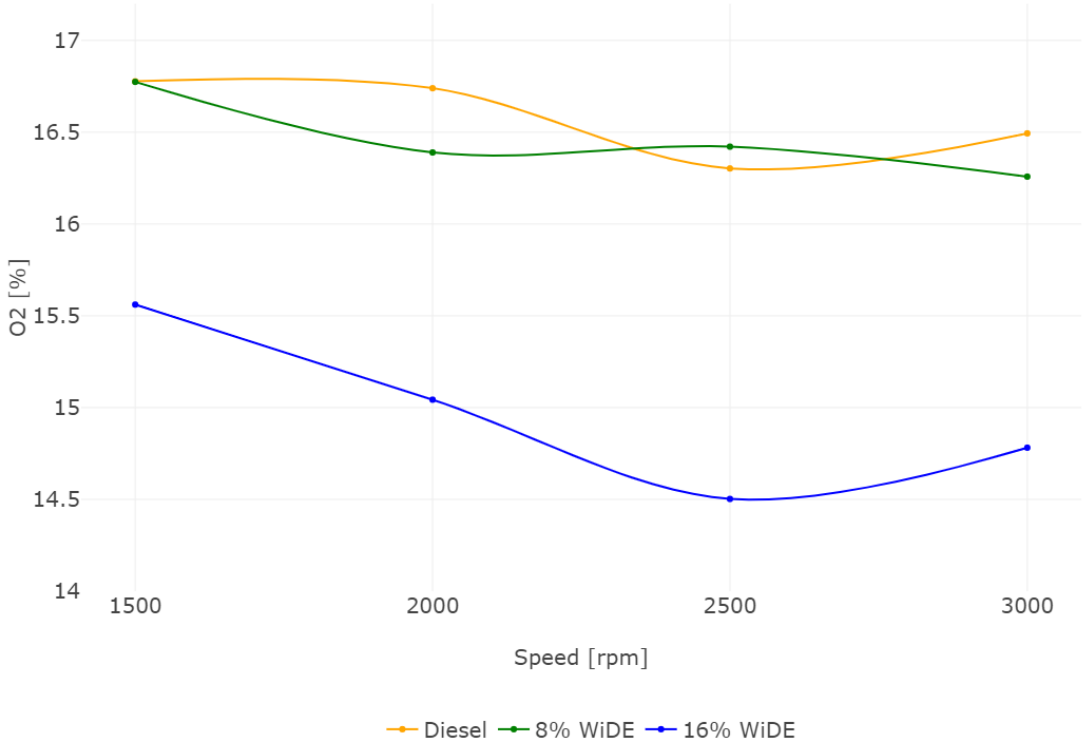

Figure 4.71. O_2 emissions at 100W load.

At 25W load, O_2 emissions of diesel are higher than 8% WiDE, followed by 16% WiDE, at every engine speed. For all fuels, these emissions increase with decreasing engine speed. At 50W load, O_2 emissions of diesel are higher than the other fuels at every engine speed. O_2 emissions of 8% WiDE are lower than 16% WiDE at every engine speed except 2000 rpm, where they are higher. For the emulsions, these emissions increase with decreasing engine speed. For diesel fuel, they decrease from 3000 rpm to 2500 rpm and then increase until 1500 rpm. At 75W load, a similar trend is found, with the exception that at 1500 rpm, the O_2 emissions of 8% WiDE are higher than 16% WiDE. At 100w load, O_2 emissions of 16% WiDE are much lower than the other fuels. O_2 emissions of 8% WiDE are similar to diesel at 1500 rpm, lower at 2000 rpm and 3000 rpm, and higher at 2500 rpm. For 16% WiDE, they decrease from 1500 rpm to 2500 rpm and increase until 3000 rpm. For 8% WiDE, these emissions decrease from 1500 rpm to 2000 rpm, increase until 2500 rpm, and decrease until 3000 rpm. For diesel fuel, O_2 emissions remain constant from 1500 rpm to 2000 rpm, decrease until 2500 rpm, and increase until 3000 rpm.

4.2.2.11 Power and smoke relationship

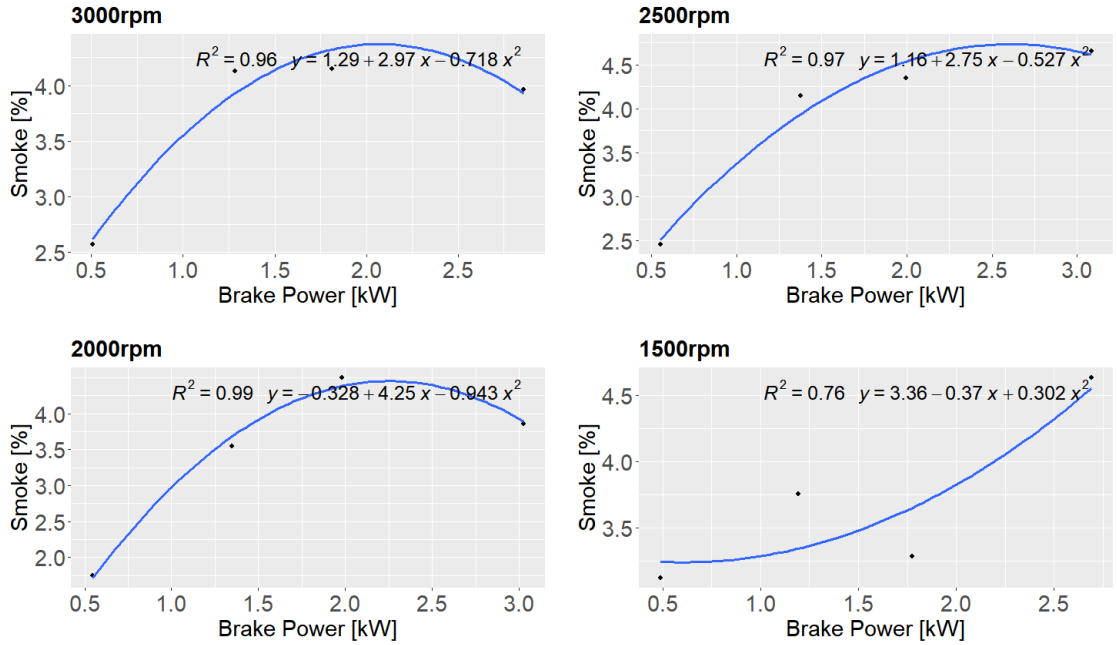

Figure 4.72. BP vs smoke relationship of diesel fuel.

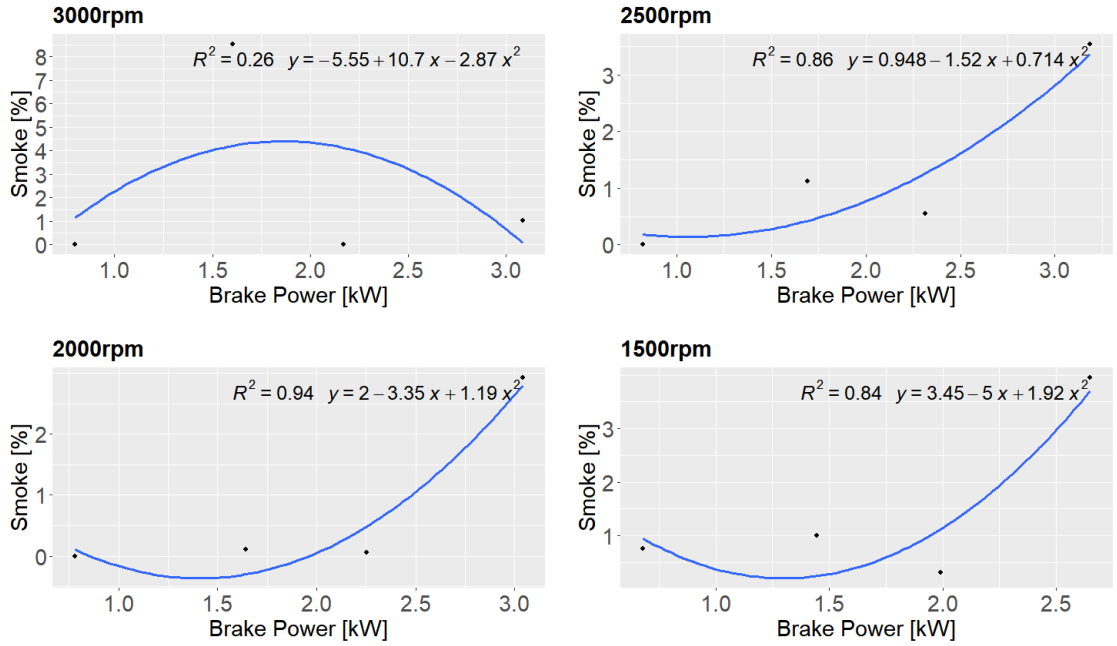

Figure 4.73. BP vs smoke relationship of 8% WiDE.

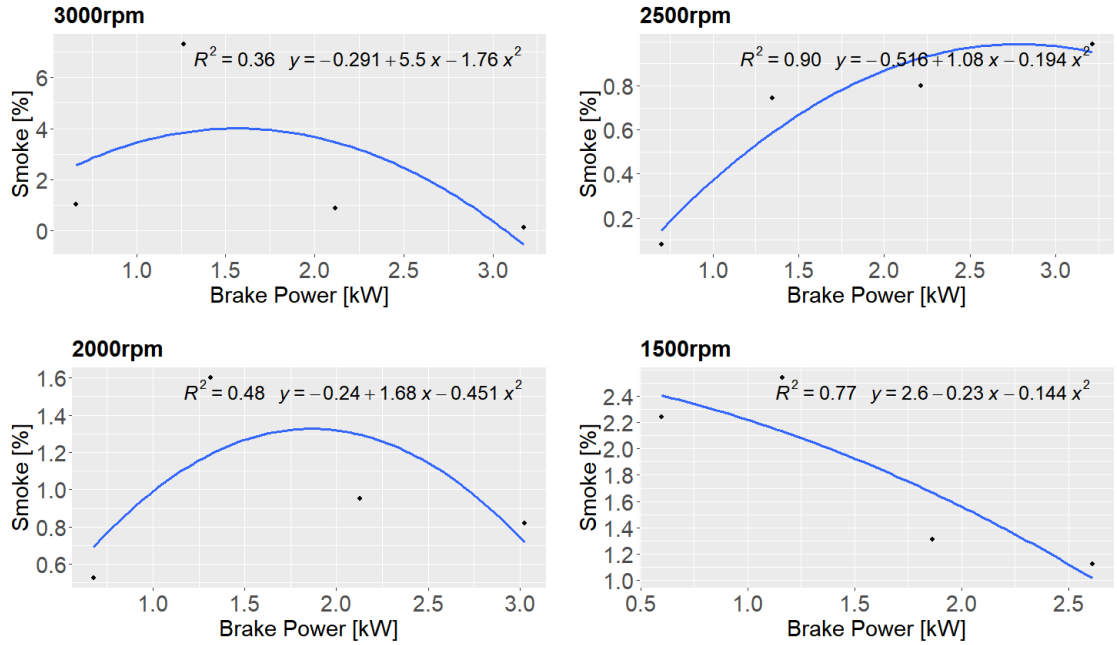

Figure 4.74. BP vs smoke relationship of 16% WiDE.

As shown in Figures 4.72 to 4.74, and similar to CO and HC emissions, a correlation between BP and smoke levels was also hard to achieve. The raw data values were also used for this case.

4.2.2.12 Smoke emissions

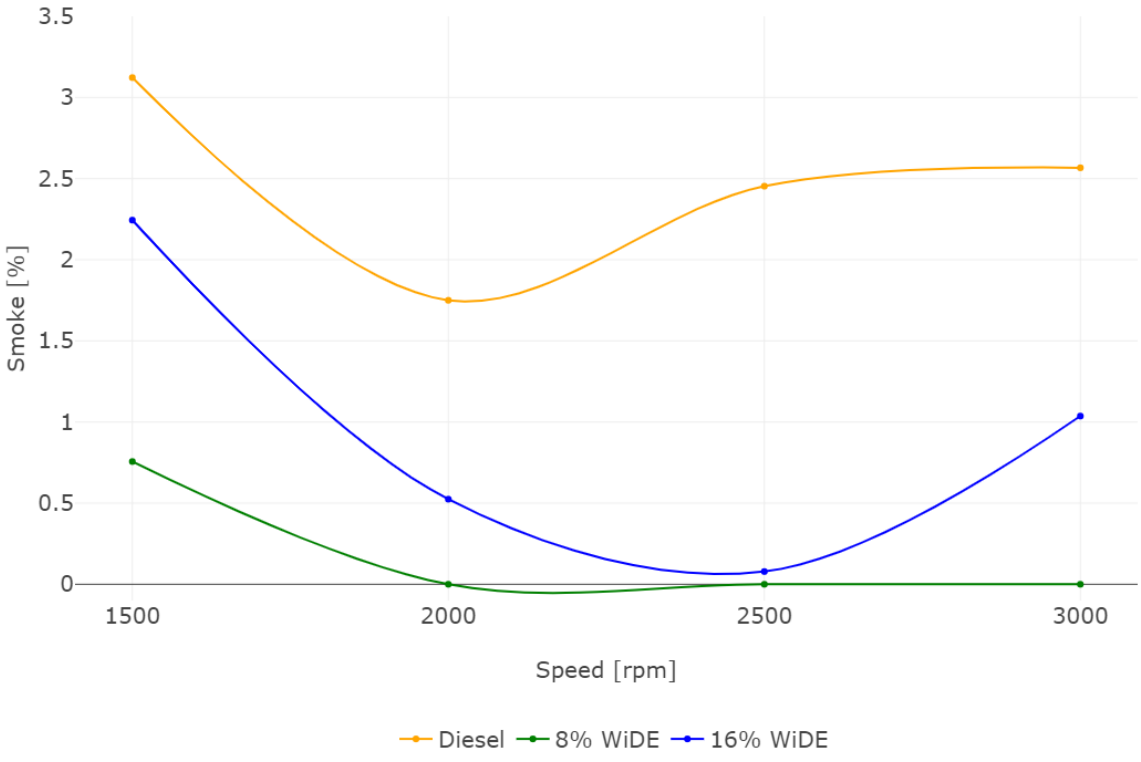

Figure 4.75. Smoke emissions at 25W load.

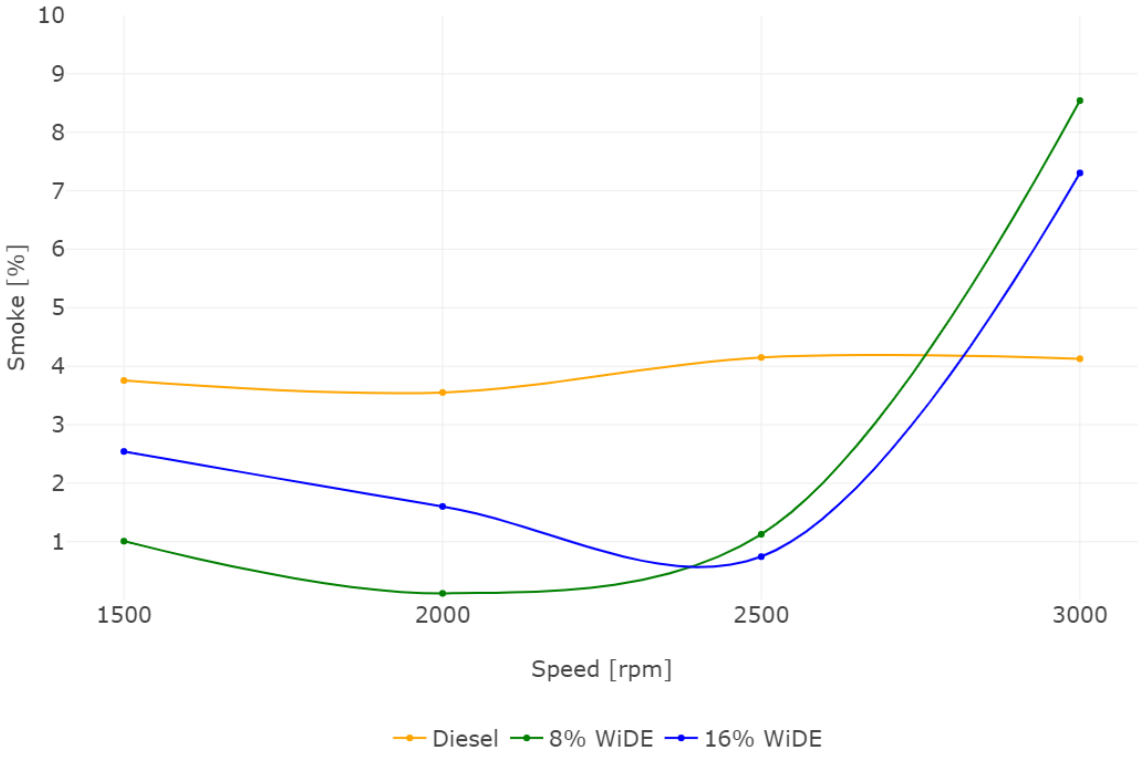

Figure 4.76. Smoke emissions at 50W load.

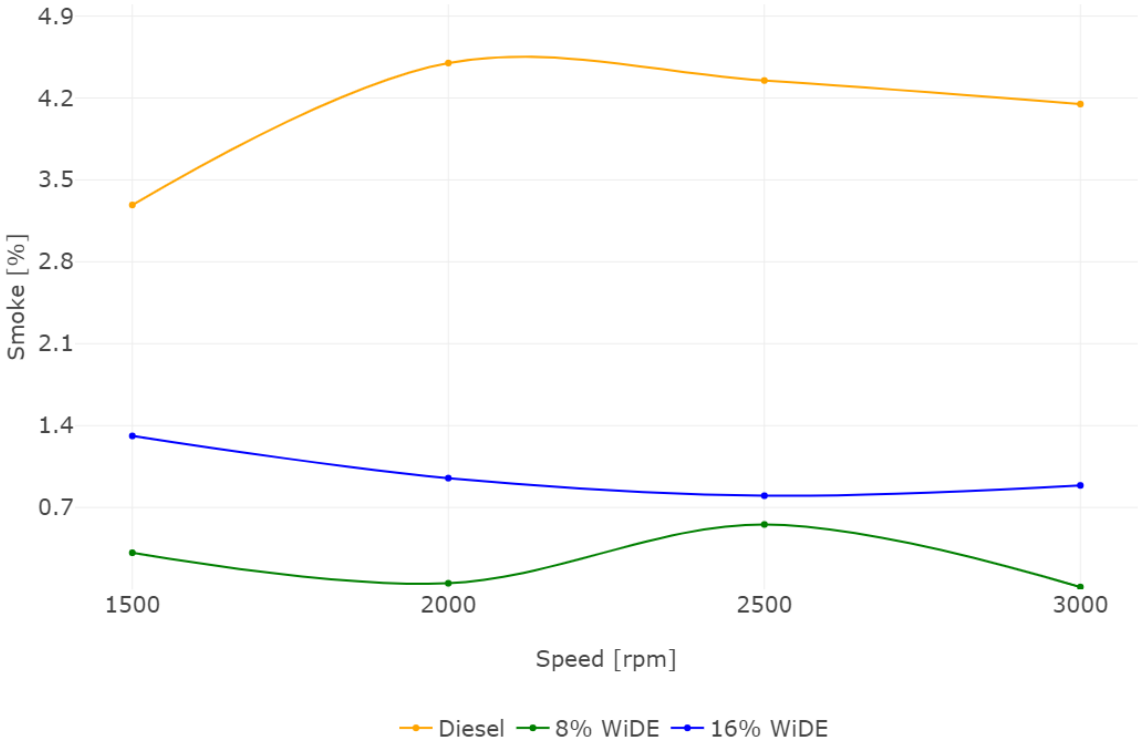

Figure 4.77. Smoke emissions at 75W load.

Figure 4.78. Smoke emissions at 100W load.

At all loads, smoke emissions for diesel are higher when compared to the emulsions, except at 50W load at 3000 rpm, where these emissions are lower. At 25W load, smoke emissions of 8% WiDE are lower than 16% WiDE. For 16% WiDE, these emissions decrease from 1500 rpm to 2500 rpm and increase until 3000 rpm. For 8% WiDE, these emissions decrease from 1500 rpm to 2000 rpm, where they remain zero until 3000 rpm. For diesel, smoke emissions decrease from 1500 rpm to 2000 rpm and increase until 3000 rpm. At 50W load, smoke emissions of 8% WiDE are lower than 16% WiDE from 1500 rpm to 2000 rpm, and higher from 2500 rpm to 3000 rpm. For 8% WiDE, these emissions decrease from 1500 rpm to 2000 rpm and increase until 3000 rpm. For 16% WiDE, these emissions decrease from 1500 rpm to 2500 rpm and increase until 3000 rpm. Smoke emissions for diesel decrease from 1500 rpm to 2000 rpm, increase until 2500 rpm, and remain constant until 3000 rpm. At 75W load, smoke emissions of 8% WiDE are always lower than 16% WiDE. For 16% WiDE, these emissions decrease from 1500 rpm to 2500 rpm and increase until 3000 rpm. For 8% WiDE, these emissions decrease from 1500 rpm to 2000 rpm, increase until 2500 rpm, and decrease until 3000 rpm. For diesel, smoke emissions increase from 1500 rpm to 2000 rpm and decrease until 3000 rpm. At 100W load, smoke emissions of 16% WiDE are always lower than 8% WiDE. For all fuels, these emissions follow the same trend. They decrease from 1500 rpm to 2000 rpm, increase until 2500 rpm, and decrease until 3000 rpm.

4.3 Flight profile vs engine load

During operation, engines experience different loads which are affected by a wide range of conditions. Their speed, torque, and power are continuously adjusted to ensure the most optimum

operational state at any given point. In the case of an aerial vehicle, during take-off, additional engine power is needed to counteract gravity. For instance, during taxiing or landing, less engine power is required to perform the procedure.

In this case, the engine was subjected to different braking torques in an attempt to reproduce the different flight conditions of a diesel-powered aerial vehicle. However, it is necessary to take into account some aspects regarding the experimental test procedures. Different currents and voltages to obtain powers of 25W, 50W, 75W, and 100W in the eddy current dynamometer were applied as a way to simulate 25%, 50%, 75%, and 100% of the engine load. However, according to the manufacturer specifications, the maximum torque obtained during the tests corresponds to 73.3% of the engine's reported peak torque, which would be similar to the maximum torque of the engine operating at an altitude close to 3 km, due to the reduced air density at this condition and less O_2 availability. Several reasons can be pointed out to explain this decision:

- Safety. Despite the maximum engine torque established by the manufacturer being 23.4 Nm, it is not recommended that the engine be kept in that condition for extended periods of time, especially on a newly acquired engine. Since the engine is being tested in stationary conditions, it is important to be careful about overheating issues associated with very high loads, not only for the different components of the engine but also for the dynamometer itself, which was found incapable of sustaining higher loads than the maximum obtained during the experiments.
- Different test procedures. The engine performance curves from the manufacturer were obtained using different test methodologies, under different conditions, and particularly with different test equipment, trying to highlight the maximum torque and power the engine was capable of reaching. It is comprehensive that by using a home-built eddy current dynamometer, the results obtained would be different from the ones specified, especially because manufacturers often publish the performance curves under full load condition over a wide range of speeds by accelerating and decelerating the engine, and not in stationary conditions as performed in this work. If higher loads were applied while measuring the torque output of the engine at 3000 rpm, decreasing the accelerator position to measure torque at the remaining lower rpms would reduce the air intake of the engine, which would lead to an engine stall as the engine wouldn't be able to keep up with the applied load at lower engine speeds, which were used for comparison between the fuels.
- Equipment limitations. After trying to maintain higher loads for long periods of time, the belt connecting the engine to the dynamometer shaft was constantly tearing due to the extreme angular velocities. On top of this, higher loads equal to a higher number of eddy currents induced in the dynamometer's aluminium disk, leading to overheating, followed by warping. A very hot rotating disk would also diminish the amount of eddy currents on its surface, reducing the torque and power available while keeping the dynamometer's load constant.

- Fuel limitations. By reducing the amount of diesel in the emulsified fuel, less energy was available to achieve the same torque. Since the results were being recorded at 3000 rpm, 2500 rpm, 2000 rpm, and 1500 rpm with the highest torque being attained at 1500 rpm, it could reach a point where due to the lower energy present in the emulsion, it wouldn't be able to maintain such low rpm without the engine stalling. By decreasing the maximum considered load, it was possible to ensure that all fuels were able to keep the engine running at every different condition, especially at the lower speed of 1500 rpm.

Having these previous factors in consideration, it was decided to assign 100W as the maximum considered load for this case and assign each engine load percentage to a specific phase of flight (following the approach taken in [214]), as described in Table 4.1.

Table 4.1. Engine load vs flight phase.

Dynamometer Load [W]	*Considered Engine Load [%]*	*Maximum BMEP [bar]*	*Average BMEP [bar]*	*Flight Phase*
25	25	1.028	0.789	Taxiing
50	50	2.241	1.698	Descent, approach, and landing
75	75	3.236	2.492	Cruising
100	100	4.534	3.585	Take-off and climb

The maximum BMEP of this engine, corresponding to its peak torque given by the manufacturer of 23.4 Nm is 6.365 bar. Even though the BMEPs obtained by using Equation 2.7 may be lower than the ones registered in an aerial vehicle during flight, they can still be differentiated as lower loads, medium loads, or higher loads, indicating how much work the engine is being subjected to in a specific operating condition, providing load conditions different enough that would allow a reasonable comparison between the different fuels over a wide range of requirements. Figures 4.79 to 4.86 show how the different variables relate to engine load and engine speed.

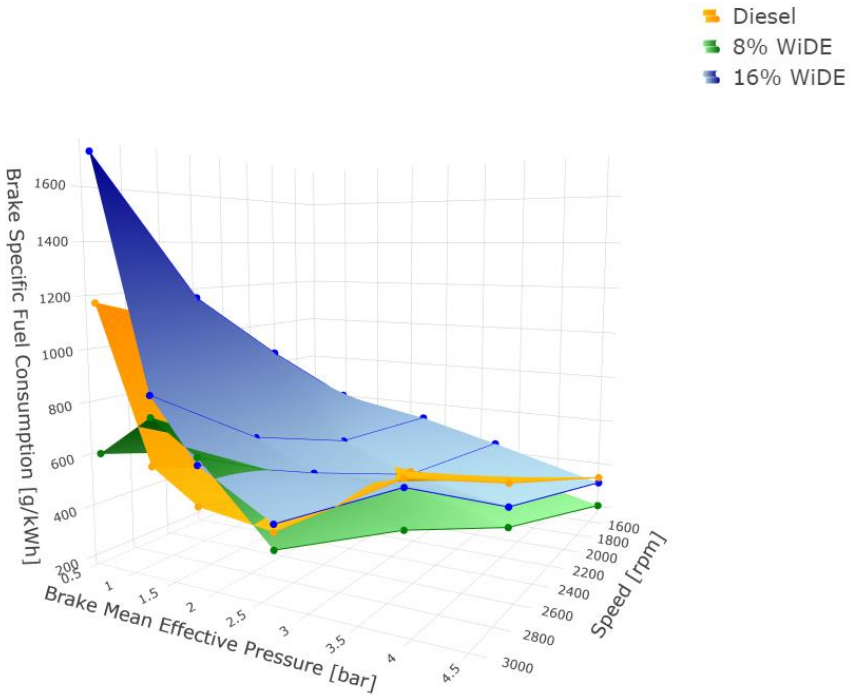

Figure 4.79. BMEP vs speed vs BSFC.

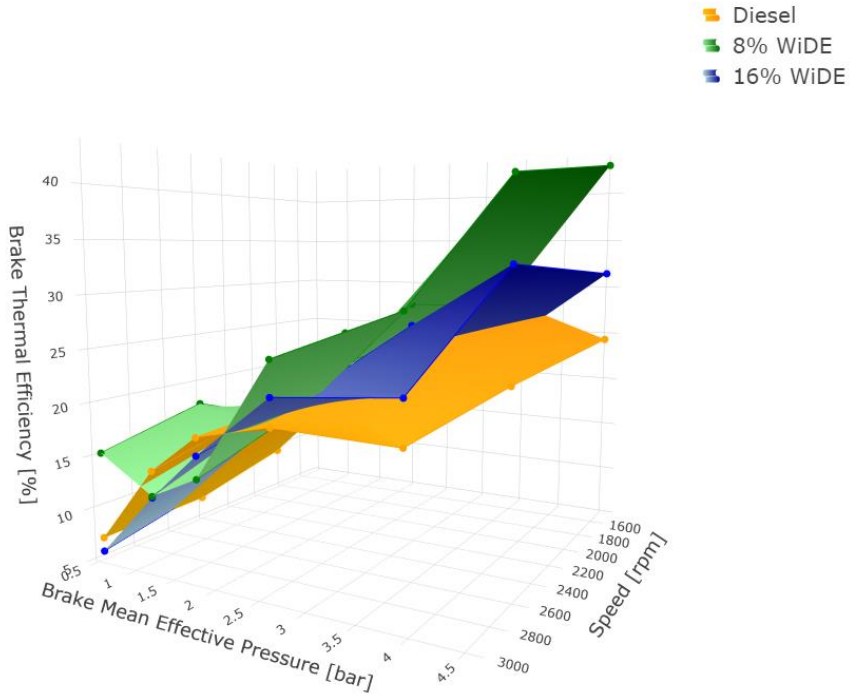

Figure 4.80. BMEP vs speed vs BTE.

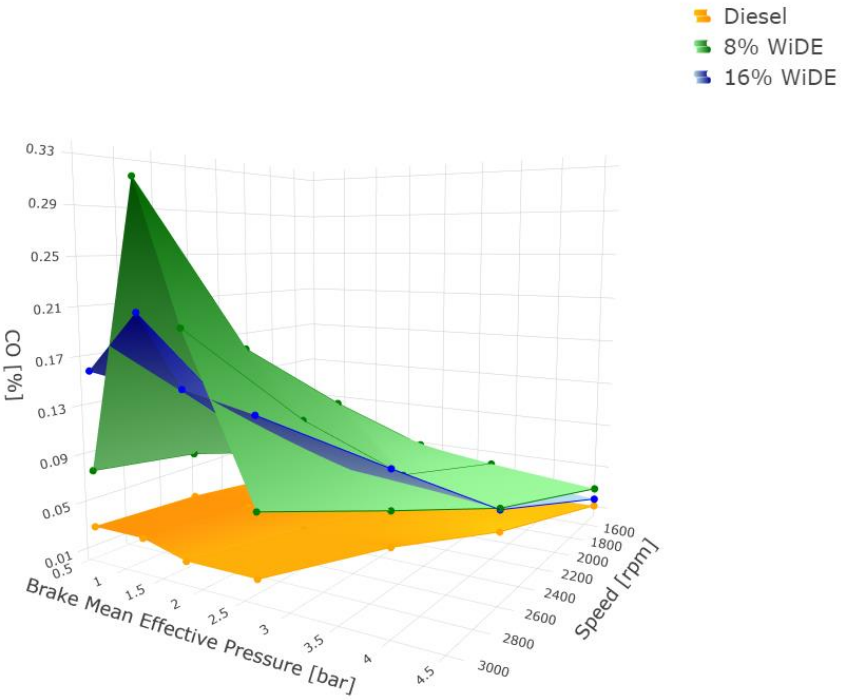

Figure 4.81. BMEP vs speed vs CO.

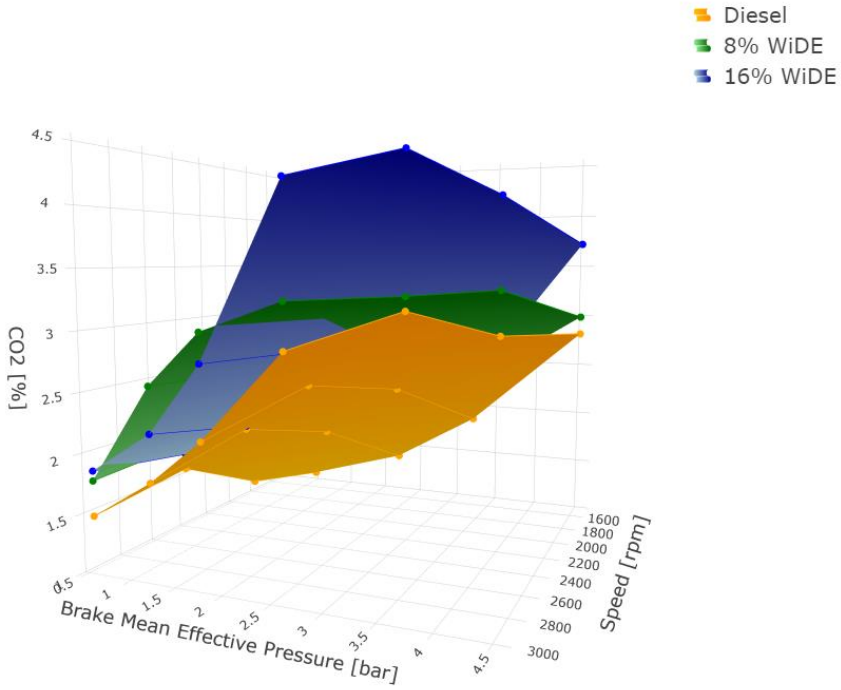

Figure 4.82. BMEP vs speed vs CO_2.

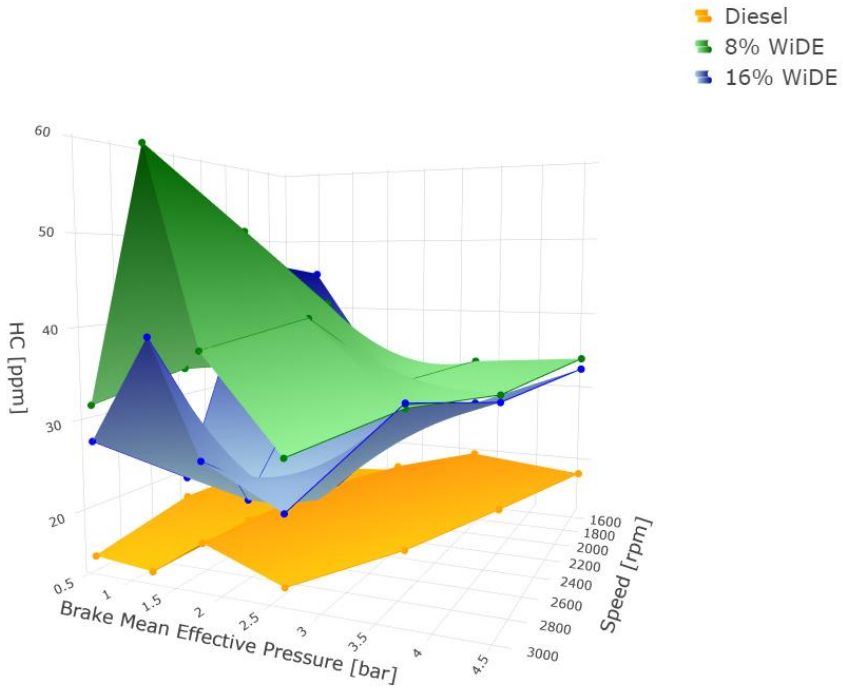

Figure 4.83. BMEP vs speed vs HC.

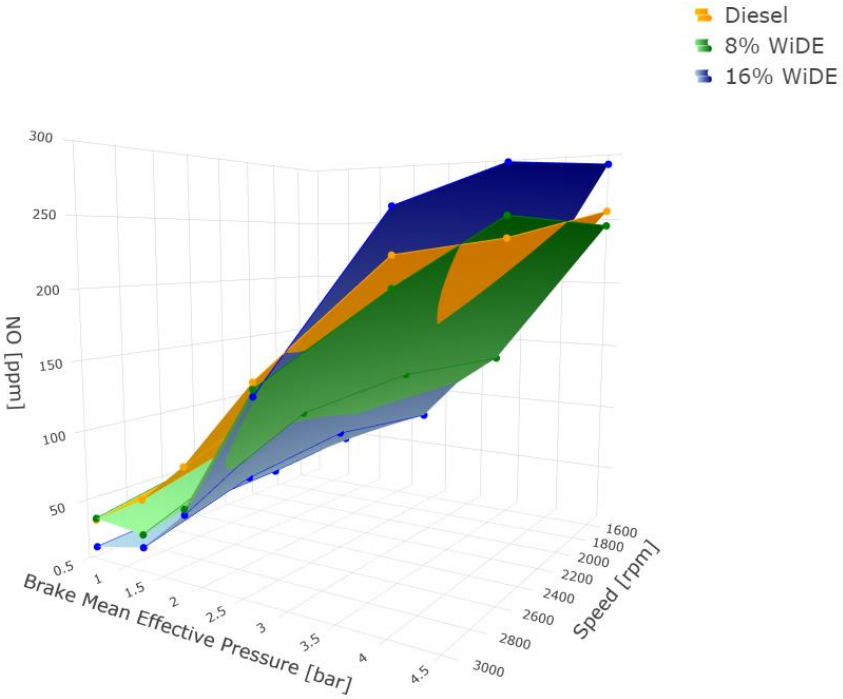

Figure 4.84. BMEP vs speed vs NO.

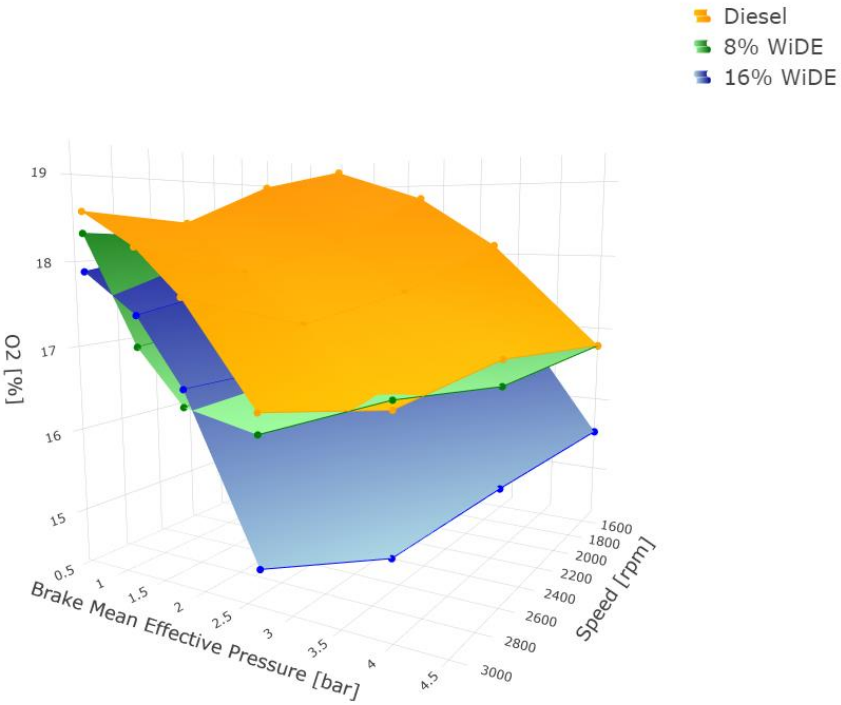

Figure 4.85. BMEP vs speed vs O_2.

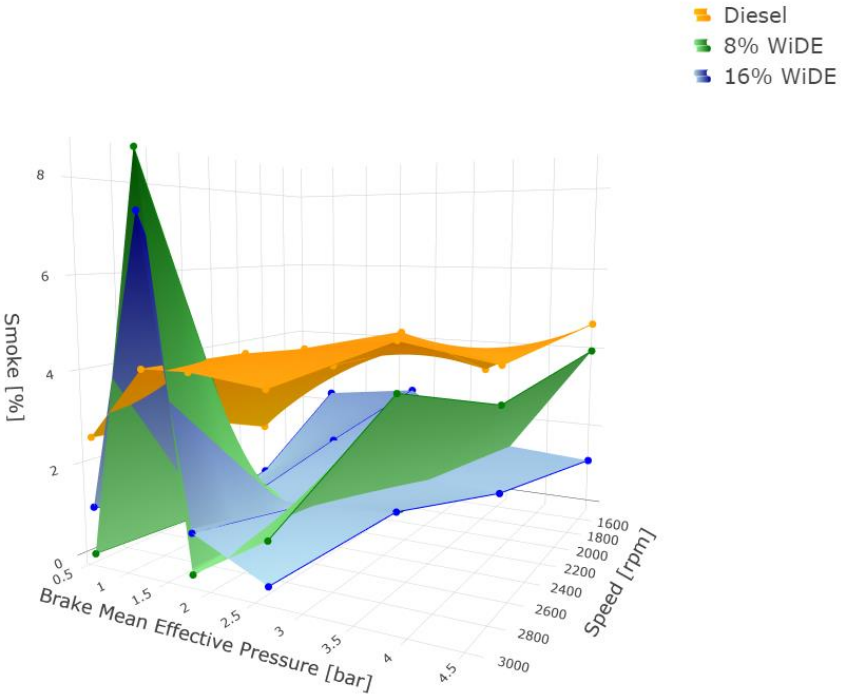

Figure 4.86. BMEP vs speed vs smoke.

Figures 4.87 to 4.95 show how the different parameters vary across the different engine loads. For these figures, the average value of the different variables was calculated across the different engine speeds to obtain a single value for each load condition.

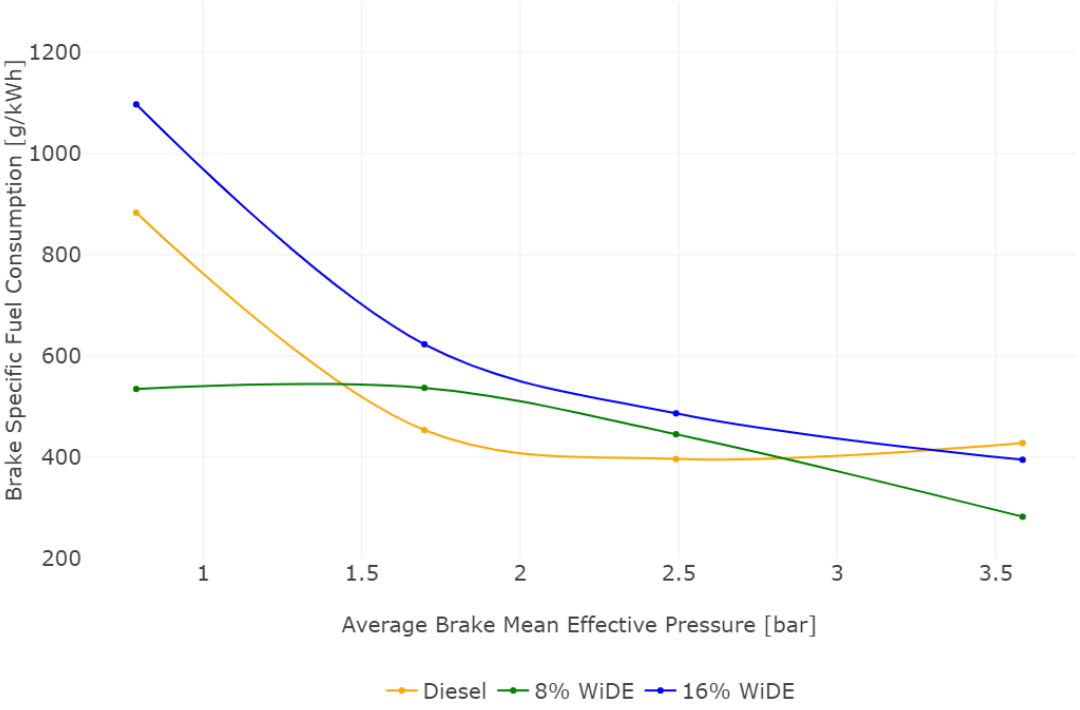

Figure 4.87. BMEP vs BSFC.

As can be seen, the BSFC of 16% WiDE is higher when compared to 8% WiDE at every load condition. It is also higher than diesel fuel in every condition except at the maximum load condition, where it is lower. The BSFC of 8% WiDE is lower than diesel fuel at the lowest and highest load condition, and higher in 1.698 bar and 2.492 bar load conditions. For 16% WiDE, BSFC decreases with the increase of engine load. For diesel fuel, BSFC decreases from 0.789 bar to 2.492 bar and then increases to 3.585 bar. For 8% WiDE, BSFC remains constant from 0.789 bar to 1.698 bar and then decreases until 3.585 bar. The occurrence of puffing and micro-explosions in emulsion droplets may be responsible for increasing the force acting on the piston during the expansion stroke [215], increasing the burning rate, and reducing the fuel flow needed to achieve a certain power, reducing BSFC in some cases. In contrast, the increased spray penetration and injection duration due to different fuel properties and the lower energy content of the fuel may increase this parameter [216].

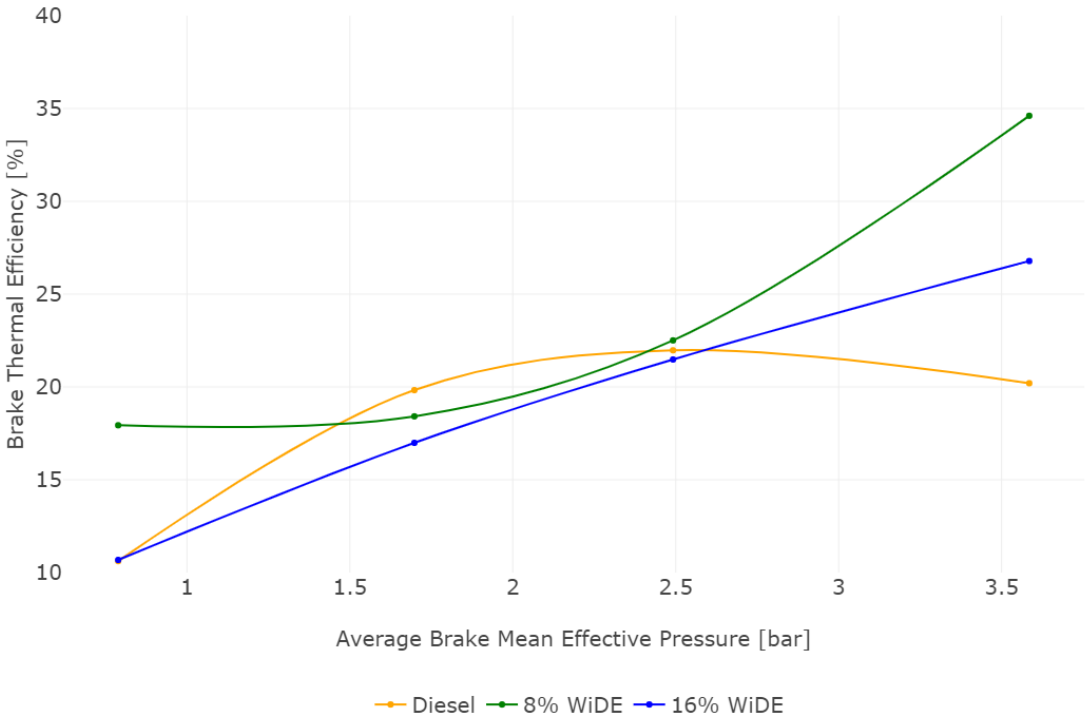

Figure 4.88. BMEP vs BTE.

Regarding BTE, 8% WiDE exhibits higher values compared to 16% WiDE at every load condition. The BTE of diesel fuel is lower than 8% WiDE and similar to 16% WiDE at 0.789 bar, higher than both emulsions at 1.698 bar, lower than both emulsions at 3.585 bar, and higher than 16% WiDE but lower than 8% WiDE at 2.492 bar. For 16% WiDE, BTE increases with engine load. For diesel fuel, it increases with engine load until 2.492 bar and then decreases until 3.585 bar. For 8% WiDE, it remains constant from 0.789 bar to 1.698 bar and then increases until 3.585 bar. As BTE is inversely proportional to BSFC, the curves are oppositely similar. Due to the lower LHV values of the emulsions (less diesel and therefore less energy content) [217], BTE can also improve, as the lower potential energy of the emulsified fuel molecules is better harvested for producing useful work, and less energy is lost in the form of heat.

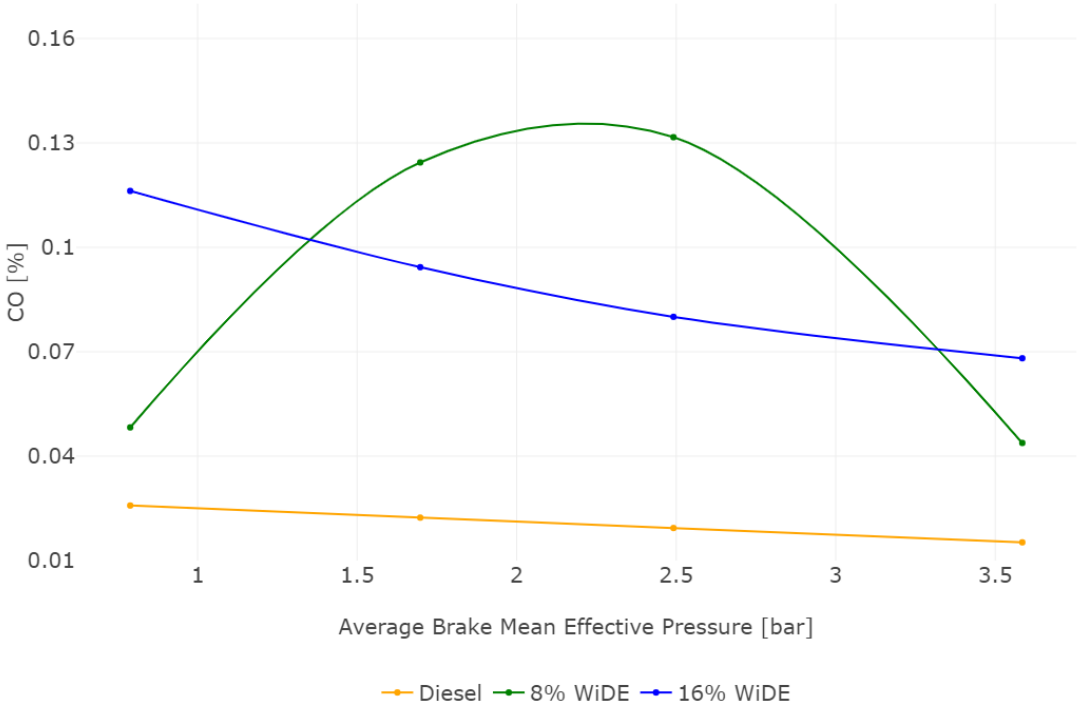

Figure 4.89. BMEP vs CO.

Regarding CO emissions, they are always lower for diesel fuel compared to both emulsions. These results are in accordance with the most recent literature [169]. For 8% WiDE, they are lower compared to 16% WiDE at the minimum and maximum load conditions, and higher at 1.698 bar and 2.492 bar. These emissions decrease for diesel fuel and 16% WiDE with the increase of engine load, and increase from 0.789 bar to 2.492 bar, followed by a decrease to 3.585 bar for 8% WiDE. Higher CO emissions for the emulsions can be a result of incomplete combustion of some fuel molecules, possibly due to the excess carbon atoms present in the surfactants that weren't fully combusted, lack of mixture uniformity, lower combustion chamber temperature, cylinder pressure, slow soot burning, and lower O_2 availability preventing CO from oxidizing to CO_2, and increased viscosity of the emulsified fuels leading to different spray characteristics after the injector [218]. On the other hand, a higher cetane number of diesel fuel due to its shorter ignition delay may reduce these emissions [219].

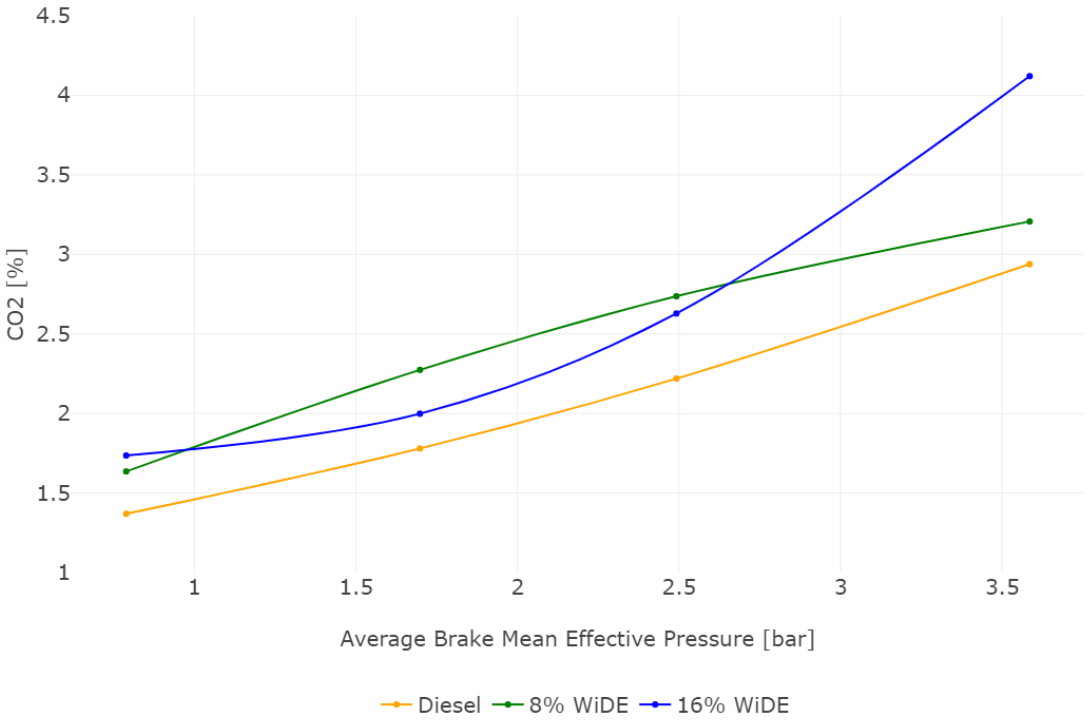

Figure 4.90. BMEP vs CO_2.

Regarding CO_2 emissions, for every fuel tested, they increase with increasing engine load. The CO_2 emissions of diesel are always lower than the emulsions at every load condition. Similar to CO emissions, CO_2 emissions for 8% WiDE are lower than 16% WiDE at the minimum and maximum load conditions, and higher at both mid-load conditions. A complete combustion of a hydrocarbon with O_2 would only produce CO_2 and water vapour. The higher CO_2 emissions of the emulsions can be due to better combustion properties and favourable conditions for CO oxidation into CO_2 [220]. Better burning characteristics can lead to a more complete combustion and therefore emit more CO_2 [221], increasing with engine load for all cases as more fuel is being burned per engine cycle.

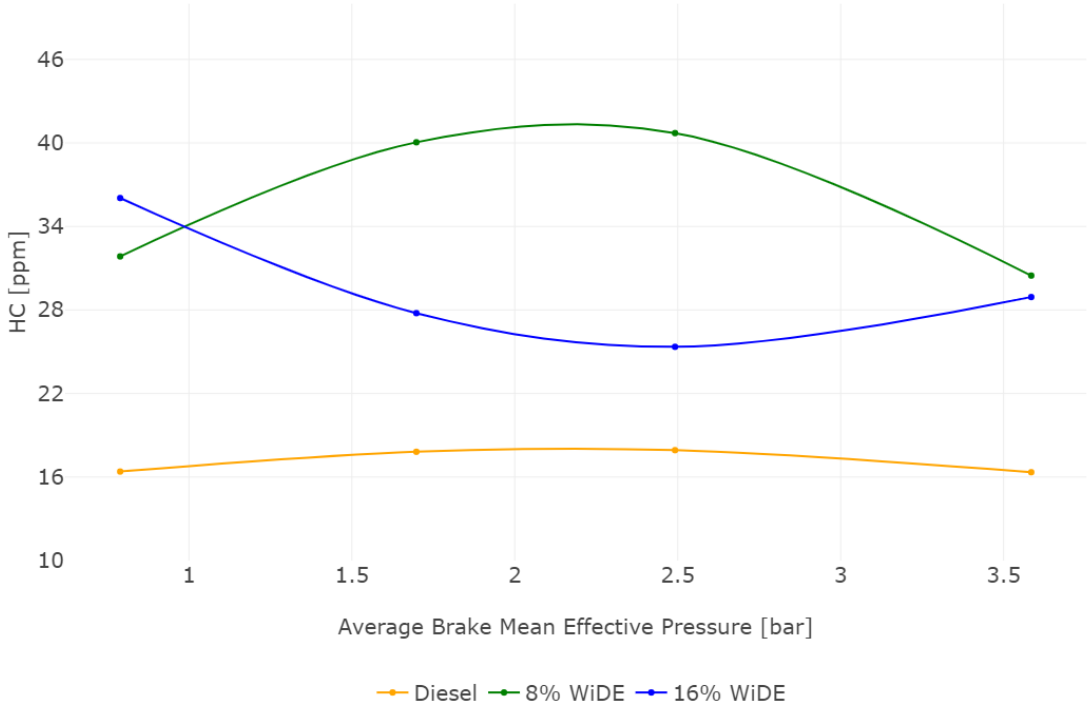

Figure 4.91. BMEP vs HC.

As for HC emissions, they are lower for diesel at every load condition compared to the emulsions. These findings are in accordance with the most recent literature [153]. For diesel fuel, they remain overall constant throughout the different load conditions. For 16% WiDE, they decrease to 2.492 bar and then increase to 3.585 bar. For 8% WiDE, they increase to 1.698 bar, remain similar until 2.492 bar, and then decrease to 3.585 bar. Similar to CO emissions, these emissions are also a result of incomplete combustion of fuel molecules, strongly influenced by the air-fuel ratio, combustion temperature [222], and cylinder pressure [223]. The higher HC emissions for the emulsions may also be due to increased hydrogen and carbon atoms in the emulsifiers. Puffing and microexplosions may also increase the spray penetration length, leading to spray wall impingement and spray wall wetting [224]. The production or breakdown of HC compounds, resulting in the formation of intermediate products, can also explain this increase [225]. During preliminary tests, it was also found that increased fuel viscosity significantly increases HC emissions in the emulsions.

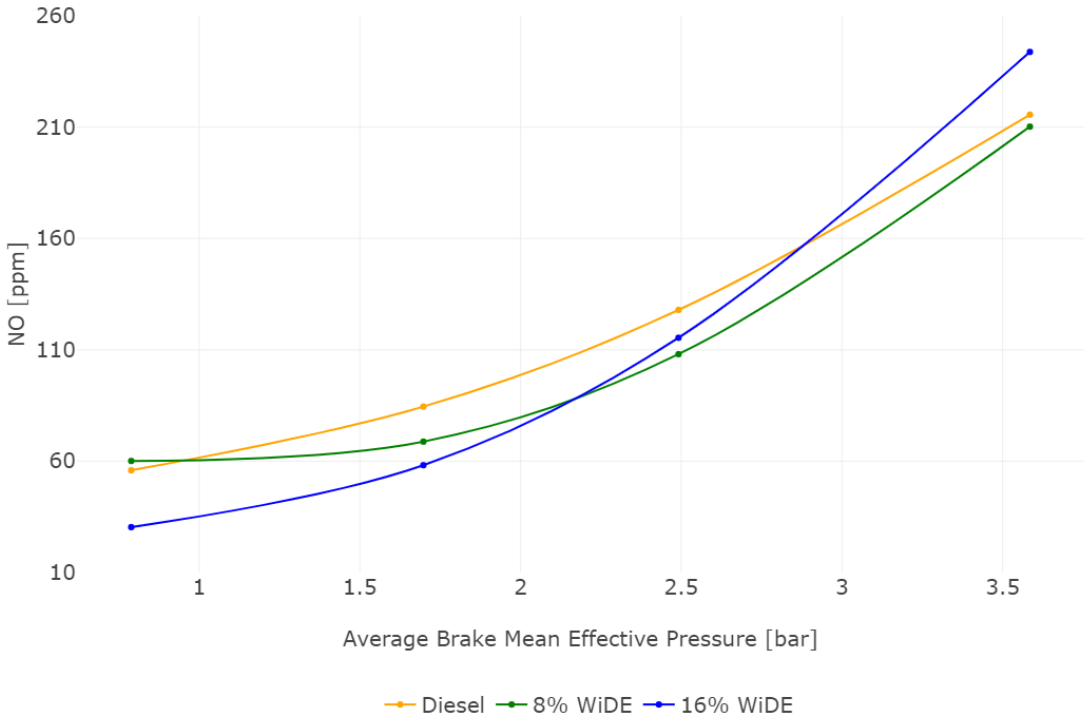

Figure 4.92. BMEP vs NO.

Regarding NO emissions, for all fuels tested, they increase with increasing engine load. For diesel fuel, these emissions are always higher compared to the emulsions, except at 0.789 bar where NO emissions of 8% WiDE are slightly higher, and 3.585 bar where NO emissions of 16% WiDE are higher. NO emissions of 16% WiDE are lower than 8% WiDE at 0.789 bar and 1.698 bar, and higher at 2.492 bar and 3.585 bar. The reduction in NO emissions for WiDE is in accordance with the most recent literature [170]. As the water molecules dispersed in the emulsified fuels need to absorb some of the heat produced during combustion to change their state from liquid to vapour, it was expected that the combustion temperature would drop as a consequence of this heat sink effect mechanism [226]. It was also expected that an increase in the water content of the emulsion would lead to a further reduction in the combustion temperature, which would prevent most of NO from being formed [227], [228]. This only happened for the 1.698 bar load condition, where NO emissions of diesel are higher, followed by 8% WiDE, followed by 16% WiDE. For the single case where NO emissions from diesel were significantly lower than 16% WiDE, higher rates of premixed combustion and increased ignition delay may explain that occurrence [229]. An increased engine temperature owing to different injection and ignition timings due to differences in fuel viscosity and the occurrence of intense micro-explosions in the combustion chamber may also have contributed to increased burning rates and improved combustion and therefore increasing these emissions [230], as longer ignition delays lead to a slower combustion and more time available for NO formation in the combustion chamber [229].

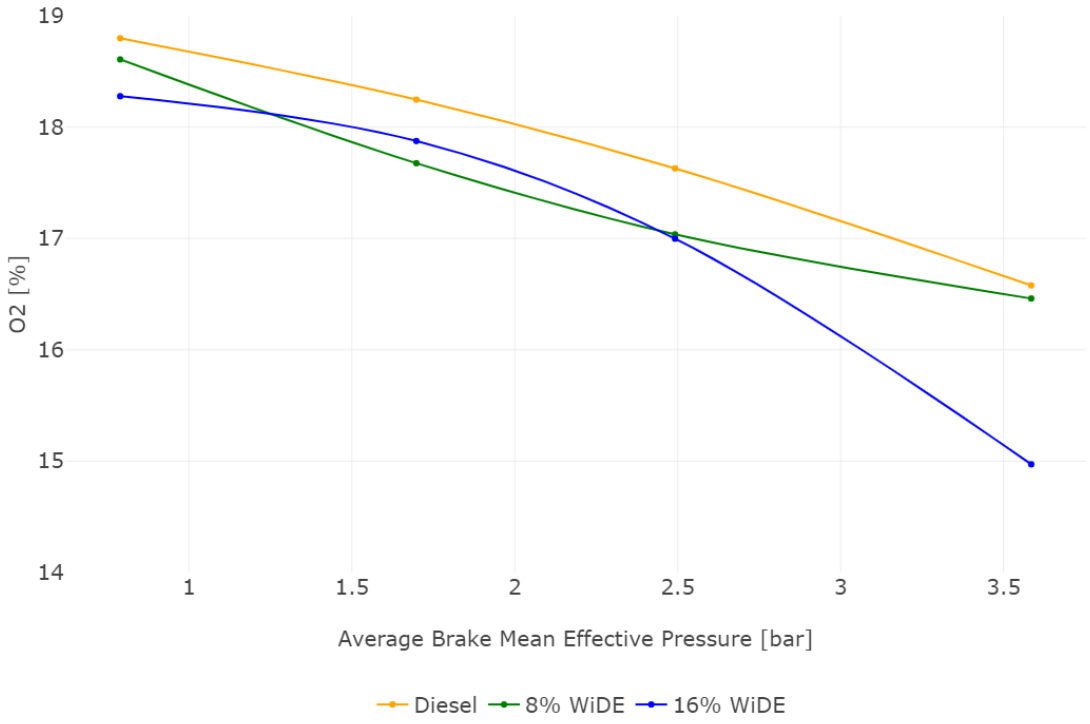

Figure 4.93. BMEP vs O_2.

Regarding O_2 emissions, for all fuels, they decrease with increasing engine load. At every load condition, O_2 emissions for diesel are higher than the emulsions. For 8% WiDE, these emissions are higher than 16% WiDE at the minimum and maximum load conditions, similar at 2.492 bar, and lower at 1.698 bar. Lower values of O_2 content measured by the gas analyser in the exhaust system may be an indication that the extra O_2 available in the emulsified fuels from the water molecules was used to react with fuel molecules and form other chemical compounds, assuring a more complete combustion [231]. If it wasn't used, it would be expected that O_2 emissions measured in exhaust would be higher.

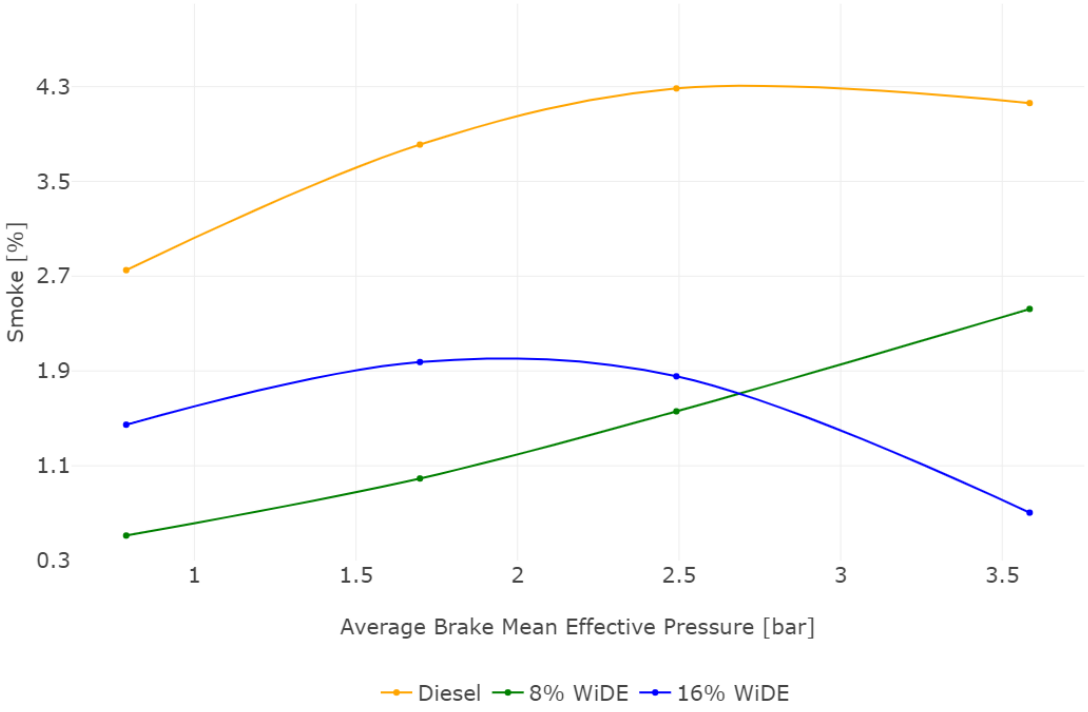

Figure 4.94. BMEP vs smoke.

As for smoke emissions, for 8% WiDE, they increase with increasing engine load. For diesel, they increase to 2.492 bar and then decrease to 3.585 bar. For 16% WiDE, these emissions increase until 1.696 bar and then decrease until 3.585 bar. The smoke emissions of diesel are always higher than the emulsions, similar to most recent studies [177]. These emissions are also always higher for 16% WiDE compared to 8% WiDE, except at the maximum load condition, where these emissions are lower. As smoke is typically formed when the combustion is incomplete, producing soot, primarily composed of carbon particles, the reduction of fuel-rich zones, characteristic of diesel's heterogenous combustion due to the oxygenated fuels [232], an improved mixing rate due to puffing and micro-explosions [233], and a longer ignition delay due to slightly higher viscosities of the emulsified fuels increasing the time for the emulsion to vaporise, mix, and auto-ignite initiating the combustion process [234] may explain these lower emissions. In addition, the decomposition of some water vapour into hydroxyl, atomic oxygen, and hydrogen radicals at high temperatures can oxidise soot in fuel-rich zones, reducing smoke emissions and improving fuel efficiency [235]. It was also expected that an increase in water content would further reduce the smoke emissions, however, this only happened at the maximum load condition.

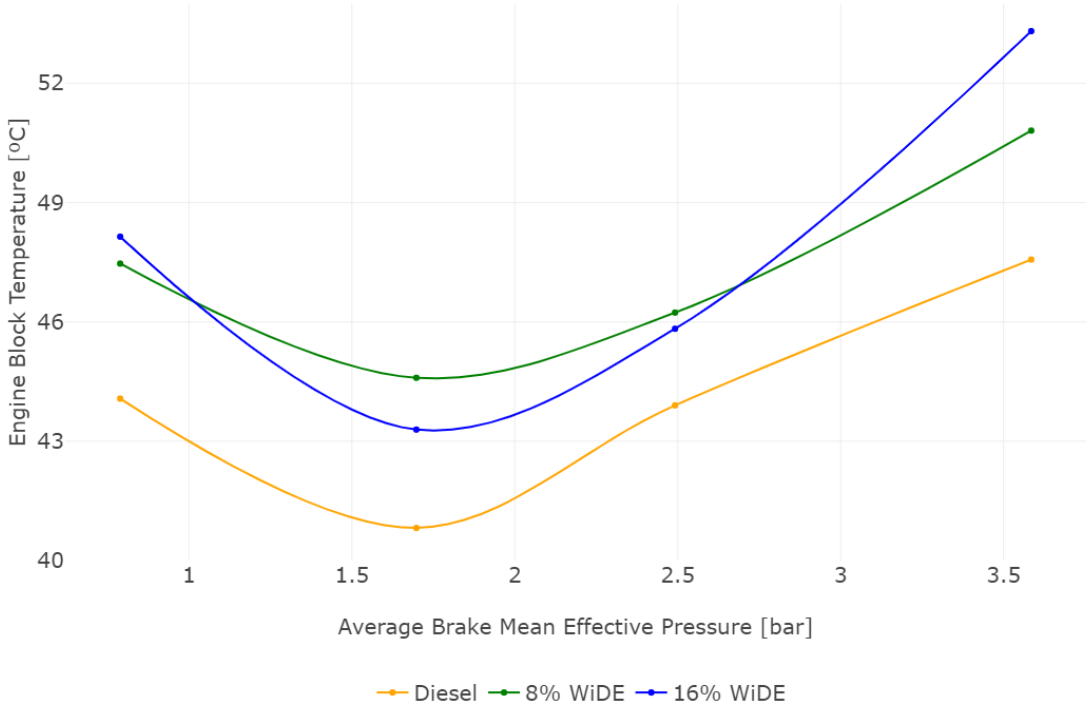

Figure 4.95. BMEP vs ET.

Due to differences in combustion characteristics between the fuels and engine cooling mechanisms, it wasn't possible to maintain a constant engine temperature for every case, and the engine stabilised at different temperatures across different operating conditions depending on the fuel being burned, as shown in figure 4.95, which calculates the mean engine block temperature across the different speeds for each load condition. As shown, for all fuels, the average temperature decreases from 25% to 50% engine load and increases from 50% to 100% engine load. The temperature registered with diesel was also always lower when compared to the emulsions. The temperature registered with 16% WiDE was lower than 8% WiDE at 50% and 75% loads and higher at the other loads. Except for these cases, the average temperature seems to increase with the increase in water content. Differences in injection timing due to changes in viscosity or the high intensity of micro-explosions can be a reason for this occurrence, as the addition of water was expected to lower the combustion temperature by absorbing the surrounding heat, even though only the block temperature was measured.

The correlation between all the different variables was also checked and can be seen in the correlation matrix, in Figure 4.96. Correlations between variables of different fuels should be ignored, as they belong to different tests, and any association is due to randomness.

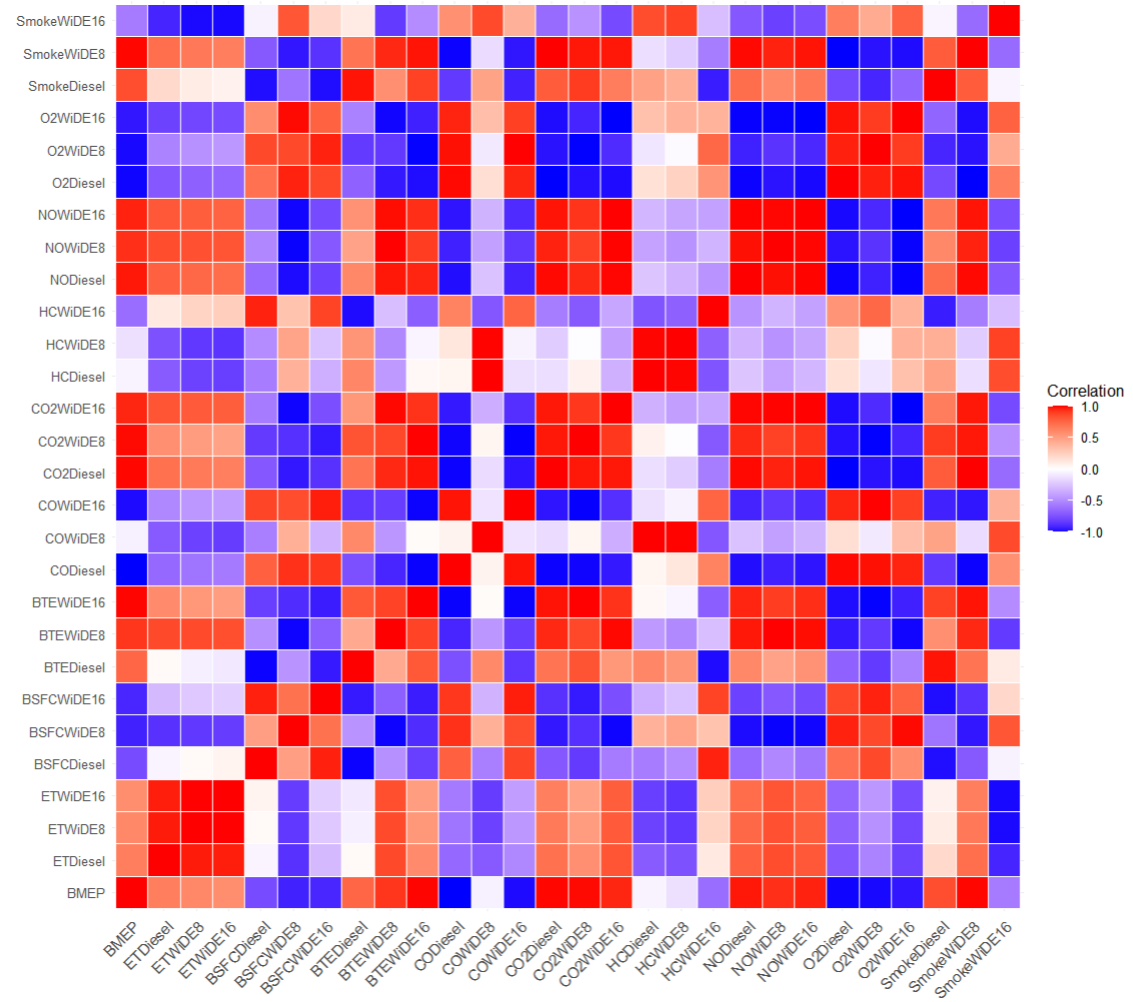

Figure 4.96. Pearson correlation matrix.

After assigning a given engine load to its corresponding flight phase, the percent change (PC) of performance and emissions parameters was calculated between the different fuels utilising Equation 4.3. The PC was calculated for the different emulsions in relation to diesel. For the particular cases where smoke levels were registered as zero, a 100% percentage decrease was considered:

$$PC = 100\frac{(\mathrm{WiDE_p} - \mathrm{Diesel_p})}{\mathrm{Diesel_p}}, \tag{4.3}$$

where PC is the percentage change of the emulsion over diesel, in %, $\mathrm{WiDE_p}$ is the emulsified fuel parameter, and $\mathrm{Diesel_p}$ is the diesel fuel parameter. Negative percentages correspond to decreases, and positive percentages correspond to increases. In Figures 4.97 to 4.104, engine block temperature is represented as ET.

Speed	BSFC	BTE	CO	CO2	HC	NO	O2	Smoke	ET
3000 rpm	-48.40%	112.61%	156.70%	19.77%	111.15%	3.21%	-1.35%	-100.00%	8.99%
2500 rpm	-51.20%	124.79%	133.33%	14.29%	89.21%	-0.63%	-1.02%	-100.00%	8.60%
2000 rpm	-21.50%	39.74%	120.62%	24.75%	83.33%	10.47%	-0.94%	-100.00%	7.85%
1500 rpm	-22.51%	41.57%	100.00%	20.66%	109.68%	13.98%	-0.75%	-75.78%	5.52%

Figure 4.97. PC of 8% WiDE over diesel at 25W load.

Speed	BSFC	BTE	CO	CO2	HC	NO	O2	Smoke	ET
3000 rpm	30.65%	-16.03%	933.33%	42.49%	174.17%	-41.53%	-6.19%	106.96%	4.50%
2500 rpm	15.59%	-5.10%	466.67%	25.50%	15.76%	-16.33%	-3.28%	-72.88%	8.60%
2000 rpm	-6.88%	17.81%	379.60%	12.74%	111.56%	-10.39%	-0.84%	-96.76%	11.61%
1500 rpm	37.33%	-20.12%	150.16%	31.80%	65.09%	-14.64%	-2.25%	-73.17%	11.68%

Figure 4.98. PC of 8% WiDE over diesel at 50W load.

Speed	BSFC	BTE	CO	CO2	HC	NO	O2	Smoke	ET
3000 rpm	37.95%	-20.48%	890.20%	38.35%	46.90%	-32.62%	-6.88%	-99.50%	8.77%
2500 rpm	12.80%	-2.75%	469.23%	21.69%	-8.43%	-16.33%	-3.30%	-87.24%	0.94%
2000 rpm	-18.83%	35.14%	136.39%	11.08%	21.03%	-5.94%	-1.11%	-98.84%	6.53%
1500 rpm	13.61%	-3.44%	300.00%	23.18%	37.16%	-13.74%	-2.16%	-90.46%	5.26%

Figure 4.99. PC of 8% WiDE over diesel at 75W load.

Speed	BSFC	BTE	CO	CO2	HC	NO	O2	Smoke	ET
3000 rpm	-14.59%	28.44%	250.00%	12.46%	49.81%	-3.04%	-1.43%	-73.88%	10.97%
2500 rpm	-38.18%	77.45%	150.48%	3.83%	110.59%	-9.87%	0.73%	-23.90%	5.14%
2000 rpm	-45.83%	102.50%	213.16%	14.59%	82.12%	6.93%	-2.09%	-24.21%	6.72%
1500 rpm	-37.59%	75.77%	122.56%	6.03%	78.86%	-4.37%	-0.02%	-14.66%	5.21%

Figure 4.100. PC of 8% WiDE over diesel at 100W load.

Speed	BSFC	BTE	CO	CO2	HC	NO	O2	Smoke	ET
3000 rpm	46.80%	-18.21%	429.05%	25.33%	84.83%	-53.40%	-3.72%	-59.61%	22.09%
2500 rpm	11.20%	7.98%	300.00%	8.29%	13.46%	-54.67%	-1.76%	-96.80%	6.30%
2000 rpm	11.08%	8.10%	335.86%	43.90%	160.82%	-47.87%	-3.19%	-70.03%	4.65%
1500 rpm	19.62%	0.38%	250.00%	36.67%	195.38%	-31.51%	-2.40%	-28.13%	4.67%

Figure 4.101. PC of 16% WiDE over diesel at 25W load.

Speed	BSFC	BTE	CO	CO2	HC	NO	O2	Smoke	ET
3000 rpm	44.54%	-16.93%	592.56%	21.57%	592.56%	-56.90%	-4.21%	76.98%	7.64%
2500 rpm	27.67%	-5.95%	230.53%	1.39%	230.53%	-36.42%	-0.79%	-82.10%	-0.05%
2000 rpm	10.07%	9.09%	248.68%	7.78%	248.68%	-16.40%	-1.07%	-54.90%	8.16%
1500 rpm	80.50%	-33.48%	78.07%	22.22%	78.07%	-24.76%	-2.06%	-32.31%	8.24%

Figure 4.102. PC of 16% WiDE over diesel at 50W load.

Speed	BSFC	BTE	CO	CO2	HC	NO	O2	Smoke	ET
3000 rpm	31.92%	-8.98%	661.78%	27.35%	46.90%	-37.15%	-5.74%	-78.57%	10.07%
2500 rpm	17.55%	2.15%	250.00%	11.98%	-8.43%	-12.33%	-2.75%	-81.59%	-4.36%
2000 rpm	-3.50%	24.43%	100.00%	12.85%	21.03%	6.29%	-2.55%	-78.86%	7.51%
1500 rpm	51.33%	-20.65%	200.00%	23.59%	37.16%	-6.43%	-3.26%	-60.08%	4.63%

Figure 4.103. PC of 16% WiDE over diesel at 75W load.

Speed	BSFC	BTE	CO	CO2	HC	NO	O2	Smoke	ET
3000 rpm	6.58%	12.66%	600.00%	42.82%	49.81%	-6.07%	-10.38%	-96.81%	18.25%
2500 rpm	-6.64%	28.61%	321.36%	41.44%	110.59%	14.24%	-11.04%	-78.79%	10.23%
2000 rpm	-24.55%	59.14%	200.00%	44.43%	82.12%	22.90%	-10.14%	-78.82%	10.73%
1500 rpm	-6.94%	29.02%	48.37%	31.83%	78.86%	14.07%	-7.25%	-75.77%	10.23%

Figure 4.104. PC of 16% WiDE over diesel at 100W load.

If we apply the previous tables to the flight profile of an aerial vehicle and calculate the mean value across all speeds for each load condition, we can obtain Figure 4.105.

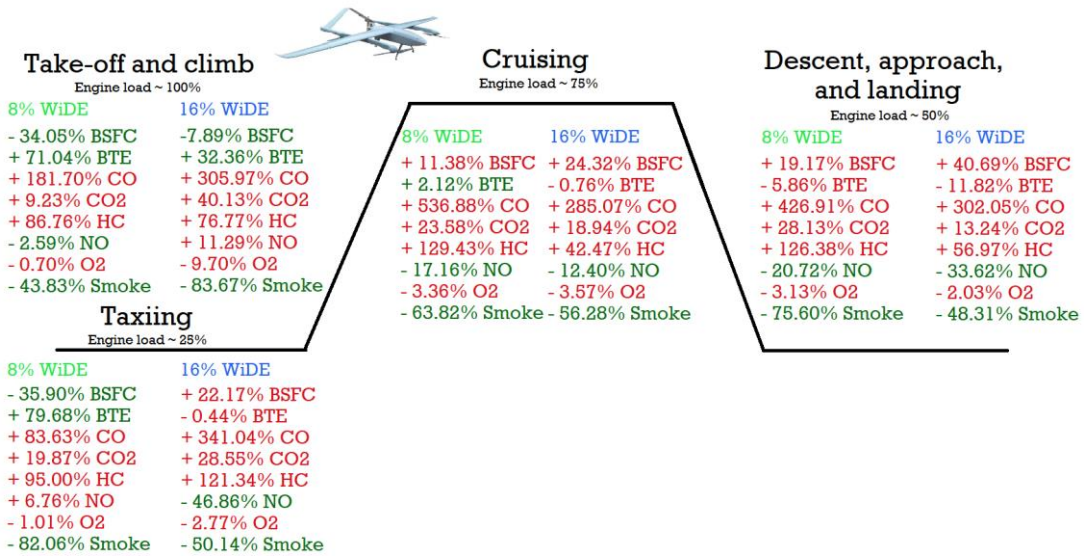

Figure 4.105. PC of WiDEs over diesel during a typical flight profile of an aerial vehicle.

As can be observed from the figure, the emulsion with 8% water offers better overall BTE at every single flight phase when compared to 16% WiDE. When compared to diesel, the biggest increase is obtained during take-off and climb, and taxiing phases with 71.04% and 79.68% increases, respectively. During cruising phase, 8% WiDE still offers a 2.12% increase of BTE when compared to diesel, even though the BSFC is increased by 11.38%. Only during descent, approach, and landing phases, it leads to a reduction of 5.86% in BTE. When compared to diesel, 16% WiDE only offers better BTE during take-off and climb, with a 32.36% increase. Regarding emissions, CO emissions are always higher for emulsions when compared to diesel, at every single flight phase. The same result is found for HC emissions. CO_2 emissions are also higher for both emulsions when compared to diesel. NO emissions are generally lower for both emulsions when compared to diesel, except during take-off and climb for 16% WiDE and taxiing for 8% WiDE. O_2 emissions are always lower for the emulsions when compared to diesel. Smoke levels are always lower for both emulsions at every flight phase when compared to diesel. Only during take-off and climb, these values are lower for 16% WiDE when compared to 8% WiDE.

4.4 Viability of emulsified fuels in a diesel engine for aeronautical applications

After analysing the various benefits and detriments of water-emulsified diesel fuel, it was reasoned that producing this fuel on-board rather than storing it would be a more optimal solution. The main factors include the higher freezing points, which could be an issue for aircraft and UAVs at higher altitudes where the temperature is lower and a heated fuel filter or fuel tank is not available, and poor storage stability of emulsified diesel, heavily dependent on temperature and pressure conditions. Even though additives could be applied to increase its freezing points and stability, it would lead to an increase in the total fuel cost, adding to the infrastructure costs for storage and handling. Although it is possible to produce an emulsion for storage purposes, its quality would drop, as the mixture remains static and is not optimised for operating conditions. An on-board system for emulsion supplying would allow real-time control of the different variables, such as water content, surfactant concentration, and diesel concentration, tailoring the mixture to the engine's immediate operational needs. This approach would ensure a more efficient and adaptable fuel use, increasing performance and reducing potential storage risks. For on-vehicle fuel tanks or other applications where the fuel is subjected to mechanical vibration or agitation, an emulsifier that both stabilises the emulsified water-in-fuel mixture and ensures the emulsified water remains in a very fine micro or nanoscale state is recommended. There is also a possibility that these disturbances can even be beneficial, as they can be a form of a low-energy mixing method that would favour kinetically stable nanoemulsions, further improving their ability to reach a lower-energy state and chemical equilibrium with the environment. Based on the findings of this work, it is possible to highlight the positive and negative aspects regarding the utilisation of WiDE in diesel-powered aerial vehicles, as well as some possible solutions to mitigate specific problems, as shown in Table 4.2.

Table 4.2. Overview of the utilisation of WiDE in aircraft CI engines.

Benefits	*Drawbacks*	*Possible Solutions*
Lower fossil content of the fuel leading to reduced fossil fuel consumption.	Lower energy content may reduce the maximum torque and power available.	Reduce water content of the emulsion.
Lower specific fuel consumption and better thermal efficiency at certain flight phases.	Lower energy density may reduce the maximum flight range.	Reduce water content of the emulsion.
Lower emissions of GHGs due to lower energy content and reduced fuel consumption.	Increased total CO_2 emissions at some flight phases.	Can be mitigated by carbon capture technologies.
Lower smoke emissions and overall lower NO emissions.	Increased CO and HC emissions at every flight phase.	Adjust injection timings to achieve a more complete combustion.
Lower sulphur emissions as less diesel is present in the fuel.	Lubricity may be reduced.	Lubricity additives.
Higher flash point leading to safer storage and risk of explosion.	Higher freezing point can result in clogging up the fuel lines at higher altitudes and very low temperatures.	Heated fuel tanks, heated fuel filters, fuel/oil heat exchangers, and antifreeze additives.
Can reduce soot build up in the engine.	-	-
Decreased oxygen availability at higher altitudes can be compensated by the additional oxygen from water present in the fuel.	-	-
Can be used without engine modifications, decreasing costs.	Poor storage and handling stability leading to degradation of the fuel.	Real-time on-board mixing system supplying optimised mixtures at specific load conditions.
Potential weight saving from emission control systems, as NO_x and PM are reduced.	-	-
Wide availability of diesel fuel, reducing the costs of the infrastructures and processes used in other alternative diesel fuels (FAME, HVO).	Fossil fuel is used instead of biofuels which are carbon neutral.	Explore water-in-biodiesel, water-in-HVO, and blends of water-in-biofuel.

Chapter 5. Final Considerations

5.1 Conclusions

Considering the challenges and difficulties of further optimising gasoline engines, specifically in general aviation applications, a transition to diesel engines seems a reasonable path that is already being pursued by some companies and flight academies as a way to mitigate some of its operating costs. This work was performed to analyse the possibility of utilising an alternative fuel for CI engines as a way to improve efficiency and reduce some of the pollutant emissions. For this work, several experiments were performed on a single-cylinder direct injection diesel engine at different load conditions represented by the different flight phases of an aerial vehicle. After analysing the results, a number of observations can be noted:

- At every flight phase, O_2 and smoke emissions are reduced for both emulsions.
- At every flight phase, CO, CO_2, and HC emissions are increased for both emulsions.
- NO emissions are reduced for both emulsions at every flight phase except during taxiing for 8% WiDE and take-off and climb for 16% WiDE.
- For 8% WiDE, TE is improved at every condition, except during descent, approach, and landing phases.
- For 16% WiDE, TE is only improved during take-off and climb phase.

On top of the results obtained, throughout this investigation, some relevant points were also identified:

- Increasing water content (from 0% to 8% to 16%) led to an increase in the measured engine block temperature, possibly due to higher intensity of microexplosions in the combustion chamber.
- Possible changes in injection timing when using WiDE may reduce some of the pollutant emissions from incomplete combustion, especially CO and HC.
- It is expected that SO_x emissions are lower for WiDE as less diesel and therefore less sulfur is present in the fuel.
- Optimising water content and surfactant content of the emulsions to specific engine operating conditions may improve performance and reduce emissions.
- It is expected that WiDE formulated for engine operating temperatures will lead to better results when compared to WiDE formulated for storage at ambient conditions.
- Higher water content of an emulsion requires higher surfactant content, and for the same proportion of hydrophilic to lipophilic surfactant, less temperature is required for stabilisation. Increasing the hydrophilic surfactant proportion will increase the stabilisation temperature for any water content.

- Storage of water-emulsified diesel fuel is not easy and relies on proper infrastructures that can assure stability, very dependent on temperature and pressure conditions.
- The stability of the emulsions is a very important aspect, as they can be volatile, especially in air transport, where pressure, temperature, and humidity conditions are constantly changing.
- Vibrations in the fuel tank and fuel lines may be beneficial and act as a low-energy mixing method to extend the stability of the emulsions.
- At higher altitudes where air is less dense and temperatures are much lower, precautions should be taken to prevent fuel from gelling.
- Increased flash point of the emulsion makes it safer for storage and handling procedures.

Taking all these aspects into consideration, and acknowledging the lengthy and meticulous process of certifying aviation fuels, water-emulsified diesel fuel may be an option for use in small aerial vehicles such as UAVs as a way to mitigate emissions of smoke and NO, and improve efficiency levels. To prevent stability issues and optimise operating conditions, an on-board mixing system can be used to supply the best formulation of diesel, water, and surfactant at every condition. To prevent cold-start associated problems, the engine may start with diesel fuel and swap to WiDE after reaching operating temperature. If not, a unique formulation should be developed and optimised for the conditions in which the vehicle will predominantly operate.

5.2 Research limitations

After completing this work, a very clear idea can be traced regarding certain aspects that were successfully achieved and others ones which leave room for improvement:

- Sensor's accuracy. The precision of the load cells for torque and fuel consumption measurement, as well as the precision of the hall sensor for speed measurement, could be improved by using better and more expensive sensors.
- Exhaust gas analyser accuracy. The precision of CO measurement could be improved by using a different gas analyser that measures its concentration in ppm instead of %, offering more precise results. The same applies to NO measurement, in which a better sensor may offer reduced errors. An exhaust gas analyser specifically designed to be operated in diesel engines would also improve the quality of the results, especially in terms of unburned HC emissions, as these emissions can vary between different fuels.
- Dynamometer's disk. After replacing the original stainless steel rotating disk with an aluminium one, due to the difficulty of inducing eddy currents on a less conductive material, it was found that the increase in load would significantly increase the temperature of the disk, increasing thermal vibrations of the atoms, which would lead to an increased resistivity due to greater scattering of electrons along the surface. On top of that, warping was also found to occur on the less rigid disk at higher braking torques.
- Dynamometer's belt. Increased braking torques led to increased temperature and very high angular accelerations on the belt connecting the pulleys. Tearing of several belts

occurred due to degradation and continuous operation during different tests. In addition, different temperatures may also lead to different tensions and mechanical efficiency losses during transmission from the engine to the dynamometer.

- Dynamometer's power supply. The current supplied to energise the coils did not remain constant during each engine operating condition, especially at lower loads. This leads to a variation in the force measured during tests, resulting from the eddy currents produced.
- Vibrations. System vibrations due to unstable engine operating conditions can lead to mechanical efficiency losses, which are hard to measure, and are also transmitted to the fuel tank by the fuel lines, increasing load cell noise during fuel consumption measurement.
- Different engine operating temperatures. Due to distinct combustion processes between the fuels, and depending on the condition, the engine stabilised at slightly different temperatures between the fuels. As this engine is cooled by forced air, and not liquid cooled (in which a thermostat would maintain similar temperatures), similar temperatures could only be achieved by controlling the airflow responsible for cooling the engine.

5.3 Perspectives for future research

After drawing the necessary conclusions and being aware of the limitations of this project, it was possible to develop a good idea of where future work and experimental tests should be directed towards:

- Acquire a modern 4-stroke aeronautical diesel engine to perform the tests.
- Perform acceleration and deceleration tests to obtain the maximum torque and power output of the engine, and observe the differences between the different fuels.
- Perform the tests at constant accelerator pedal positions and different atmospheric conditions (pressure and temperature), often encountered at higher altitudes where aircraft and UAVs fly.
- Analyse the stability of the emulsions over a wide range of temperatures, as experienced during the different flight phases.
- Experimentally verify if the presence of anti-freeze additives in the fuel influences the emulsions' thermal stability and performance.
- Prepare stable emulsions at ambient temperature and analyse the difference in performance.
- Utilise different percentages of water, surfactant, and formulation to verify their impact on the stability and performance of the emulsions.
- Prepare emulsions with jet fuel, biodiesel, or other biofuels instead of diesel, and observe its stability behaviour, as well as its performance in comparison with the other fuels in a diesel engine.

Bibliography

[1] S. Gumy, “Personal Interventions and Risk Communication on Air Pollution,” Geneva, 2019.

[2] E. Stavropoulou, I. Manisalidis, A. Stavropoulos, and E. Bezirtzoglou, “Environmental and Health Impacts of Air Pollution: A Review,” *Front. Public Heal.*, vol. 8, pp. 1–13, 2020.

[3] E. Institute, “Statistical Review of World Energy,” 2024.

[4] BP, “Statistical Review of World Energy,” London, 2020.

[5] Our World in Data, “Energy consumption by source, World,” 2024. [Online]. Available: https://ourworldindata.org/grapher/energy-consumption-by-source-and-country. [Accessed: 08-Oct-2024].

[6] Bioenergy International, “EU transportation sector still overly dependant on fossil fuels,” 2019. [Online]. Available: https://bioenergyinternational.com/markets-finance/eu-transport-still-overly-dependant-on-fossil-fuels. [Accessed: 23-Sep-2020].

[7] Center For Climate And Energy Solutions, “Global Emissions,” 2017. [Online]. Available: https://www.c2es.org/content/international-emissions/. [Accessed: 23-Sep-2020].

[8] S. Woo and K. Lee, “Effect of injection strategy and water content on water emulsion fuel engine for low pollutant compression ignition engines,” *Fuel*, vol. 343, 127809, 2023.

[9] D. Hall and N. Lutsey, “Estimating the infrastructure needs and costs for the launch of zero-emissions trucks,” Washington DC, 2019.

[10] S. C. Davis and R. G. Boundy, *Transportation Energy Data Book*, 38th ed. Oak Ridge, 2020.

[11] FAA Office of Environment and Energy, “Aviation Emissions, Impacts & Mitigation: A Primer,” 2015.

[12] Chevron Products Company, “Aviation Fuels Technical Review,” San Ramon, 2007.

[13] S. L. Deore and S. N. Kale, “Emulsion Micro Emulsion and Nano Emulsion: A Review,” *Syst. Rev. Pharm.*, vol. 8, no. 1, pp. 39–47, 2017.

[14] N. H. C. Marzuki, R. A. Wahab, and M. A. Hamid, “An overview of nanoemulsion: Concepts of development and cosmeceutical applications,” *Biotechnol. Biotechnol. Equip.*, vol. 33, no. 1, pp. 779–797, 2019.

[15] P. K. Mondal and B. K. Mandal, “A comparative study on the performance and emissions from a CI engine fuelled with water emulsified diesel prepared by mechanical homogenization and ultrasonic dispersion method,” *Energy Reports*, vol. 5, pp. 639–648, 2019.

[16] J. Hansen, M. Sato, R. Ruedy, A. Lacis, and V. Oinas, “Global warming in the twenty-first century: An alternative scenario,” *Proc. Natl. Acad. Sci. U. S. A.*, vol. 97, no. 18, pp. 9875–9880, 2000.

[17] J. Houghton, “Global warming,” *Reports Prog. Phys.*, vol. 68, no. 6, pp. 1343–1403, 2005.

[18] D. J. Easterbrook, “Greenhouse Gases,” in *Evidence-Based Climate Science: Data Opposing CO2 Emissions as the Primary Source of Global Warming*, 2nd ed., Bellingham, 2016, pp. 163–173.

[19] L. Chiari and A. Zecca, “Constraints of fossil fuels depletion on global warming projections,” *Energy Policy*, vol. 39, no. 9, pp. 5026–5034, 2011.

[20] L. Al-Ghussain, “Global warming: review on driving forces and mitigation,” *Environ. Prog. Sustain. Energy*, vol. 38, no. 1, pp. 13–21, 2019.

[21] Ü. Ağbulut and S. Sarıdemir, “A general view to converting fossil fuels to cleaner energy source by adding nanoparticles,” *Int. J. Ambient Energy*, vol. 42, no. 13, pp. 1569–1574, 2021.

[22] S. Vellaiyan, “Recent advancements in water emulsion fuel to explore efficient and cleaner production from various biodiesels: A retrospective review,” *Renew. Sustain. Energy Rev.*, vol. 187, 113704, 2023.

[23] J. E. Jonson, J. Borken-Kleefeld, D. Simpson, A. Nyíri, M. Posch, and C. Heyes, “Impact of excess NOx emissions from diesel cars on air quality, public health and eutrophication in Europe,” *Environ. Res. Lett.*, vol. 12, no. 9, pp. 1–11, 2017.

[24] “Emission Standards: Europe: Cars and Light Trucks.” [Online]. Available: https://dieselnet.com/standards/eu/ld.php. [Accessed: 12-Sep-2024].

[25] ACEA, “Position Paper Views on proposals for Euro 7 emission standard,” 2020.

[26] S. Wijeyakulasuriya *et al.*, “Enabling Powertrain Technologies for Euro 7/VII Vehicles with Computational Fluid Dynamics,” *Transp. Eng.*, vol. 9, 100127, 2022.

[27] E. EEA, EASA, “European Aviation Environmental Report,” 2019.

[28] H. Ritchie, “Climate change and flying: what share of global CO2 emissions come from aviation?,” 2020. [Online]. Available: https://ourworldindata.org/co2-emissions-from-aviation. [Accessed: 22-Oct-2021].

[29] “Engine,” *SKYbrary*, 2017. [Online].

Available: https://www.skybrary.aero/index.php/Engine. [Accessed: 03-May-2021].

[30] A. F. El-Sayed, *Aircraft Propulsion and Gas Turbine Engines* , 2nd ed. CRC Press, 2017.

[31] A. Fernandes, C. Granjeiro, and J. Gomes, *Compêndio sobre Motores Alternativos*. 2008.

[32] T. Z. Quazi, C. Mhatre, S. Khanolkar, P. Patil, and S. Pawar, “A Review on Internal Combustion Engines,” *Int. J. Eng. Res. Eng. Sci. Manag.*, vol. 1, no. 10, pp. 790–792, 2018.

[33] V. Ganesan, *Internal Combustion Engines*, 3rd ed. Tata McGraw-Hill Publishing Company Limited, 2007.

[34] J. Heywood, *Internal Combustion Engine Fundamentals*. McGraw-Hill, Inc., 1988.

[35] V. Smil, “The two prime movers of globalization: History and impact of diesel engines and gas turbines,” *J. Glob. Hist.*, vol. 2, no. 3, pp. 373–394, 2007.

[36] J. Martins, *Motores de Combustão Interna*, 2nd ed. Publindústria, 2006.

[37] R. Stone, *Introduction to Internal Combustion Engines*, 2nd ed. Uxbridge: Palgrave Macmillan, 1992.

[38] C. Proctor and L. Horn, “Diesel engine,” *Encyclopedia Britannica*. [Online]. Available: https://www.britannica.com/technology/diesel-engine. [Accessed: 29-Apr-2021].

[39] A. Parlak, “The effect of heat transfer on performance of the Diesel cycle and exergy of the exhaust gas stream in a LHR Diesel engine at the optimum injection timing,” *Energy Convers. Manag.*, vol. 46, no. 2, pp. 167–179, 2005.

[40] “Diesel Cycle - Diesel Engine .” [Online]. Available: https://www.nuclear-power.com/nuclear-engineering/thermodynamics/thermodynamic-cycles/diesel-cycle-diesel-engine/. [Accessed: 11-Oct-2022].

[41] F. A. Administration and U. S. D. of Transportation, “Aircraft Systems,” in *Pilot’s*

Handbook of Aeronautical Knowledge, A. S. & Academics, Ed. Aviation Supplies & Academics, Inc., 2016.

[42] M. Dubovský, M. Božek, and M. Olšovský, "Degradation of aviation sealing materials in rapeseed biodiesel," *J. Appl. Polym. Sci.*, vol. 132, no. 28, pp. 1–7, 2015.

[43] K. Meng, L. Bao, F. Li, C. Wang, and Q. Lin, "Experimental understanding on combustion and micro-explosion characteristics of mixed droplets of aviation fuel, biodiesel and ethanol," *J. Energy Inst.*, vol. 97, pp. 169–179, 2021.

[44] G. Cican, M. Deaconu, R. Mirea, L. C. Ceatra, and M. Cretu, "An experimental investigation to use the biodiesel resulting from recycled sunflower oil, and sunflower oil with palm oil as fuels for aviation turbo-engines," *Int. J. Environ. Res. Public Health*, vol. 18, no. 10, pp. 1–18, 2021.

[45] N. E. Daidzic, L. Piancastelli, and A. Cattini, "Diesel engines for light-to-medium helicopters and airplanes," *Int. J. Aviat. Aeronaut. Aerosp.*, vol. 1, no. 3, pp. 1–18, 2014.

[46] M. Gęca, Z. Czyż, and M. Sułek, "Diesel engine for aircraft propulsion system," *Combust. Engines*, vol. 169, no. 2, pp. 7–13, 2017.

[47] W. W. Pulkrabek, *Engineering Fundamentals of the Internal Combustion Engine*, 2nd ed. Platteville: Pearson, 2003.

[48] İ. Dinçer and C. Zamfirescu, "Fossil Fuels and Alternative Fuels," in *Sustainable Energy Systems and Applications*, 1st ed., Springer, Boston, MA, 2012, pp. 169–201.

[49] H. Schobert, "Fuels and the global carbon cycle," in *Chemistry of Fossil Fuels and Biofuels*, 1st ed., Cambridge University Press, 2013, pp. 1–9.

[50] C. K. Otto, "Fossil fuel," *Encyclopedia Britannica*. [Online]. Available: https://www.britannica.com/explore/savingearth/fossil-fuel. [Accessed: 09-May-2021].

[51] Shell Aviation, *The Aeroshell Book*, 20th ed. 2021.

[52] M. Al Qubeissi, A. El-kharouf, and H. S. Soyhan, *Renewable Energy: Resources, Challenges and Applications*. London: IntechOpen, 2020.

[53] K. O. P. Bjørgen, D. R. Emberson, and T. Løvås, "Combustion and soot characteristics of hydrotreated vegetable oil compression-ignited spray flames," *Fuel*, vol. 266, 116942, 2020.

[54] R. W. Jenkins, M. Munro, S. Nash, and C. J. Chuck, "Potential renewable

oxygenated biofuels for the aviation and road transport sectors," *Fuel*, vol. 103, pp. 593–599, 2013.

[55] M. A. Mayorga *et al.*, "Production of aviation biofuel from palm kernel oil," *Chem. Eng. Trans.*, vol. 80, pp. 319–324, 2020.

[56] L. Shao *et al.*, "Advanced combustion in heavy fuel aircraft piston engines: A comprehensive review and future directions," *Fuel*, vol. 370, 131771, 2024.

[57] Galp, "The process of refining." [Online].

Available: https://www.galp.com/corp/en/about-us/what-we-do/industrial-energy-management/refining-and-logistics/fundamentals-of-refining. [Accessed: 10-Feb-2023].

[58] S. S. Doliente, A. Narayan, J. F. D. Tapia, N. J. Samsatli, Y. Zhao, and S. Samsatli, "Bio-aviation Fuel: A Comprehensive Review and Analysis of the Supply Chain Components," *Front. Energy Res.*, vol. 8, pp. 1–38, 2020.

[59] ACEA, Auto Alliance, Ema, and Jama, "Worldwide Fuel Charter: Gasoline and Diesel Fuel," 2019.

[60] E. Goodger and R. Vere, "Current Aviation Fuel Types," in *Aviation Fuels Technology*, Macmillan Education UK, 1985, pp. 15–21.

[61] T. J. Fortin and A. Laesecke, "Viscosity Measurements of Aviation Turbine Fuels," *Energy and Fuels*, vol. 29, no. 9, pp. 5495–5506, 2015.

[62] M. Hilgers and W. Achenbach, "Vehicle and Energy Loss," in *Fuel Consumption and Consumption Optimization*, 1st ed., Springer Vieweg, 2021, pp. 5–8.

[63] H. Solmaz, H. Yamık, A. Uyumaz, and S. P. ve E. Yılmaz, "An experimental Study on the Effects of Diesel and Jet-A1 Fuel Blends on Combustion, Engine Performance and Exhaust Emissions in a Direct Injection Diesel Engine," *J. Therm. Sci. Technol.*, vol. 36, no. 2, pp. 51–60, 2016.

[64] Chevron Products Company, "Alternative Jet Fuels," San Ramon, 2006.

[65] R. Liu, W. Zhao, Z. Wang, and X. Liu, "Investigation on performance and combustion of compression ignition aviation piston engine burning biodiesel and diesel," *Aircr. Eng. Aerosp. Technol.*, vol. 93, no. 3, pp. 384–393, 2020.

[66] European Parliamentary Research Service, "Sustainable aviation fuels," 2020.

[67] Airbus, "This A380 is the latest to test 100% SAF ," 2022. [Online]. Available: https://www.airbus.com/en/newsroom/news/2022-03-this-a380-is-the-latest-to-test-100-saf. [Accessed: 28-Sep-2022].

[68] Airbus, “First A380 powered by 100% Sustainable Aviation Fuel takes to the skies,” Toulouse, 2022.

[69] J. Ringbeck and V. Koch, “Aviation biofuels: A roadmap towards more carbon-neutral skies,” *Biofuels*, vol. 1, no. 4, pp. 519–521, 2010.

[70] EASA, “Sustainable Aviation Fuel ‘Facilitation Initiative,’” 2019.

[71] M. Bracha, “Liquid Hydrogen – Status and Trends as potential Aviation Fuel,” in *Fuel Cell and Hydrogen Technologies in Aviation*, Springer, Cham, 2022, pp. 23–53.

[72] B. V. Sethi *et al.*, “Enabling Cryogenic Hydrogen-Based CO2 -Free Air Transport: Meeting the demands of zero carbon aviation,” *IEEE Electrification Magazine*, vol. 10, no. 2, pp. 69–81, 2022.

[73] R. Domingues, F. Brójo, and P. Oliveira, “CFD Analysis of the Combustion of Hydrogen Fuel on a CFM56-3 Combustor,” in *Proceedings of the ASME 2022 International Mechanical Engineering Congress and Exposition. Volume 3: Advanced Materials: Design, Processing, Characterization and Applications; Advances in Aerospace Technology*, 2023.

[74] R. W. Howarth and M. Z. Jacobson, “How green is blue hydrogen?,” *Energy Sci. Eng.*, vol. 9, no. 10, pp. 1676–1687, 2021.

[75] M. Aziz, “Liquid Hydrogen: A Review on Liquefaction, Storage, Transportation, and Safety,” *Energies*, vol. 14, no. 18, 5917, 2021.

[76] J. Baumi, C. Milani Bertosse, and C. Luisa Barbosa Guedes, “Aviation Fuels and Biofuels,” in *Renewable Energy - Resources, Challenges and Applications*, IntechOpen, 2020, pp. 1–21.

[77] S. Blakey, L. Rye, and C. W. Wilson, “Aviation gas turbine alternative fuels: A review,” *Proc. Combust. Inst.*, vol. 33, no. 2, pp. 2863–2885, 2011.

[78] N. Yilmaz and A. Atmanli, “Sustainable alternative fuels in aviation,” *Energy*, vol. 140, pp. 1378–1386, 2017.

[79] C. Bae and J. Kim, “Alternative fuels for internal combustion engines,” *Proc. Combust. Inst.*, vol. 36, no. 3, pp. 3389–3413, 2017.

[80] A. de Klerk, “Aviation Turbine Fuels Through the Fischer–Tropsch Process,” in *Biofuels for Aviation - Feedstocks, Technology and Implementation*, Academic Press, 2016, pp. 241–259.

[81] F. Dawood, M. Anda, and G. M. Shafiullah, “Hydrogen production for energy: An overview,” *Int. J. Hydrogen Energy*, vol. 45, no. 7, pp. 3847–3869, 2020.

[82] D. R. Vardon, B. J. Sherbacow, K. Guan, J. S. Heyne, and Z. Abdullah, “Realizing ‘net-zero-carbon’ sustainable aviation fuel,” *Joule*, vol. 6, no. 1, pp. 16–21, 2022.

[83] P. K. Maurya, S. Mondal, V. Kumar, and S. P. Singh, “Roadmap to sustainable carbon-neutral energy and environment: can we cross the barrier of biomass productivity?,” *Environ. Sci. Pollut. Res.*, vol. 28, no. 36, pp. 49327–49342, 2021.

[84] Bio-Rad, “Carbon Cycle.” [Online]. Available: https://www.bio-rad.com/en-pt/education/overlay/carbon-cycle?ID=Carbon-Cyc_1265324612. [Accessed: 03-Mar-2023].

[85] J. Q. da Silva, D. Q. Santos, J. D. Fabris, L. V. L. Harter, and S. P. Chagas, “Light biodiesel from macaúba and palm kernel: Properties of their blends with fossil kerosene in the perspective of an alternative aviation fuel,” *Renew. Energy*, vol. 151, pp. 426–433, 2020.

[86] M. Lapuerta, O. Armas, and J. Rodríguez-Fernández, “Effect of biodiesel fuels on diesel engine emissions,” *Prog. Energy Combust. Sci.*, vol. 34, no. 2, pp. 198–223, 2008.

[87] E. Mattarelli, C. A. Rinaldini, and T. Savioli, “Combustion Analysis of a Diesel Engine Running on Different Biodiesel Blends,” *Energies*, vol. 8, no. 4, pp. 3047–3057, 2015.

[88] Neste, *Neste Renewable Diesel Handbook*. 2020.

[89] K. P. Brooks *et al.*, “Low-Carbon Aviation Fuel Through the Alcohol to Jet Pathway,” in *Biofuels for Aviation - Feedstocks, Technology and Implementation*, C. Chuck, Ed. Academic Press, 2016, pp. 109–150.

[90] ETIP Bioenergy - European Technology and Innovation Platform, “Hydrogenated vegetable oil (HVO),” 2020.

[91] R. Khujamberdiev and H. M. Cho, “Biofuels in Aviation: Exploring the Impact of Sustainable Aviation Fuels in Aircraft Engines,” *Energies* , vol. 17, no. 11, 2650, 2024.

[92] T. G. Mason, J. N. Wilking, K. Meleson, C. B. Chang, and S. M. Graves, “Nanoemulsions: Formation, structure, and physical properties,” *J. Phys. Condens. Matter*, vol. 18, no. 41, pp. 635–666, 2006.

[93] M. R. Noor El-Din, S. H. El-Hamouly, H. M. Mohamed, M. R. Mishrif, and A. M. Ragab, “Water-in-diesel fuel nanoemulsions: Preparation, stability and physical properties,” *Egypt. J. Pet.*, vol. 22, no. 4, pp. 517–530, 2013.

[94] D. J. McClements, “Nanoemulsions versus microemulsions: Terminology,

differences, and similarities," *Soft Matter*, vol. 8, no. 6, pp. 1719–1729, 2012.

[95] J. C. F. Serôdio, "The effect of Water in Diesel Nanoemulsion on Light-Duty Diesel Vehicle," MSc dissertation, Swansea University, Swansea, 2022.

[96] S. Gowrishankar, P. Rastogi, A. Krishnasamy, M. G. Basavaraj, N. Kaisare, and I. S. Aidhen, "Synthesis and characterization of emulsion fuels –Implications to spray and engine studies," *Prog. Energy Combust. Sci.*, vol. 101, 101133, 2024.

[97] J. Eastoe, "Microemulsions," in *Surfactant Chemistry*, Bristol, 2003, pp. 59–95.

[98] I. K. Salleh, S. Misra, J. M. B. M. Ibrahim, and S. R. Panuganti, "Micro-emulsion-based dissolver for removal of mixed scale deposition," *J. Pet. Explor. Prod. Technol.*, vol. 9, no. 4, pp. 2635–2641, 2019.

[99] H. Kapadia, H. Brahmbhatt, Y. Dabhi, and S. Chourasia, "Investigation of emulsion and effect on emission in CI engine by using diesel and bio-diesel fuel: A review," *Egypt. J. Pet.*, vol. 28, no. 4, pp. 323–337, 2019.

[100] T. Tadros, "Applied Surfactants," in *Applied Surfactants: Principles and Applications*, 1st ed., Wokingham: Wiley-VCH, 2005, pp. 1–22.

[101] M. D. Anil, V. B. Hemadri, and M. Swamy, "Experimental investigation on impact of water in diesel emulsion in a single-cylinder research diesel engine," *Int. J. Ambient Energy*, vol. 44, no. 1, pp. 399–412, 2023.

[102] S. Woo, W. Kim, J. Lee, and K. Lee, "Fuel properties of water emulsion fuel prepared using porous membrane method for low pollutant engine at various temperatures," *Energy Reports*, vol. 7, pp. 6638–6650, 2021.

[103] V. Vinodhini and C. Krishnamoorthi, "Effect of dispersants on cytotoxic properties of magnetic nanoparticles: a review," *Polym. Bull.*, 2021.

[104] Ken Research, "Growth in Landscape of Surface Active Agents Global Market Outlook," 2020. [Online].

Available: https://kenresearchreport.wordpress.com/2020/08/28/global-surface-active-agents-market/. [Accessed: 25-Sep-2024].

[105] M. Yahaya Khan, Z. A. Abdul Karim, F. Y. Hagos, A. R. A. Aziz, and I. M. Tan, "Current Trends in Water-in-Diesel Emulsion as a Fuel," *Sci. World J.*, pp. 1–15, 2014.

[106] I. Ayad, M. T. Ghannam, and M. Y. E. Selim, "Experimental stability investigation of different water-in-jojoba biodiesel emulsions," *Fuel*, vol. 357, 129782, 2024.

[107] S. Abbott, "Surfactant Science: Principles and Practice," 2015.

[108] S. Abbot, “Hydrophilic Lipophilic Difference.” [Online].

Available: https://www.stevenabbott.co.uk/practical-surfactants/hld.php. [Accessed: 26-Sep-2022].

[109] S. Abbot, “Fishtail Diagrams.” [Online].

Available: https://www.stevenabbott.co.uk/practical-surfactants/fishtail.php. [Accessed: 26-Sep-2022].

[110] J.-L. Salager, R. Marquez, J. Bullon, and A. Forgiarini, “Formulation in Surfactant Systems: From-Winsor-to-HLDN,” *Encyclopedia*, vol. 2, no. 2, pp. 778–839, 2022.

[111] J. M. Aubry, J. F. Ontiveros, J. L. Salager, and V. Nardello-Rataj, “Use of the normalized hydrophilic-lipophilic-deviation (HLDN) equation for determining the equivalent alkane carbon number (EACN) of oils and the preferred alkane carbon number (PACN) of nonionic surfactants by the fish-tail method (FTM),” *Adv. Colloid Interface Sci.*, vol. 276, 102099, 2020.

[112] Z. Chen, L. Wang, Z. Wei, Y. Wang, and J. Deng, “Effect of components on the emulsification characteristic of glucose solution emulsified heavy fuel oil,” *Energy*, vol. 244, 123147, 2022.

[113] D. I. Horsup, “Microemulsion and Macroemulsion Behaviour of Systems Containing Oil, Water and Nonionic Surfactant,” University of Hull, 1991.

[114] S. Abbot, “Creaming.” [Online].

Available: https://www.stevenabbott.co.uk/practical-surfactants/creaming.php. [Accessed: 26-Sep-2022].

[115] S. Abbot, “Flocculation .” [Online].

Available:

https://www.stevenabbott.co.uk/practical-surfactants/flocculation.php. [Accessed: 26-Sep-2022].

[116] S. Abbot, “Coalescence .” [Online].

Available:

https://www.stevenabbott.co.uk/practical-surfactants/coalescence.php. [Accessed: 26-Sep-2022].

[117] S. Abbot, “Ostwald Ripening .” [Online].

Available: https://www.stevenabbott.co.uk/practical-surfactants/ostwald.php. [Accessed: 26-Sep-2022].

[118] S. Gowrishankar and A. Krishnasamy, “Emulsification – A promising approach to improve performance and reduce exhaust emissions of a biodiesel fuelled light-duty diesel engine,” *Energy*, vol. 263 Part C, 125782, 2023.

[119] S. S. Sazhin *et al.*, “A simple model for puffing/micro-explosions in water-fuel emulsion droplets,” *Int. J. Heat Mass Transf.*, vol. 131, pp. 815–821, 2019.

[120] D. C. K. Rao, S. Syam, S. Karmakar, and R. Joarder, “Experimental investigations on nucleation, bubble growth, and micro-explosion characteristics during the combustion of ethanol/Jet A-1 fuel droplets,” *Exp. Therm. Fluid Sci.*, vol. 89, pp. 284–294, 2017.

[121] D. C. K. Rao, S. Karmakar, and S. K. Som, “Puffing and micro-explosion behavior in combustion of butanol/Jet A-1 and acetone-butanol-ethanol (A-B-E)/Jet A-1 fuel droplets,” *Combust. Sci. Technol.*, vol. 189, no. 10, pp. 1796–1812, 2017.

[122] S. Park, S. Woo, H. Kim, and K. Lee, “The characteristic of spray using diesel water emulsified fuel in a diesel engine,” *Appl. Energy*, vol. 176, pp. 209–220, 2016.

[123] C. Confidence, E. H. Ndiritu, and B. Gathitu, “Effect of Emulsified Diesel Fuel on Performance and Emissions Characteristics,” *Energy Power Eng.*, vol. 11, no. 9, pp. 333–341, 2019.

[124] B. K. Debnath, U. K. Saha, and N. Sahoo, “A comprehensive review on the application of emulsions as an alternative fuel for diesel engines,” *Renew. Sustain. Energy Rev.*, vol. 42, pp. 196–211, 2015.

[125] A. Jhalani, D. Sharma, S. L. Soni, P. K. Sharma, and S. Sharma, “A comprehensive review on water-emulsified diesel fuel: chemistry, engine performance and exhaust emissions,” *Environ. Sci. Pollut. Res.*, vol. 26, no. 5, pp. 4570–4587, 2019.

[126] K. R. Patel and V. D. Dhiman, “A review on emission and performance of water diesel micro-emulsified mixture-diesel engine,” *Int. J. Environ. Sci. Technol.*, vol. 19, no. 8, pp. 8027–8042, 2022.

[127] A. Ali, A. R. A. Aziz, M. A. Ismael, and S. Alqaed, “Biosurfactants as an alternative eco-friendly solution for water-in-diesel emulsions-A review paper,” *Heliyon*, vol. 10, no. 17, e37485, 2024.

[128] A. Sartomo, B. Santoso, Ubaidillah, and O. Muraza, “Recent progress on mixing technology for water-emulsion fuel: A review,” *Energy Convers. Manag.*, vol. 213, 112817, 2020.

[129] A. Mostafa, A. Mustafa, I. Youssef, and M. Mourad, “Assessment of Performance and Emissions Characteristics of Diesel Engine using Water Diesel Emulsion: A

Review," *EnvironmentAsia*, vol. 15, no. 1, pp. 117–130, 2022.

[130] K. Park, I. Kwak, and S. Oh, "The effect of water emulsified fuel on a motorway-bus diesel engine," *KSME Int. J.*, vol. 18, no. 11, pp. 2049–2057, 2004.

[131] M. Nadeem, C. Rangkuti, K. Anuar, M. R. U. Haq, I. B. Tan, and S. S. Shah, "Diesel engine performance and emission evaluation using emulsified fuels stabilized by conventional and gemini surfactants," *Fuel*, vol. 85, no. 14–15, pp. 2111–2119, 2006.

[132] M. Y. E. Selim and M. T. Ghannam, "Combustion study of stabilized water-in-diesel fuel emulsion," *Energy Sources, Part A Recover. Util. Environ. Eff.*, vol. 32, no. 3, pp. 256–274, 2010.

[133] M. E. A. Fahd, Y. Wenming, P. S. Lee, S. K. Chou, and C. R. Yap, "Experimental investigation of the performance and emission characteristics of direct injection diesel engine by water emulsion diesel under varying engine load condition," *Appl. Energy*, vol. 102, pp. 1042–1049, 2013.

[134] S. S. Hoseini and M. A. Sobati, "Performance and emission characteristics of a diesel engine operating on different water in diesel emulsion fuels: optimization using response surface methodology (RSM)," *Front. Energy*, vol. 13, no. 4, pp. 636–657, 2019.

[135] F. Okumuş, C. Kaya, and G. Kökkülünk, "NOx based comparative analysis of a CI engine fueled with water in diesel emulsion," *Energy Sources, Part A Recover. Util. Environ. Eff.*, pp. 1–20, 2020.

[136] K. R. Patel and V. D. Dhiman, "Effect of hybrid nanoparticles MgO and Al2O3 added water-in-diesel emulsion fueled diesel engine using hybrid deep neural network-based spotted hyena optimization," *Heat Transf.*, vol. 51, pp. 5748–5788, 2022.

[137] M. Abu-Zaid, "Performance of single cylinder, direct injection Diesel engine using water fuel emulsions," *Energy Convers. Manag.*, vol. 45, no. 5, pp. 697–705, 2004.

[138] M. Abu-Zaid, "An experimental study of the evaporation characteristics of emulsified liquid droplets," *Heat Mass Transf.*, vol. 40, no. 9, pp. 737–741, 2004.

[139] K. Kannan and M. Udayakumar, "NOx and HC emission control using water emulsified diesel in single cylinder diesel engine," *J. Eng. Appl. Sci.*, vol. 4, no. 8, pp. 59–62, 2009.

[140] A. Alahmer, J. Yamin, A. Sakhrieh, and M. A. Hamdan, "Engine performance

using emulsified diesel fuel," *Energy Convers. Manag.*, vol. 51, no. 8, pp. 1708–1713, 2010.

[141] A. Alahmer, "Influence of using emulsified diesel fuel on the performance and pollutants emitted from diesel engine," *Energy Convers. Manag.*, vol. 73, pp. 361–369, 2013.

[142] M. R. Seifi, S. R. Hassan-Beygi, B. Ghobadian, U. Desideri, and M. Antonelli, "Experimental investigation of a diesel engine power, torque and noise emission using water-diesel emulsions," *Fuel*, vol. 166, pp. 392–399, 2016.

[143] H. Hosseinzadeh-Bandbafha *et al.*, "Effects of aqueous carbon nanoparticles as a novel nanoadditive in water-emulsified diesel/biodiesel blends on performance and emissions parameters of a diesel engine," *Energy Convers. Manag.*, vol. 196, pp. 1153–1166, 2019.

[144] A. M. Khathri, M. Y. Ismail, A. A. Abdullah, R. Mamat, and Sutiman, "Performance, Exhaust Emissions and Optimization Using Response Surface Methodology of a Water in Diesel Emulsion on Diesel Engine," *J. Adv. Res. Fluid Mech. Therm. Sci.*, vol. 93, no. 1, pp. 1–12, 2022.

[145] P. K. Mondal and B. K. Mandal, "Experimental investigation on the combustion, performance and emission characteristics of a diesel engine using water emulsified diesel prepared by ultrasonication," *J. Brazilian Soc. Mech. Sci. Eng.*, vol. 40, no. 11, pp. 1–17, 2018.

[146] F. Barnaud, P. Schmelzle, and P. Schulz, "AQUAZOLE™: An original emulsified water-diesel fuel for heavy-duty applications," *SAE Tech. Pap.*, 2000.

[147] J. W. Park, K. Y. Huh, and J. H. Lee, "Reduction of NOx, smoke and brake specific fuel consumption with optimal injection timing and emulsion ratio of water-emulsified diesel," *Proc. Inst. Mech. Eng. Part D J. Automob. Eng.*, vol. 215, no. 1, pp. 83–93, 2001.

[148] W. Zhang *et al.*, "Influence of water emulsified diesel & oxygen-enriched air on diesel engine NO-smoke emissions and combustion characteristics," *Energy*, vol. 55, pp. 369–377, 2013.

[149] N. Singh and R. Bharj, "An Experimental Investigation of Emulsified Fuel in a Slow Speed Diesel Engine for Performance and Emission," *Int. J. Ind. Eng. Technol.*, vol. 6, no. 1, pp. 1–9, 2014.

[150] N. A. Ramlan *et al.*, "Performance and emissions of light-duty diesel vehicle fuelled with non-surfactant low grade diesel emulsion compared with a high grade diesel in Malaysia," *Energy Convers. Manag.*, vol. 130, no. 2016, pp. 192–199,

2016.

[151] A. M. Ithnin *et al.*, "Emulsifier-free Water-in-Diesel emulsion fuel: Its stability behaviour, engine performance and exhaust emission," *Fuel*, vol. 215, pp. 454–462, 2018.

[152] K. Ramalingam, E. P. Venkatesan, and A. Aabid, "Assessment of CI Engine Performance and Exhaust Air Quality Outfitted with Real-Time Emulsion Fuel Injection System," *Sustainability*, vol. 14, pp. 1–19, 2022.

[153] H. A. Rahman, M. M. Rahman, W. J. Yahya, T. E. Kaonain, and H. A. Kadir, "Implementation of a Non-Surfactant Water-in-Diesel Emulsion Fuel in a Common Rail Direct Injection Diesel Vehicle," *Int. J. Automot. Technol.*, vol. 24, no. 5, pp. 1349–1358, 2023.

[154] M. Q. Mohd Tamam *et al.*, "Performance and emission studies of a common rail turbocharged diesel electric generator fueled with emulsifier free water/diesel emulsion," *Energy*, vol. 268, 126704, 2023.

[155] D. Holt, "Effects of PuriNOx™ water-diesel fuel emulsions on emissions and fuel economy in a heavy-duty diesel engine," in *Alternative Diesel Fuels*, SAE, 2004, pp. 1–11.

[156] V. Suresh and K. S. Amirthagadeswaran, "Combustion and performance characteristics of water-in-diesel emulsion fuel," *Energy Sources, Part A Recover. Util. Environ. Eff.*, vol. 37, no. 18, pp. 2020–2028, 2015.

[157] A. M. Ithnin, M. A. Ahmad, M. A. A. Bakar, S. Rajoo, and W. J. Yahya, "Combustion performance and emission analysis of diesel engine fuelled with water-in-diesel emulsion fuel made from low-grade diesel fuel," *Energy Convers. Manag.*, vol. 90, pp. 375–382, 2015.

[158] D. Ogunkoya, S. Li, O. J. Rojas, and T. Fang, "Performance, combustion, and emissions in a diesel engine operated with fuel-in-water emulsions based on lignin," *Appl. Energy*, vol. 154, pp. 851–861, 2015.

[159] N. A. Mazlan *et al.*, "Effects of different water percentages in non-surfactant emulsion fuel on performance and exhaust emissions of a light-duty truck," *J. Clean. Prod.*, vol. 179, pp. 559–566, 2018.

[160] S. Vellaiyan, A. Subbiah, and P. Chockalingam, "Effect of Titanium dioxide nanoparticle as an additive on the working characteristics of biodiesel-water emulsion fuel blends," *Energy Sources, Part A Recover. Util. Environ. Eff.*, vol. 43, no. 9, pp. 1087–1099, 2021.

[161] C. Y. Lin and K. H. Wang, “Diesel engine performance and emission characteristics using three-phase emulsions as fuel,” *Fuel*, vol. 83, pp. 537–545, 2004.

[162] C. Y. Lin and L. W. Chen, “Engine performance and emission characteristics of three-phase diesel emulsions prepared by an ultrasonic emulsification method,” *Fuel*, vol. 85, pp. 593–600, 2006.

[163] E. Tzirakis *et al.*, “Diesel-water emulsion emissions and performance evaluation in public buses in attica basin,” *SAE Tech. Pap.*, 2006.

[164] J. Ghojel, D. Honnery, and K. Al-Khaleefi, “Performance, emissions and heat release characteristics of direct injection diesel engine operating on diesel oil emulsion,” *Appl. Therm. Eng.*, vol. 26, no. 17–18, pp. 2132–2141, 2006.

[165] A. Alahmer, J. Yamin, A. Sakhrieh, and M. A. Hamdan, “Engine performance using emulsified diesel fuel,” *Energy Convers. Manag.*, vol. 51, no. 8, pp. 1708–1713, 2010.

[166] A. Maiboom and X. Tauzia, “NOx and PM emissions reduction on an automotive HSDI Diesel engine with water-in-diesel emulsion and EGR: An experimental study,” *Fuel*, vol. 90, no. 11, pp. 3179–3192, 2011.

[167] E. Perumal Venkatesan *et al.*, “Performance and emission reduction characteristics of cerium oxide nanoparticle-water emulsion biofuel in diesel engine with modified coated piston,” *Environ. Sci. Pollut. Res.*, vol. 26, pp. 27362–27371, 2019.

[168] Rosid, B. Sudarmanta, L. Atmaja, I. S. Krisandika, and A. W. Arohman, “Effect of 35% water in diesel emulsion fuel and AFR enriched combustion on the combustion and emissions characteristics,” *AIP Conf. Proc.*, vol. 2187, 2019.

[169] Z. U. Hassan *et al.*, “Use of diesel and emulsified diesel in CI engine: A comparative analysis of engine characteristics,” *Sci. Prog.*, vol. 104, no. 2, pp. 1–19, 2021.

[170] P. S. Gautam, P. K. Vishnoi, and V. K. Gupta, “The effect of water emulsified diesel on combustion, performance and emission characteristics of diesel engine,” *Mater. Today Proc.*, vol. 52, pp. 1041–1047, 2022.

[171] O. Armas, R. Ballesteros, F. J. Martos, and J. R. Agudelo, “Characterization of light duty Diesel engine pollutant emissions using water-emulsified fuel,” *Fuel*, vol. 84, pp. 1011–1018, 2005.

[172] O. Badran, S. Emeish, M. Abu-Zaid, T. Abu-Rahma, M. Al-Hasan, and M. Al-

Ragheb, “Impact of Emulsified Water/Diesel Mixture on Engine Performance and Environment,” *Int. J. Therm. Environ. Eng.*, vol. 3, no. 1, pp. 1–7, 2010.

[173] J. S. Basha and R. B. Anand, “An experimental study in a CI engine using nanoadditive blended water-diesel emulsion fuel,” *Int. J. Green Energy*, vol. 8, no. 3, pp. 332–348, 2011.

[174] J. Y. Syu *et al.*, “Effects of water-emulsified fuel on a diesel engine generator’s thermal efficiency and exhaust,” *J. Air Waste Manag. Assoc.*, vol. 64, no. 8, pp. 970–978, 2014.

[175] A. M. A. Attia and A. R. Kulchitskiy, “Influence of the structure of water-in-fuel emulsion on diesel engine performance,” *Fuel*, vol. 116, pp. 703–708, 2014.

[176] P. Baskar and A. Senthil Kumar, “Experimental investigation on performance characteristics of a diesel engine using diesel-water emulsion with oxygen enriched air,” *Alexandria Eng. J.*, vol. 56, no. 1, pp. 137–146, 2017.

[177] P. K. Mondal and B. K. Mandal, “A comprehensive review on the feasibility of using water emulsified diesel as a CI engine fuel,” *Fuel*, vol. 237, pp. 937–960, 2019.

[178] K. A. Subramanian and A. Ramesh, “A Study on the use of Water-Diesel Emulsions in a di Diesel Engine,” *SAE Tech. Pap.*, 2001.

[179] M. A. A. Nazha, H. Rajakaruna, and S. A. Wagstaff, “The use of emulsion, water induction and EGR for controlling diesel engine emissions,” *SAE Tech. Pap.*, 2001.

[180] A. Lif and K. Holmberg, “Water-in-diesel emulsions and related systems,” *Adv. Colloid Interface Sci.*, vol. 123–126, pp. 231–239, 2006.

[181] M. A. Ahmad *et al.*, “Combustion performance and exhaust emissions fuelled with non-surfactant water-in-diesel emulsion fuel made from different water sources,” *Environ. Sci. Pollut. Res.*, vol. 25, pp. 24266–24280, 2018.

[182] D. A. Sugeng *et al.*, “Diesel engine emission analysis using fuel from diverse emulsification methods,” *Environ. Sci. Pollut. Res.*, vol. 25, no. 27, pp. 27214–27224, 2018.

[183] M. Saravanan, A. Anbarasu, and B. M. Gnanasekaran, “Study of performance and emission characteristics of IC engines by using diesel-water emulsion,” *Int. J. Adv. Manuf. Technol.*, vol. 69, no. 9–12, pp. 2531–2544, 2013.

[184] N. H. Abdurahman, Y. M. Rosli, N. H. Azhari, and A. Abdul Adam, “The Potential of a Water-in-Diesel Emulsion for Increased Engine Performance and as an Environmentally Friendly Fuel,” *MATEC Web Conf.*, vol. 70, 2016.

[185] J. S. Basha and M. Al Balushi, “Performance and Emission Features of a Light Duty Diesel Engine Generator Powered with Water-Diesel Emulsions,” *Eur. J. Eng. Sci. Technol.*, vol. 2, no. 4, pp. 72–78, 2019.

[186] A. M. Al-Sabagh, M. M. Emara, M. R. N. El-Din, and W. R. Aly, “Water-in-Diesel Fuel Nanoemulsions Prepared by High Energy: Emulsion Drop Size and Stability, and Emission Characteristics,” *J. Surfactants Deterg.*, vol. 15, no. 2, pp. 139–145, 2012.

[187] N. Samec, B. Kegl, and R. W. Dibble, “Numerical and experimental study of water/oil emulsified fuel combustion in a diesel engine,” *Fuel*, vol. 81, no. 16, pp. 2035–2044, 2002.

[188] D. R. Emberson, B. Ihracska, S. Imran, A. Diez, M. Lancaster, and T. Korakianitis, “Hydraulic characterization of Diesel and water emulsions using momentum flux,” *Fuel*, vol. 162, pp. 23–33, 2015.

[189] S. Vellaiyan and K. S. Amirthagadeswaran, “The role of water-in-diesel emulsion and its additives on diesel engine performance and emission levels: A retrospective review,” *Alexandria Eng. J.*, vol. 55, no. 3, pp. 2463–2472, 2016.

[190] E. Rajasekar, A. Murugesan, R. Subramanian, and N. Nedunchezhian, “Review of NOx reduction technologies in CI engines fuelled with oxygenated biomass fuels,” *Renew. Sustain. Energy Rev.*, vol. 14, no. 7, pp. 2113–2121, 2010.

[191] K. A. Subramanian, “A comparison of water-diesel emulsion and timed injection of water into the intake manifold of a diesel engine for simultaneous control of NO and smoke emissions,” *Energy Convers. Manag.*, vol. 52, no. 2, pp. 849–857, 2011.

[192] D. Scarpete, “Diesel-Water Emulsion , an Alternative Fuel To Reduce Diesel Engine Emissions . a Review,” *Mach. Technol. Mater.*, no. 7, pp. 7–10, 2013.

[193] N. A. Ramlan *et al.*, “Performance and emissions of light-duty diesel vehicle fuelled with non-surfactant low grade diesel emulsion compared with a high grade diesel in Malaysia,” *Energy Convers. Manag.*, vol. 130, pp. 192–199, 2016.

[194] T. Kadota and H. Yamasaki, “Recent advances in the combustion of water fuel emulsion,” *Prog. Energy Combust. Sci.*, vol. 28, no. 5, pp. 385–404, 2002.

[195] Z. Wang *et al.*, “Effects of water content on evaporation and combustion characteristics of water emulsified diesel spray,” *Appl. Energy*, vol. 226, no. 1037, pp. 397–407, 2018.

[196] L. Corral-Gómez, G. Rubio-Gómez, S. Martínez-Martínez, and F. A. Sánchez-Cruz,

"Effect of diesel-biodiesel-ethanol blends on the spray macroscopic parameters in a common-rail diesel injection system," *Fuel*, vol. 241, pp. 876–883, 2019.

[197] M. A. Ismael, A. R. A. Aziz, S. E. Mohammed, E. Z. Zainal A, M. B. Baharom, and F. Y. Hagos, "Macroscopic and microscopic spray structure of water-in-diesel emulsions," *Energy*, vol. 223, 120040, 2021.

[198] A. Stark, "Power vs. Torque." [Online]. Available: https://x-engineer.org/power-vs-torque/. [Accessed: 17-Nov-2021].

[199] T. Liao, R. Wang, X. Zheng, Y. Sun, K. Butterbach-Bahl, and N. Chen, "Automated online measurement of N2, N2O, NO, CO2, and CH4 emissions based on a gas-flow-soil-core technique," *Chemosphere*, vol. 93, no. 11, pp. 2848–2853, 2013.

[200] I. A. Reşitoɨlu, K. Altinişik, and A. Keskin, "The pollutant emissions from diesel-engine vehicles and exhaust aftertreatment systems," *Clean Technol. Environ. Policy*, vol. 17, no. 1, pp. 15–27, 2015.

[201] R. Van Basshuysen and F. Schaefer, *Internal Combustion Engine Handbook: Basics, Components, Systems, and Perspectives*, 2nd ed. SAE International, 2016.

[202] C. Baukal, "Everything you need to know about NOx," *Met. Finish.*, vol. 103, no. 11, pp. 18–24, 2005.

[203] R. Y. Mamuad and A. E. S. Choi, "Biodesulfurization Processes for the Removal of Sulfur from Diesel Oil: A Perspective Report," *Energies*, vol. 16, no. 6, 2738, 2023.

[204] E. Alptekin and M. Canakci, "Determination of the density and the viscosities of biodiesel-diesel fuel blends," *Renew. Energy*, vol. 33, no. 12, pp. 2623–2630, 2008.

[205] M. El-Adawy, M. A. Ismael, I. B. Dalha, A. R. A. Aziz, and W. El Maghlany, "Unveiling the status of emulsified water-in-diesel and nanoparticles on diesel engine attributes," *Case Stud. Therm. Eng.*, vol. 44, 102824, 2023.

[206] "Viscosity." [Online]. Available: https://www.britannica.com/science/viscosity. [Accessed: 14-Feb-2023].

[207] R. P. Chhabra, "Non-Newtonian fluids: An introduction," in *Rheology of Complex Fluids*, Springer New York, 2010, pp. 3–34.

[208] J. Mak, "Hydrodynamic Stability of Newtonian and Non-Newtonian Fluids," 2009.

[209] M. R. G. Contreras, "Estudio de mezclas basadas en bioetanol sobre las emisiones de un motor diesel," PhD dissertation, Universidad de Castilla-La Mancha, Toledo, 2009.

[210] R. Arévalo-Ramírez and J. Aros-Taglioni, “Parametric analysis based on energy and exergy balances of a condensing boiler,” *J. Mech. Sci. Technol.*, vol. 37, no. 3, pp. 1463–1471, 2023.

[211] A. José Rosa Nunes and F. Miguel Ribeiro Proença Brojo, “Designing an Eddy Current Brake for Engine Testing,” in *International Congress on Engineering - Engineering for Evolution, KnE Engineering*, 2020, pp. 743–756.

[212] M. R. Madireddy, “Methods for Reconstruction of Transient Emissions from Heavy-Duty Vehicles,” West Virgina University, 2008.

[213] R. Viskup, “Comparison of Different Techniques for Measurement of Soot and Particulate Matter Emissions from Diesel Engine,” in *Introduction to Diesel Emissions*, IntechOpen, 2020.

[214] Ł. Grabowski, Z. Czyż, and M. Porzak, “The study on loads on an aircraft piston engine continental motors IOF-240-B5B in training flights,” *Transport*, vol. 33, no. 3, pp. 773–778, 2018.

[215] E. A. El Shenawy *et al.*, “Investigation and performance analysis of water-diesel emulsion for improvement of performance and emission characteristics of partially premixed charge compression ignition (PPCCI) diesel engines,” *Sustain. Energy Technol. Assessments*, vol. 36, 100546, 2019.

[216] Z. Wang *et al.*, “Experimental investigation on spray, evaporation and combustion characteristics of ethanol-diesel, water-emulsified diesel and neat diesel fuels,” *Fuel*, vol. 231, pp. 438–448, 2018.

[217] A. Khanjani and M. A. Sobati, “Performance and emission of a diesel engine using different water/waste fish oil (WFO) biodiesel/diesel emulsion fuels: Optimization of fuel formulation via response surface methodology (RSM),” *Fuel*, vol. 288, 119662, 2021.

[218] W. Zhang, Z. Zhang, H. Chen, Z. Ji, Y. Ma, and F. Sun, “A review on performance, combustion and emission of diesel and alcohols in a dual fuel engine,” *J. Energy Inst.*, vol. 116, 101760, 2024.

[219] K. Kim *et al.*, “Effects of the cetane number on chemical ignition delay,” *Energy*, vol. 264, 126263, 2023.

[220] J. Liu, P. Booma Devi, A. Chinnathambi, and S. Ali Alharbi, “Mitigating fossil fuel deficiency and environmental impacts: Performance analysis of Scenedesmus obliquus microalgae biodiesel in a diesel engine,” *Fuel*, vol. 364, 131033, 2024.

[221] M. Abdollahi, B. Ghobadian, G. Najafi, S. S. Hoseini, M. Mofijur, and M. Mazlan,

"Impact of water – biodiesel – diesel nano-emulsion fuel on performance parameters and diesel engine emission," *Fuel*, vol. 280, 118576, 2020.

[222] C. Cengiz and S. Ozen Unverdi, "Effect of early intake valve closing, exhaust gas recirculation and split injection on combustion and emissions characteristics of a HDDI diesel engine operating in PCCI combustion mode," *Fuel*, vol. 353, 129079, 2023.

[223] Ü. Ağbulut and S. Sarıdemir, "Synergistic effects of hybrid nanoparticles along with conventional fuel on engine performance, combustion, and environmental characteristics," *Energy*, vol. 292, 130267, 2024.

[224] S. Gowrishankar and A. Krishnasamy, "Experimental investigations on biodiesel-water emulsion as a potential fuel for early and late injection based premixed lean combustion," *Energy Convers. Manag.*, vol. 273, 116386, 2022.

[225] Neha, R. Prasad, and S. V. Singh, "A review on catalytic oxidation of soot emitted from diesel fuelled engines," *J. Environ. Chem. Eng.*, vol. 8, 103945, 2020.

[226] R. Vigneswaran, D. Balasubramanian, and B. D. S. Sastha, "Performance, emission and combustion characteristics of unmodified diesel engine with titanium dioxide (TiO2) nano particle along with water-in-diesel emulsion fuel," *Fuel*, vol. 285, 119115, 2021.

[227] N. A. Ramlan *et al.*, "Emissions and performance analysis of diesel powered road vehicle equipped with real-time non-surfactant emulsion fuel supply system," *Fuel*, vol. 273, 117257, 2020.

[228] S. Vellaiyan, "Enhancement in combustion, performance, and emission characteristics of a biodiesel-fueled diesel engine by using water emulsion and nanoadditive," *Renew. Energy*, vol. 145, pp. 2108–2120, 2020.

[229] X. Su *et al.*, "Combustion and emission characteristics of diesel engine fueled with diesel/cyclohexanol blend fuels under different exhaust gas recirculation ratios and injection timings," *Fuel*, vol. 332, 125986, 2023.

[230] I. Veza *et al.*, "Effects of Acetone-Butanol-Ethanol (ABE) addition on HCCI-DI engine performance, combustion and emission," *Fuel*, vol. 333, 126377, 2023.

[231] P. V. Elumalai, M. Nambiraj, M. Parthasarathy, D. Balasubramanian, V. Hariharan, and J. Jayakar, "Experimental investigation to reduce environmental pollutants using biofuel nano-water emulsion in thermal barrier coated engine," *Fuel*, vol. 285, 119200, 2021.

[232] Z. Yin, S. Liu, D. Tan, Z. Zhang, Z. Wang, and B. Wang, "A review of the

development and application of soot modelling for modern diesel engines and the soot modelling for different fuels," *Process Saf. Environ. Prot.*, vol. 178, pp. 836–859, 2023.

[233] X. Chen, X. Xi, L. Zhang, Z. Wang, Z. Cui, and W. Long, "Experimental study on nucleation and micro-explosion characteristics of emulsified heavy fuel oil droplets at elevated temperatures during evaporation," *Appl. Therm. Eng.*, vol. 224, 120114, 2023.

[234] X. Wang, H. Bu, H. Chen, J. Liu, Z. Chen, and J. Gao, "Numerical investigation of diesel spray combustion characteristics in the ammonia/air atmosphere," *J. Energy Inst.*, vol. 116, 101718, 2024.

[235] S. Shen, K. Sun, Z. Che, T. Wang, M. Jia, and J. Cai, "Mechanism of micro-explosion of water-in-oil emulsified fuel droplet and its effect on soot generation," *Energy*, vol. 191, 116488, 2020.

Annex A. Publications

A.1 Articles in international peer-reviewed journals

1. Pedro Oliveira, Francisco Brójo, An Experimental Study on the Performance and Emissions of an 8% Water-in-Diesel Emulsion Stabilized by a Hydrophilic Surfactant Blend, *Energies*, vol 16, no. 6, 1328, 2024.
2. Pedro Oliveira, Francisco Brójo, Fuel properties, performance, and emissions of water-emulsified diesel in an IDI diesel engine, *Thermal Science and Engineering*, vol 7, no. 2, 8821, 2024.
3. Pedro Oliveira, Francisco Brójo, Rogério Serôdio, João Serôdio, Investigation of Water-in-Diesel Emulsion Behavior Formulated for Performance Conditions on a Single-Cylinder Diesel Engine, *Energies*, vol 18, 934, 2025.

A.2 Articles in international peer-reviewed conferences

1. Pedro Oliveira, Francisco Brójo, Water-in-Diesel Emulsion: Torque, Fuel Consumption and Emission Analysis, *International Mechanical Engineering Congress and Exposition*, New Orleans, LA, October 29 - November 2, 2023.
2. Pedro Oliveira, Francisco Brójo, Rafael Domingues, Influence of Fuel Temperature on Performance and Emissions of Water-emulsified Diesel Fuel, *International Mechanical Engineering Congress and Exposition*, Portland, OR, November 17 - November 21, 2024.
3. Pedro Oliveira, Francisco Brójo, Rogério Serôdio, Influence of Water Percentage on Performance and Emissions of a Diesel Engine Fuelled with Water-emulsified Diesel, *ICEUBI - International Congress on Engineering*, Covilhã, Portugal, November 27 - November 29, 2024.
4. Pedro Oliveira, Francisco Brójo, Rogério Serôdio, João Serôdio, Effect of Water-in-Diesel Blends on Efficiency and Pollutant Emissions at Medium Engine Load, International Mechanical Engineering Congress and Exposition, Memphis, TN, November 16 – November 20, 2025. (Accepted, under review)

A.3 Oral presentations

1. Pedro Oliveira, Water-in-Diesel Emulsions, C-MAST Seminar, 13 July 2022, Covilhã, Portugal.

Annex B. Arduino Code

B.1 Arduino 1: Load cell and hall effect sensor

```
// Include libraries
#include <Wire.h>                                                  // I2C Library
#include <LiquidCrystal_I2C.h>                                     // LCD Library
#include <HX711.h>                                                // HX711 Library

// Initialise interface pins
HX711 scale;                                          // Start link with HX711
LiquidCrystal_I2C lcd(0x27, 16, 2);              // (address, #columns, #rows)

// Variables for speed
const int rpmPin = 2;                              // Pin 2 detects hall sensor
int rpm;                                          // Speed value to be displayed
float PrevTime = 0;                 // Time of previous magnet detection in µs
float Duration = 0;             // Time elapsed between magnet detection in µs

// Variables for torque and power
const int CLK = 4;                                 // Pin 4 connects to HX711 CLK
const int DOUT = 5;                               // Pin 5 connects to HX711 DOUT
const int ResetPin = 6;                  // Pin 6 connects to reset push button
const int Distance = 500;                           // Distance of the arm in mm
float Weight;                              // Weight measured by load cell in g
float Calibration = 218.5;                      // Load cell calibration factor
float Torque;                                        // Torque calculated in Nm
bool ResetButton;
float PowerKW;
float PowerHP;


void setup()
{
  pinMode(ResetPin, INPUT_PULLUP);
  attachInterrupt(digitalPinToInterrupt(rpmPin), RPMISR, RISING);

  scale.begin(DOUT, CLK);                                 // Start link with HX711
  scale.tare();                                              // Tare scale to zero
  scale.set_scale(Calibration);          // Adjust scale to calibration factor

  Serial.begin(9600);

  lcd.init();                                          // Start I2C link with LCD
  lcd.backlight();                                       // Turn on LCD backlight
  lcd.setCursor(0, 0);
  lcd.print(" The Dyno Bench ");      // Delay routine to stabilise scale.tare
  lcd.setCursor(0, 1);
  lcd.print("   C-MAST UBI   ");
  delay(1500);
}


void loop()
{
  RPM();
  TORQUE();
  POWER();
  LCD();
  SERIALCOM();
}

void RPMISR()
{
```

```
  Duration = micros() - PrevTime;
  PrevTime = micros();
}

void RPM()
{
  rpm = 60000000 / Duration;
  if (micros() - PrevTime  > 2*1000000)
  {
    rpm = 0;
  }
}

void TORQUE()
{
  ResetButton = digitalRead(ResetPin);            // Read state of push button
  if (ResetButton == LOW)
  {
    scale.tare();                       // Tare scale if push button is pressed
  }
  Weight = scale.get_units();                              // Average 3 readings
  Torque = Weight * Distance * 0.001 * 9.81 * 0.001;
}

void POWER()
{
  PowerKW = rpm*Torque/9550;
  PowerHP = PowerKW*1.341;
}

void LCD()
{
  lcd.clear();
  lcd.setCursor(0, 0);
  lcd.print("SPD: ");
  lcd.print(rpm);
  lcd.print(" rpm");
  lcd.setCursor(0, 1);
  lcd.print("TRQ: ");
  lcd.print(Torque);
  lcd.print(" N.m ");
}

void SERIALCOM()
{
  Serial.print(rpm);
  Serial.print(" ");
  Serial.print(Torque);
  Serial.print(" ");
  Serial.print(PowerKW);
  Serial.print(" ");
  Serial.println(PowerHP);
}
```

B.2 Arduino 2: Load cell and type K thermocouple

```
// Include libraries
#include <HX711.h>                                          // HX711 Library
#include "max6675.h"                                      // max6675.h Library

HX711 scale;

// Variables for temperature
int ktcSO_1 = 5;
int ktcCS_1 = 6;
int ktcCLK_1 = 7;
float termo_k_1;
```

```
// Variables for weight
const int CLK = 2;
const int DOUT = 3;
float weight;
float initialweight;
float finalweight;
float Calibration = 437;


void setup()
{
  scale.begin(DOUT, CLK);
  scale.tare();
  scale.set_scale(Calibration);
  Serial.begin(9600);
}


void loop()
{
  EBT();                                        // For engine block temperature
  FF();                                                    // For fuel flow
  SERIALCOM();
}

void EBT()
{
  MAX6675 ktc_1(ktcCLK_1, ktcCS_1, ktcSO_1);
  termo_k_1 = ktc_1.readCelsius();
  delay(250);                                   // If delay <250, it overclocks
}

void FF()
{
  weight = scale.get_units();
}

void SERIALCOM()
{
  Serial.print(termo_k_1);
  Serial.print(" ");
  Serial.println(weight);
}
```

Annex C. Raw Data

C.1 25W load

C.1.1 Performance

Table C.1. Mean and standard deviation for speed, BT, and BP at 25W load.

	Speed [rpm]	BT [Nm]	BP [kW]
Diesel	1469.81 ± 29.86	3.21 ± 0.03	0.49 ± 0.01
	1961.07 ± 43.51	2.57 ± 0.04	0.53 ± 0.02
	2532.98 ± 4.43	2.01 ± 0.02	0.53 ± 0.01
	3001.68 ± 5.07	1.69 ± 0.09	0.53 ± 0.03
8% WiDE	1444.36 ± 17.60	4.43 ± 0.04	0.67 ± 0.01
	1934.27 ± 13.62	3.77 ± 0.04	0.76 ± 0.01
	2470.39 ± 16.63	3.10 ± 0.04	0.80 ± 0.01
	2978.39 ± 17.84	2.62 ± 0.20	0.82 ± 0.06
16% WiDE	1497.57 ± 27.35	3.93 ± 0.03	0.62 ± 0.01
	2037.18 ± 16.58	2.89 ± 0.06	0.62 ± 0.01
	2560.36 ± 14.01	2.84 ± 0.05	0.76 ± 0.01
	2976.87 ± 17.77	2.07 ± 0.13	0.65 ± 0.04

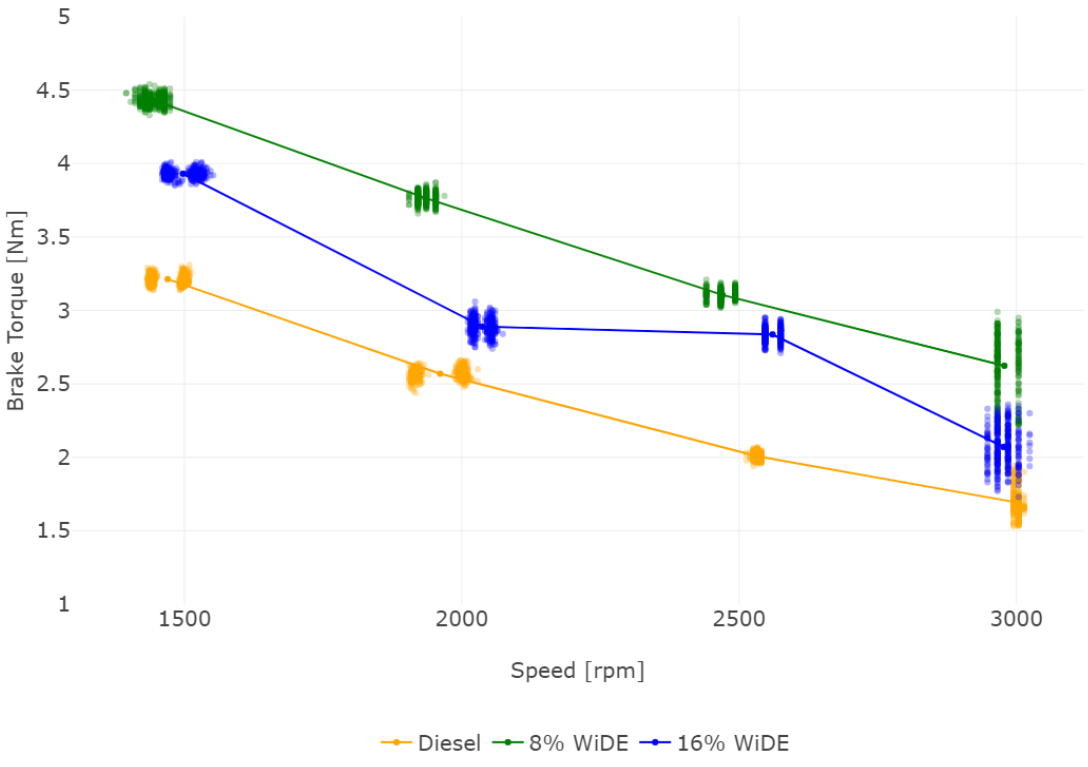

Figure C.1. Engine BT at 25W load (raw data).

Figure C.2. Engine BP at 25W load (raw data).

Figure C.3. Engine BSFC at 25W load (raw data).

Figure C.4. Engine BTE at 25W load (raw data).

C.1.2 Emissions

Table C.2. Mean and standard deviation for speed, CO, CO_2, HC, NO, O_2, and smoke at 25W load.

	Speed [rpm]	CO [%]	CO_2 [%]	HC [ppm]	NO [ppm]	O_2 [%]	Smoke [%]
Diesel	1469.81 ± 29.86 1961.07 ± 43.51 2532.98 ± 4.43 3001.68 ± 5.07	0.02 ± 0.00 0.02 ± 0.00 0.03 ± 0.00 0.03 ± 0.00	1.05 ± 0.01 1.16 ± 0.01 1.51 ± 0.01 1.40 ± 0.02	15.26 ± 0.71 18.00 ± 0.00 17.97 ± 0.17 14.99 ± 0.72	60.61 ± 0.95 56.57 ± 0.53 52.46 ± 0.74 33.95 ± 1.12	19.20 ± 0.01 19.05 ± 0.01 18.63 ± 0.01 18.67 ± 0.05	3.12 ± 0.08 1.75 ± 0.09 2.45 ± 0.15 2.57 ± 0.15
8% WiDE	1444.36 ± 17.60 1934.27 ± 13.62 2470.39 ± 16.63 2978.39 ± 17.84	0.04 ± 0.00 0.05 ± 0.00 0.07 ± 0.00 0.08 ± 0.00	1.37 ± 0.01 1.64 ± 0.00 2.00 ± 0.00 1.91 ± 0.02	32.00 ± 0.00 33.00 ± 0.00 34.00 ± 0.00 31.66 ± 0.86	75.05 ± 0.85 69.11 ± 0.69 60.62 ± 0.76 35.37 ± 1.03	19.03 ± 0.01 18.66 ± 0.01 18.08 ± 0.01 18.13 ± 0.02	0.76 ± 0.14 0.00 ± 0.00 0.00 ± 0.00 0.00 ± 0.00
16% WiDE	1497.57 ± 27.35 2037.18 ± 16.58 2560.36 ± 14.01 2976.87 ± 17.77	0.07 ± 0.00 0.10 ± 0.01 0.12 ± 0.00 0.16 ± 0.00	1.51 ± 0.01 1.77 ± 0.02 1.77 ± 0.01 1.86 ± 0.02	45.08 ± 0.27 46.95 ± 4.42 20.39 ± 1.45 27.71 ± 1.60	44.07 ± 0.79 34.31 ± 0.75 27.02 ± 0.49 18.11 ± 1.17	18.76 ± 0.01 18.37 ± 0.03 18.09 ± 0.01 17.90 ± 0.01	2.24 ± 0.14 0.52 ± 0.04 0.08 ± 0.04 1.04 ± 0.97

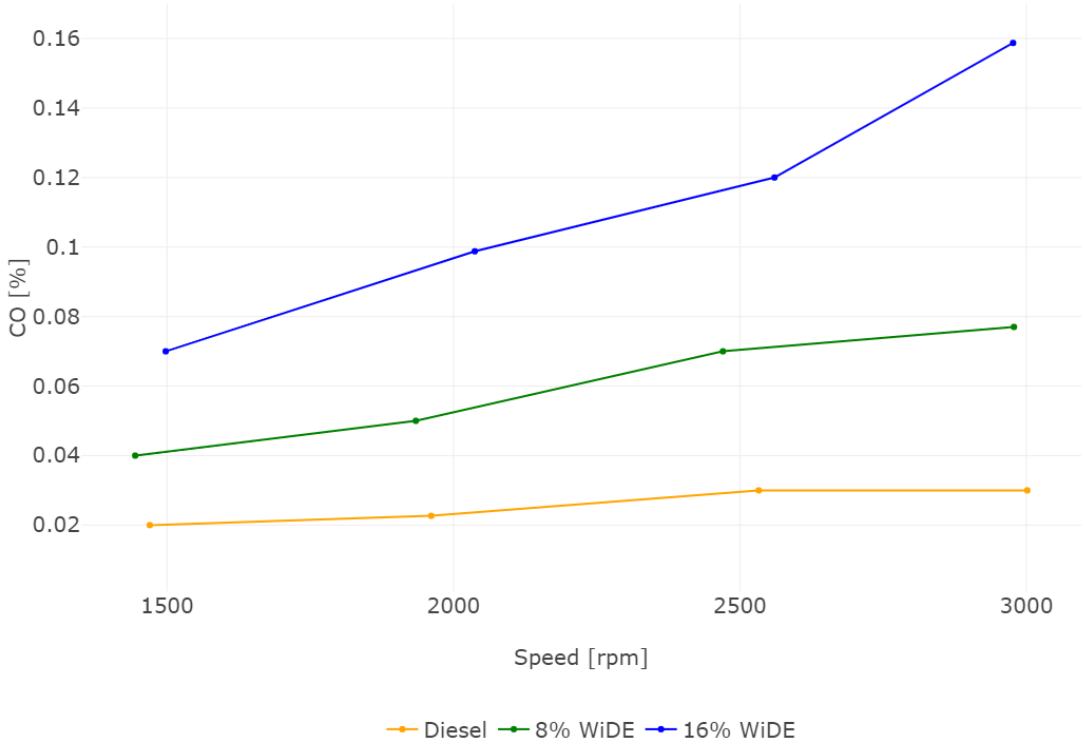

Figure C.5. CO emissions at 25W load (raw data).

Figure C.6. CO_2 emissions at 25W load (raw data).

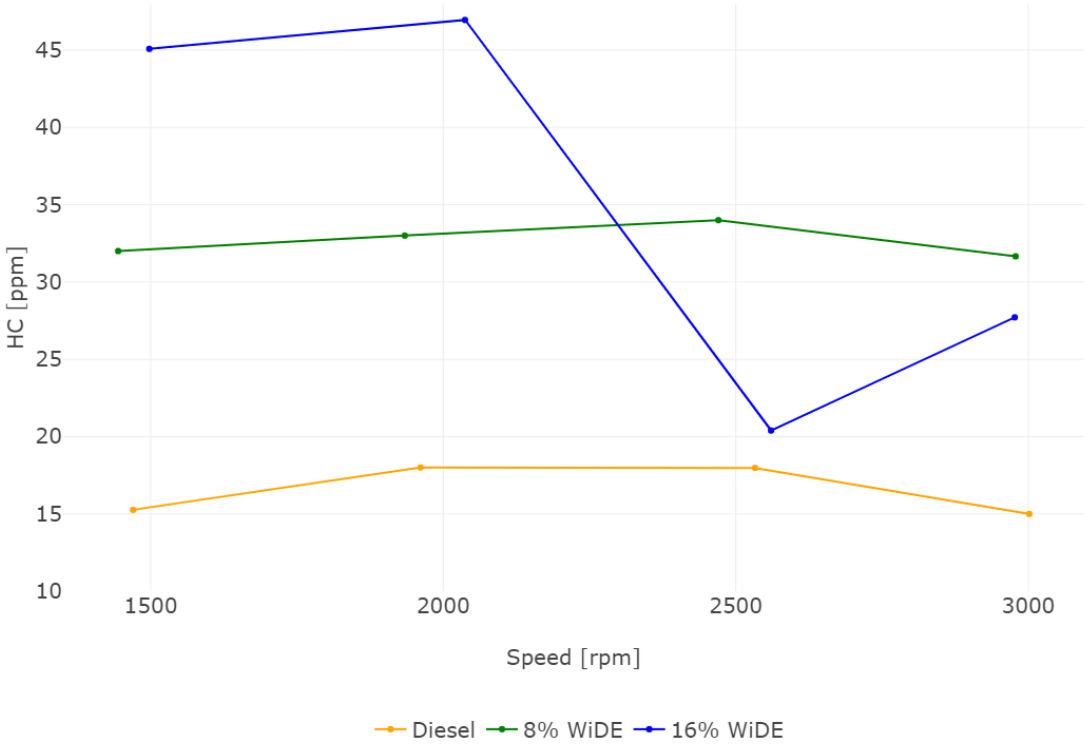

Figure C.7. HC emissions at 25W load (raw data).

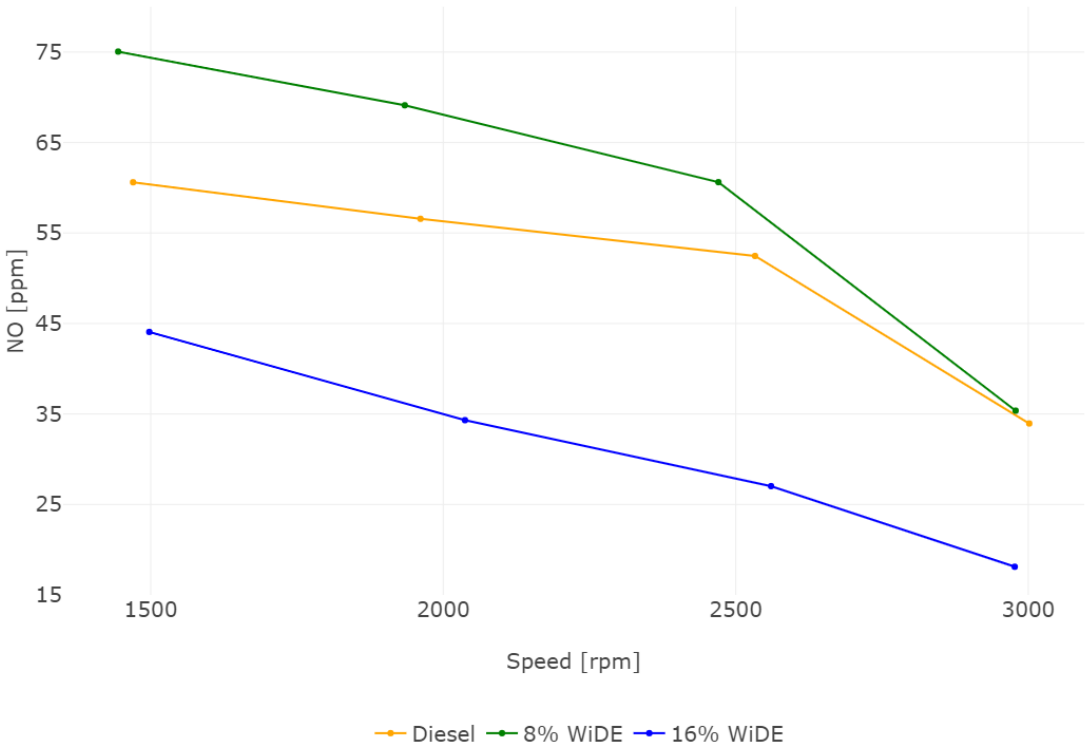

Figure C.8. NO emissions at 25W load (raw data).

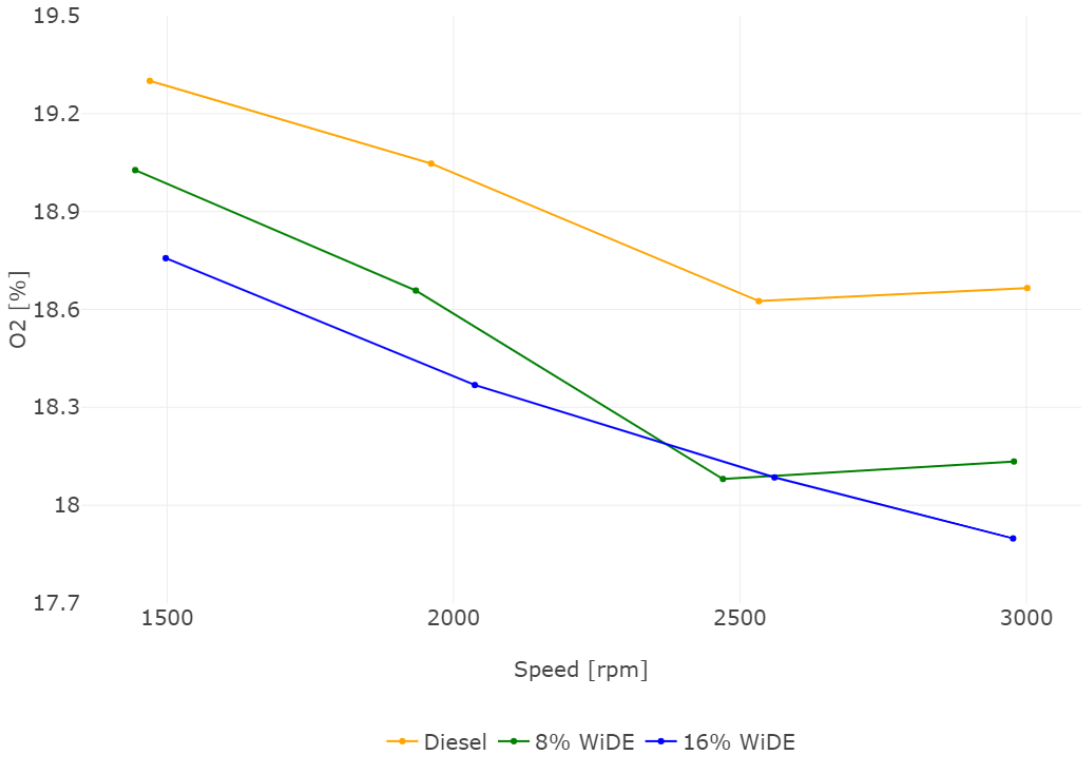

Figure C.9. O_2 emissions at 25W load (raw data).

Figure C.10. Smoke emissions at 25W load (raw data).

C.2 50W load

C.2.1 Performance

Table C.3. Mean and standard deviation for speed, BT, and BP at 50W load.

	Speed [rpm]	BT [Nm]	BP [kW]
Diesel	1511.34 ± 5.98	7.61 ± 0.04	1.20 ± 0.01
	2007.24 ± 34.96	6.42 ± 0.09	1.35 ± 0.03
	2527.82 ± 15.05	5.07 ± 0.04	1.34 ± 0.01
	3015 ± 12.18	4.14 ± 0.21	1.31 ± 0.07
8% WiDE	1521.43 ± 18.81	9.29 ± 0.05	1.48 ± 0.02
	2036.42 ± 19.99	7.59 ± 0.04	1.62 ± 0.02
	2512.87 ± 25.88	6.33 ± 0.04	1.67 ± 0.02
	2975.44 ± 21.19	5.30 ± 0.25	1.65 ± 0.08
16% WiDE	1457.24 ± 30.44	7.85 ± 0.05	1.20 ± 0.03
	2063.87 ± 56.55	5.62 ± 0.05	1.22 ± 0.03
	2504.44 ± 16.52	5.00 ±0.08	1.31 ± 0.02
	3014.35 ± 13.28	4.29 ± 0.25	1.35 ± 0.08

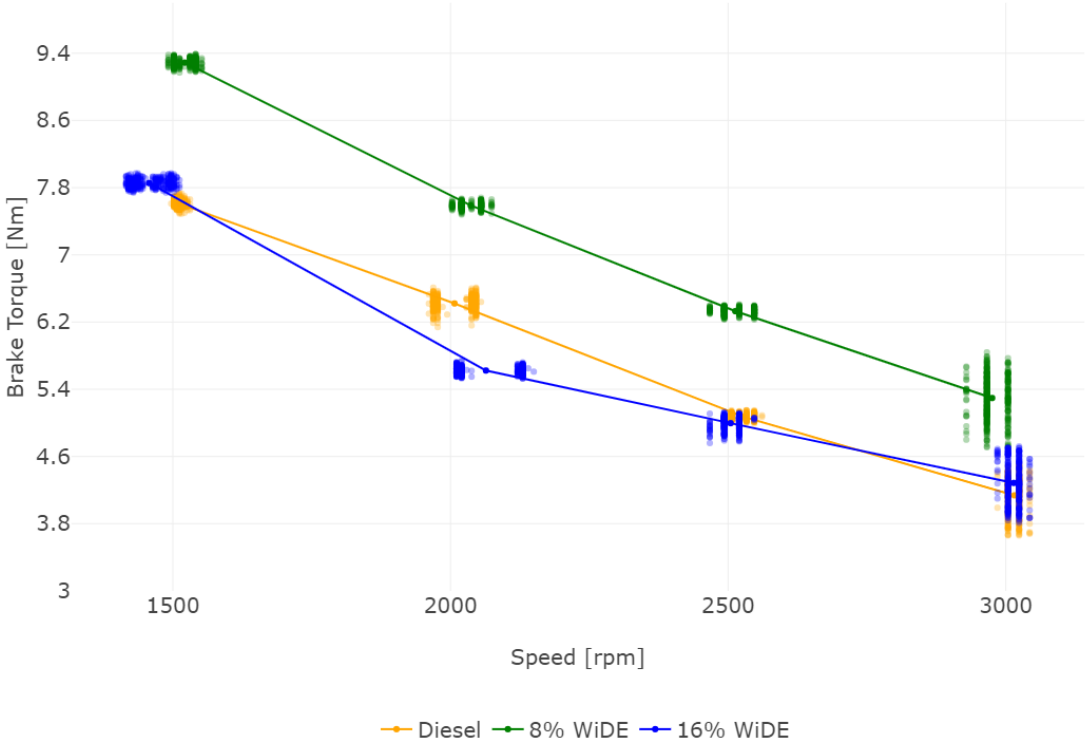

Figure C.11. Engine BT at 50W load (raw data).

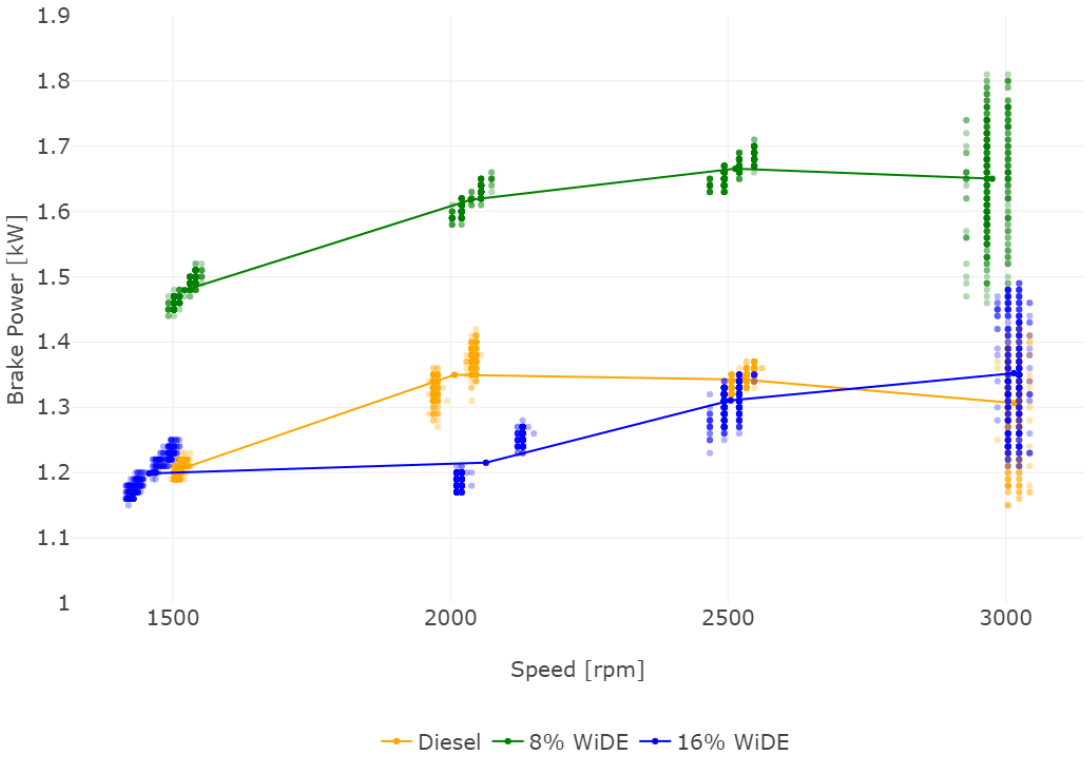

Figure C.12. Engine BP at 50W load (raw data).

Figure C.13. Engine BSFC at 50W load (raw data).

Figure C.14. Engine BTE at 50W load (raw data).

C.2.2 Emissions

Table C.4. Mean and standard deviation for speed, CO, CO_2, HC, NO, O_2, and smoke at 50W load.

	Speed [rpm]	CO [%]	CO_2 [%]	HC [ppm]	NO [ppm]	O_2 [%]	Smoke [%]
Diesel	1511.34 ± 5.98	0.02 ± 0.00	1.47 ± 0.01	16.22 ± 0.41	106.64 ± 0.79	18.74 ± 0.01	3.76 ± 0.12
	2007.24 ± 34.96	0.02 ± 0.00	1.86 ± 0.01	16.99 ± 0.11	102.54 ± 0.78	18.18 ± 0.01	3.55 ± 0.06
	2527.82 ± 15.05	0.03 ± 0.00	2.19 ± 0.02	16.00 ± 0.00	89.08 ± 1.23	17.65 ± 0.01	4.15 ± 0.17
	3015.00 ± 12.18	0.03 ± 0.00	1.84 ± 0.01	14.32 ± 0.47	53.02 ± 0.59	18.13 ± 0.03	4.13 ± 0.15
8% WiDE	1521.43 ± 18.81	0.05 ± 0.00	2.02 ± 0.01	30.50 ± 0.50	96.02 ± 1.18	18.13 ± 0.01	1.01 ± 0.20
	2036.42 ± 19.99	0.11 ± 0.00	2.32 ± 0.00	41.46 ± 0.50	88.36 ± 1.06	17.62 ± 0.02	0.11 ± 0.06
	2512.87 ± 25.88	0.17 ± 0.00	2.81 ± 0.01	50.5 ± 0.96	74.13 ± 2.26	16.92 ± 0.03	1.13 ± 0.22
	2975.44 ± 21.19	0.31 ± 0.00	2.84 ± 0.01	58.92 ± 2.12	35.96 ± 2.04	16.61 ± 0.01	8.54 ± 1.00
16% WiDE	1457.24 ± 30.44	0.04 ± 0.00	1.61 ± 0.01	26.78 ± 0.42	71.19 ± 0.95	18.57 ± 0.01	2.54 ± 0.17
	2063.87 ± 56.55	0.08 ± 0.00	2.01 ± 0.01	35.94 ± 0.71	67.72 ± 1.39	17.96 ± 0.01	1.60 ± 0.17
	2504.44 ± 16.52	0.10 ± 0.00	2.02 ± 0.02	18.52 ± 1.03	47.65 ± 1.27	17.85 ± 0.02	0.74 ± 0.05
	3014.35 ± 13.28	0.21 ± 0.00	2.09 ± 0.02	39.26 ± 2.55	18.79 ± 0.82	17.54 ± 0.02	7.30 ± 0.55

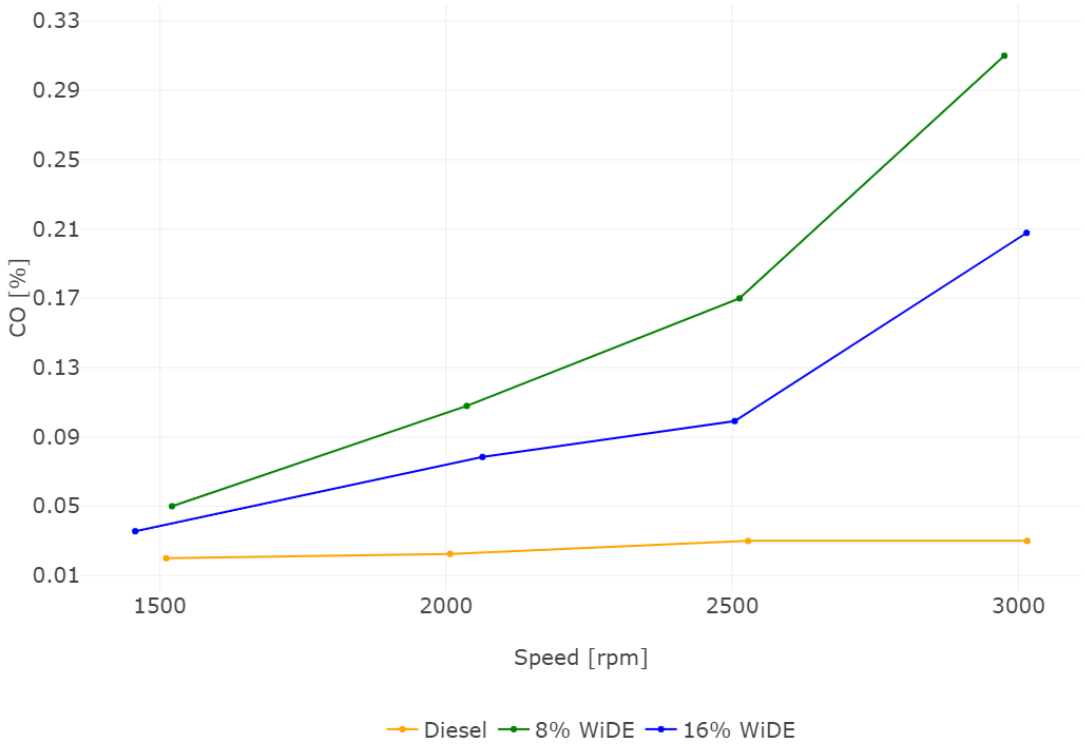

Figure C.15. CO emissions at 50W load (raw data).

Figure C.16. CO_2 emissions at 50W load (raw data).

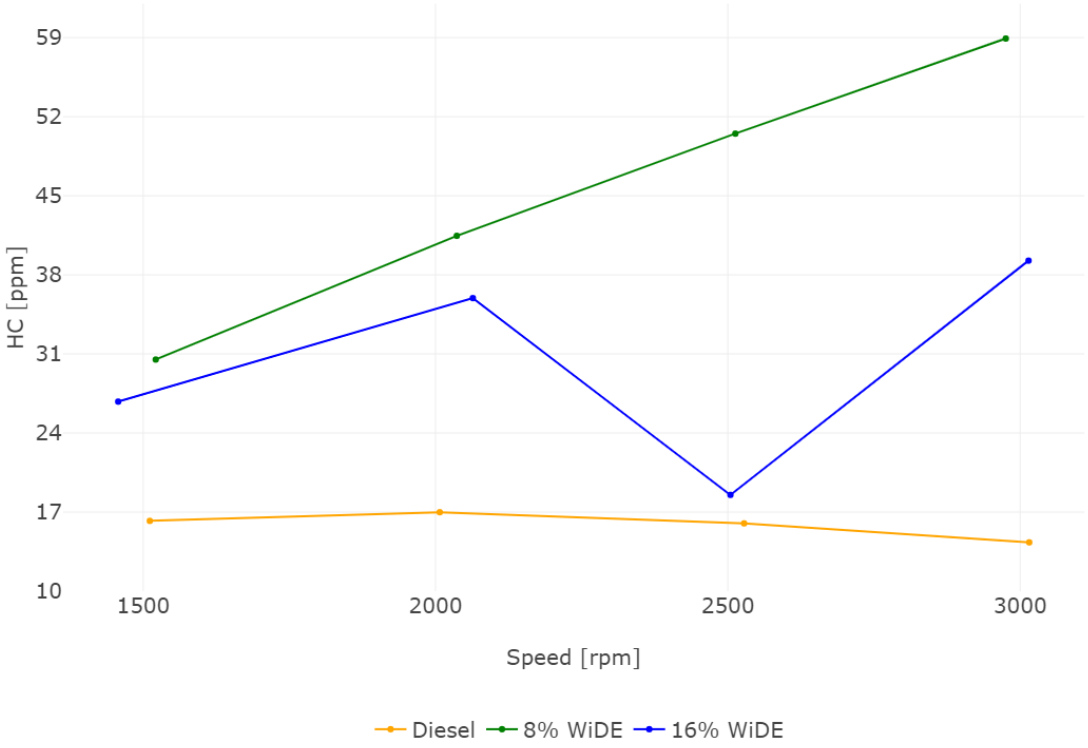

Figure C.17. HC emissions at 50W load (raw data).

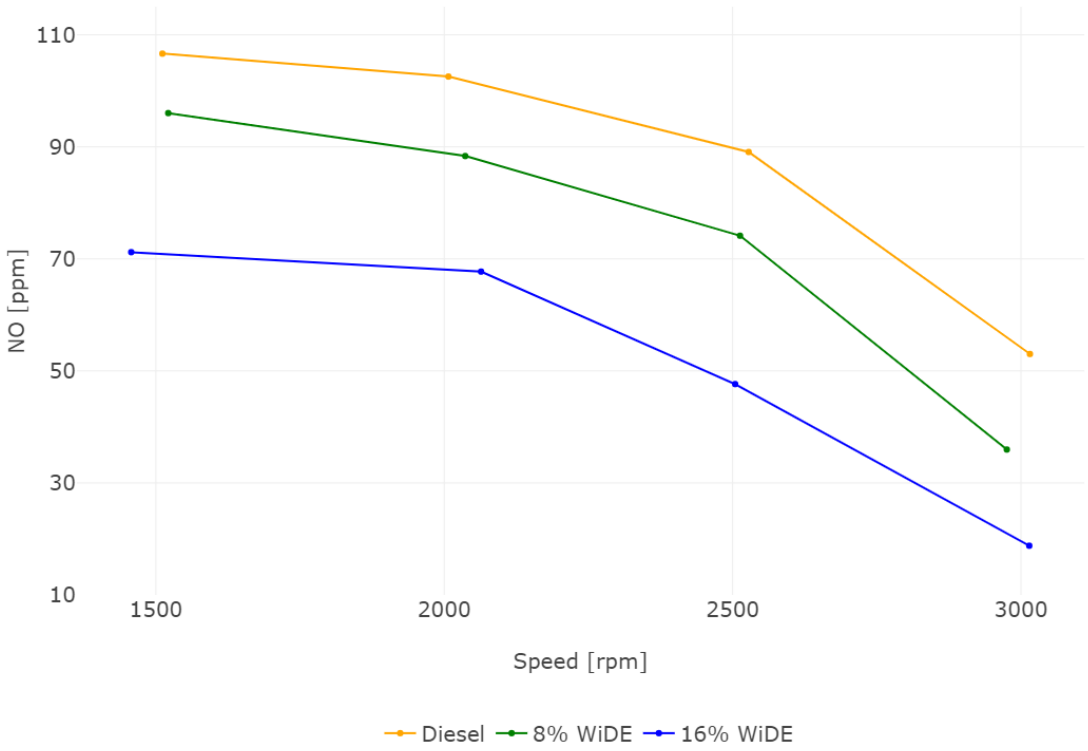

Figure C.18. NO emissions at 50W load (raw data).

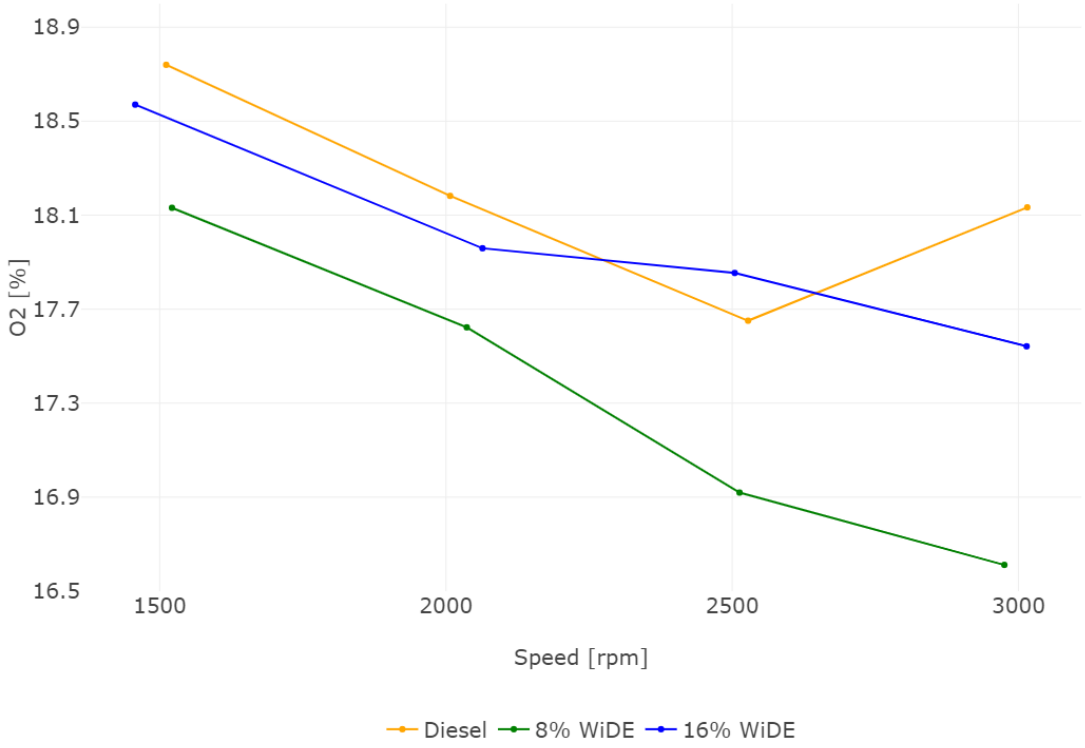

Figure C.19. O_2 emissions at 50W load (raw data).

Figure C.20. Smoke emissions at 50W load (raw data).

C.3 75W load

C.3.1 Performance

Table C.5. Mean and standard deviation for speed, BT, and BP at 75W load.

	Speed [rpm]	BT [Nm]	BP [kW]
Diesel	1454.13 ± 31.77	11.57 ± 0.06	1.76 ± 0.04
	2050.86 ± 56.65	9.13 ± 0.12	1.96 ± 0.06
	2533.33 ± 24.73	7.42 ± 0.10	1.97 ± 0.03
	2985.36 ± 20.03	5.92 ± 0.31	1.85 ± 0.10
8% WiDE	1470.37 ± 17.62	12.83 ± 0.05	1.98 ± 0.02
	1947.49 ± 15.01	11.02 ± 0.10	2.25 ± 0.03
	2489.47 ± 13.18	8.65 ± 0.07	2.26 ± 0.02
	2941.33 ± 21.53	7.27 ± 0.27	2.24 ± 0.08
16% WiDE	1445.58 ± 10.27	12.35 ± 0.07	1.87 ± 0.02
	1953.27 ± 14.12	9.91 ± 0.04	2.03 ± 0.02
	2534.22 ± 15.86	8.33 ± 0.05	2.21 ± 0.02
	3020.09 ± 19.85	6.80 ± 0.26	2.15 ± 0.08

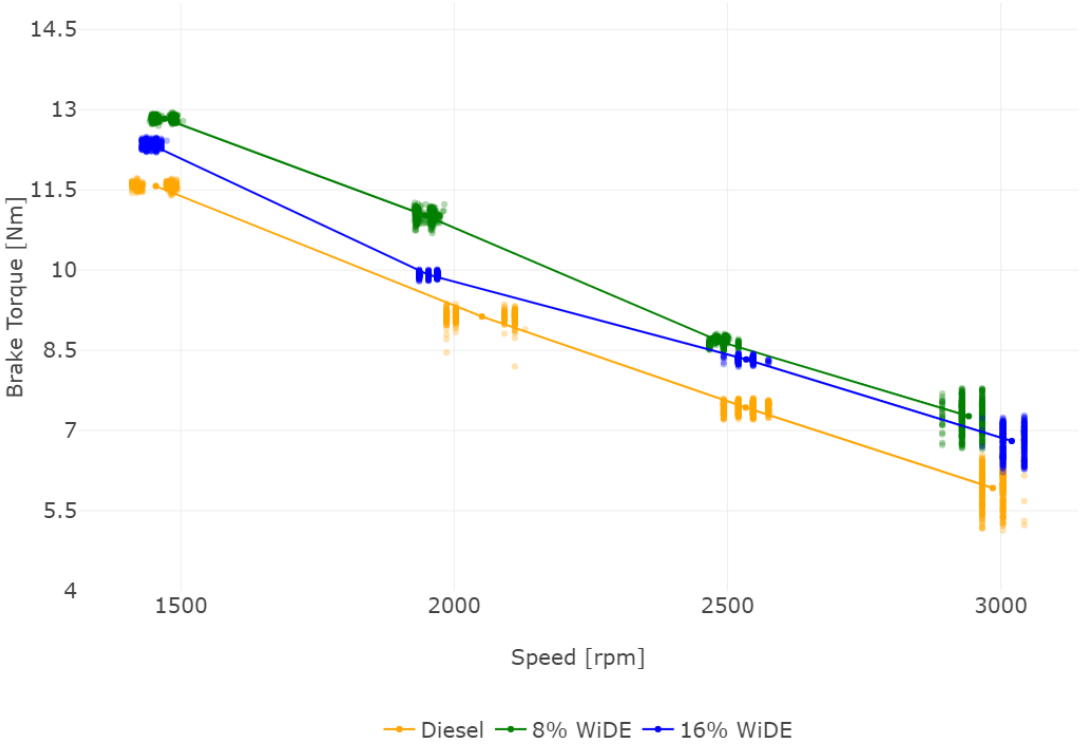

Figure C.21. Engine BT at 75W load (raw data).

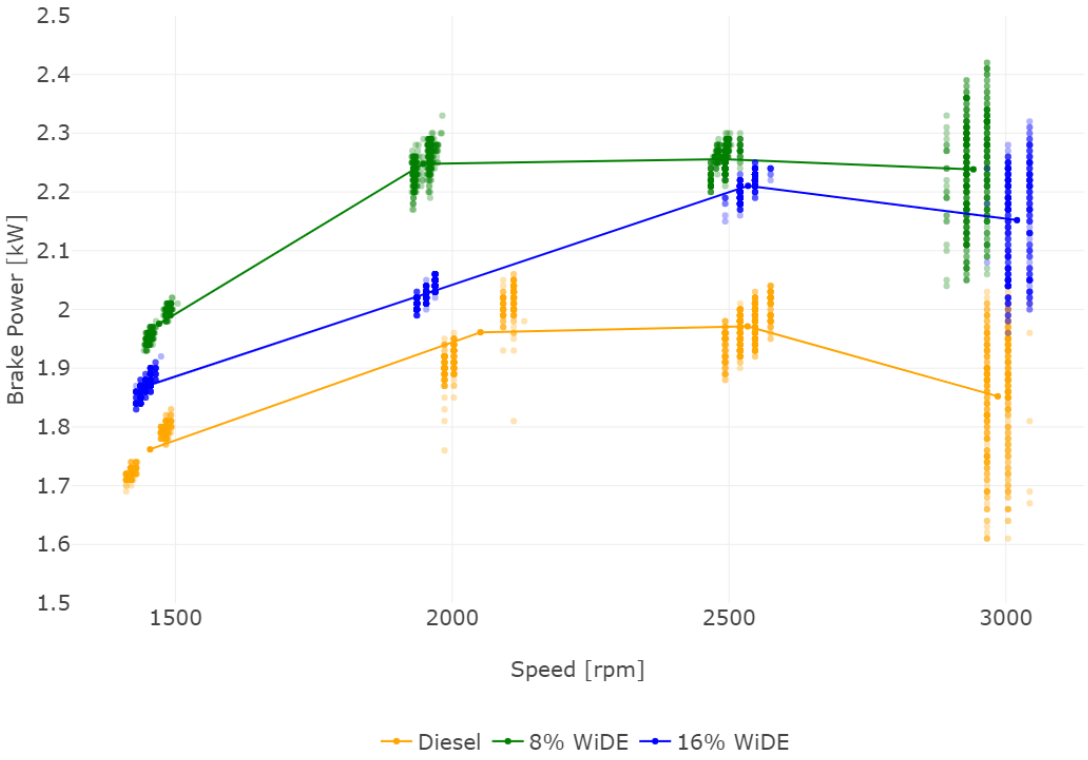

Figure C.22. Engine BP at 75W load (raw data).

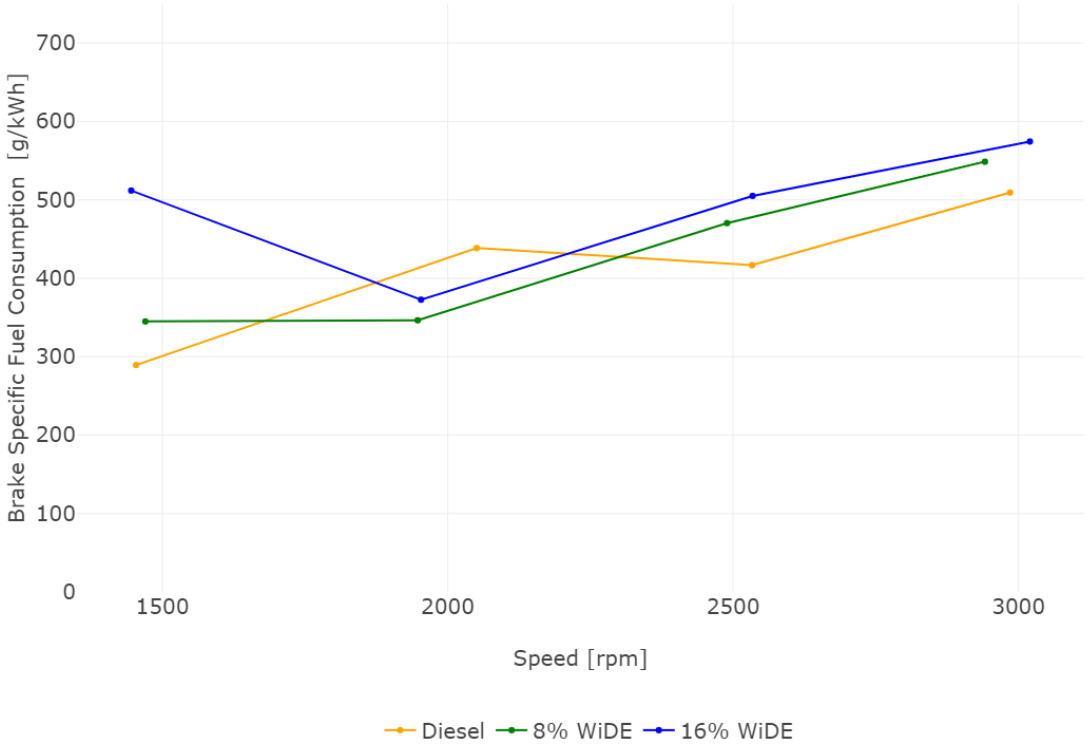

Figure C.23. Engine BSFC at 75W load (raw data).

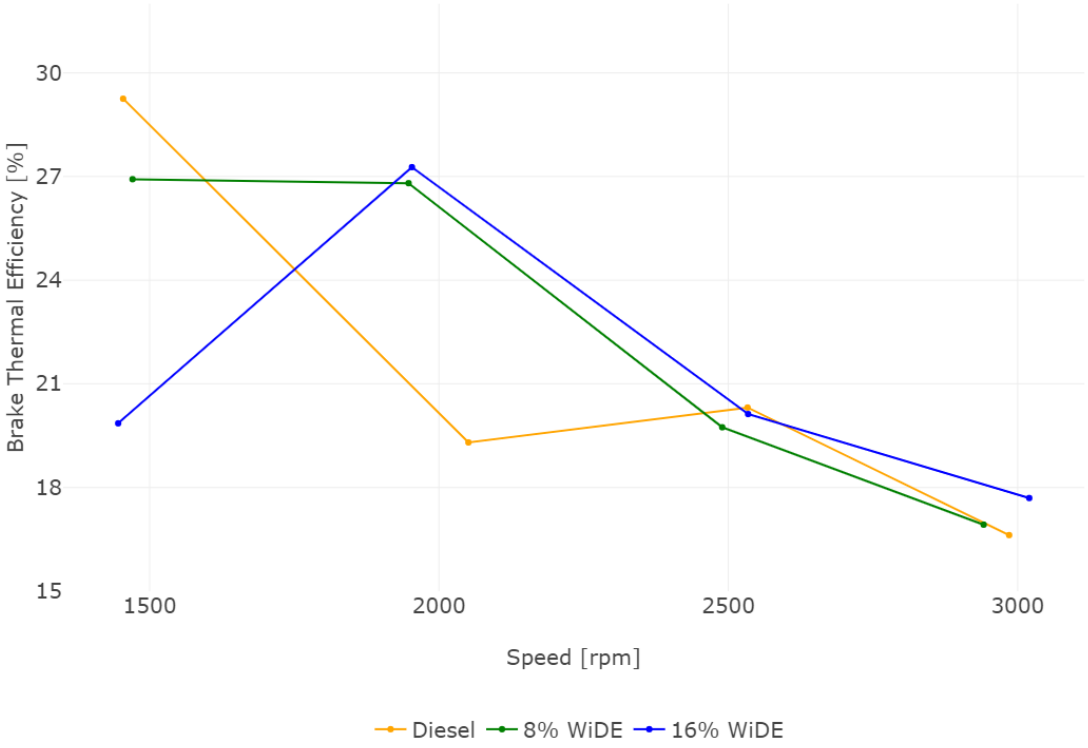

Figure C.24. Engine BTE at 75W load (raw data).

C.3.2 Emissions

Table C.6. Mean and standard deviation for speed, CO, CO_2, HC, NO, O_2, and smoke at 75W load.

	Speed [rpm]	CO [%]	CO_2 [%]	HC [ppm]	NO [ppm]	O_2 [%]	Smoke [%]
Diesel	1454.13 ± 31.77 2050.86 ± 56.65 2533.33 ± 24.73 2985.36 ± 20.03	0.01 ± 0.00 0.02 ± 0.00 0.02 ± 0.00 0.02 ± 0.00	1.66 ± 0.00 2.22 ± 0.01 2.25 ± 0.00 1.93 ± 0.00	19.69 ± 0.46 20.55 ± 0.50 20.00 ± 0.00 18.25 ± 0.49	135.89 ± 1.34 115.00 ± 0.59 115.88 ± 0.95 74.73 ± 2.29	18.40 ± 0.01 17.63 ± 0.01 17.56 ± 0.02 18.03 ± 0.02	3.29 ± 0.11 4.50 ± 0.14 4.35 ± 0.15 4.15 ± 0.15
8% WiDE	1470.37 ± 17.62 1947.49 ± 15.01 2489.47 ± 13.18 2941.33 ± 21.53	0.04 ± 0.00 0.05 ± 0.00 0.11 ± 0.00 0.20 ± 0.00	2.35 ± 0.00 2.65 ± 0.01 3.06 ± 0.01 2.96 ± 0.02	33.00 ± 0.00 31.45 ± 0.66 40.56 ± 0.60 38.08 ± 1.17	149.68 ± 1.24 152.74 ± 1.37 131.77 ± 1.41 66.34 ± 1.60	17.68 ± 0.02 17.29 ± 0.01 16.63 ± 0.03 16.62 ± 0.03	0.31 ± 0.14 0.05 ± 0.05 0.56 ± 0.21 0.02 ± 0.04
16% WiDE	1445.58 ± 10.27 1953.27 ± 14.12 2534.22 ± 15.86 3020.09 ± 19.85	0.03 ± 0.00 0.04 ±0.00 0.07 ± 0.00 0.15 ± 0.00	2.32 ± 0.01 2.64 ± 0.00 2.88 ± 0.05 2.83 ± 0.02	27.00 ± 0.00 24.87 ± 0.99 18.31 ± 0.51 26.81 ± 1.30	141.72 ± 2.44 152.82 ± 1.48 124.45 ± 3.32 58.69 ± 0.89	17.52 ± 0.02 17.05 ± 0.02 16.57 ± 0.04 16.60 ± 0.03	1.31 ± 0.14 0.95 ± 0.05 0.80 ± 0.15 0.89 ± 0.08

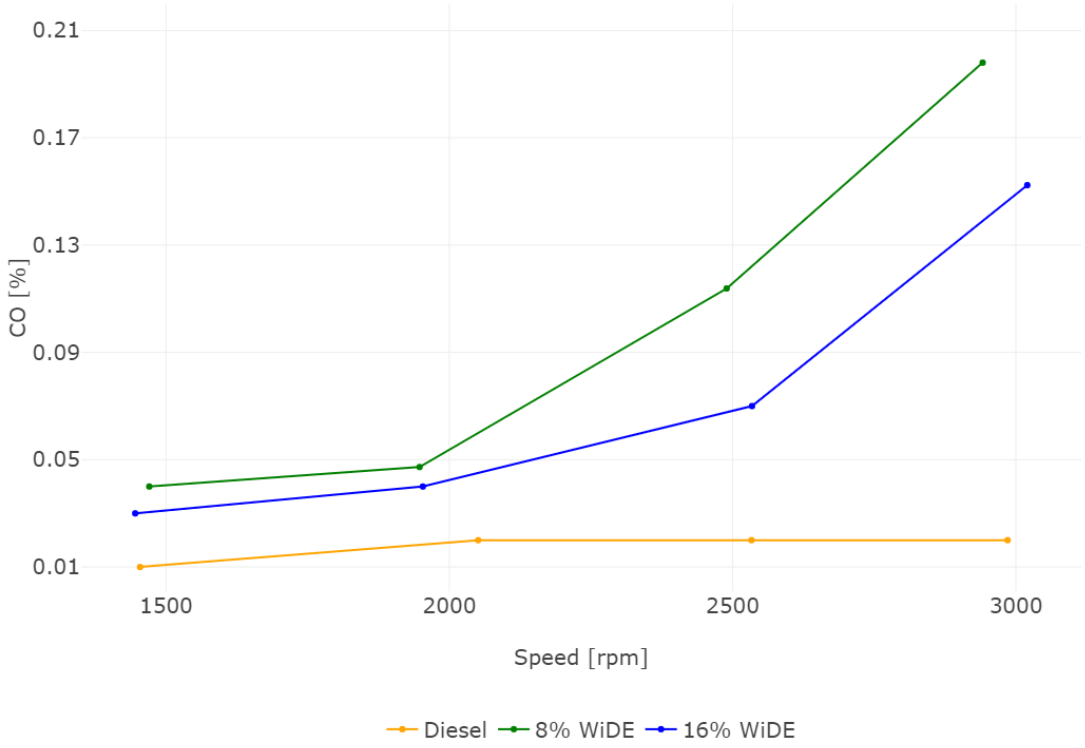

Figure C.25. CO emissions at 75W load (raw data).

Figure C.26. CO_2 emissions at 75W load (raw data).

Figure C.27. HC emissions at 75W load (raw data).

Figure C.28. NO emissions 75W load (raw data).

Figure C.29. O_2 emissions at 75W load (raw data).

Figure C.30. Smoke emissions at 75W load (raw data).

C.4 100W load

C.4.1 Performance

Table C.7. Mean and standard deviation for speed, BT, and BP at 100W load.

	Speed [rpm]	BT [Nm]	BP [kW]
Diesel	1506.42 ± 8.02	16.99 ± 0.05	2.68 ± 0.02
	2003.03 ± 14.97	14.48 ± 0.05	3.04 ± 0.02
	2476.97 ± 17.79	12.08 ± 0.08	3.13 ± 0.03
	3005.17 ± 28.86	8.93 ± 0.27	2.81 ± 0.09
8% WiDE	1442.20 ± 14.34	17.07 ± 0.05	2.58 ± 0.03
	1909.46 ± 9.31	15.13 ± 0.07	3.02 ± 0.02
	2515.13 ± 35.49	11.94 ± 0.04	3.14 ± 0.05
	2949.83 ± 24.23	10.12 ± 0.34	3.13 ± 0.10
16% WiDE	1446.23 ± 19.66	17.15 ± 0.07	2.60 ± 0.04
	1937.35 ± 17.45	14.37 ± 0.07	2.91 ± 0.03
	2531.21 ± 32.32	11.96 ± 0.07	3.17 ± 0.04
	3031.39 ± 21.00	10.20 ± 0.32	3.24 ± 0.10

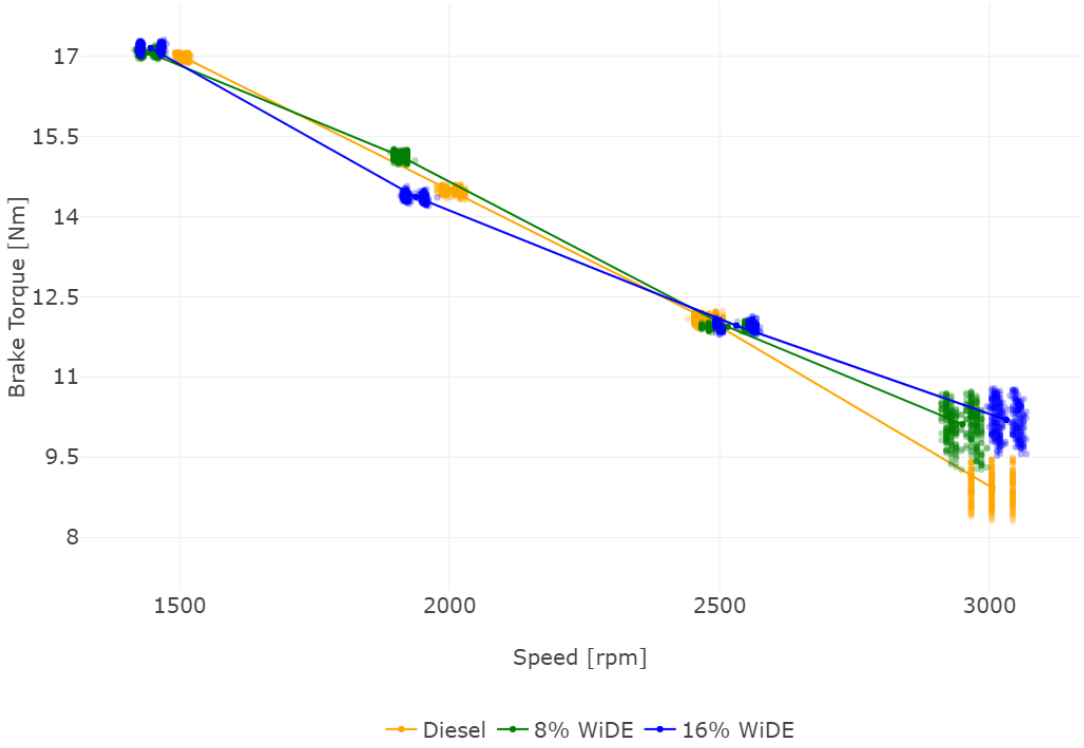

Figure C.31. Engine BT at 100W load (raw data).

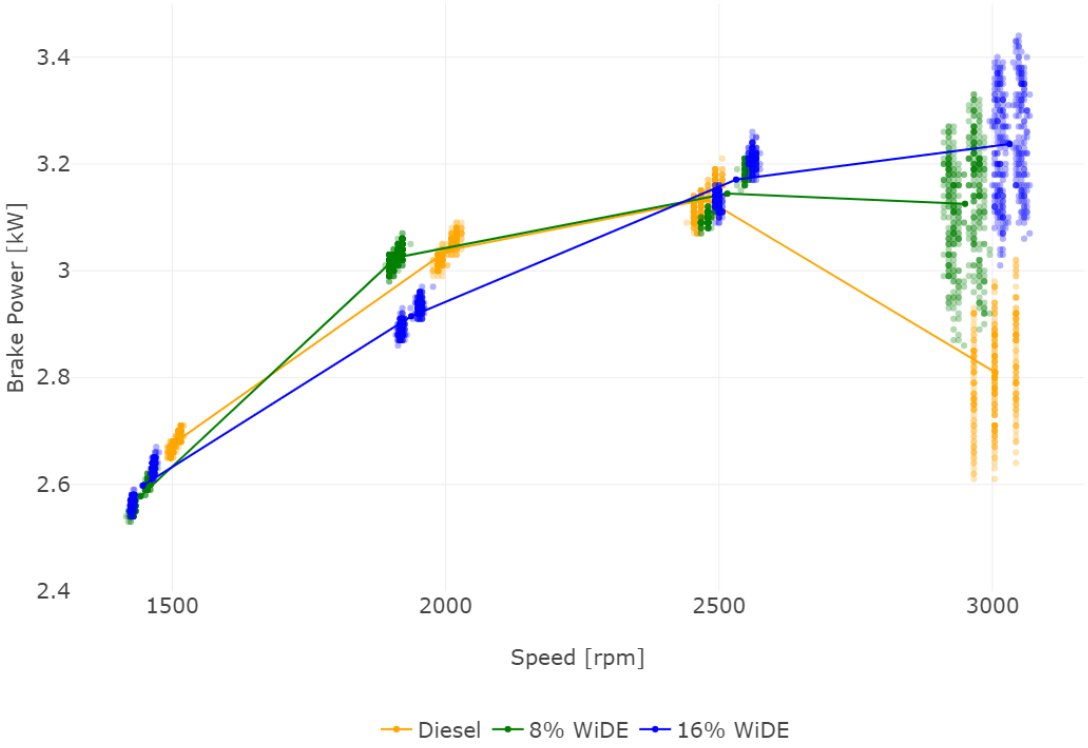

Figure C.32. Engine BP at 100W load (raw data).

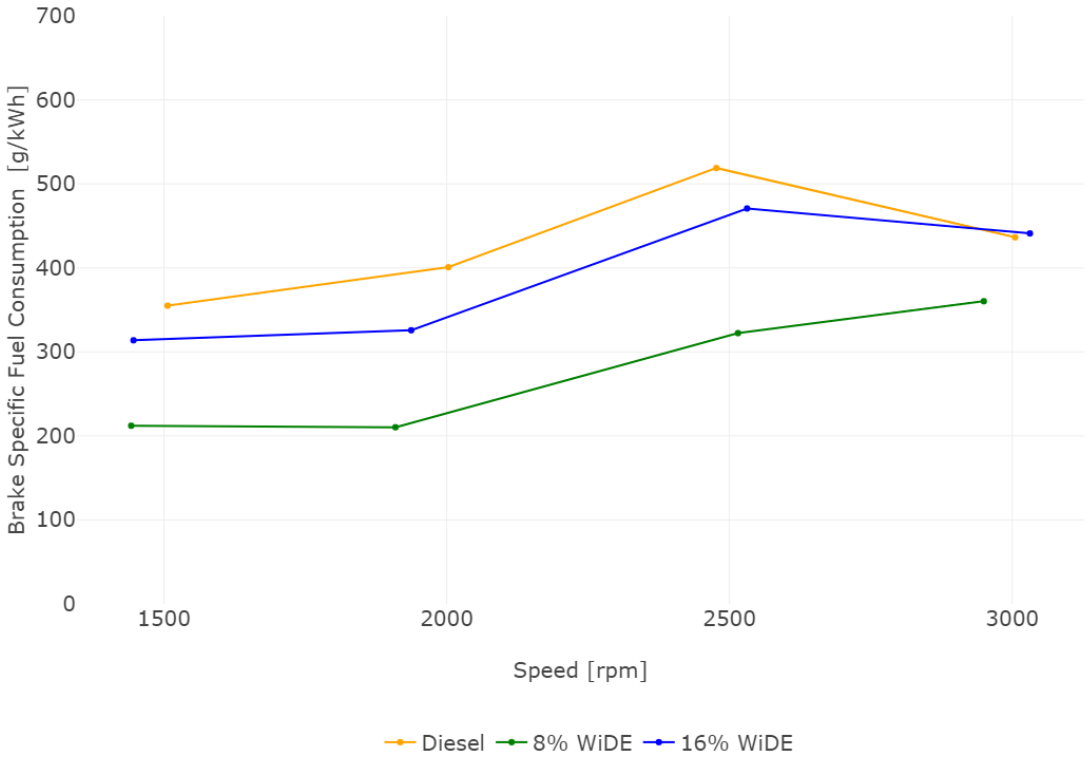

Figure C.33. Engine BSFC at 100W load (raw data).

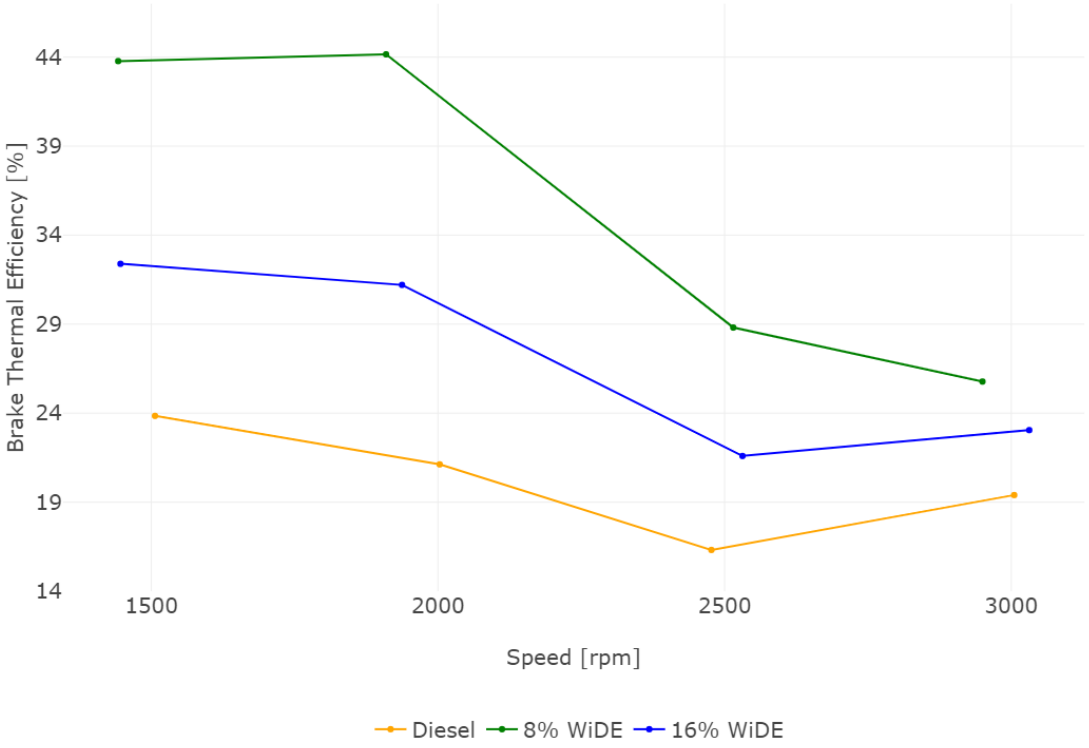

Figure C.34. Engine BTE at 100W load (raw data).

C.4.2 Emissions

Table C.8. Mean and standard deviation for speed, CO, CO_2, HC, NO, O_2, and smoke at 100W load.

	Speed [rpm]	CO [%]	CO_2 [%]	HC [ppm]	NO [ppm]	O_2 [%]	Smoke [%]
Diesel	1506.42 ± 8.02 2003.03 ± 14.97 2476.97 ± 17.79 3005.17 ± 28.86	0.01 ± 0.00 0.01 ± 0.00 0.02 ± 0.00 0.02 ± 0.00	2.96 ± 0.01 2.90 ± 0.01 3.13 ± 0.00 2.76 ± 0.03	18.22 ± 0.42 16.38 ± 0.60 15.00 ± 0.00 15.00 ± 0.00	269.72 ± 2.46 242.30 ± 1.29 217.19 ± 1.00 133.58 ± 2.13	16.59 ± 0.01 16.71 ± 0.01 16.32 ± 0.01 16.74 ± 0.04	4.63 ± 0.29 3.86 ± 0.19 4.66 ± 0.20 3.96 ± 0.14
8% WiDE	1442.20 ± 14.34 1909.46 ± 9.31 2515.13 ± 35.49 2949.83 ± 24.23	0.03 ± 0.00 0.03 ± 0.00 0.05 ± 0.00 0.07 ± 0.00	3.04 ± 0.01 3.35 ± 0.02 3.28 ± 0.03 3.30 ± 0.02	34.00 ± 0.00 30.77 ± 0.84 31.00 ± 0.00 28.00 ± 0.00	250.65 ± 1.45 258.13 ± 2.18 203.18 ± 1.39 146.09 ± 2.64	16.70 ± 0.02 16.30 ± 0.01 16.41 ± 0.03 16.21 ± 0.04	3.95 ± 0.24 2.93 ± 0.19 3.54 ± 0.17 1.03 ± 0.23
16% WiDE	1446.23 ± 19.66 1937.35 ± 17.45 2531.21 ± 32.32 3031.39 ± 21.00	0.02 ± 0.00 0.03 ± 0.00 0.08 ± 0.00 0.14 ± 0.00	3.70 ± 0.01 4.23 ± 0.01 4.59 ± 0.01 4.36 ± 0.05	32.60 ± 0.49 29.84 ± 0.74 31.59 ± 0.49 22.47 ± 1.23	291.42 ± 3.07 294.88 ± 1.51 265.98 ± 1.48 151.61 ± 6.55	15.59 ± 0.02 14.93 ± 0.02 14.34 ± 0.02 14.50 ± 0.10	1.12 ± 0.05 0.82 ± 0.06 0.99 ± 0.05 0.13 ± 0.09

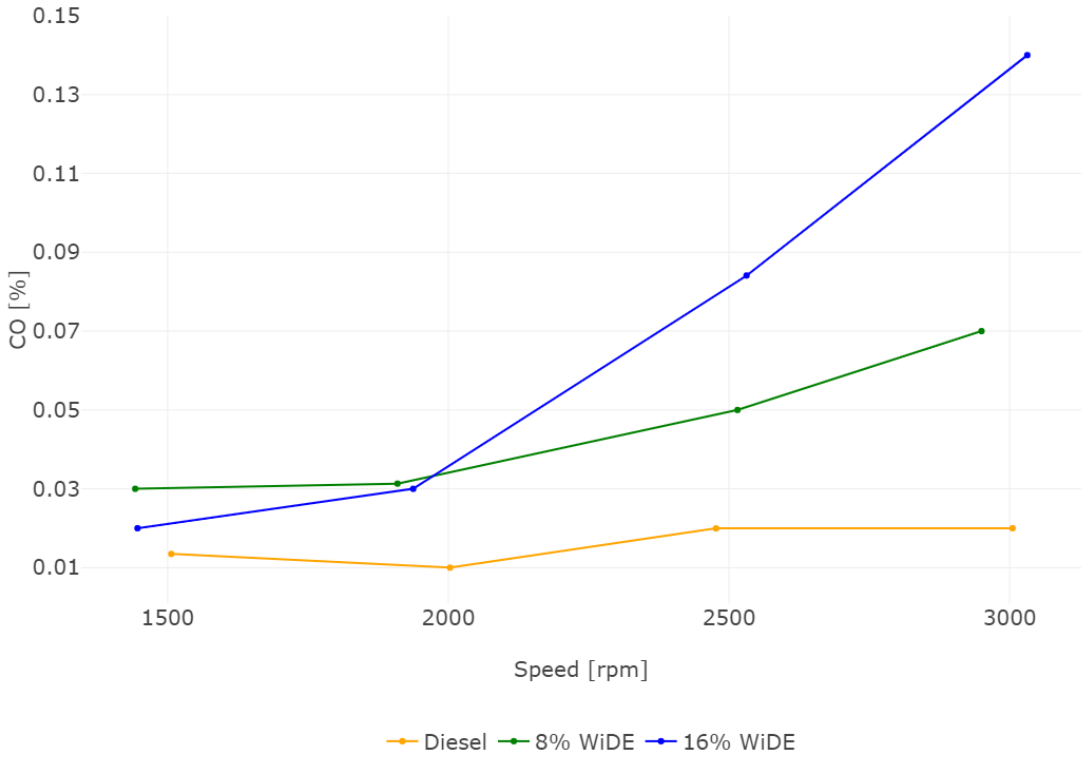

Figure C.35. CO emissions at 100W load (raw data).

Figure C.36. CO_2 emissions at 100W load (raw data).

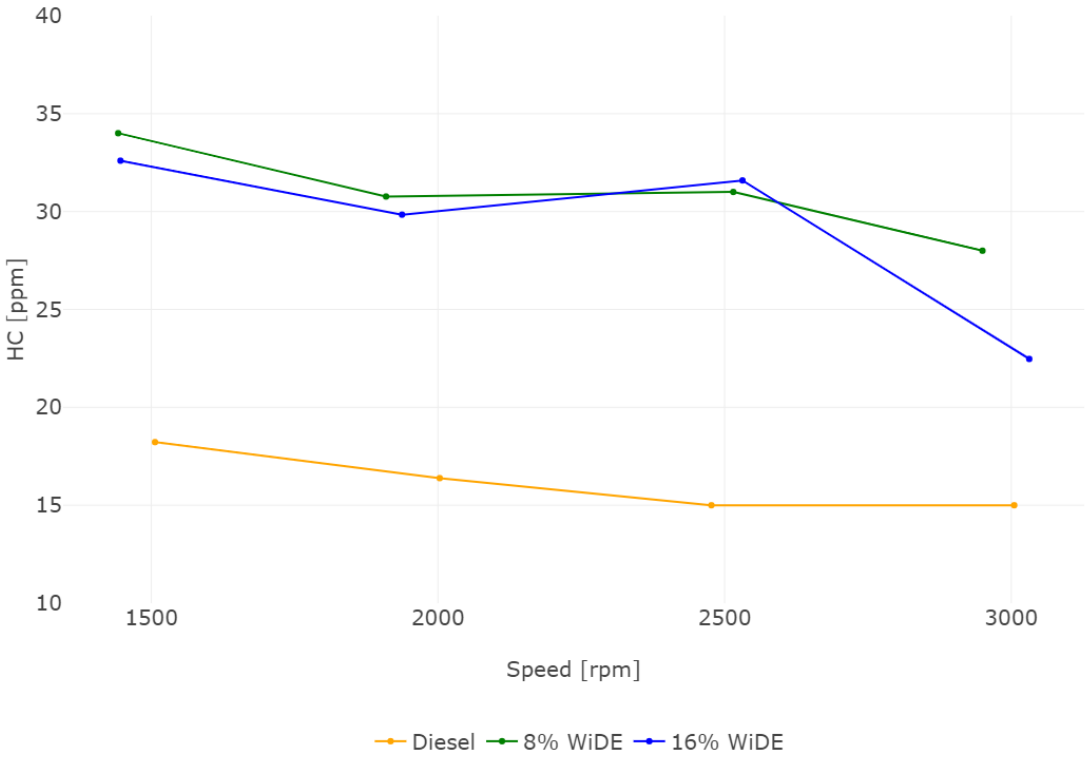

Figure C.37. HC emissions at 100W load (raw data).

Figure C.38. NO emissions at 100W load (raw data).

Figure C.39. O_2 emissions at 100W load (raw data).

Figure C.40. Smoke emissions at 100W load (raw data).